INVESTIGATING UNCERTAINTIES IN SHEAR RESISTANCE PREDICTION OF BEAMS WITHOUT STIRRUPS

Abayomi Bolarinwa, David

B.Eng. (Civil Engineering)

(221118905)

Submitted in fulfilment of the requirements for the degree of
Master of Science in Civil Engineering

College Of Agriculture, Engineering and Science
University Of Kwazulu-Natal
Durban, South Africa.

JANUARY 2023

Under The Supervision Of;

Dr. Oladimeji B. Olalusi

B.Eng, M.Eng, PhD (Stellenbosch), CPEng NER RPEQ (Australia)

Structural Engineering & Computation Mechanics Group (SECM), University of Kwazulu-Natal

PLAGIARISM DECLARATION

I, Abayomi Bolarinwa David, declare that

1. The research reported in this thesis, except where otherwise indicated, is my original research.

2. This research has not been submitted for any degree or examination at any other university.

3. This thesis does not contain other persons' data, pictures, graphs, or other information unless specifically acknowledged as being sourced from other persons.

4. This research does not contain other persons' writing unless specifically acknowledged as being sourced from other researchers. Where other written sources have been quoted, then:

a. Their words have been re-written but the general information attributed to them has been referenced.

b. Where their exact words have been used, then their writing has been placed in italics and inside quotation marks and referenced.

5. This thesis does not contain text, graphics or tables copied and pasted from the Internet, unless specifically acknowledged, and the source is detailed in the thesis and the References sections.

ABAYOMI BOLARINWA DAVID

____

JANUARY,2023

PREFACE

Under the supervision of Dr Oladimeji Benedict Olalusi, the study that is reported in this thesis was carried out at the University of KwaZulu-Natal's civil engineering department, Howard campus, Durban from February 2022 to April 2023.

As the Candidate's Supervisor, I agree to the submission of this thesis.

.... signed at; Sydney, Australia on 29/01/2023

DEDICATION

This thesis is dedicated to my beautiful and kind-hearted fiancée, Queen. Thank you for always being there for me, for believing in me and for respecting my career path.

ACKNOWLEDGEMENTS

May God be praised for giving me the privilege to start this study and furnishing me with the ability to complete it in due time, I am grateful to Him. The following individuals deserve my gratitude for significantly contributing to the success of this research work.

- My supervisor and mentor, Dr Oladimeji Benedict Olalusi, encouraged me to work hard throughout my study because of his passion for academic excellence. His superb direction and priceless assistance had a significant influence on this dissertation. I wish to express my profound gratitude for his patience and timely corrections. Without his assistance, this study would not have been possible.

- Sincere thanks to my parents, Prof. Olatunji Ayodeji Aiyetan and Mrs Abimbola Aiyetan, for their untiring love, support, and prayers during my entire academic career. I would not have been able to accomplish any of my goals without them.

- My Uncle, Mr Olatunde Ajibola Samson, for accommodating me on my arrival to South Africa and for his unending support and care.

ABSTRACT

Optimizing a model's performance should keep the functionality within the confines of safety and economy; deviation from these calls for a reliability investigation of such models. In a bit to optimize shear models for simplicity, safety functionality and economic performance have been an issue of a trade-off as the overestimation or underestimation of the model's intended purpose may occur. Overestimating the shear resistance of flexural members raises safety concerns since it might lead to unsafe design practices that ultimately cause the entire structure to collapse. In the same manner, underestimating the shear resistance may give rise to uneconomical designs. In this research, the predictions of various code-based & authorial shear resistance models in terms of their structural performance were assessed through the model uncertainties. According to Gino *et al.* (2017), identifying and quantifying the uncertainty related to a specific model is of high relevance to structural safety verification in the course of reliability assessment. Uncertainties related to models adequately capture the inconsistency of models' performance across varied structural conditions. Hence, the extent of conservatism demonstrated by shear models of beams without stirrups is investigated towards structural reliability assessment and calibration.

A database of 784 experimental beams without shear reinforcements compiled by Reineck *et al.* (2013), consisting of beams with varying geometrical properties was investigated in this study. Analyses conducted in this study include a mean values analysis (best-estimate prediction without any form of bias) and a deterministic design value analysis (inclusion of partial safety factor or reduction factor and characteristic material properties). Shear values derived from mean value analysis are used as the input parameter to determine the uncertainty of each model for the same structural condition. Supervised machine learning models based on the architecture of the Artificial Neural Networks, Support Vector Machine, Decision Tree Regressor and Random Forest were also used for shear resistance predictions. Model uncertainty was also derived for machine learning predictive shear models.

A comparative analysis between the experimental shear resistance and all considered predictive model was done. Statistical characterization of each model factor in terms of the bias, standard deviation, coefficient of variation and skewness was carried out to evaluate the model's performance in order to adopt a general probabilistic model for subsequent reliability evaluation. Sensitivity analysis of model uncertainty to parametric variation of input parameters was also carried out with the measured value of correlation.

The provision of a carefully calibrated partial factor for model uncertainties that will take into account the uncertainty associated with shear methods is the most efficient management of the reliability performance for any resistance method. To this end, the calibration of a partial factor of safety according to EN 1992-4

was done for models with poor performance in terms of uncertainty performance indexes such as sensitivity to model parameters, a large degree of variability in shear prediction and significant bias in prediction.

CONTENTS

Chapter 3

Chapter 4

List of Figures

Chapter 2

Chapter 3

Chapter 4

Chapter 5

List of Tables

Chapter 2

Chapter 3

Chapter 4

Chapter 5

LIST OF SYMBOLS

a	shear span
A_c	area of the concrete section
A_{sl}	area of tensile reinforcement
Av	stirrup area within the distance of the stirrup spacing
a/d	ratio of their shear span to effective depth
Av, min	minimum stirrup reinforcement ratio
A_g	the gross area of the concrete section
Asw	area of shear reinforcement within spacing, *s*
b_{tens}	the width of the tension flange
bv, eff	effective shear width
bw	beam width
β	reliability index
β_T	target reliability index
β	size effect factor according to (gb50010-2010)
c	depth of the compression zone
d	effective depth of the beam
dv	effective shear depth
d_g	maximum nominal aggregate size
ε_x	longitudinal strain
ε_1	principal strain defined by mohr's circle of strain

ε_2	principal compressive strain
Es	modulus of elasticity of the reinforcement steel
Ec	modulus of elasticity of the concrete
fc	concrete compressive cylinder strength
f_{cd}	the design value of concrete compressive strength
fck	characteristic value of concrete compressive cylinder strength
fcm	mean value of concrete compressive cylinder strength
fcu	characteristic value of concrete cube strength
$f_{ct,ef}$	effective tensile strength
$f_{y\mathrm{wk}}$	characteristic strength of the web reinforcement
$fx(X)$	joint probability density distribution of the vector of basic variables X
G_F	fracture energy
G_{cr}	shear modulus of the cracked concrete
$h_{f,tens}$	height of compression flange.
k_v	product of the strain effect factor and the size effect factor
k_s	shear stiffness factor
l_{eff}/d	effective length-to-depth ratio
M_o	the flexural moment required to cancel the stress induced by the axial force at the extreme tension fibre
Mu	factored design moment
MF	model factor
M	bending moment
M_f	flexural moment
M_{ud}	flexural strength without consideration of the axial force

N_{Ed} the axial force in the cross-section due to loading or prestressing

η_{fc} brittleness factor which reduces the strength for fck > 30 MPa.

NV tension in the longitudinal direction

N_u axial load acting at the critical zone of the concrete section

P_v the vertical component of prestress crossing the section under consideration (according to AS3600-18)

V_{Rd} the design value of the shear resistance force

$V_{Rd,c}$ concrete contribution to design shear resistance

$V_{Rd,s}$ stirrup contribution to the design shear resistance

$V_{Rd,max}$ the upper limit of design shear resistance

V_C shear strength of concrete contribution

vc contribution of the uncracked compression to resisting shear force

V_f shear force

V_l contribution of the longitudinal reinforcement/dowel action to shear resistance

V_w shear transferred across web cracks

V_{uc} design shear resistance from the concrete (according to AS3600-18)

V_{us} design shear resistance from the shear reinforcement (according to AS3600-18)

$V_{Rd,c,min}$ minimum shear strength contribution by concrete to design shear resistance

Vu design value of acting shear force

Vcc shear in the compression zone

V_d contribution of dowel action to shear resistance

V_{az} contribution of aggregate interlock to shear resistance

Vcr residual tensile stress in concrete

Vp vertical component of prestressing steel

$v1$	strength reduction factor
s	stirrup spacing
sx	the perpendicular spacing of cracks inclined at angle θ
ϕ	the angle of the initial inclined cracks.
ϕ	strength reduction factor
θ	concrete compressive strut angle
θ_v	angle of inclination of the concrete compression strut to the longitudinal axis of the member
ζ	size and slenderness effect factor
γ	slenderness ratio
λ_s	size effect modification factor (according to ACI 318-19)
ρl	longitudinal reinforcement ratio
w	crack opening
δ	the relative crack slips
γc	partial material factor for concrete
γs	partial material factor for steel
z	internal lever arm
f_t	tensile strength of concrete
vs	contribution of the sum of the shear resisted by the transverse reinforcement
αcw	coefficient accounting for stress in the compression chord
x	basic random variables on which the resistance and loads depend.
X_k	the characteristic value of material strength
X_m	the mean value of variable X
g(x)	limit state function of random variables (X)
φ	cumulative distribution function of the standardized normal distribution

α_{xi}	sensitivity factor of xi
P_f	probability of failure
μ_{MF}	the mean value of the model factor
σ_{MF}	the standard deviation of the model factor
Ω_{MF}	coefficient of variation of the model factor
η_{MF}	the skewness of the model factor
r	Pearson's correlation coefficient
υ	Poisson's ratio
$\propto$	the angle of stirrups
r^2	coefficient of determination
λ	modification factor
σ_{cp}	compressive stress in the concrete from axial load or prestressing
α_e	the modular ratio of concrete
x	neutral axis depth of the cracked section

Abbreviations

CCC	Compression Chord Capacity (for concrete shear resistance)
DP	Demerit Point
FORM	First Order Reliability Method
GPM	General probabilistic model
JCSS	Joint Committee on Structural Safety
LEFM	Linear Elastic Fracture Mechanics
LN	Lognormal distribution
LoA	Level of Approximation
LSF	Limit State Function
MCFT	Modified Compression Field Theory (for concrete shear resistance)
MASM	Multi Action Shear Model
N	Normal distribution
RC	Reinforced concrete
SMCFT	Simplified Modified Compression Field Theory
TDP	Total Demerit Point
VSIM	Variable Strut

CHAPTER 1
INTRODUCTION

Beams are structural components that are susceptible to transverse loads and are crucial to the load transfer process in any kind of structure, whether it be a reinforced concrete building, a composite structure, or a steel-framed building. The structural significance of this component cannot be overstated. As a result, the role of the structural engineer is to ensure a safe design by critically taking into consideration the failure mode (shear failure) of this element and providing a suitable design that meets the demands of serviceability, safety and economy. A structural model (code-based or literature-based) that predicts the resistance strength is required to appropriately account for the complexity of the shear transfer mechanism and capacity estimate in beams without stirrups since the resistance strength of beams without stirrups does not depend on the availability of stirrups in a practical situation. According to Gino *et al.* (2017), a model typifies reality in a simplified expression and may provide predictions that differ from the actual response due to uncertainties relating to the formulation of the simplified assumption or the neglection of important parameters that contributes to shear resistance. Hence, Controversy arises when the shear model proposed by design codes and authorial models gives different estimates largely because of the variation in theories and shear phenomenon as interpreted by each body of knowledge. Consequently, a conflict of adoption for general use becomes eminent as the inconsistencies associated with the various shear resistance models raise an issue for debate.

1.1 Background of study

The reinforced concrete beam is primarily subjected to bending moment as it is a majorly flexural member. In addition to the predominant flexural force in a concrete beam are forces such as shear force (responsible for shear failure in beams), axial force, and torsion. Shear failure also termed diagonal tension failure, a combination of flexural stress and shear stress, is a brittle failure that naturally occurs abruptly and does not give significant prior signs of distress and warnings before total failure. A combination of non-homogeneity, cracks, reinforcements, and nonlinearity in reinforced concrete contributes to the complex behaviour of reinforced concrete under shear, as described by Hunegnaw and Aure (2021). This makes the inadequacy associated with shear design more dangerous and of much concern than that associated with flexural designs. Collins *et al.* (2015) further said that because shear failures can happen suddenly and without the ability to redistribute internal stresses, they are fundamentally more harmful than flexural design flaws in concrete structures. For the sake of public safety, it is imperative to accurately assess a reinforced concrete structure's shear capability, yet the present approaches are questionable. The "plane sections theory," a simple, precise approach that is generally and universally accepted, can be used by engineers to model the bending resistance of concrete beams. However, for determining shear strength, engineers frequently rely on limited empirical formulae whose application and accuracy can be somewhat disputed.

Shear models are typically laborious and excessively time-consuming because all relevant variables must be taken into account to produce an accurate predictive model. Because shear failure is brittle and should not be the initial mode of failure, design codes are always unnecessarily simplistic and integrate more caution in their assessment of shear resistance than their provisions for bending by adding large factors of safety to the expression for shear.

According to Holicky *et al.* (2015), typically, a hypothetical model for resistance or load effect is incomplete and erroneous because of a lack of information or because the model has been purposefully modified for usability. Hence reliability analysis is employed in assessing the extent to which design codes and authorial model gives a significant margin away from unreliability and inconsistency. Fundamentally, structural reliability analysis concerns itself with the accurate characterization of model uncertainties and the improvement of models by introducing partial factors to enhance the performance of analyzed models.

The following definition of model uncertainty has been put forward by various bodies of knowledge, and each definition accurately captures the entirety of the theme. Model uncertainty is explained by Mandic *et al.* (2020) as a quantitative marker that relates a predefined threshold to the anticipated performance of a structural framework. ISO 2394 (2015) specifies model uncertainty as a basic variable related to the reliability of physical or empirical models. Following the Joint Committee on Structural Safety's Probabilistic Model Code, model uncertainty is often an independent factor expressing the influences excluded in a model's formulation and approximation.

A model is a way of expressing reality in simple terms, structural engineering is surrounded by a whole lot of uncertainties, both in the materials for construction(aleatory) and in the design models(epistemic) for simulating practical conditions (Mensah, 2015). Therefore, before models such as those employed to forecast the shear resistance of beams without shear reinforcement can be completely accepted on a broad scale and represent reliability, their underlying epistemic uncertainties need to be thoroughly assessed. To develop a generic probabilistic model that properly accounts for the complexities of shear resistance models and accurately reflects an experimental setup under a variety of real-world conditions, the assessment and characterization of the uncertainties of shear resistance must be carried out.

Machine learning, a subset of artificial intelligence, is being used as a tool to solve a variety of technical challenges, including design improvement, stochastic simulation, reliability analysis, and performance assessment of structural systems of great complexities (Olalusi and Spyridis, 2020). This is possibly attributed to the enormous volume of experimental data acquired over time, as machine learning is more associated with the science of data. Innovation in the computation power of hardware and software systems has made soft computation a generally acceptable solution to engineering problems. This tool is largely used in research work related to the evaluation of shear resistance due to the availability of shear experimental datasets, the precision in the output of machine learning models since the algorithm computerizes the inherent knowledge in a type of dataset and builds an accurate input and output relationship as suggested by Jung and Kim (2008), and its ability to express model uncertainty as a tool for structural reliability analysis.

1.2 Motivation and problem statement

According to Tran and Carl-Alexander (2018), due to the difficulty, cost, and length of time involved in conducting experiments to discover how various factors or parameters such as the type of concrete, its strength, and composition impact the concrete shear properties, the concrete parameters' uncertainty estimation constitutes the majority of a shear capacity prediction model's uncertainty. As a result, uncertainties occur when these factors are estimated as a function of other concrete parameters (majorly concrete compressive strength). In addition, ignoring the influence of essential properties of concrete toward the simplification of a model may also lead to uncertainty. The objective of the flexural members shear model is to provide shear capacity estimates with an adequate degree of safety that is economical for usage.

This consequently implies that for an accurate prediction of shear, due account should be taken of all basic variables in an appropriate calculation model which results in a difficult and time-consuming design procedure which is seen when manually applying the Modified Compression Field Theory (MCFT). Most codes of practice have elected to base their shear design methods on simplified design approaches that have typically been calibrated in one way or another to provide acceptable safety and economy, though this is not always achieved transparently. (Mensah *et al.*, 2013).

The Canadian code (CSA A23.3) considers shear strength to be a function of concrete compressive strength and effective depth, whereas EC2 (2003) incorporates reinforcement ratio, effective depth, and concrete compressive strength in its formulation for the shear strength of beams without stirrups. The Fib Model code 2010 addresses beam shear strength as a function of longitudinal strain in the web. In determining the concrete contribution to shear, ACI 318, CSA A23.3, and NBR 6118 (Brazilian standard) regulations depend only on concrete strength, ignoring aggregate interlock and the dowel action supplied by longitudinal reinforcement.

Shear approaches as stated in design codes have restrictions on a number of design variables, for example, the compressive strength for CSA A23.3 and ACI 318 has a maximum boundary value of 60MPa and 70 MPa accordingly, but EC2 and NBR 6118 permit values up to 90MPa. These constraints are some kinds of bias that have been incorporated into the design model that affects the reliability performance. A measure of divergence in shear strength prediction is created between the models provided by these codes of design. It should be noted that the variation in the codes is majorly due to the assumptions the codes were based on. Due to this reason, a reliability-based assessment of these codified models and other analytical models should be conducted.

Retief (2007) reported, "reliability studies conducted at Stellenbosch University showed the model uncertainty reduced considerably when the shear span to effective depth (a/d) and effective depth (d) increased, but it is not sensitive to trends in the other shear parameters when examining shear resistance models for RC beams without stirrups following EN 1992-1-1 shear model". Cladera and Mari (2004) noted that as the effective depth and longitudinal reinforcement (%) increased, the model uncertainty for the same shear model decreased. It is important to look at the differences in the results reported by Retief (2007) and Cladera and Mari (2004). It is crucial to stress that members without shear reinforcement break suddenly due to their brittleness, hence, sufficient dependability must be guaranteed.

Empirical models are by all means only applicable to the set of data from which they were produced, and they are occasionally oversimplified by omitting some fundamental factors to produce even more basic models (Mensah *et al.*, 2013). Specifications for the construction of reinforced concrete structures often use empirical modelling techniques for beams without stirrups and can only be as valid as the extent of data available during the derivation. To alleviate the uncertainties associated with such models and assist their effective deployment, reliability evaluation of such models is therefore necessary following the acquisition of an extended dataset.

The evaluation of uncertainty in available shear prediction models for beams without stirrup in this study is predicated on shortcomings surrounding the formulation and application of shear models, such as those stated earlier. This paper concentrates on investigating the underlying uncertainties in available shear methods with appropriate quantification through the use of an extended dataset of 784 experimental observations of beams with no stirrups. Additionally, this study provides a partial factor that takes into consideration the shear model uncertainties that may be identified after a comprehensive evaluation.

1.3 Research Aim and Objectives

The primary purpose of this research is to characterize and measure model uncertainty in shear modelling techniques provided for estimating the shear resistance of beams without stirrups. The shear models to be investigated include code-based models (such as EN 2003, ACI 318, AS 3600, *Fib* Model Code 2010 and SANS10100), relevant authorial models (such as CCC, MASM, NLT and the modified SNiP shear model) and machine learning based shear models (ANN, SVM, RF and DT) to arrive at a probabilistic model, which would be recommended for future reliability analysis. Specific objectives include;

1. To review recent works of literature on; the mechanics of shear failure and transfer in RC beams without stirrups taking into account the influence of shear parameters that contribute to shear resistance, the assessment of model uncertainty related to shear resistance, as well as other aspects of engineering interest, and, finally, to study research work on the use of machine learning to get a complete understanding of its usage as a tool in engineering.
2. To develop machine learning-based shear models with the use of python (a high-level object-oriented programming language).
3. To compare predictions from various shear models (code-based models, authorial models and machine learning-based models) to experimental results.
4. Model factor estimation and characterization for the aforementioned shear resistance models, as well as the inclusion of a parametric assessment to further explore how sensitive the identified model uncertainty is to input parameters (shear design parameters).
5. To identify the probabilistic model that would be proposed for future reliability analysis.
6. To derive a partial factor that would account for model uncertainties in shear models.

1.4 Summary of Chapters

This dissertation is divided into six (6) chapters, which are organized as follows;

Chapter 2 examines the broad subject of shear as a delicate mode of failure in RC beams, the behaviour of beams in shear which doubles as the mode of shear failure is also reviewed. The shear transfer actions of reinforced concrete beams with and without stirrups are presented in chapter 2 of this study. An in-depth discussion is carried out on the shear contributions of aggregate interlock, dowel action, residual stress, arch action and the uncracked compression zone. The chapter highlights the key characteristics and the underlying phenomenon of the shear models (code-based and literature-based models) proposed for forecasting the shear capacity of beams without shear reinforcements as specified in this study. A3600-18, ACI 318-19 building code, *fib* Model Code 2010 Level of Approximation II, Eurocode 2, and the South African National Standard SANS 10100-1 are the international standards considered, while authorial models include the compression chord capacity model (CCCM), the multi-action shear model (MASM), mechanical shear model based on structural mechanics and the modified Russian SNiP model. Additionally, a summary of structural reliability and its evaluation is provided in this chapter, with a focus on model uncertainty and reliability index. The chapter ends with a review of machine learning and the mathematical theory behind the machine learning (ML) models that were selected for this study, such as the artificial neural network (ANN), support vector machine (SVM), decision tree (DT), and random forest (RF).

Chapter 3 analyzes and discusses the characteristics of the dataset that was used in this investigation provided by Reinick et al. (2013). This chapter presents the techniques used in model factor uncertainty studies and reliability assessments for various shear approaches. The approaches covered in this chapter are sequential; they include a mean value-based deterministic analysis and a design value analysis. Additionally, a flowchart illustrating the sequence of machine learning prediction and performance evaluation is provided. Also included are the model factors that were derived for various shear design techniques. A thorough examination of the parametric (Mean, standard deviation, coefficient of variation, correlation, and regression, and Pearson coefficient of skewness) and non-parametric (goodness of fit test, probability distribution function) analytical techniques for the assessment of model factor is also presented in this chapter.

Chapter 4 centres on statistically characterizing and quantifying model factors for the reviewed shear resistance models. The EC2 mean shear value, the ACI 318-19 best-estimate predictions, the *fib* Model Code 2010 (II) best-estimate model, the AS 3600-18 mean shear value, the SANS true shear estimate, the CCC true shear value, the MASM best estimate, mean predictions from the mechanical model by Tran (2020) and the modified Russian SNiP shear model were all taken into consideration. To characterize the relevant model uncertainties and bias, statistical methods were applied to a database of assembled experimental observations in this chapter. Using a sensitivity analysis, model factors were examined with crucial shear factors as it is a requisite for statistical investigation. As a result, an appropriate GPM for shear resistance was proposed. Different visualizations to buttress the investigation is also presented in chapter 4 of this study.

Chapter 5 presents an introduction to the model uncertainty partial factor calibration following EN 1990. After the investigation concerning model uncertainty in chapter 4 of this study, the deterministic approach in EN 1990 for calibrating model uncertainty partial factor is applied to the EC2 and fib model code LOA II shear provision to take into account the uncertainty related to the shear methods and reported

Chapter 6 presents the objectives achieved in the course of this dissertation. A summary of the thesis and an outline of the dissertation's key findings about the uncertainties associated with the EC2, ACI, AS, MC-10 (II), SANS, CCC, MASM, modified SNiP and Tran (2019) shear design formulations are documented as well as research recommendations.

CHAPTER 2

Literature Review

This chapter gives an extensive review of the mechanism of shear transfer in beams without shear reinforcement, it gives an account of the factors (shear parameters) that contributes to the shear capacity of RC beams. Also, it provides details that relate to the shear failure mode in beams without shear reinforcement. It highlights the codes of design and authorial models for estimating the shear resistance of beams without stirrups and gives a comprehensive examination of the premise surrounding the formulation of each model mentioned. This chapter also reviews existing literature that has quantified uncertainties due to resistance models, load effects or other engineering interests. Works of literature related to the machine learning models considered in this research would also be discussed to gain an in-depth understanding of the underlying principles.

2.1 Review of Shear in Beams Without Stirrups

Tao *et al.* (2016) gave a chronological presentation of various methodologies proposed by different researchers from the year 1966 – 2013. In their study, Tao *et al.* (2016) reported 24 shear models proposed by different research within 47 years, however, the subject of shear and its estimation is yet to receive a conclusive solution. This is due to the intricacies that surround the shearing mechanism, the shear resistance of reinforced concrete has been difficult to predict, and even with various proposed models for prediction, it is still a continued area of interest in reinforced concrete design for safety evaluation and material science.

According to Cladera *et al.* (2016), Diagonal cracks occur when a reinforced/prestressed concrete structural element undergoes both shear and flexure. This results in the development of a multi-axial stress state that occurs in regions along a flexural beam that displays a particularly intricate response, hence, the actions of shear-resisting agents. The mechanics of these shear-resisting actions are considerably different from each other and displays a complicated relationship among themselves. Subsequently, the development of a generally acknowledged formulation to represent shear forces has not been accomplished at this point and it is important to take significant presumptions to determine compact expressions.

Changes in the load application plane result in changes in the structure's performance, due to this, special attention should be given to assessing the critical state of structural elements, in the case of reinforced concrete beams, determining the shear strength and shear strengthening method is an evolving problem with all sense of urgency (Vegera *et al.*, 2016).

Shear modelling of beams with stirrups has achieved a degree of stability with the underlying theory of equilibrium such as strut & tie models and stress field models (ASCE-ACI Committee 445). This is not true for the shear estimation of beams without stirrups as there is no consensus in the research community concerning the parameters and peculiarities overseeing shear strength in beams without shear reinforcement (Ruiz *et al.*, 2015). Amani and Moeini (2012) and Filatov (2017) also agreed with Ruiz *et al.* (2015) as they said distinctively that “a generally accepted design philosophy for shear is non-existence unlike the case of design provisions for bending”.

The consequence of this becomes obvious in the design models used to estimate the shear strength of beams with no stirrups as there is preferential consideration of mechanism that governs the shear transfer while neglecting the influence of others and this ultimately affects the shear strength evaluation from each model (ACI Committee 318).

Bentz *et al.* (2006) and yang (2014) recognize the contribution of aggregate interlock as the dominant governing mechanism in shear transfer in beams without stirrups. Contrarily, Zararis (2003) identified the shear carried by the compression chord as the most important parameter that contributes to the shear transfer mechanism.

Considering the estimation of shear in beams without stirrups, design models from different country codes have also been analyzed under their presumptions about the governing parameters that are responsible for the quantification of shear resistance. The Ukrainian and European design code does not account for the influence of the load type and location and the shear span-effective depth ratio. The American code of design provides a very simplified and basic expression for the estimation of shear strength which neglects the impact of the longitudinal reinforcement, the shear span- effective depth ratio and the loading type but gives a quick assessment of shear, the Australian code of design takes into consideration much of the design parameters, but according to Vegera *et al.* (2016), the design model still shows notable variation with true experimental shear prediction.

The international regulations for concrete designs and their parameter considerations for evaluating shear are shown in the table below.

Table 2.1 International regulations for concrete designs and their parameter considerations

Codes of design	**Considered Parameter**
Canadian code (CSA-A23.3, 2004)	longitudinal strain (ε_x), shear force (V_f), effective depth (d), and bending moment (M_f)
JSCE (1986)	member depth (d), compressive strength (f_{ck}), bending moment (M_o), longitudinal reinforcement ratio (ρ), and bending strength (M_{ud})

GB50010-2010	effective depth (d), slenderness factor (β), and concrete tensile strength (f_t)

Various authorial empirical models have also been proposed, some of which include the Compression Chord Capacity Model ($CCCM$) by Cladera *et al.* (2016) which is a simplification of the model put forward by Mari *et al.* (2015) called the Multi-Action Shear Model ($MASM$). The Multi-Action shear model which is based on the principle of mechanics considers the contribution of the sum of all the shear-resisting actions, but in a case where the contribution of the transverse reinforcement doesn't exist, the expression can be modified by neglecting its effect as in the case of beams without stirrups. Unlike the $MASM$, the compression chord capacity model ($CCCM$) generalizes on the premise that the shear transferred by the uncracked compression chord is the main transfer mechanism in the considered failure state. The theories, assumptions and conditions for the use of these models would be further reviewed in this research work.

Yerzhanov *et al.* (2019) reviewed and modified the shear design model for RC members without shear reinforcement specified in the SNiP code (This code is used by structural engineers in CIS nations to design RC structures). The inadequacy of the original SNiP code was primarily due to the insufficient quantity of experimental data used to develop the model which then led to a poor generalization of the model concerning inferencing. Yerzhanov *et al*. (2019) used the ACI 445-DafStb shear database which is more comprehensive with more datasets to propose a modification factor chosen as a function of the effective depth (d) and consideration given to tensile strength rather than compressive strength to improve the analytical accuracy and safety level of the original SNiP model.

In contrast to every other empirical and semi-empirical model mentioned above, a mechanical model which is purely based on the theory of structural mechanics was developed and presented by Tran (2020). The author of this model made use of technological advancements by using the digital image correlation approach to gather comprehensive knowledge on a concrete member's behaviour under shear, especially the formation of cracks with an emphasis on crack width and crack spacing. The parameters from the crack inspection together with the fracture energy (G_F), the tensile strength of concrete (f_{Ct}), the modulus of elasticity (E_C) and Poisson's ratio (υ) were considered the most important mechanical characteristics of concrete relating to shear capacity and were used in the mathematical formulation of the mechanical model.

All that these models aim to do is to capture the true estimation of the shear strength by applying their underlying theory and assumptions and translating it into an empirical equation as is common with shear strength modelling.

2.2 Shear behaviour of RC beams without stirrups

According to Tran (2020), there are three response stages to the behaviour of a concrete structural member in shear which is explained below and further represented graphically. See Fig 2.1

- In the first stage, when the concrete is in its uncracked state, the entire concrete cross-section experiences a distribution of shear stress that is parabolic and the shear transfer mechanism is restricted as there are no resisting actions from the aggregate interlock, the residual tensile stress and the dowel effect.
- The section attains a cracked state in the second stage, with shear cracks limited to the tension zone and not passing through the neutral axis. Parabolic distribution of shear stress occurs at the uncracked region of the flexural member. At this point, some resisting mechanism begins to take effect; interface shear transfer, an inconsequential dowel action and residual tensile stresses.
- Stage 3 shows the major shear crack's total extension deep inside the compression zone. In uncracked concrete, it is quite feasible that the shear stress will be redistributed parabolically. At this stage, full resisting actions begin to interact with each other. Shear failure occurs when the concrete section loose hold of the unstable region C under the influence of incremental loadings.

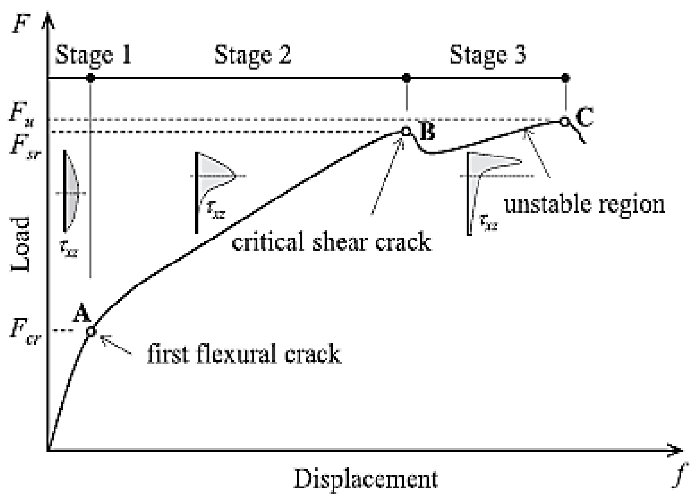

Fig 2.1. Shear failure response for an RC beam under incremental loading (Tran, 2020).

As stated by Olalusi (2018), the absence of stirrups limits and affects the individual influence of the various shear-resisting actions, particularly the aggregate interlock and dowel action. The Multi-Action Shear Model by Cladera and Mari (2015) initially put this into consideration in their formulation of the $MASM$ expression for shear;

$$if \;\; v_s > 0 \rightarrow v_l = {}^{0 \cdot 23 \frac{\alpha_e \cdot \rho_l}{1-x}}\!/_{d} \tag{2.1}$$

$$if \;\; v_s \;=\; 0 \rightarrow v_l = 0 \tag{2.2}$$

The first expression provides a way to estimate the contribution of shear resistance of the dowel action ($\boldsymbol{v_l}$) if the contribution from the stirrup is not equal to zero as in the case of the RC beam with stirrups. In the second expression, the contribution of the stirrup ($\boldsymbol{v_s}$) is zero and this significantly limits the impact of the dowel action.

When studying the behaviour of reinforced concrete beams without shear reinforcement, all other factors are kept constant and the shear span-effective depth ratio is varied. This categorizes the beams into four classes. The behaviour of RC beams without stirrup is such that different responses are derived from different classes according to the size orientation along with the crack formation, stress distribution and mode of shear failure. These classifications with further explanations are based on the categorization by the Joint ACI-ASCE 426 committee (1973).

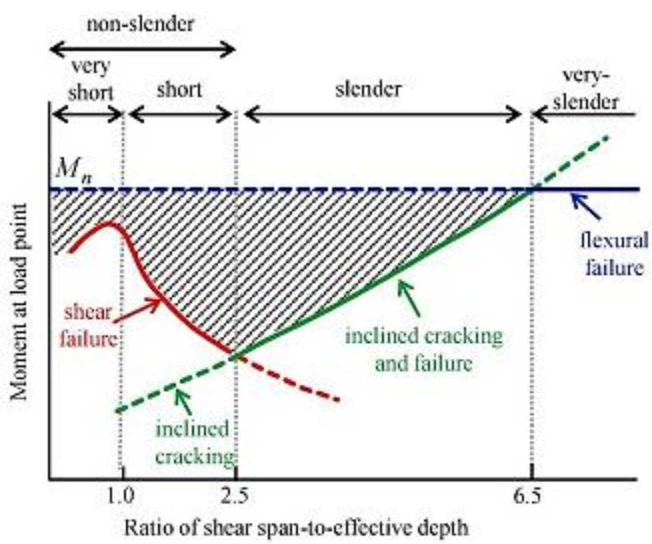

Fig 2.2. Variation in shear capacity with shear span- effective depth ratio (Parsi *et al.*, 2022)

2.2.1 Deep Beams

As seen from Fig 2.2, deep beams also known as very short beams have the ratio of their shear span to effective depth (a/d) < 1. The deep beams develop inclined cracks that join the point of loading with the supports. These cracks disrupt the horizontal shear transfer from the longitudinal reinforcement to the compression zone and this behaviour changes the beam action to arch action. When arch action occurs, the longitudinal tensile reinforcement has the same amount of tension force throughout its span. The anchoring failure at the extremity of the tension tie, also known as shear tension failure, is a typical failure associated with deep beams.

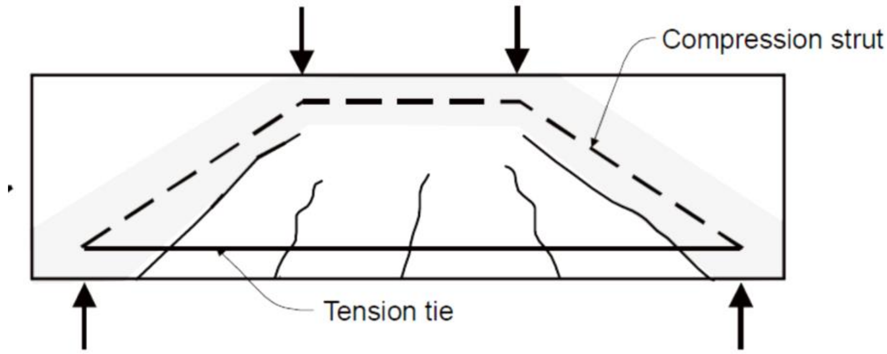

Fig 2.3. Tied-arch structural system (Kuchma *et al.,* 2004)

2.2.2 Short Beams

Short beams have the expression for the ratio of their shear span to effective depth (a/d) as 1<a/d<2.5 i.e., the allowable depth for short beams lies between 1-2.5m. short beams also develop inclined cracks as in the case of deep beams, but after the development of inclined cracks, redistribution of internal forces allows the beam still carry additional loads. As the value of the additional load increases, a final failure occurs whereby the crack crosses over to the top of the compression zone. This mode of failure is known as shear compression failure.

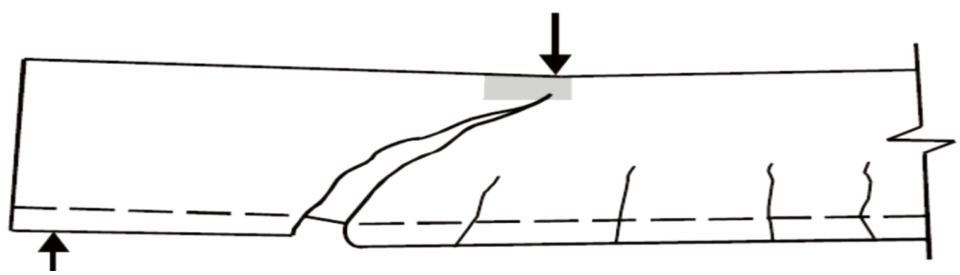

Fig 2.4. Shear compression failure (Kuchma *et al.,* 2004)

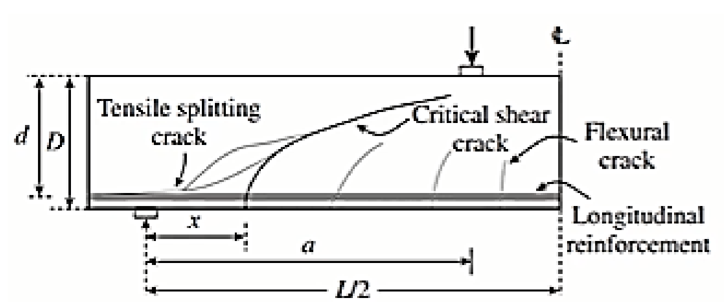

Fig 2.5. Typical crack pattern for short beams without shear reinforcement ACI-ASCE 426 (1973)

In Fig 2.5, the inclined crack propagates in a backward direction and causes a bond failure between the longitudinal steel and the concrete resulting in a splitting action, and the beam then fails by a splitting failure. Short beams may fail due to splitting/bond failure or shear compression failure depending on the direction of crack propagation.

2.2.3 Slender beams

The shear span to effective depth ratio of a slender beam is given as 2.5<a/d<6. Slender beams fail in the plane of the diagonal tension failure, and inclined cracks in slender beams cause sufficient instability to cause the beam to break under the load of the inclined cracking.

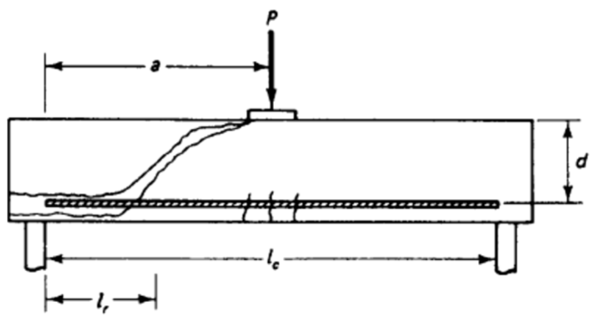

Fig 2.6. Diagonal tension failure (Nawy, 2009).

2.2.4 Very slender beams

Very slender beams often have a shear span to effective depth ratio higher than 6. (a/d > 6m). Fig 2.2 shows that only the very slender beam attains a full flexural capacity, as it fails in flexural moment capacity before failing in the shear before the formation of inclined cracks as there is no formation of inclined cracks.

When an inclined crack appears in an uncracked region of a beam without initially forming vertical flexural cracks, such cracks are said to be web-shear cracks. These types of cracks are dominant in thin webbed beams subjected to high shear and low moments i.e., near the supports where shear force is maximum. Contrarily, for flexural-shear cracks, there is an initial formation of vertical flexural cracks at regions where the moment is maximum, the vertical flexural cracks continue to propagate up to the compression zone in an inclined manner.

2.3 Shear transfer mechanism

The shear transfer in beam types differs from each other considerably due to the use of different constituent materials and governing shear transfer mechanism that contributes to the shear capacity of each beam type and the theories that govern the existence of such beams (Jung and Kim, 2008). For example, following the findings by the joint ASCE-ACI Committee 426 and joint ASCE-ACI Committee

445 for conventional reinforced concrete, the shear is transferred by the stirrups, the longitudinal reinforcement, the aggregate interlock, the uncracked compression zone, dowel effect and residual tensile stresses across the crack (Jung and Kim, 2008).

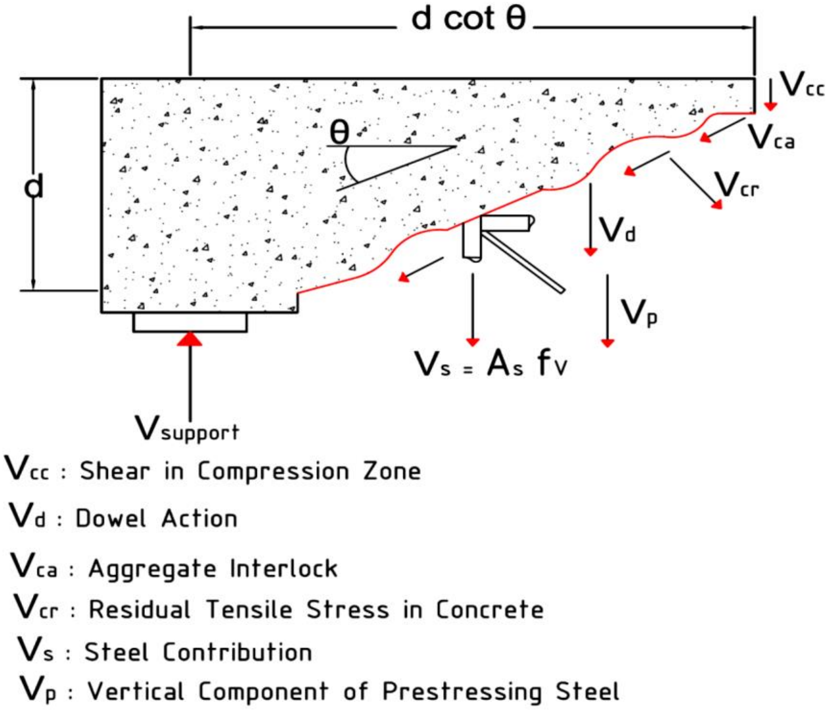

Fig 2.7. Dimensionless shear-resisting actions and forces that contribute to the shear resistance of an RC beam with stirrups (Olalusi, 2018; Kuchma *et al.*, 2004).

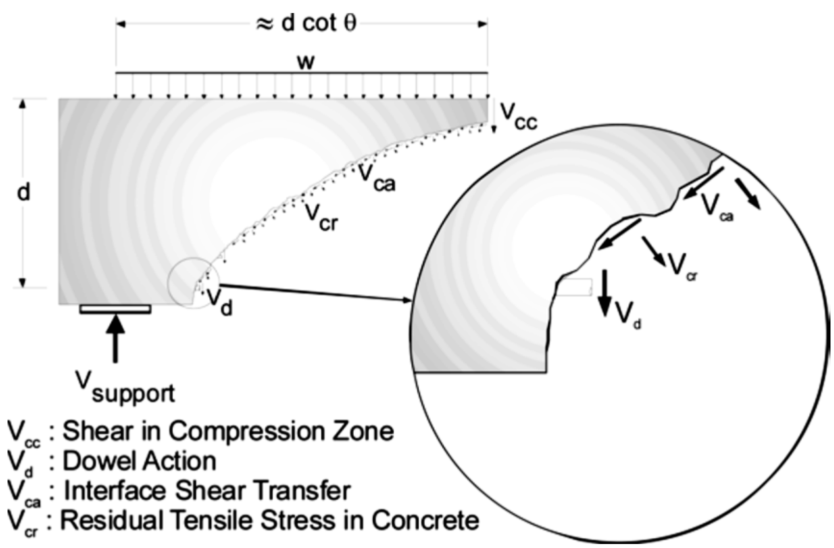

Fig 2.8. Shear-resisting actions for beams without web reinforcement (Song *et al.*, 2010).

The shear transfer mechanisms dominant in beams without shear reinforcement are shear resistance in the uncracked concrete, the dowel action, the aggregate interlock and the residual tensile stress in concrete. According to Campana *et al*. (2013), the activation of these shear transfer actions largely depends on the pattern or shape of the critical shear crack and its failure dynamics. The above-mentioned shear transfer mechanisms are purely beam-shear transfer actions. According to Nakamura *et al.* (2018), there are two classes of shear transfer mechanisms based on the shear-span to effective depth ratio (slenderness) namely arch action and beam-shear transfer action. Jayasinghe *et al.* (2022) cited Sherwood *et al.* (2008) saying the beam action is initially responsible for carrying the total shear in a reinforced concrete beam without stirrups. After the failure of the beam action, a redistribution of shear stresses occurs, allowing the activation of the arch action. When this arch action reaches its capacity, the shear failure of beams without stirrups becomes inevitable.

Fig. 2.9 gives a graphical representation of the slenderness ratio (γ) relevance, a function of the shear span to effective depth ratio ($^a/_d$), in determining the governing shear transfer mechanism in reinforced concrete beams based on a series of experimental observations by Kani (1967).

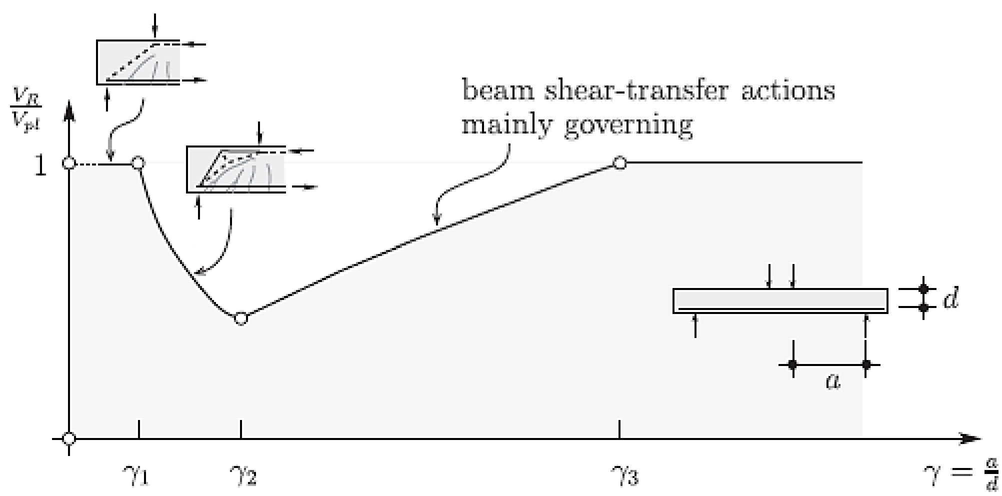

Fig 2.9. Kani’s valley: dominancy of shear actions as a function of slenderness (Ruiz *et al.*, 2015).

The Arching action is associated with plot points in Fig. 2.9 where the slenderness ratio is within the boundary condition ($\gamma < \gamma_1$), this typifies a low shear-span to effective depth ratio as in the case of deep beams and the shear which causes failure (v_R) at this condition compares well with the plastic strength (v_{pl}) of the reinforced concrete beam without stirrups. According to Muttoni and Ruiz (2008), this may be the case for deep beams since flexural cracks do not extend inside the compression zone. The plastic strength (v_{pl}) is responsible for the crushing of concrete and the yielding of the longitudinal reinforcement. In Kani's Valley (1964), regions where $\gamma_1 < \gamma < \gamma_2$, a plastic strength larger than the shear failure is developed in the beam section which gives rise to an overestimation of the plastic strength (Kani, 1964) as a result, cracks may partially propagate into the compression zone. When $\gamma > \gamma_2$, the ratio between the shear responsible for the failure of a section when exceeded and the plastic strength gradually increases and the beam-shear transfer mechanism gains dominance in combination with the arching action (Ruiz *et al*., 2015).

2.3.1 Shear in uncracked compression zone (v_{cc})

The shear capacity contributed by the uncracked compression zone to the total shear strength of a reinforced flexural member is about 20 – 40% (Taylor & Brewer, 1963). The contribution of this shear transfer mechanism is dependent on the depth of the uncracked compression zone (Frosch &Wolf, 2003) and the compressive strength of the member (Jayasinghe et al, 2022). Thus, the participation of this mechanism in the shear transfer in very slender flexural members is limited and negligible but provides a significant contribution to the total shear strength in members with little slenderness ratio as in the case of deep beams. According to Tureyen *et al* & Ribas *et al* (2003, 2014 as cited in Cladera *et al.*, 2015), the shear transferred by the uncracked concrete chord has a linear dependency with the neutral axis depth. Cladera *et al.* (2015) further added that since the neutral axis depth depends on the longitudinal reinforcement ratio and the modular ratio, a high ratio of longitudinal reinforcement would affect the neutral axis depth. This enhances the capacity of the uncracked compression chord in resisting shear.

As the critical shear crack propagates in a quasi-horizontal trend, Ruiz *et al.* (2015) reported that the compression chord's shear capacity contribution is still viable despite the cantilever action in slender members, which transfers force by the inclination of the compression chord, has been disabled. According to the crack kinematics evaluation, it was seen that the compression chord remains functional provided that an inclined compression strut develops. Additionally, the height and placement of the critical shear crack as well as the angle of the compression strut determine how much shear force may be transmitted.

2.3.2 Dowel action (v_d)

The flexural reinforcements in a reinforced concrete member contribute to the shear transference by acting as a dowel between the lips of cracks (Krefeld & Thurston, 1966). Shear displacement which occurs along the cracks in a concrete section may cause slippage, the longitudinal bars provide resistance by averting such slippage (Olalusi, 2018). According to Campana *et al.* (2015), When the critical shear crack propagates through the compression reinforcement and prevents spalling cracks from developing close to the loading plate, the dowel action's influence is significant. Additionally, the use of transverse reinforcement in RC members or the inability of concrete to form spalling fractures, as in the case of short-span beams, makes this mechanism effective. However, in agreement with Jelic *et al.* (1999), Muttoni *et al.* (2008) said that as a/d decreases in the case of slender beams without transverse reinforcement, the influence of the dowelling action becomes significantly negligible. As also stated by Kuchma *et al.* (2004), the spacing of cracks caused by bending, lateral reinforcement arrangement and the concrete cover, all determine how the dowelling action influences shear strength.

2.3.3 Aggregate interlock (v_{ca})

Aggregate interlocking stresses (normal and tangential contact stresses surrounding a crack formation in concrete) happen whenever the cement paste on one side of the crack comes into contact with the aggregate on the other side. According to the study of crack kinematics in the work of Ruiz *et al.* (2015), the shear strength provided by this transfer mechanism is limited by the crack opening (w) and the relative crack slip (δ). The compression field theory generalizes on the premise that the shear contribution from the aggregate interlock is the most significant of all the shear transfer mechanisms (Collins *et al.*, 2006). It should be noted that the failure of this shear transfer mechanism is associated with the development of a delamination crack at the level of flexural reinforcement (Ruiz *et al.*, 2015). A delamination crack is explained as a horizontal splitting, cracking or separation near the upper surface of a rectangle cross-section specimen, it is known as a mode of failure where a material fractures into layers as in the case of the failure mode of 3D printed cementitious concrete.

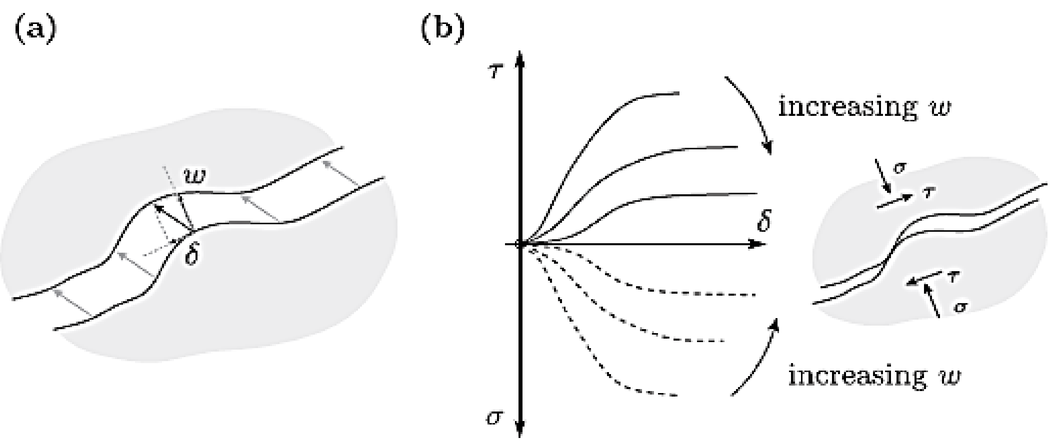

Fig 2.10. Aggregate interlock: (a) kinematics of a shear crack with relative components of opening (w) and slip (δ); and (b) contact stresses (Ruiz *et al.*, 2015).

2.3.4 Residual tensile stress in concrete (v_{Cr})

The capacity of concrete to transfer tensile stresses remains significant even after cracking has occurred provided that the crack width is within the permissible range. Stresses develop near the tip of the crack (the fracture process zone) and soften upon incremental opening of crack width (Hillerborg, 1983). Ruiz *et al.* (2015) established that the capacity of the shear transfer accounted for by this mechanism depends on the aggregate size of the concrete.

Tensile stresses can continue to be transmitted in fractured concrete up until crack widths of 0.05-0.15 mm (ACI-ASCE Committee 445, 2009), while Hordjick (1992) made it clear that a flexural member with a crack opening wider than 0.2 mm cannot continue to transfer tensile loads.

2.3.5 Shear reinforcement contribution (v_s)

The shear reinforcement can be placed either perpendicular to the flexural bars, in an inclined manner or laterally as demonstrated in experiments carried out by Hunegnaw and Aure (2021) and Sayyad *et al.* (2013). The presence of stirrups does not significantly alter or modify the shear transfer mechanism in RC beams, rather, it contributes to the strength of the shear transfer actions collectively and individually by carrying part of the shear, improving the capacity of the dowel action by effectively supporting the flexural bars that are being crossed by flexural cracks, limiting the opening or width of diagonal cracks within the elastic range, as the shear reinforcement cannot stop the formation of cracks. Hence, the inclusion of web reinforcement proves to be important to the behaviour of the shear action by the interface shear transfer (aggregate interlock). Stirrups provide confinement to the concrete when closely spaced. As a result, the compressive strength of concrete is increased and this helps in regions affected by the arching action. The web reinforcements also prevent bond failure when splitting cracks develop in the anchorage zones due to the dowel and anchorage forces.

The overall objective of the stirrup is to guarantee that complete flexural capacity may be reached since inclined cracking decreases the shear strength of beams below flexural capacity. Fig 2.11 is a graph of the positive linear relationship between the internal resisting shear and the applied shear, it shows that whatever the applied shear is, there should be a corresponding or equal magnitude of internal resisting shear through the section of a beam with web reinforcement. The different points on the x-axis of the graph represent the progressive response of a reinforced concrete section to applied shear force which determines the distribution of the dominating shear transfer action. Before the formation of the inclined cracks, the contribution of shear capacity by the stirrups is zero i.e., there is no action by stirrups. All of the applied shear at this point is resisted by the contribution from the concrete only. The flexural crack occurs before the formation of the inclined crack, the concrete also dominates the resistance mechanism at this point. Between the flexural cracks and the inclined crack, the shear resistance provided by the concrete can be resolved into three (3), the shear resisted by the uncracked compression zone (v_C), shear resisted by the dowelling action (v_d), and the contribution from the interface shear transfer/aggregate interlock (v_{az}). As the applied shear gradually increases beyond the inclined crack, the stirrups would provide shear resistance.

A further increase of the applied shear would cause the stirrups to yield and as a result, the resistance capacity of the stirrups remains constant for higher values of applied shear. To resist the increasing applied shear forces at this point, the value of v_C and v_d increases rapidly, while v_{az} decreases due to the presence of wider cracks caused by the yielding of the stirrups. As v_C and v_d increases along with the applied shear, failure occurs due to dowel splitting, loss of interface shear transfer or the failure of the compression zone due to the combined action of shear and compression. At this point, it is safe to say the ultimate failure has been attained.

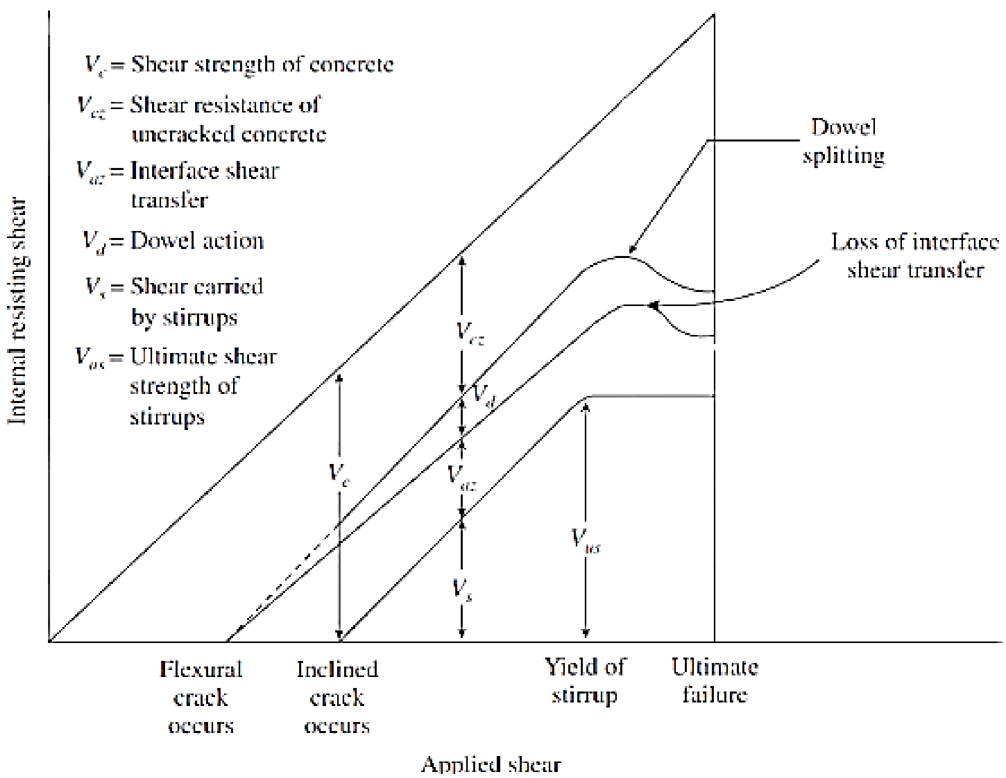

Fig 2.11 Distribution of internal shear in beam with web reinforcement (Subramanian, 2014).

2.3.6 Arch action

Deep beams with short spans exhibit behaviour synonymous with that of an arch. In conventional beams, applied loads are carried through flexural bending and shear, and deep beam responds to loadings as trusses would via arch action. In such beams, the applied load is close to the support and a larger portion of the load is directly transferred to the support in compression. This mechanism facilitates the formation of a compression strut between the applied load and the support. By keeping a constant lever arm (z) between the compression and tension chords, beam-transfer actions permit the carrying of shear in a member. As a result, the tension reinforcement's force varies depending on how significant the beam's bending moments become. However, arching action gives room for shear to be carried by assuming a constant force in the longitudinal reinforcement. Anchorage failure may be the controlling failure mechanism in deep beams, instead of shear failure. Arch action is not a shear transfer mechanism, but for beams where arch action gains dominancy over beam actions, such beams usually have a higher shear resistance than similar beams which are slenderer. Kim and Park (1996) state that induced loads is transmitted directly to the supports in relatively short beams by the arch action. The span-to-height ratio of the corresponding arch and the strength of the compression strut are the major variables affecting this shear action. The shear span-to-depth ratio and the span-to-height ratio of the corresponding arch are almost equivalent, while the compressive strength of concrete and the area of tension reinforcement strongly impact the strength of the compression strut.

2.4 Parameters contributing to shear strength

2.4.1 Longitudinal reinforcement ratio

By using a low ratio of flexural reinforcement, as opposed to when using a significant percentage of longitudinal reinforcement, flexural cracks rapidly propagate over the neutral axis into the surrounding region of the compression zone. Insufficient steel ratio in steel-reinforced concrete causes an increase in crack width. Consequently, this results in a decrease in the capacity of shear transferred by the dowel effect and the aggregate interlock as in the case of slightly reinforced beams. According to Collins and Kuchma (1999), quoted by Olalusi (2018), beams with longitudinal reinforcement spread along the depth of the beam exhibit closely spaced, thinner cracks with high shear strengths.

According to Angelakos *et al.* (1999; 2001 as cited in Jayasinghe *et al.*, 2022), changing the percentage composition of the longitudinal reinforcement ratio from 0.5% to 2.09% caused a 62% rise in the observed shear strength of large concrete beams. This shows that the greater the steel ratio, the greater the strength of contributing shear actions. The absence of transverse reinforcement causes a vertical movement of the flexural longitudinal bars. Hence, the longitudinal bars are rendered incapable of transferring shear due to the lack of constraint from stirrups (Cladera *et al.*, 2015).

Slowik (2018) conducted experimental studies that demonstrated how the quantity of longitudinal reinforcement affects its effectiveness. Additionally, the longitudinal reinforcement ratio can affect the failure mode in flexural beams without stirrups.

2.4.2 Concrete strength

The strength of concrete is generally known to be its ability to resist forces. In more precise knowledge relating to structural engineering, concrete strength is defined as the unit force required to cause a rupture in a concrete member. Concrete strength can either be compressive or tensile. According to Angelakos *et al*. (2001), the effect of the tensile strength of concrete on the shear strength is more critical than that of the compressive strength. This may be because concrete as a brittle material is weak in tension and strong in compression, so more concern should be given to the tensile capacity of concrete. Shetty (2005) confirmed this as well saying that the tensile strength of concrete for a grade M25 concrete and above is about 8-11% of the corresponding compressive strength. With increased concrete strength, the shear capacity of the uncracked compression chord and dowel action increases as well (Olalusi, 2018). Due to the fracture of aggregates, increasing the compressive strength of concrete in beams void of shear reinforcement does not significantly enhance the resistance of such beams against shear (Cladera *et al.*, 2004).

Since the flexural cracking that initiates the inclined cracking disturbs the elastic-stress field to the point at which inclined cracking occurs at a principal tensile stress of approximately half of the tensile strength of the uncracked section, the inclined cracking load in a flexural member tends to depend on the tensile strength of the concrete.

2.4.3 Size effect

According to Muttoni & Ruiz (2008) and Lee *et al.* (2017), the shear strengths of reinforced concrete members without transverse reinforcement tend to decrease as the effective member depth (d) increases depicting an inverse relationship between both entities, this phenomenon is known as the size effect. Fernandez Ruiz *et al.* (2015) further explained the size effect as the decrease in the unitary (normalized) shear strength for beam samples with the same geometrical and mechanical properties but with increasing member sizes (d). As reported by Tran (2020), the size effect expresses the material strength concerning the structural size and is therefore associated with material failure.

The negative linear relationship as shown in Fig. 2.12 at increasing values of Log d demonstrates the size-effect law stated by Bazant *et al.* (1984), the rule specifies that a size-effect law should regulate the decline in concrete shear strength, making the transition from a yield criteria for small member sizes (without a size effect) to the behaviour anticipated by linear elastic fracture mechanics (LEFM) for large sizes (strength reduction controlled by d^(-0·5)).

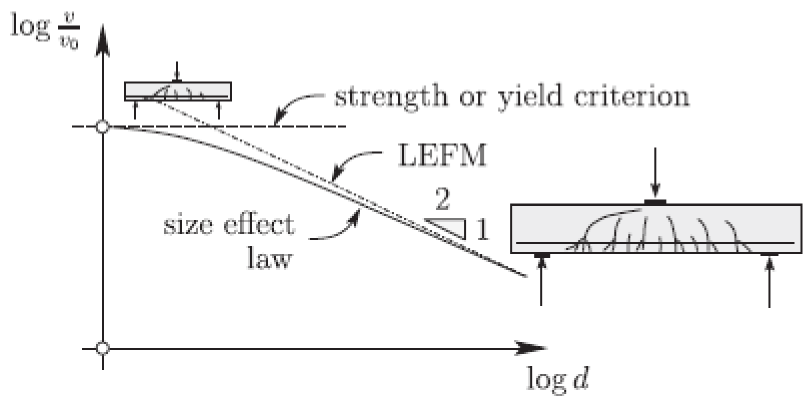

Fig 2.12 Using a double-logarithmic scale to demonstrate size effect (Fernandez Ruiz *et al.*, 2015)

The conflict on how best to model the size effect remains. Although, there is a generalized knowledge that the main reason for this is the phenomenon of concrete cracking and structural energy release (Hunegnaw and Aure, 2021). The product of the strain in the reinforcement passing through the crack and the crack spacing determines the width of an inclined crack. The crack widths and spacings tend to widen as the depth of the beam increases. This in turn largely affects the capacity of shear contributed by the residual tensile strength of concrete and the interface shear transfer as they vary proportionally to the width of the crack. Therefore, for a deep beam with a large crack width, the aggregate interlock and residual tensile stress become limited. Slowik (2014) reported that the size effect should not only be associated with the member depth but should be considered for all the geometrical properties namely the effective length, depth and width.

2.4.4 Shear span – effective depth ratio

The shear span-to-depth ratio (a/d) can be explained as the ratio between the shear force and flexural moment in the critical section (Yerzhanov *et al.*, 2019). This is true when bending moment (M) and shear force (v_f) occurs simultaneously in the same cross-section given as M / (v_f). But for a three -four-point bend test, the shear span to depth ratio is taken as (a/d) where the shear span (a) is the distance from the point of force applied to the support, and (d) is the member size as in depth. In a bit to show that the effective length-to-depth ratio (l_{eff}/d) of flexural concrete members without web reinforcement affects the shear strength, an experimental study by Slowik (2014) was conducted and it was concluded that the shear span-depth ratio (a/d) is the fundamental parameter that substantially affects the shear strength in concrete members reinforced longitudinally and without shear reinforcement, it was also seen that the failure process in the investigated members was influenced by shear span-to-depth ratio along with the effective length-to-depth ratio.

Sneed and Ramirez (2010) discovered that in addition to size effects, changes in the behaviour of RC beams and the method of shear transfer at failure also determine the reduction in shear with increasing effective depth in beams (beam action versus arch action).

2.4.5 Axial force

Olalusi (2018) cited Kuchma *et al.* (2004) saying when a reinforced concrete beam is subjected to axial tension, it experiences a decrease in its shear strength. Contrarily, axial compression increases shear strength. He continued by saying that the start of a critical failure in the section is accelerated by the axial tensile forces which also tend to increase the inclination of the crack angle.

Other factors which affect the shear strength of concrete include the grade of concrete and the size of the coarse aggregate used in the mix.

2.5 Review of current national codes of design

2.5.1 European code (EC2)

Clause 6.2.2 of the European standard, Eurocode 2: Design of concrete structures – Part 1-1: General rules and rules for buildings (EN 1992-1-1 (2004)), gives the expression for estimating the design shear resistance of beam without shear reinforcement. The expression is as written in Equation (2.3);

$$V_{Rd,c} = \left[C_{Rd,c}k(100\rho l f_{ck})^{1/3} + k_1\sigma_{cp}\right]b_{\mathrm{w}}d \geq V_{Rd,c,min} \tag{2.3}$$

The code also makes provisions for the minimum amount of shear contributed by the concrete which can be termed as $\boldsymbol{V_{Rd,c,min}}$ and determined by;

$$V_{Rd,c,min} = (V_{min} + k_1\sigma_{cp})b_{\mathrm{w}}d \tag{2.4}$$

Where $V_{min} = 0.035^{3/2} f_{ck}^{1/2}$ (2.5)

Hence,

$$V_{Rd,c,min} = (0.035^{3/2} f_{ck}^{1/2} + k_1\sigma_{cp})b_{\mathrm{w}}d \tag{2.6}$$

Where:

b_{w}= beam width

ρl = longitudinal reinforcement ratio = $\frac{A_{sl}}{b_{\mathrm{w}}d} < 0.02\ or\ 2\%$

A_{sl} = Area of tensile reinforcement

d = effective beam depth

f_{ck}= Concrete characteristic compressive cylinder strength at 28 days (Mpa)

$C_{Rd,c}= \frac{0.18}{\gamma_c}$

σ_{cp}= Axial load or prestressing-induced compression stress in the concrete

$$= \frac{N_{Ed}}{A_c} < 0.2 f_{cd} (MPa) \tag{2.7}$$

N_{Ed} = Axial force from loading or prestressing in the cross-section [in N]

A_c = Area of the concrete section

K= size effect factor = $1 + \sqrt{\frac{200}{d}}$

Clause 6.2.1 of the EN 1992-1-1 (2004) clearly states that the total shear resistance of a reinforced concrete member is the sum of the contribution from the shear reinforcement ($V_{Rd,s}$), concrete ($V_{Rd,c}$) and the shear component of the force in the compression area, if there is an inclined compression chord (V_{ccd}) and it is represented by the expression below;

$$V_{Rd} = V_{Rd,s} + V_{Rd,c} + V_{ccd} \tag{2.8}$$

2.5.1.1 Shear Resistance by Shear Reinforcement ($V_{Rd,s}$)

The shear design for the web reinforcement is based on a truss model and a lower-bound plasticity theory. The model permits the concrete compressive strut angle (θ) to be kept within the range of $21.8° \leq \theta \leq 45°$. This concept is introduced to control the propagation of cracks since an incremental shear force on the beam widens the strut angle (θ) which eventually reduces the shear strength of the member. Olalusi (2018) asserts that the EC2 variable strut inclination method shear design's limited strut angle is a kind of bias applied to the concrete compressive strut angle to increase conservatism in the model. The maximum boundary of 45˚ serves to prevent excessively conservative estimations, while the lower limit of 21.8˚ is imposed to produce a more conservative approximation of shear predictions. The diagram below gives a pictorial representation of the reinforced concrete beam in shear using the truss model mechanism.

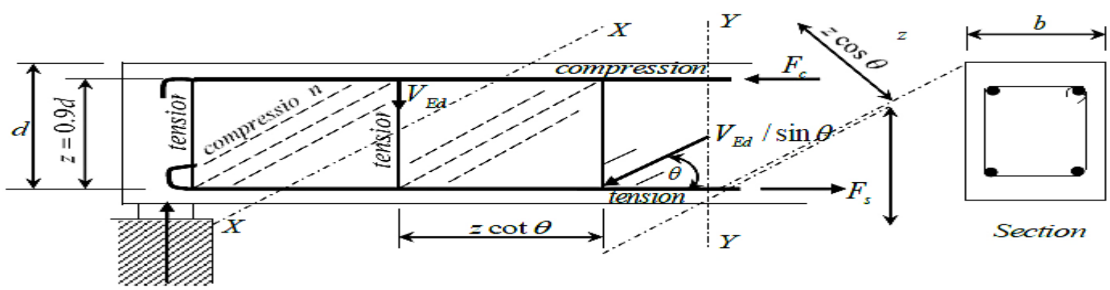

Fig 2.13 Truss model (Mosley *et al*., 2007)

The equation for the design value of the shear force that the resisting reinforcement can withstand ($V_{Rd,s}$) is as follows;

$$V_{Rd,s} = \frac{A_{sw}}{S} Z f_{\text{ywd}} cot\theta \tag{2.9}$$

Where A_{sw} = cross-sectional area of the shear reinforcement

S = spacing of the stirrups

f_{ywd} = design yield strength of the shear reinforcement

Z = the inner lever arm. The approximate value z = 0.9d may often be adopted in the shear calculation of reinforced concrete in the absence of axial force.

θ = angle between the concrete compression strut and the beam axis perpendicular to the shear force.

An upper limit of shear resistance is provided by the code of design to avoid premature web-crushing failure. According to EN 1992-1-1 (2004), $V_{Rd,max}$ is calculated as

$$V_{Rd,max} = \frac{\alpha_{cw} b_w Z v_1 f_{cd}}{cot\theta + tan\theta} \tag{2.10}$$

Where;

α_{cw} is the coefficient accounting for stress in the compression chord, value = 1 for non-prestressed structures.

f_{cd} is the design value of concrete compressive strength

v_1 is the strength reduction factor with a value

$$v_1 = 0.6\left[1 - \frac{f_{ck}}{250}\right] \tag{2.11}$$

θ, the concrete strut angle is given by;

$$\theta = sin^{-1}\sqrt{\frac{A_{sw}(\frac{f_{ywk}}{\gamma_s})}{\alpha_{cw} b_w s v_1 (\frac{f_{ck}}{\gamma_c})}} \tag{2.12}$$

f_{ck} = concrete characteristic strength

γ_c = proposed value of 1.5 for the concrete partial material factor

f_{ywk} is the characteristic strength of the web reinforcement

γ_s is the partial material factor for steel with a recommended value of 1.15

2.5.2 Australian code (AS 3600 – 2018)

The Australian standard for concrete structures was first published in March 1988 as AS 3600-1988. Since then, it has been subjected to four revisions; AS 3600-1994, AS 3600-2001, AS 3600-2009 and the recent revision, AS 3600-2018. According to Chowdury and Loo (2018), there have been substantial updates/changes to the most current edition (2018), which now incorporates an improved approach to capacity estimation. According to Chowdury and Loo (2018), the modifications which were introduced in the recent publication resulted in a more arduous procedure and additional computational efforts would be required for practitioners. Jayasinghe et al (2022) stated that the AS 3600-2018 together with some other concrete design codes such as the Canadian Concrete Code, Fib Model Code and the AASTHO-LFRD based their provisions for designing RC beams without shear reinforcement on the simplified modified compression field theory.

In the estimation of the concrete contribution to the shear strength, the k_v factor and the concrete compressive strength are the dependent factors. The factor k_v is a parameter that has been adopted from the SMCFT. Due to the difficulties of determining this variable, it has been concluded that AS 3600-2018's computational efforts and intricacy requirements are often difficult for the designing of reinforced and prestressed concrete for shear. (Chowdury and Loo, 2018).

Clause 8.2.3.1 of the AS 3600-2018 states that the design shear resistance of a reinforced concrete section can be considered as the sum of the 3 explicit contributions as shown in Equation (2.13);

$$V_u = V_{uc} + V_{us} + P_v \tag{2.13}$$

Where V_{uc} is the design shear resistance from the concrete

V_{us} is the design shear resistance from the shear reinforcement

P_v is the vertical component of prestress crossing the section under consideration.

For the design of beams with no shear reinforcement, the other two terms (V_{us}, P_v) can be neglected since there is no shear contribution from either of the terms. Clause 8.2.4.1 gives the expression for determining the concrete contribution to the shear strength, and it can be calculated by

$$V_{uc} = k_v b_v d_v \sqrt{f_c'} \tag{2.14}$$

Where:

f_c' = Characteristic compressive (cylinder) strength of concrete at 28 days (f_c'<8Mpa (1160 psi)). b_v = Width of the section

d_v = Effective shear depth of the member

According to AS 3600-2018, the value of k_v shall be determined as follows

a. For $A_{sv}/s < A_{sv,min}/s$;

$$k_v = \left(\frac{0.4}{1+1500\varepsilon_x}\right)\left(\frac{1300}{1000+k_{dg}d_v}\right) \tag{2.15}$$

Where:

1. If $f_c' \leq$ 65Mpa (9427Psi) and not lightweight concrete

   $$k_{dg} = \left[\frac{32}{(16+d_g)}\right] \nless 0.8 \tag{2.16}$$

   d_g is the maximum nominal aggregate size

   k_{dg} can be taken as 1.0 provided that the d_g is not less than 16mm

2. If $f_c' > 65$Mpa or lightweight concrete

   k_{dg}= 2.0

b. For $A_{sv}/s \geq A_{sv,min}/s$;

$$k_v = \left[\frac{0.4}{1+1500\varepsilon_x}\right] \tag{2.17}$$

Determination of the longitudinal strain in concrete

$$\varepsilon_x = \frac{\left|\frac{M^*}{d_v}\right| + |V^*| - P_v + 0.5N^* - A_{pt}f_{po}}{2(E_sA_{st} + E_pA_{pt})} \leq 3.0 * 10^{-3} \tag{2.18}$$

The web shearing capacity $V_{u,max}$ is given by

$$V_{u,max} = 0.55\left[f_c' b_{\mathrm{w}} d_v \left(\frac{cot\theta_v}{1+cot^2\theta_v}\right)\right] \tag{2.19}$$

θ_v, the angle of inclination of the concrete compression strut to the longitudinal axis of the member shall be calculated as follows;

$$\theta_v = (29 + 7000\varepsilon_x) \tag{2.20}$$

2.5.3 American code (ACI 318-19)

The one-way shear design equations for non-prestressed concrete were changed in the ACI 318-19 Code. According to the American Building Code Requirements for Structural Concrete (ACI 318-19), this was done to include the size effect factor (λ_s) developed by professor Bazant and the ACI committee 446. The influence of the longitudinal reinforcement ratio and axial load, if there be any axial force acting alongside the shearing force and the resulting moment on a member, were also included. The previous shear equations had some safety concerns for members with a minimum amount of longitudinal reinforcement and large depth. For non-prestressed concrete (reinforced concrete), V_c shall be calculated following the table below.

Table 2.2 Selection of shear expression based on shear reinforcement requirement (ACI 318-19)

Criteria		V_c	
$\boldsymbol{A_v \geq A_{v,min}}$	Either of:	$\left[2\lambda\sqrt{f_c'} + \frac{N_u}{6A_g}\right] b_{\mathrm{w}} d$	(a)
		$\left[8\lambda(\rho)^{1/3}\sqrt{f_c'} + \frac{N_u}{6A_g}\right] b_{\mathrm{w}} d$	(b)
$\boldsymbol{A_v < A_{v,min}}$		$\left[8\lambda_s\lambda(\rho)^{1/3}\sqrt{f_c'} + \frac{N_u}{6A_g}\right] b_{\mathrm{w}} d$	(c)

Where λ_s is the size effect modification factor, it can be determined by;

$\lambda_s = \sqrt{\frac{2}{1+\frac{d}{10}}} \leq 1$

(2.21)

λ, 1.0 is used as the modification factor for normal-weight concrete for lightweight concrete.

fc, is the concrete compressive cylinder strength

ρl is the flexural reinforcement ratio

A_g is the gross area of the concrete section

bw is the beam width

d is the effective depth of the beam

N_u is the axial load acting at the critical zone of the concrete section

Note that when calculating $\boldsymbol{V_c}$, according to ACI 318-19, an axial tension force can cause $\boldsymbol{V_c}$ to have a negative value. In those cases, $\boldsymbol{V_c}$ should be taken as zero.

Limit Values

$V_c \ngtr 5\lambda b_{\mathrm{w}} d$ (2.22)

$\frac{N_u}{6A_g} \ngtr 0.05 f_c'$

(2.23)

If shear reinforcement is required, $A_{v,min}$ (minimum amount of shear reinforcement) shall be taken as the greater of;

(a) $0.75\sqrt{f_c'}\frac{b_{\mathrm{w}} s}{f_{yt}}$ (2.24)

(b) $50\frac{b_w s}{f_{yt}}$

(2.25)

The above expression can be neglected for beams that are unreinforced in their web.

Table 2.2 Cases where $A_{V,min}$ is not required if $V_u \leq \Phi V_c$

Beam Type	**Condition ≤ ≥**
Shallow beam	h ≤ 10 in.
Integral with slab	h ≤ greater of $2.5t_f$ or $0.5b_w$ and h ≤ 24 in
Constructed with steel fibre-reinforced normal-weight concrete conforming to specific requirements and with $\boldsymbol{f'_c}$ ≤ 6000 psi	h ≤ 24 in. and $V_u \leq \emptyset 2\sqrt{f'_c} b_w d$
One-way joint system	Conforming to specific requirements

2.5.4 The South African national standard (SANS 10100-1. (2000))

The South African concrete specification (SANS 10100-1(2000)) incorporates the previous British standard for the design of reinforced concrete buildings (BS8110). The design code employs the 45° truss model methodology as the design philosophy for shear reinforcement and also takes into account the impact of the concrete in resisting shear by including a concrete contribution term calculated empirically. As a result, the nominal shear strength (V_n) is calculated by adding the concrete contribution (V_c) and the shear reinforcement (V_s), as follows:

$$V_n = V_s + V_c \tag{2.26}$$

The shear reinforcement contribution is given as

$$V_s = \frac{A_v f_v d}{\gamma_{m,s} b_w s} \tag{2.27}$$

Where f_v is the yield strength of shear reinforcement

A_v is the area of shear reinforcement

$\gamma_{m,s}$ is the partial material safety factor for steel = 1.15

The concrete contribution is given as

$$V_c = \frac{0.75}{\gamma_{m,c}}(\frac{f_{cu}}{25})^{\frac{1}{3}}(\frac{100A_s}{b_{\mathrm{w}}d})^{\frac{1}{3}}(\frac{400}{d})^{\frac{1}{4}} \tag{2.28}$$

Where $\frac{100A_s}{b_{\mathrm{w}}d}$ = reinforcement ratio

fcu is the characteristic concrete cube strength

$\gamma_{m,c}$ is the partial material safety factor for concrete = 1.4

Hence the nominal shear capacity according to SANS10100(200) is given by;

$$V_n = \frac{A_v f_v d}{\gamma_{m,s} b_{\mathrm{w}} s} + \frac{0.75}{\gamma_{m,c}}(\frac{f_{cu}}{25})^{\frac{1}{3}}(\frac{100A_s}{b_{\mathrm{w}}d})^{\frac{1}{3}}(\frac{400}{d})^{\frac{1}{4}} \tag{2.29}$$

The contribution of the shear reinforcement can be neglected in cases where stirrups are not required, as in the case of beams without shear reinforcement considered in this study.

2.5.5 *Fib* Model Code 2010 (LOA II)

The fib Model Code 2010 procedures were developed from physical-mechanical models that are based on behavioural observation of test subjects at a mesoscale level, they represent a significant advancement over previous standardized empirical methods (Sigrist *et al.*, 2013). The shear resistance expression provided by the fib model code 2010 is categorized into four approximation levels (LoA I-IV) which determine the complexity, computation time and effort, level of detail needed (i.e., preliminary design, detailed design or assessment of existing structures), the importance of structural element and level of accuracy associated each procedure. LoA II would be considered in this study as LoA III is associated with the shear estimation of beams with shear reinforcement, while LoA IV looks more into numerical modelling and finite element analysis. The code offers practitioners the freedom to alter the design procedures for members with and without shear reinforcement as it explicitly states that the components of the design shear resistance include the resistance attributed to the concrete and the shear strength provided by the shear reinforcement.

According to Sigrist *et al.* (2013), the *fib* Model Code 2010 shear provisions for members without shear reinforcement are based on Simplified Modified Compression Field Theory (SMCFT). While for members with shear reinforcement, the design principle is based on a general stress field approach combined with SMCFT. The shear resistance provided by the fib model code is as given below;

$$V_{Rd} = V_{Rd,s} + V_{Rd,c} \geq V_{Ed} \tag{2.30}$$

where $V_{Rd,c}$ is the resistance attributed to the concrete given as;

$$V_{Rd,c} = 0.9k_v\sqrt{\frac{f_{ck}}{\gamma_c}}b_w d \tag{2.31}$$

$V_{Rd,s}$ is the resistance attributed to the shear reinforcement given as;

$$V_{Rd,s} = 0.9\frac{A_{sw}}{s_w}{f_{ywk}}/{\gamma_s}\,d(cot\theta + cot\alpha)sin\alpha \tag{2.32}$$

Hence,

$$V_{Rd} = 0.9\frac{A_{sw}}{s_w}{f_{ywk}}/{\gamma_s}\,d(cot\theta + cot\alpha)sin\alpha + 0.9k_v\sqrt{\frac{f_{ck}}{\gamma_c}}b_w d \geq V_{Ed} \tag{2.33}$$

V_{Ed} is the design shear force at the control section

where f_{ck} is the characteristic value of concrete compressive strength

To determine the shear resistance attributed to concrete, k_v, a factor dependent on the longitudinal strain of concrete is calculated as shown below

$$k_v = \frac{0.4}{(1+1500\varepsilon_x)}(1 - {V_{Ed}}/{V_{Rd,max}(\theta_{min})} \geq 0 \tag{2.34}$$

ε_x = the longitudinal strain of concrete = $\frac{{M_{Ed}}/{z} + V_{Ed}}{2E_sA_s} < 3 * 10^{-3}$ (2.35)

where A_s comprises the main longitudinal reinforcing bars in the tension chord.

$$\theta = 20° + 7000\varepsilon_x \tag{2.36}$$

$$\theta_{min} = 20° + 10000\varepsilon_x \tag{2.36b}$$

$$\theta_{min} \leq \theta \leq 45° \tag{2.37}$$

Fib Model Code 2010 (LoA III) Web crushing strength capacity ($V_{Rd,max}$)

The shear strength is limited by the crushing of the concrete $V_{Rd,max}$ calculated as shown below

$$V_{Rd,max} = 0.9k_c{f_{ck}}/{\gamma_c}\,b_w d\frac{cot\theta + cot\alpha}{1+cot^2\theta} \tag{2.38}$$

Where k_c Evaluates the effects of cracked concrete in the calculation of the decline in concrete strength = $K_\varepsilon\eta_{fc}$

K_ε = factor for the strain effect given as;

$$K_\varepsilon = \frac{1}{1.2+55\varepsilon_1} \leq 0.65 \tag{2.39}$$

ε_1 =the principal strain defined by Mohr’s circle of strain given as;

$$\varepsilon_1 = \varepsilon_x + (\varepsilon_x + 0.002)cot^2\theta \tag{2.40}$$

α is the angle of the stirrups

η_{fc}= the brittleness factor concrete given as;

$$\eta_{fc} = (\frac{30}{f_{ck}})^{\frac{1}{3}} \leq 1 \tag{2.41}$$

2.6 Literature–based shear models

2.6.1 Multi-action shear model (MASM)

The Multi-Action Shear Model ($MASM$) proposed by Cladera *et al*. (2015) is an extension of a flexural shear model based on the principle of mechanics originally developed to evaluate the resisting capacity of concrete flexural members reinforced with fibre polymers longitudinally and/or transversally. According to Cladera *et al.* (2015), the model can be applied to both prestressed and reinforced concrete with or without shear reinforcement. Also, the cross-section of the beams could either be T-shaped or rectangular. Cladera *et al.* (2019) stated that the main assumption of the multi-action shear model is that as the second branch of the critical shear begins to form, the load does not considerably increase as the flexural compression zone's concrete softening occurs. This was also seen in the works of Zararis and Papadakis (2001), Carmona *et al.* (2007) and Yu *et al*. (2016).

By subjecting slender beams to shear and bending, a critical shear crack which can be divided into two parts occurs; first, the flexural cracks occur at the tension zone and propagates in a quasi-vertical manner through the web to the neighbourhood of the flexural neutral axis. Under incremental loading, a second branch of the critical shear crack, the inclined crack, develops inside the compression chord in a quasi-horizontal manner, which eventually connects the flexural crack and the point of load application, producing failure (Zararis and Papadakis, 2001; Muttoni *et al.* 2008 as cited in Cladera *et al.* 2015). Cladera *et al*. (2015) further added that the critical shear crack experiences more damage as the load increases.

Fig 2.14 Critical crack evolution under incremental shear loading (Mari et al, 2016)

As the name implies, the shear model considers the shear strength as the sum of the various shear transfer actions namely shear contribution from the uncracked compression chord, residual tensile stress, shear contribution by the stirrups and, the shear by the dowelling actions of the longitudinal reinforcements. The dimensionless expression according to Cladera *et al.* (2015) is given below;

$$V = (v_c + v_w + v_l)\, f_{ctm}.b.d + v_s \;\leq\; V_{max} \tag{2.42}$$

where v_c, v_w v_l and v_s are the non-dimensional representation of the concrete shearing transfer actions of the uncracked compression chord, shear transferred along web cracks, dowelling action of the longitudinal reinforcement and the web reinforcement while V_{max} is the shear force that causes failure(crushing) in concrete struts. The explicit Dimensionless equations of these actions are given below;

Uncracked compression chord

$$v_c = \zeta\left[\left(0.88 + \left(0.20 + 0.50\frac{b}{b_{\mathrm{w}}}\right)v_s\right)\frac{x}{d} + 0.02\right]\frac{b_{v,eff}}{b}K_p \tag{2.43}$$

Shear transferred along web cracks

$$v_w = 167\frac{f_{ctm}}{E_{cm}}\frac{b_{\mathrm{w}}}{b}\left(1 + \frac{2G_F E_{cm}}{f_{ctm}^2 d_0}\right) \tag{2.44}$$

Longitudinal reinforcement

$$v_l = \frac{0\cdot 23\frac{\alpha_e \cdot \rho_l}{1-x}}{d},\; if \;\; v_s > 0 \tag{2.45}$$

$$v_l = 0, \qquad\qquad if \;\; v_s \;=\; 0$$

Shear reinforcement

$$v_s = (d_s - x)cot\theta\,\frac{A_{\mathrm{sw}}\cdot f_{\mathrm{yw}}}{s.f_{ctm}.b.d} \approx \frac{0.85 d_s A_{\mathrm{sw}}\cdot f_{\mathrm{yw}}}{s.f_{ctm}.b.d} \tag{2.46}$$

Maximum strut strength equation

$$V_{u,max} = \propto_{cw} b_{\mathrm{w}} z v_1 f_{cm}\frac{cot\,\theta}{1+cot^2\theta} \tag{2.47}$$

The neutral axis $\boldsymbol{x}$ is considered to be equivalent to the height of the uncracked compression zone and it is given as;

$$\frac{x_0}{d} = \alpha_e\rho_l\left(-1 + \sqrt{1 + \frac{2}{\alpha_e\rho_l}}\right) \approx 0.75((\alpha_e\rho_l)^{1/3} \tag{2.48}$$

$\frac{x_0}{d}$ is a parameter used to control the depth or the different zone of the critical crack. The above expression is valid for reinforced concrete members where $\alpha_e = \frac{E_s}{E_c}$ is the modulus of elasticity ratio between steel and concrete.

For RC members $x = x_o$, while for a prestressed member, x would be computed from x_o with the expression below

$$x = \; x_0 + (\frac{h}{d} - x_0)(\frac{d}{h})\frac{\sigma_{cp}}{\sigma_{cp}+f_{ctm}} \tag{2.49}$$

Where, σ_{cp}, the mean normal stress of concrete caused by prestressing or axial loads =*P/Ac* (*P* is the prestressing force and *Ac* is the concrete cross-sectional area).

The inclination of the first part of the flexural shear critical crack is given as;

$$cot\,\theta = \frac{0{\cdot}85\,d_s}{d_s - x} \leq 2 \cdot 50 \tag{2.50}$$

G_f is the concrete fracture energy, given as G_f = $0.0028 f_{cm}^{0.18} d_g^{0.32}$

d_0 = effective depth, d ≥100 mm.

ζ = size effect coefficient at critical shear crack failure, ζ =1.2 – 0.2a ≥ 0.65, with a in m.

$b_{v.eff}$ = effective beam width for compression flange. Note that for a rectangular beam, $b_{v.eff} = b_v = b$

$$\text{When } x \leq h_f,\ b_{v.eff} = b_v = b_{\mathrm{w}} + 2h_f \leq b \tag{2.51}$$

$$\text{When } x > h_f,\ b_{v.eff} = b_{\mathrm{w}} + (b_v - b_{\mathrm{w}})(\frac{h_f}{x})^{3/2} \tag{2.52}$$

For T or I-shaped beams with compression flange, K_T , a coefficient to take into account the mechanical difference of flange effect is given as;

$$K_T = \frac{M_{cr,T}}{M_{cr,R}}\frac{b_{\mathrm{w}}}{b} \approx 0.1 + 0.9\frac{b_{\mathrm{w}}}{b} + 2.5\frac{h_{f,tens}}{h}(\frac{b_{tens} - b_{\mathrm{w}}}{b}) \tag{2.53}$$

Where $h_{f,tens}$ and b_{tens} are the depth and the width of the tension flange of an I-shaped beam

For rectangular sections, K_T is taken as 1

K_P is a coefficient for considering the effect of the prestressing force in the cracking moment given as;

$$K_P = 1 + 0.24\frac{P\ y_t + M_v}{f_{ctm}^{bd^2}} \tag{2.54}$$

When applying this model to evaluate shear strength, the individual actions are explicitly calculated and summed up to give the total shear strength of the flexural member.

2.6.2 Compression chord capacity model (CCCM)

Cladera *et al.* (2016) simplified the $MASM$ (2015) model and developed a more compact expression by incorporating the explicit expression of v_w, v_l into v_c with constant average values and named the model Compression Chord Capacity Model ($CCCM$). Cladera *et al.* (2016) claim that the model is based on the idea that the compression chord's shear transfer function is the primary transfer action that resists or predominates in the failure condition under consideration.

Following Cladera *et al.* (2016) compression chord model, the nominal shear resistance can be taken as the summation of the concrete (v_{cu}) and stirrup contributions (v_{su}) contributions.

Unlike the $MASM$ which explicitly states the contribution of the individual transfer mechanism, the $CCCM$ only provides expressions for concrete contribution as well as steel, with boundary values. The expressions are given below;

$$V_{cu} = 0.3\zeta \frac{x}{d} f_{cd}^{2/3} b_{v,eff} d \ \nleq v_{cu,min} = 0.25(\zeta \frac{x}{d} + \frac{20}{d_0}) f_{cd}^{2/3} b_{\mathrm{w}} d \tag{2.55}$$

$v_{cu,min}$, the permitted minimum shear strength provided by concrete, is given because, for members with small depths and light reinforcement, the shear transmitted by the residual tensile stress is significantly equivalent to the shear transferred by the uncracked compression zone. This theory serves as the foundation of the CCCM. Hence, the contribution of the uncracked compression chord is limited (Cladera *et al.*, 2019).

$$V_{su} = 1.4 \frac{A_{\mathrm{sw}}}{s} f_{\mathrm{ywd}} (d_s - x) cot\theta \tag{2.56}$$

The total shear strength is given as;

$$V_{Rd} = V_{cu} + V_{su} \leq V_{Rd,max} \tag{2.57}$$

Where $V_{Rd,max}$ is the web crushing capacity given as;

$$V_{Rd,max} = \ \alpha_{\mathrm{cw}} b_{\mathrm{w}} z v_1 f_{cd}^{2/3} \frac{cot\theta + cot\alpha}{1 + cot^2\theta} \tag{2.58}$$

Hence,

$$V_{Rd} = \ 0.3\zeta \frac{x}{d} f_{cd}^{2/3} b_{v,eff} d \ + \ 1.4 \frac{A_{\mathrm{sw}}}{s} f_{\mathrm{ywd}} (d_s - x) cot\theta \ \leq \ V_{Rd,max} \tag{2.59}$$

For the determination of f_{cd} & f_{ywd}, f_{ck} shall not be taken greater than 60 Mpa

$$f_{cd} = \frac{f_{ck}}{\gamma}, f_{\mathrm{ywd}} = \frac{f_{y\mathrm{wk}}}{\gamma}$$

When compared to the mean inclination of the shear crack, the compression strut's inclination is deemed to be identical and it is given by;

$$cot\,\theta = \frac{0{\cdot}85\, d_s}{d_s - x} \leq 2 \cdot 5$$

where x is the neutral axis depth of the cracked section and can be computed from the equation below;

$$\frac{x_0}{d} = \alpha_e\rho_l\left(-1 + \sqrt{1 + \frac{2}{\alpha_e\rho_l}}\right) \approx 0.75((\alpha_e\rho_l)^{1/3}$$

When determining the value of V_{cu}, the size and slenderness effect (ζ) can be calculated from the expression below;

$$\zeta = \frac{2}{\sqrt{1+\frac{d_0}{200}}}(\frac{d}{a})^{0.2} \not< 0.45 \quad (2.60)$$

$b_{v.eff}$ = effective beam width for compression flange. Note that for a rectangular beam, $b_{v.eff} = b_v = b$

When $x \le h_f,\ b_{v.eff} = b_v = b_{\mathrm{w}} + 2h_f \le b$

When $x > h_f, b_{v.eff} = b_{\mathrm{w}} + (b_v - b_{\mathrm{w}})(\frac{h_f}{x})^{3/2}$

In a situation whereby there is no provision for shear reinforcement as in the case of beams without stirrups, the contribution of the stirrups can be omitted and then the expression below is considered in estimating total shear strength.

$$V_{Rd} = V_{cu}$$

2.6.3 Modification of the SNiP model

The modified SNiP shear design model by Yerzhanov *et al.* (2019) is an improvement of the already existing shear model for beams without stirrups from the Russian SNiP code of design. The original SNiP model design was based on the Plane Minimum Resistance (PMR) approach/model. The following describes the PMR idea, as described by Borishansky (1961) and Palaskas & Darwin (1980);

$$v_c = kb_w dR_b tan\phi = k\frac{R_b b_w d^2}{a} \quad (2.61)$$

According to Borishansky (1961), In the shear strength model, the principal compressive stress direction may be taken into account using $cot\,\phi = {}^{d}/_{a}$. The stress direction is given due consideration so as to include the effect of the inclination angle of the principal compressive stress (ϕ) and to make the effects of the interaction between shear resistance and the major compressive stress' inclination angle, as given in the equation above more comprehensible.

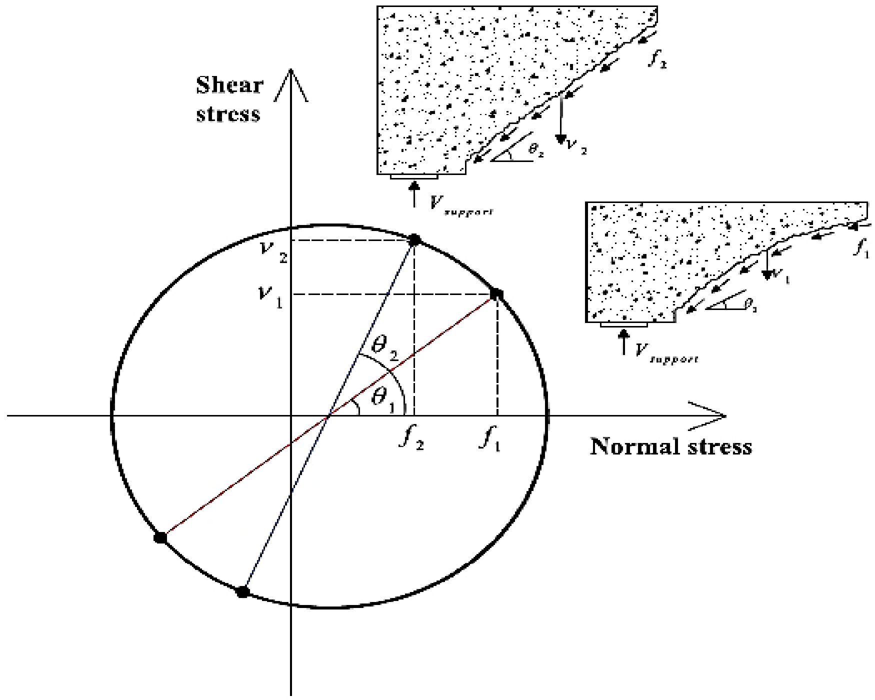

Fig 2.15. Effect of Principal compressive stress on shear resistance (Yerzhanov et al, 2019)

To determine the value of the factor k ($strength\ modification\ factor$), Borishansky (1961) utilized the test result from 75 shear experiments, as he reported that the value of the factor k would be difficult to determine theoretically. The PMR model was modified as follows;

$$Q_b = \frac{0.15F_{cu}b_\omega d^2}{a} \tag{2.62}$$

The expression above becomes unrealistic to use due to the high possibility of poor inference generalization with practical design conditions. The basis for determining the modification factor was limited to a few experimental setups. Unlike the PMR model which forms the basis for the SNiP shear design model, more emphasis is placed on the tensile strength of concrete. Therefore, the shear resistance of concrete as described in the SNiP code (SNIP2.03.01-84, 2012) becomes;

$$v_c = k_{SniP} b_w d f_t \tan\varphi = \frac{k_{SniP} f_t b_w d^2}{a} \tag{2.63}$$

Where k_{SniP} is the experimental adjustment factor to be taken as 1.5, φ is the inclination angle of the diagonal shear crack and f_t is the concrete tensile strength. The expression above can then be written as;

$$v_c = \frac{1.5 f_t b_w d^2}{a} \tag{2.64}$$

The following are the maximum and minimum shear strengths where concrete's shear contribution is permitted: $v_c\text{min} \leq v_c \leq v_c\text{max}$. The values for $v_c$min and $v_c$max has been experimentally established for the shear estimation of structures with a large shear span – effective depth ratio and smaller values of the shear span – effective depth ratio.

$$v_c\text{min} = 0.5 f_t b_w d \ , \quad v_c\text{max} = 2.5 f_t b_w d \tag{2.65}$$

Therefore,

$$0.5 f_t b_w d \leq \frac{1.5 f_t b_w d^2}{a} \leq 2.5 f_t b_w d \tag{2.66}$$

The SNiP code also has a provision for the shear contributed by the transverse reinforcement given as;

$$v_{sw} = 1 \cdot 5 \frac{A_{sw} F_y}{s} d \tag{2.67}$$

This allows for the estimation of the total shear in a reinforced concrete beam with shear reinforcement ($v_n = v_c + v_{sw}$), but in the case of beams without stirrups, v_{sw} can be omitted.

According to Yerzhanov *et al.* (2019), the shear model in the SNiP code provides unconservative estimations of shear strength for flexural members without stirrups and a minimal number of test results was used to determine the factor K that is stated in the SNiP code as said earlier which makes for a poor generalization of the model. To overcome such impediment and provide a more rational adjustment for the value K, the ACI-DafStb shear database collected and compiled by Reineck *et al*. (2013) was utilized to develop a new modification factor (K) to improve the analytical accuracy and safety level of the SNiP model proposed by Yerzhanov et al (2019) given as:

$$K_m = k \cot \alpha = \frac{v_c}{Ft b_w d} \tag{2.68}$$

Yerzhanov *et al.* (2019) expressed the new modification factor as a function of the effective depth (d). the modification factor is reduced as follows;

$$k_m = \frac{v_c}{f_t b_w d} = 6 \sqrt{\frac{1}{d}} \tag{2.69}$$

The modified SNiP model for shear design can then be finally simplified as;

$$v_c = 6 \sqrt{\frac{1}{d}} f_t b_w d \tag{2.70}$$

2.6.4 Mechanical model based on structural mechanics

The new approach developed by Tran (2020) to evaluate the shear capacity of slender beams without stirrups is based on the fundamentals of structural mechanics with the assumption that the shear strength correlates to a failure that happens at the neutral axis given that the major tensile stress is comparable to the concrete tensile strength and resulting in a rapid crack connecting to the critical shear crack tip. The distribution of stresses that leads to failure along the neutral axis is shown diagrammatically in the figure below, along with the formation of shear cracks.

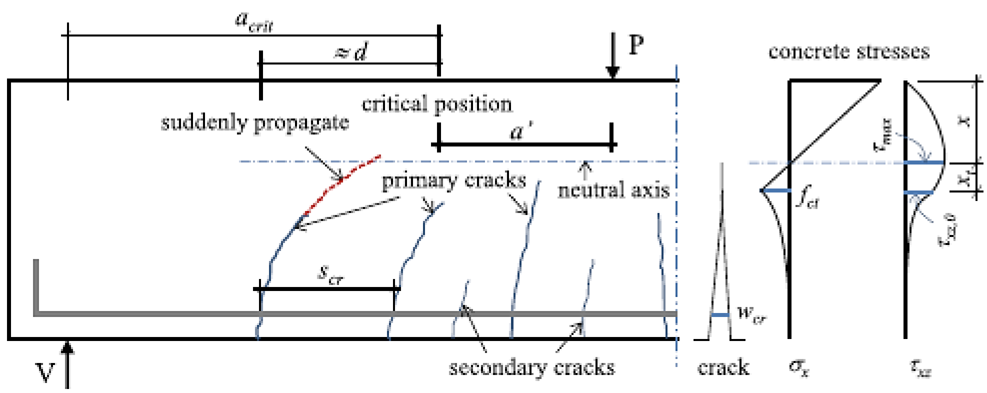

Fig 2.16. Failure along the neutral axis owning to stress distribution and crack formation (Tran, 2020)

The shear capacity expression proposed by Tran (2020) is considered to be the sum of the shear transfer mechanism in the tension zone (v_{ct}) and the compression zone (v_{cc}) accordingly, i.e., there are two explicit expressions summed up as one. One caters for the strength at the bottom area of the concrete section just before the neutral axis (the tension zone), and the other provides an estimation for the shear capacity of the uncracked compression zone where the critical area is located as shown in the fig above.

$$V_c = V_{ct} + V_{cc} \tag{2.71}$$

Tran (2020) considered concrete properties such as tensile strength (f_{ct}), effective tensile strength ($f_{ct,ef}$), fracture energy (G_F), elastic modulus (E_c), crack width (w_{cr}), crack slip (s) and crack spacing (s_{cr}) in the formulation of the model.

Shear capacity in the compression zone (V_{cc})

According to Tran (2020), the shear capacity in the compression zone can be estimated based on the assumption that in the uncracked zone of the cracked concrete, the concrete stress (σ_x) increases linearly with an applied load. This leads to a parabolic distribution of the shear stresses in the compression zone with a maximum value of shear stress (τ_{max}) at the neutral axis and shows a solidity factor (ψ) = 2/3. The shear capacity in the compression zone can be determined as follows;

$$V_{cc} = \frac{2}{3}\tau_{max}.bdk_x \tag{2.72}$$

Where $k_x = x/d$ is the relative depth of the compression zone

ψ is the solidity factor

Shear capacity in the tension zone (V_{ct})

According to Tran (2020), the aggregates are in control of transmitting shear stresses across cracks in the tension zone, and this shear behaviour generates consistency in the response of the structural concrete and its load-bearing performance in cracks. Tran (2020) further added that the shear distortion and shear modulus of the uncracked compression zone has a significant impact on the shear deformation of the cracked concrete in the tension zone.

Assuming that the maximum crack width (w_c) is greater than the crack width at the bottom end of the shear crack (w_a) and substituting η , V_{ct} can be rewritten as;

$$V_{ct} = bd\frac{(1-k_x)}{\mathrm{w}_{cr}}\int_0^{\mathrm{w}_a}\sigma_{ct(\mathrm{w})}\,d\mathrm{w} = bd\frac{G_F}{\mathrm{w}_{cr}}(1-k_x) \tag{2.73}$$

By combining the shear resistance in the tension zone and the compression zone, the total shear capacity of a reinforced concrete beam without shear reinforcement can be written as;

$$V_c = bd\frac{G_F}{\mathrm{w}_{cr}}(1-k_x) + \frac{2}{3}\tau_{max}.bdk_x \tag{2.74}$$

$$V_c = \frac{2}{3}f_{ct,ef}.bd\left[k_x + \frac{1.5G_F}{f_{ct,ef}\mathrm{w}_{cr}}(1-k_x)\right] \tag{2.75}$$

Where $\boldsymbol{G_F}$ the fracture energy is given as $0.03f_c^{0.18}a_g^{0.32}$ and a_g= maximum aggregate size.

$\boldsymbol{f_{ct,ef}}$ the effective tensile strength = $f_{ct}.\frac{1}{1+v} \approx 0.83f_{ct}$

the crack width $\mathbf{w}_{cr}$ is taken as

$$\mathrm{w}_{cr} = \varepsilon_{sm} - \varepsilon_{cm} \tag{2.75}$$

2.7.0 Structural reliability assessment

As stated by Holicky (2009), the concept of structural reliability is primarily focused on the demand that the structural resistance has to be in comparison greater than the action effect, the failure to meet this demand leads to a failed state of the structural mechanism. This is depicted below;

$$R > E \tag{3.1}$$

The trilemma of resistance reliability assessment in structures involves the examination and validation of resistance models that are functionally adequate in their safety performance, economically wise and less sophisticated for use i.e., simplicity.

When representing actions and their combinations, structural reliability modelling makes a deliberate attempt to develop adequate probability models, particularly for variable actions, and to account for these flaws in the design methods by including partial elements as necessary. Research on structural reliability and resistance focuses primarily on enhancing prediction models by calibrating loading and resistance functions in design codes to ensure that a particular degree of reliability is maintained in all possible design scenarios. Other concerns include the economic implication in terms of cost and ease of use when applying the design models in practice (Huber, 2005). Measurement of a structure's failure likelihood while taking into account resistance and load uncertainty is the goal of structural reliability evaluation (Olalusi, 2018). It has been proven that by properly modelling material characteristics, geometric parameters, and uncertainty factors related to a model under consideration, structural resistances may be anticipated. The difference between the predicted values of the structural resistance and those of the applied loads may be used to determine the reliability performance of a particular failure mechanism, such as that taken into account in this study. The performance function is as seen in Equation (3.1b);

$$g(\boldsymbol{X}) = P(X) - \mathrm{Q(X)} \tag{3.1b}$$

$g(\boldsymbol{X})$ is representative of the performance function and is defined based on the values of Q and P, Q is the action effect and P is the structural resistance value.

The performance function explicitly characterizes the outcome of its evaluation into three 3 possible design condition

(1) $g(\boldsymbol{X}) = 0$ depicts the limit state

(2) $g(\boldsymbol{X}) > 0$ depicts the safe design condition

(3) $g(\boldsymbol{X}) < 0$ depicts an unsafe design condition (the failure region)

Hence, the probability of a failure event may conveniently be described in terms of the functional relationship in Equation (3.2)

$$P_f = P(g(X) < 0) = \int_{g(X) \leq 0} f_x(X)\, dx \tag{3.2}$$

$$P_f = \Phi(-\beta) \tag{3.3}$$

The probability of failure can be easily evaluated by integrating the joint probability distribution function of the random variables (X) or the equivalence of the domain where the limit state function is less or equal to zero.

When the disparity between the anticipated value of structural resistance $P(X)$ and the anticipated value of the applied loads $\mathrm{Q(X)}$ is greater, the safety level is increased.

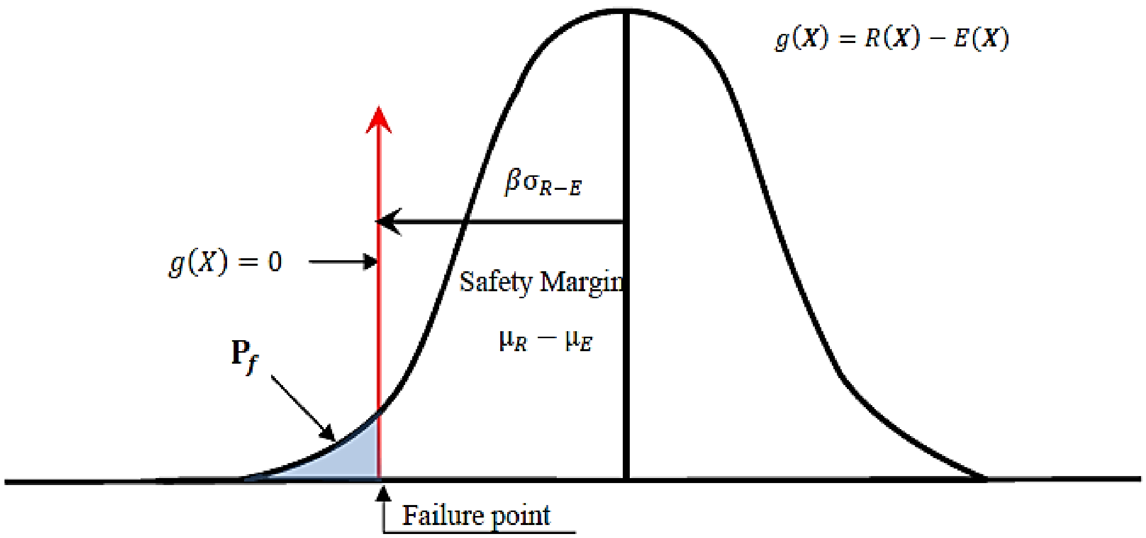

Fig 2.18 Representation of the limit state function (Olalusi, 2018)

The conclusion of reliability-based investigations might be to introduce the use of different partial safety factors for various modes of resistance across respective construction materials, the application of different values of constants and coefficients in various design models, or place constraints to restrict or limit the use of particular methods or applications (Mensah *et al.*, 2013). It is important to note that this also depends on the scope of the investigation. During the reliability investigation of a shear resistance model, the scope of investigation must be stated to understand the extent to which the investigation has to be carried out (Full or partial/preliminary calibration). This is also because most times, shear models involve binary design functions and calibration must be specific to design functions.

EN 1990 (2002) specify a required target reliability level value of β_T=3.8 while the SANS 10160-1 (2011) stipulates a value of β_T=3.0 for Class of RC2 structures. The preliminary reliability-based investigation comes to an end when the target reliability index of the investigated model meets the demands specified earlier. The expression below captures well;

$$\beta_R \approx \beta_T \tag{3.4}$$

Here, the reliability index (β_R) can easily be computed by an assessment of the limit state function through FORM analysis as seen in Equation (3.5);

$$g(X) = R(X) - R_d(X_{k,\gamma}) = 0 \quad (3.5)$$

Where $R(X)$ is the probabilistic distribution representing real shear resistance

$R_d(X_{k,\gamma})$ denotes a deterministic value of shear resistance for which the reliability index is investigated.

In a situation where the expression above is not satisfied i.e., if $\beta_R < \beta_T$ further actions seem cogent towards an appropriate calibration of the model to demonstrate an adequate level of safety in practice. Conversely, if $\beta_R > \beta_T$, the model should be calibrated to achieve cost-effective design functions.

Holicky *et al.* (2010) stated that to adequately take care of the shortcomings in the reliability performance of a specific model observed in the course of reliability investigation as regards attaining specified reliability levels, applying partial factors to the variables that most affect or dominate reliability performance (mostly model uncertainty; concluded from existing works of literature) could prove effective in attaining such required reliability levels.

Following the instructions in EN 1990, the partial factor may be derived analytically; however, it should be noted that the probability distribution of the model uncertainty data must follow a lognormal distribution for the formula below to be valid.

$$\gamma_{Rd} = 1/[\mu_\theta . exp.(-\alpha_R . \beta . V_\theta)] \quad (3.6)$$

Here, γ_{Rd} = derived partial factor of model uncertainty

μ_θ = mean of the model uncertainty random variable

V_θ = coefficient of variation of model uncertainty random variable

β = reliability index provided in design codes

α_R= direction cosine (FORM sensitivity factor)

The influence of the calculated resistance model partial factor may be integrated into the design expression using the expression provided by EN 1990, as shown below.;

$$R_d = R\left[\eta \frac{X_k}{\gamma_m}; a_d ..\right]/\gamma_{Rd} \quad (3.7)$$

R_d represents the calibrated design resistance, X_k is the characteristic values of the material property, η conversion factor applicable to the material property and a_d is the design geometric parameter.

Besides the First Order Reliability Method (FORM), other reliability investigative methods which include Numerical integration, Computer-based Monte Carlo Simulation and Cost Optimization (Sykora and Holicky, 2012) can be used to evaluate the reliability index of a system.

2.7.1 Model uncertainty

Uncertainty study is generally composed of two types of uncertainties; aleatoric (Data uncertainty) or epistemic (Knowledge uncertainty). Aleatoric uncertainty arises from uncertainness in the actual data as a result of natural variability while epistemic uncertainty is a result of poor knowledge or oversimplification during the formulation of a model and the parameters of the model. The uncertainty considered in this research work is the epistemic uncertainty hereafter referred to as model uncertainty.

Uncertainties in resistance models play an important aspect in the reliability assessment of structure and calibration of partial factors for semi-probabilistic design in codes of practice, these uncertainties should always be treated for a definite model, a peculiar mode of failure and scope of application (Holicky *et al.*, 2015). According to Gino *et al.* (2017), identifying and quantifying the uncertainty factor related to a specific model is of high relevance to structural safety verification in the course of reliability assessment.

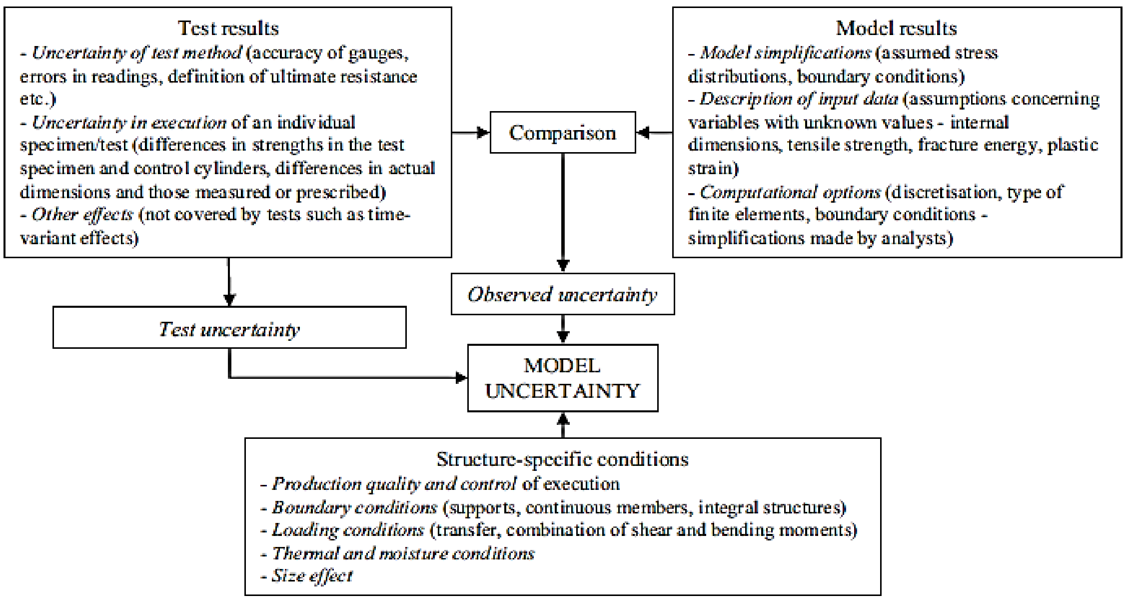

Fig 2.19 General concept of model uncertainty (Holicky *et al.*, 2015).

Epistemic uncertainty can be due to the limitation of knowledge or constraint in the application of a model (Riberio *et al.*, 2016). Riberio *et al.* (2016) further cited Melchers (1999) saying that epistemic uncertainties refer to those uncertainties which can be mitigated with additional data or information, better modelling and accurate estimation of the model parameter.

According to Sykora *et al.* (2012), model uncertainties can be associated with strength characteristics models such as shear models, bending resistance models, and load effects models (load effects assessment and their combination). They also mentioned that while considering resistance models, the following conditions should be covered;

- ✓ overcomplicating existing physical principles should be avoided in a model's framework
- ✓ assumptions in analytical models

- ✓ The impact of conflicting inference of advanced software packages and human mistakes.

JCSS (2006) provided two expressions for estimating the uncertainties in resistance models based on the nature of the relationship (multiplicative or additive) between the actual resistance (experimental observations) and the deterministic resistance.

By a means of the multiplicative relationship as seen in Equation (3.8);

$$R(X,Y) = \theta . R_{mod}(X) \tag{3.8}$$

by a means of an additive relationship as seen in Equation (3.9)

$$R(X,Y) = \theta + R_{mod}(X) \tag{3.9}$$

Where $R(X,Y)$ is the resistance from an observed experimental setup which consists of a series of tests over a practical range of design parameters.

$R_{mod}(X)$ is the resistance estimated deterministically from specific resistance models.

X is a vector of basic input parameters (variables) included in the resistance models, and Y is the vector of variables that have been disregarded or omitted in the deterministic models but influence the resistance evaluation.

To determine the use case of either of the uncertainty model expression becomes difficult as the choice is dependent on the task-specific condition. Though, in existing studies, the multiplicative representation of model uncertainty is commonly applied to resistance models while the additive relationship is used to account for errors in systematic measurements.

Due to the nature of the statistical distribution of the model uncertainty factor, Sykora *et al.* (2012) suggested that the multiplicative relationship is more appropriate when considering a resistance model since the real resistance (R) and resistance from numerical modelling (R_{mod}) is described by the same lognormal distribution as the model uncertainty, then the additive relationship becomes preferable when a normal distribution is significant.

Hence, the model uncertainty can be calculated by;

$$\theta_n = \frac{R_n(X,Y)}{R_{mod,n}(X)} \tag{3.10}$$

Here, θ_n represents the n-th event of the estimated model uncertainty comparing the values of the experimental tests with results from deterministic simulation.

$R_n(X,Y)$ and $R_{mod,n}(X)$ represents values obtained from the n-th iteration of the experimental test and deterministic model.

The deliberate simplifications and disregard of some design input parameters are majorly responsible for modelling uncertainty related to shear performance; simplification is done to achieve an easy-to-use functional design model. It is quite important to note that the modelling uncertainty is affected by a vast number of causes like human error and quality control, as well as issues of model adjustment (Mensah *et al.*, 2013).

Holicky *et al.* (2015) stated that the primary aim of model uncertainty assessment is to reflect its contribution to the reliability performance of the model as characterized by the dispersion of the distribution function.

In conclusion, investigating uncertainties in specific models with appropriate value allocation is an effective and fundamental principle in the reliability calibration of such models.

2.7.2 Uncertainty modelling in existing literature

2.7.2.1 Mensah *et al.* (2013)

Concerns stem from the predictions of the EC 2's Variable Struct Inclination method for diagonal tension failure as it gives very conservative capacity predictions for RC beams with a low percentage of shear reinforcement, while for members with relatively large amounts of shear, very unconservative prediction is provided. As a result, Mensah *et al.* (2013) performed a proper calibration of the model to achieve both economic and safe performance in practice. The first step towards reliability calibration was to characterize the modelling uncertainty associated with the EC2 shear prediction model for diagonal tension failure and assess its effect on shear reliability performance. To further substantiate the need to calibrate the design function of the EC 2's VSIM, Mensah *et al.* (2013) carried out a preliminary reliability evaluation to determine the test case reliability index following a FORM limit state function analysis. The EC 2's VSIM fell below the required target reliability index recommended by EN 1990 but satisfied the requirement of the SANS 10160-1. Hence, Mensah *et al.* (2013) concluded that logical actions should be taken for proper calibration. The model uncertainty earlier characterized in their work was used to derive partial factors for model uncertainty during full reliability calibration and incorporated into the design function.

2.7.2.2 Sykora *et al.* (2014)

Sykora *et al.* (2014) investigated the uncertainties associated with resistance models of sound structural members (members not affected by the corrosion of reinforcement) and corrosion-damaged structural members as well. Failure modes particular to the two structural conditions as provided by the EN 1992-1-1 were looked into. Statistical characteristics of the model uncertainties were adopted from existing works of literature that have quantified the uncertainty factor in the respective models, these model uncertainty factors were used in the calibration of a partial factor for the model uncertainty. Sykora *et al.* (2014) concluded based on the performance evaluation of the model uncertainties in terms of sample space that the uncertainty related to corrosion-damaged RC models is more severe than that of the models in the sound RC models. Hence, Further efforts are required to develop appropriate models for calculating the resistance of corrosion-damaged structures. In the course of the investigation, Sykora *et al.* (2014) conducted a deterministic reliability verification according to EN 1990 to calibrate a partial factor which describes the uncertainty associated with the resistance models.

2.7.2.3 Sykora *et al.* (2017)

Sykora *et al.* (2017) used a dataset of 459 experimental observations of beams with stirrups and another database of 184 shear tests of beams without shear reinforcement to assess the uncertainty in the shear provision of the fib model code. They adopted the same investigative measures in determining the uncertainty inherent in all levels of approximation (I-III) of the shear models. The study focused on identifying the biases and scatters in the shear model provision at each level of approximation. By appropriately analyzing the sample moments of the uncertainty factor in all the shear provisions for beams with stirrups, Sykora *et al.* (2017) identified the MC2010 LoA III shear model as the most appropriate model with a model uncertainty factor close to unity, typifying a low bias, and the smallest coefficient of variation. While for beams without stirrups, the MC2010 LoA II seems to have a favourable evaluation performance over the MC2010 LoAI in terms of model uncertainty. Sykora *et al.* (2017) concluded that the accuracy of the MC2010 LoA III over the others may be due to the additional input data as it contributes shear strength by summing the contributions of concrete and stirrups.

2.7.2.4 Nadolski and Sykora (2014)

Considering the engineering formulas provided by the EN 1993-1-1 for the prediction of the resistance of steel members, Nadolski and Sykora (2014) interpreted the model uncertainty and quantification in resistance models of steel members including uniform bending moment, gradient bending moment, yielding resistance for bending, bending resistance with the loss of stability (rolled or equivalent welded profiles), bending resistance with the loss of stability (general case) and Axial compression with the loss of stability. The model uncertainty of each failure mode and its corresponding descriptive statistical distribution was obtained from probabilistic models proposed in the literature of other researchers, though the results were recognized by the EN 1993-1-1. Nadolski and Sykora (2014) utilized the sample moments of the probabilistic models proposed to compute and recommend model uncertainty partial factor to facilitate practical application.

2.7.2.5 Gino *et al.* (2017)

Gino *et al.* (2017) quantified the model uncertainties in non-linear finite element analysis of reinforced concrete shear walls subjected to incremental cyclic loading. The context of their research involves the comparative assessment of the level of uncertainties associated with two commercial NLFEM software to be adopted for structural safety verification. Results of the simulation of the structural behaviour of two families of shear walls were obtained from the scientific literature by different authors. The scope of the investigation was limited to the quantification of the uncertainties related to the maximum load and maximum displacement. As a result, Gino *et al*. (2017) concluded that further investigation has to be done to consider the influence of more finite element model parameters on 2D NLFEM model uncertainties and the prediction of the structural response of R.C structures subjected to cyclic loading.

Other pieces of literature that have quantified model uncertainties as a measure of reliability assessment include Holicky *et al.* (2015), Lukas & Vladmir (2016), McLeod *et al*. (2016), Ribeiro *et al*. (2016), McLeod *et al.* (2017), Olalusi & Viljoen (2017), Engen *et al*. (2018), Olalusi & Spyridis (2020b), Olalusi & Awoyera (2021), Olalusi (2020), Olalusi & Viljoen (2021b), Olalusi & Viljoen (2021a).

2.7.3 Reliability index & target reliability index

The minimum level of reliability is expressed as the reliability index β , defined as the number of standard deviations (σ_{R-E}) that the difference between the expected value of the structural resistance and the expected value of the loads (μ_{R-E}) i.e., the safety margin is situated from the failure point (Huber, 2005).

According to EN 1990 (2002), the overall reliability index, β, can be separated into two parts; the resistance reliability index expressed as $\beta_R = \alpha_R\beta$ and the load effects index expressed as $\beta_E = -\alpha_E\beta$. α_R and α_E denote FORM sensitivity factors (direction cosines) and are recommended in EN 1990 and SANS 10160-1 as α_R=0.8 and α_E=−0.7. To meet the demands of structural reliability investigations, it is only ideal to require that the resistance index β_R should be almost equal, equal or greater than the target reliability index. In any case, it must not be significantly less than the target reliability index.

SANS 10160-1 provides a value of $\beta_{RT,SANS}$ = 0.8×3.0 = 2.4 for its target reliability while the EN 1990 gave a value of $\beta_{RT,EC2}$ = 0.8×3.8= 3.04 as the required target reliability index for the same class of RC2 structures. Concerns arise when the condition for safety is not met. Hence, further investigative measures may be needed to identify the parameter that largely affects the structural performance of the model by conducting a comparative analysis of the direction cosines of the basic variables and providing a partial factor as appropriate. The direction cosine of the i^{th} basic variable as given by Ang & Tang (1984) is as seen below;

$$\alpha_{X_i} = (\partial g(X)/\partial X_i)/[\sum_i(\partial g(X)/\partial X_i)^2]^{1/2} \qquad \text{and } \left[\sum_i(\alpha_{X_i}^2)\right]^{1/2} = 1 \tag{3.11}$$

2.7.4 General Probabilistic Model

According to Olalusi & Viljoen (2017), in the reliability assessment of a shear model, a general probabilistic model that accurately represents shear failure behaviour concerning the material and geometric parameters over the range of practical applications is required.

A general probabilistic model for shear capacity can be obtained as a product of any unbiased prediction model and its corresponding uncertainty, it should be noted that not all GPMs are suitable for reliability assessment as their accuracy may differ respectively (Olalusi & Viljoen, 2017).

$$V_{GPM=}MF.V_m \tag{3.12}$$

The Limit State Function is given as;

$$g(X) = V_{GPM} - V_{Rd,S} \tag{3.13}$$

The general probabilistic model for shear corresponds to the real shear resistance subject to uncertainties in parameters that affect the shear resistance. Consequently, the general probabilistic model for shear includes a model factor as one of the basic variables to quantify the uncertainty in the model to predict the true shear resistance as seen above (Huber,2005). The general probabilistic model is derived from design procedures with the least uncertainty factor among other selected models during reliability assessment.

2.8.0 Overview of artificial intelligence & machine learning

Artificial intelligence has three (3) key characteristics namely; intention, intelligence, and adaptability. The intentionality of Artificial intelligence (AI) is in its ability to make judgments based on information rather than automatically responding to questions with prepared replies. This can only be accomplished when an AI system has access to extensive datasets. According to Skansi (2018), machine learning was created as a result of artificial intelligence and cognitive science. Hence, AI gains its intelligence through interactions with machine learning and data analytics.

The intelligent answer to inquiries is determined by the interplay between computer systems, data analytics, and machine learning. The ability of AI systems to adapt to new data entry and make conclusions based on the most recent data quality makes them unique, and this is referred to as the adaptation of artificially intelligent algorithms.

Machine learning, a subset of artificial intelligence, is the act of programming a computer system to learn from available data without being explicitly programmed i.e., it is not hard coded. In machine learning, computer system learns to take decisions by themselves based on a certain policy. Image data or tabular data is given to a computer system, and the computer establishes an intrinsic relationship between the data for future prediction either classification or regression.

The application of machine learning is dependent on the problem scope. A problem which can be solved by traditional algorithms, e.g., linear programming, does not require the use of machine learning. The complex use of machine learning includes non-linear multivariate problems, spam filtering or speech recognition, these problems cannot be solved via a traditional algorithm, hence the need for machine learning. The ability of machine learning to adapt to new data makes it a preferable choice as a tool to solve robust engineering problems.

There may be a lot of fine-tuning needed when using a conventional approach such as structural equation modelling to estimate shear resistance. Instead, this arduousness may be readily prevented by using a machine learning method. Aldakheel, Satari, & Wriggers, (2021) agreed that data-driven models like machine learning, deep learning, and artificial neural networks are utilized to simplify a conventional model's complexity.

2.8.1 Applications of machine learning

- Image classification e.g., production line of an industry (CNN; Convolution neural network)
- Semantic segmentation to detect a tumour in a brain scan by classifying pixels of the image scan to determine the exact location and shape of the tumour. (CNN)
- Text classification using Natural Language Processing (NLP) (RNN, CNN)

- Chatbot or Virtual Personal Assistant using Natural Language Processing, Natural Language Understanding and Natural Language Generation Concepts e.g., Cortana
- Forecast companies' revenue based on performance metrics (Linear or polynomial regression, SVM, RF, ANN, RNN, LSTN)
- Predicting the compressive strength or shear resistance of a beam (Linear or polynomial regression, SVM, RF, ANN, RNN, LSTN, GEP)
- Anomaly detection or recognizing outliers in a dataset
- Dimensionality reduction for high dimensional dataset i.e., multiple features. (Auto encoders, principal component analysis)
- Product recommendation system
- Building a reinforcement learning robotic agent for game development or robotic application without being supervised e.g., in the assembly line of an automotive industry.

The ability to employ a machine learning model is determined by its application, hence domain expertise is more crucial in machine learning than building the model itself.

2.8.2 Classification of machine learning algorithm

- Classification based on human supervision; machine learning algorithms can be classified as supervised, unsupervised, semi-supervised or reinforcement learning algorithms. These classifications are based on the provision of human supervision in terms of labelling data to guide computer systems in their learning process. Unsupervised learning and reinforcement learning are prerequisites for achieving AGI or Strong A.I (Artificial General Intelligence). AGI is a level of intelligence a machine system possesses where its intelligence level is like that of humans. The application of machine learning in this thesis would be restricted to the confines of Weak A.I (Artificial Narrow Intelligence), where a machine learning system can only perform a single function, unlike humans or AGI.
- Classification based on Training Methodology; Training may be online or offline (batch) learning.
- Classification based on Generalization; Instance-based learning or Model-based learning.

Supervised learning can be classified into two kinds of problems; classification and regression. Classification-supervised learning is used to predict discrete values e.g., spam filtering systems. While regression models are used to predict a continuous numerical value. Some of the supervised machine learning models include;

- Linear regression
- Logistic regression
- Support vector machine
- Random forest
- Decision tree
- Neural networks (Artificial, Convolutional, Recurrent)
- Naïve Bayes
- Polynomial regression
- K-Nearest Neighbors
- Gene Expression Programming

Unsupervised learning models are examples of models that do not require human supervision. Or providing a label to data. These models can be majorly used for clustering purposes and Novelty/Anomaly detection. Examples include;

- K-means clustering
- DB Scan
- Hierarchical clustering analysis
- Dimensionality reduction and visualization-based algorithms e.g., PCA (principal component analysis), GNN (Graph neural network).

2.9.0 Theory and Mathematical Intuition of Machine Learning models

In this section, the history of the considered machine learning models, the concept and underlying theory together with the mathematical intuition and expressions are presented.

2.9.1 Support Vector Machine

Vladimir N. Vapnik, a Russian researcher was responsible for the development of the support vector machine. His research on the support vectors algorithm started in 1963 (Vapnik and Lerner, 1963; Vapnik and Chervonenkis, 1964) and was successful by 1997 (Vapnik *et al.*, 1997). In 1963, Vapnik published a research paper in which the SVM concept was first introduced based on the generalized portrait algorithm. Hence, the support vector algorithm was then termed a non-linear generalization of the general portrait algorithm (Smola and Scholkopf, 2003). The SV algorithm has evolved significantly over the past 60 years, and the sub-variants will be examined in more detail below. It should be known that the support vector algorithm was initially developed to provide solutions to classification problems. A variant, support vector regressor, was later developed to address regression problems.

The validity of SVM as a tool for solving complicated, non-linear engineering problems has been confirmed in both recent and previous literature, making it an established and credible approach in engineering analysis. The use of SVM can be found in the following research papers;

Wakjira *et al.* (2022) employed the support vector machine together with alternative machine learning models to predict the load and flexural capacities of reinforced concrete beams strengthened with fabric-reinforced cementitious matrix (FRCM) composites in flexure. Results from the prediction were compared to existing analytical methods. In structural health monitoring, Deng *et al*. (2020) used SVM to simulate the relationship between fatigue damage and traffic load for the Nanxi suspension bridge hangers. Also, Chou et *al*. (2014) adopted the support vector algorithm and other ML models to simulate the mechanical strength of concrete using data from several countries.

According to Noble (2006), to understand the entirety of a support vector machine, an individual only needs to have an in-depth knowledge of the following four fundamental concepts.

- Hyperplane
- The maximum margin classifier/hyperplane
- The soft margin (support vector classifier)
- The kernel function (support vector machine)

Hyperplane

A hyperplane is a higher dimensional generalization of a given plane that is often used to separate mixed variable classes in an n-dimensional Euclidean space. For a classification or regression problem, the dimension of the hyperplane adopted by the support vector algorithm is dependent on the number of input features in a dataset.

Consider a situation where there are two input variables, N = 2 for x and y, the hyperplane would then have N-1 dimensions to perfectly separate both variable classes. Suppose you have 3 input variables, a 2-dimensional plane is considered as the appropriate hyperplane. An N-dimensional plane greater than 3 cannot be visualized, hence the name, Hyperplane.

Selecting the hyperplane with the largest margin is an effective method of determining which of the infinite number of separating hyperplanes to employ (Bentsen, 2019). The maximal margin hyperplane maximizes the distance to the nearest point from each class and divides the two classes. This provides an efficient way of optimizing the separating hyperplane.

The maximum margin classifier/hyperplane

The definition of the maximum margin classifier takes the form of a hyperplane, which is a planar linear subspace of dimension p-1 in a p-dimensional space (Bentsen, 2019). Only perfectly separable classes may be classified with the maximum margin classifier. This indicates that the maximum margin classifier has a restriction and cannot perform an appropriate classification when the classes are not perfectly separable, as would be in a real-world scenario.

Our aim in the maximum margin classifier is to derive the equation of hyperplane based on the best ѳ-coefficient, as in linear regression, that will maximize the margin with subjection to some constraints.

Constraint 1; given $(\theta_0, \theta_1, \theta_2, \dots \dots . \theta_p)$ then $\sum_{j=1}^{p} \theta_j^2 = 1$ (3.14)

Constrain 2; the sum of the orthogonal or perpendicular distance must not be less than M.

$$y_i\left(\theta_0 + \theta_1 x_{i1} + \theta_2 x_{i2} + \cdots \dots \dots \dots \dots . . \theta_p x_{ip}\right) \geq M \quad (3.15)$$

Where $\theta's$ are model coefficients and $x's$ are model features.

M = Maximum margin.

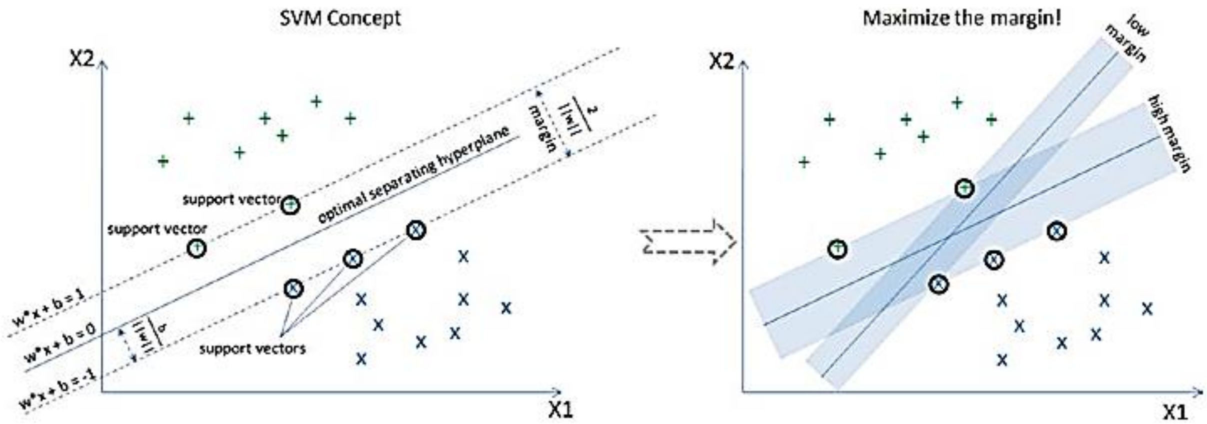

Fig 2.20. A maximum margin hyperplane that separates two perfectly separable classes with just five support vectors for the optimal solution of the optimization problem (Swamynathan, 2017).

The soft margin (support vector classifier)

In a situation whereby the classes are not perfectly separable as seen in Fig. 2.21 below, the maximum margin classifier cannot be applied because applying a maximum margin classifier to imperfectly separable class results in the misclassification of both classes.

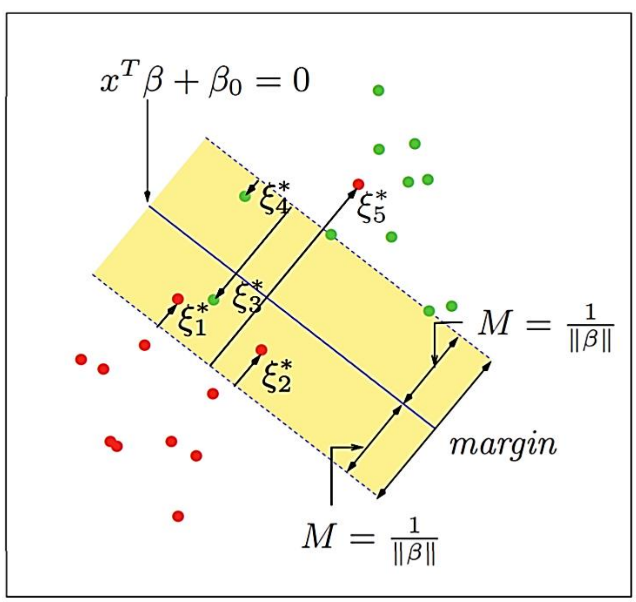

Fig 2.21. An imperfectly separable data set and the support vector classifiers. The labelled points are wrongly classified (Bentsen, 2019)

The support vector classifier uses the soft margin approach for this sort of problem. The soft margin allows a misclassification inside a margin for a test point. The support vector algorithm attempts to conduct a bias-variance trade-off by lowering the variance and raising the bias. Without this misclassification, by permitting a misclassification inside the margin, the support vector classifier model fails to generalize properly, and it would generate unsatisfactory predictions.

Hence, with the inclusion of a slack variable ξ to allow misclassification, the constraint as seen in the maximum margin classifier is modified to maximize M.

Constraint 1; given $(\theta_0, \theta_1, \theta_2, \dots \dots . \theta_p)$ then $\sum_{j=1}^{p} \theta_j^2 = 1$

Constraint 2; given $(\xi_1, \xi_2, \xi_3, \dots \dots . \xi_n)$, $\xi_i > 0$; then $\sum_{i=1}^{n} \xi_i \leq C$ (3.16)

Where C is a regularization parameter that controls the allowable degree of misclassification in the soft margin. The strength of regularization is inversely proportional to C i.e. if the value of C is high, the strength of regularization is less and vice-versa.

Constrain 3; the sum of the orthogonal or perpendicular distance must not be less than M (1-ξ_i).

$$y_i\left(\theta_0 + \theta_1 x_{i1} + \theta_2 x_{i2} + \cdots \dots \dots \dots \dots . . \theta_p x_{ip}\right) \geq M(1\text{-}\xi_i) \quad (3.17)$$

The kernel function (support vector machine)

The main principle of support vector machines is that the training set can always be projected from the original input space, which has dimension p, to a higher-dimensional feature space where the training set is more linearly separable. The constraint is also modified into;

Constraint 1 applies as well.

Constraint 2; $y_i\left(\theta_0 + \sum_{j=1}^{p} \theta_{ji} x_{ij} + \sum_{j=1}^{p} \theta_{j2} x_{ij}^{k}\right) \geq M(1\text{-}\xi_i)$ (3.18)

The power k denotes that the original input space has been projected into a higher dimensional space.

The support vector algorithm becomes more complex when projecting into a higher-dimension space, which might result in an overfitting issue. The kernel function and trick are used to address this problem.

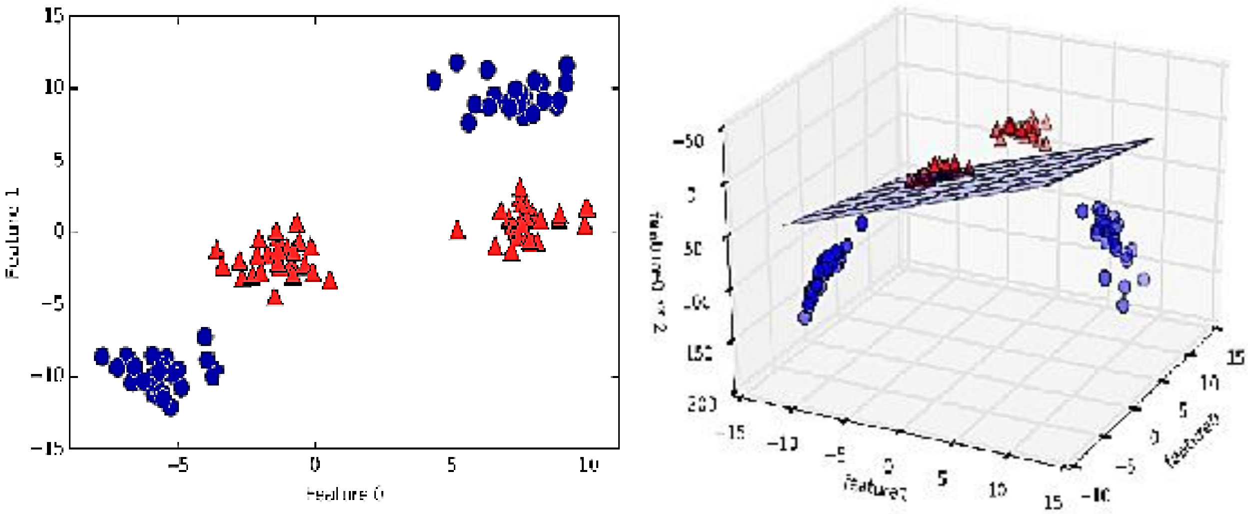

a. Two classes not linearly separable b. Projection into a higher dimension

Fig 2.22 (a) Two-class classification dataset in which classes are not linearly separable (b) A linear SVM on the larger three-dimensional dataset determined the decision boundary (Muller and Guido, 2016).

The kernel function and trick concept

By applying the kernel trick, we try to calculate the dot product of the training observations in a linear support vector classifier.

$$F(x) = \theta_0 + \sum_{i=1}^{n} \alpha_i \langle x, x_i \rangle \tag{3.19}$$

$\sum_{i=1}^{n} \alpha_i \langle x, x_i \rangle$= Dot product of all training observations or data points.

$$= \alpha_1 x_1 + \alpha_2 x_2 + \alpha_3 x_3 + \cdots \ldots \ldots \ldots \ldots + \alpha_n x_n \tag{3.20}$$

α controls or selects the non-zero support vectors, the idea of the kernel trick is to only select the non-zero support vectors and not the entire data points to save the computation time and reduce the complexity of the algorithm.

To complete the kernel trick transformation, the kernel function is introduced into the Dot product equation above to completely decrease the algorithm complexity in a higher dimensional feature space. The speciality of the kernel function is that it tries to quantify the similarity between the original feature space and the enlarged feature space by showing the equivalence of the data in each feature space regardless of the dimension in which the data was defined.

The support vector machine equation then becomes;

$$F(x) = \theta_0 + \sum_{i=1}^{n} \alpha_i K \langle x, x_i' \rangle \tag{3.21}$$

The term '$K\langle x, x_i' \rangle$' performs the kernel transformation and also controls the complexity of the algorithm with the Dot-product concept.

For a polynomial kernel function, $K\langle x, x_i' \rangle$ is given as

$$K\langle x, x_i' \rangle = (1 + \sum_{i=1}^{p} x_{ij}, x_{ij}')^d \tag{3.22}$$

The equation of the support vector machine with a polynomial kernel function becomes;

$$F(x) = \theta_0 + \sum \alpha_i \,(1 + \sum_{i=1}^{p} x_{ij}, x_{ij}')^d \tag{3.23}$$

For a Radial basis kernel function, $K\langle x, x_i' \rangle$ is given as

$$K\langle x, x_i' \rangle = \exp(-\gamma \; \sum_{i=1}^{p} (x_{ij} - x_{ij}')^2) \tag{3.24}$$

The equation of the support vector machine with a Radial based kernel function becomes;

$$F(x) = \theta_0 + \sum \alpha_i \exp(-\gamma \; \sum_{i=1}^{p} (x_{ij} - x_{ij}')^2) \tag{3.25}$$

Support Vector Regressor

When one is conversant with the support vector algorithm, understanding regression in a support vector machine is simple. The fundamental idea behind support vector regression is that the maximum margin is populated with data points, and the optimal data points inside the margin are used to establish a line of best fit, much like in linear regression. A corresponding y-value (prediction) is derived from the x-values (optimal data points) that generated the line of best fit in the maximum margin.

2.9.2 Artificial Neural Network

McCulloch and Pitts (1943) established the idea of the perceptron, an artificial neuron that serves as the fundamental component of an artificial neural network as seen in Fig. 2.23. The term 'Neural Network' was not only given as a biological name but because the activity was fashioned like that of the neurons in the human brain (Swamynathan, 2017).

An artificial neural network (ANN) is simply a mathematical depiction of the human brain whose underlying phenomenon was modelled after the characteristics and function of the human brain. While neuronal cells (roughly 1011) make up the brain, the neural network or brain is composed of about 10,000 connections between these cells, or neurons. The artificial neural network (ANN) imitates the natural neural network as seen in the brain by similarly connecting its artificial neurons (Kukreja *et al.*, 2016).

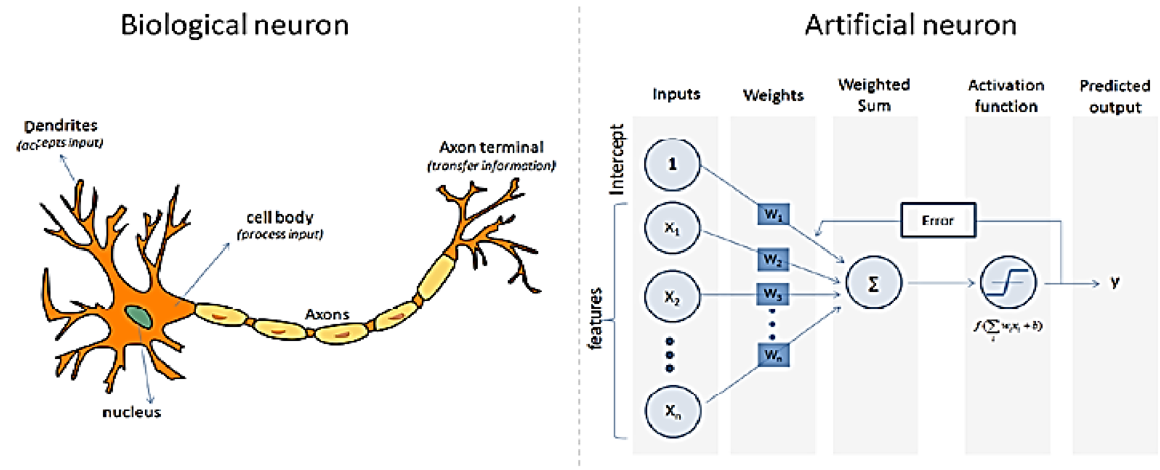

Fig 2.23 Similarities between the natural neural network and the artificial neural network (Swamynathan, 2017).

It is significant to note that by altering the basic components of the neural network architecture, we modify how the neural network computes results, how it connects to other networks, and how it uses input values. Consequently, this alters how the network learns and affects how accurate the predictions are (Michelucci, 2018).

Assume you have a real number input where $\mathrm{w}_i \in R$ with $i = 1,2,\dots.,n_x$. Here, the number of input variables is n_x and $i \in N$ (set of integers). The neural network aims to apply a function to a linear combination of all inputs. Mathematical equations for the neural network algorithm are seen below.

$$z = \mathrm{w}_1 x_1 + \mathrm{w}_2 x_2 + \cdots \dots + \mathrm{w}_{m_x} x_{m_x} + b \quad (3.26)$$

An output y will then be produced by applying a function f to z.

$$y(k) = f(z) = f(\textstyle\sum_{i=0}^{m} \mathrm{w}_i(k).\, x_i(k) + b) \quad (3.27)$$

Where b is a modifiable value called bias

$x_i(k)$ represents input value in discrete time k where i goes from 0 to m

$\mathrm{w}_i(k)$ represents weight value in discrete time k where i goes from 0 to m

f is an activation function.

$y(k)$ is the predicted value in discrete time k

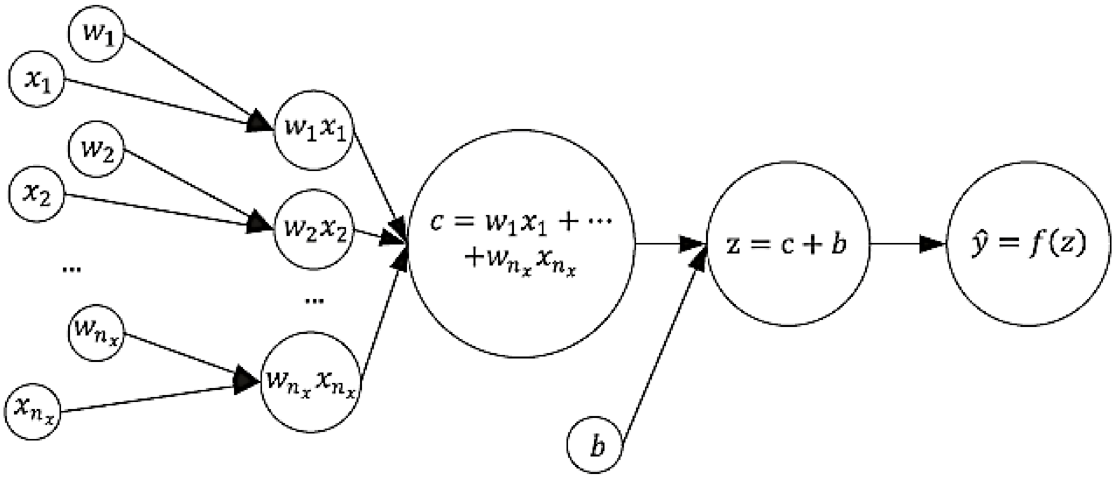

Fig 2.24. The computational diagram for the neural network is described above (Michelucci, 2018).

Components of the artificial neural network

1. **Input Layer**; Just like the human biological neuron possesses dendrites that receive signals externally for processing, the artificial neural network also has multiple input layers that are responsible for accepting training samples as a row vector $(x_1, x_2, x_3 .. x_m)$ or a column vector $(x_1, x_2, x_3 .. x_m)^T$. When computing a neural network, it is important to note that having too many input parameters will considerably slow down the learning process, but the training accuracy will significantly increase. The input layer has a collection of synapses, or connecting links, each of which is distinguished by a weight as seen in Fig. 2.23.
2. **Hidden layer**; The hidden layer is the second point of contact in the neural network architecture. It serves as an intermediary between the input layer and the output layer with the sole responsibility of applying weights to inputs and directing the product through an activation function. The hidden layer also utilizes information stored in the input layers. According to Jayasinghe *et al.* (2022), too many hidden neurons will cause over-fitting, and minimal hidden layers will not be able to capture the function's underlying behaviour. Hence, the optimal numbers of hidden layers and neurons present in a neural network may be largely decided by a trial-and-error process or by cross-validation.

   According to Haykin (2009), the activation function, also known as a squashing function, limits the acceptable amplitude range of the output signal to a certain finite value, hence restricting the amplitude of a neuron's output. Haykin (2009) also added that the output of a neural network is largely dependent on the nature of the activation function $(\varphi(v))$ in the neural network, in terms of the induced local field v. Hence, the common activation functions adopted in building a neural network architecture are found below.

- Sigmoid function; The most typical type of activation function utilized in the creation of neural networks is the sigmoid function, whose graph is "S"-shaped. It is regarded as a strictly increasing function with a fine balance between linear and nonlinear behaviour. The expression is given by;

$$\varphi(v) = \frac{1}{e^{(-av)}+1} \tag{3.28}$$

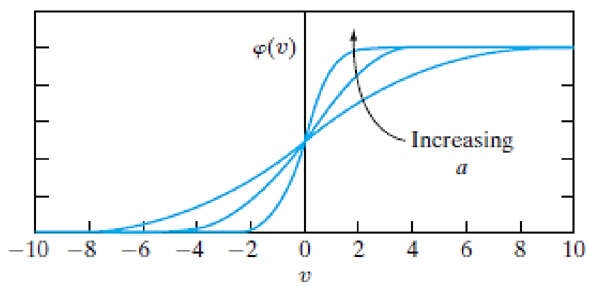

Fig 2.25. Sigmoid function for varying slope parameter a (Haykin, 2009)

- Purelin activation function; is a linear activation function whose range of function has an unlimited number of points, and it has no impact on how sophisticated the data set could be (Aldakheel *et al.*, 2021). The expression is given by;

$$f(x) = x \tag{3.29}$$

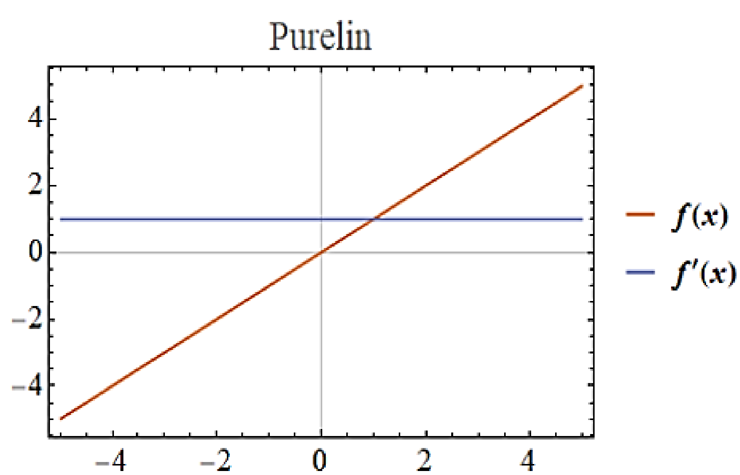

Fig 2.26. The Graph of Purlin Activation Function (Aldakheel *et al.*, 2021).

- The threshold function; also known as a heavy side function, is given as;

$$\varphi(v) = \begin{cases} 1 \; if \; v \; \geq 0 \\ 0 \; if \; v \; < 0 \end{cases} \tag{3.30}$$

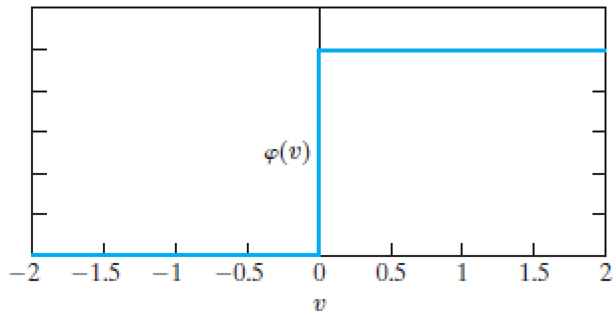

Fig 2.27. Threshold function (Haykin, 2009)

Some other activation functions include hyperbolic tangent activation function, Rectified linear activation (ReLu) and leaky ReLu.

3. Output layer; The results of the neural network computation are given by the output layer.

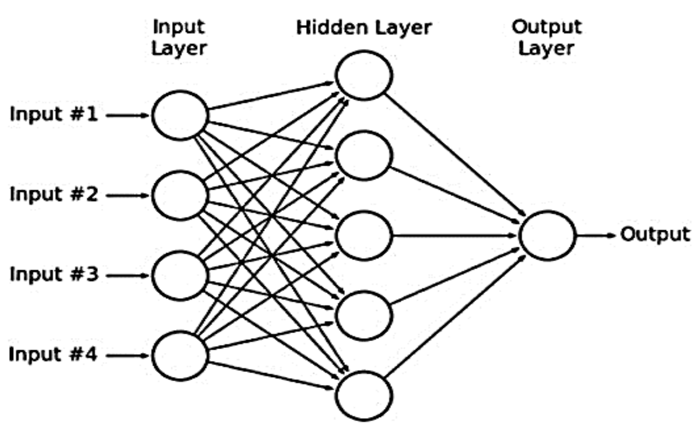

Fig 2.27. Typical architecture of the ANN (Aldakheel, Satari, & Wriggers, 2021).

One of the advantages the neural network has over alternative machine learning algorithms is its ability to overcome the limitation of a single perceptron as it is composed of many perceptrons that are connected in various ways and acting on various activation functions to provide improved learning mechanisms. The training sample propagates forward through the network and the output error is back-propagated. The computation error is minimized by applying the gradient descent approach, which will calculate a loss function for all the weights in the network and re-compute in epochs (Swamynathan, 2017).

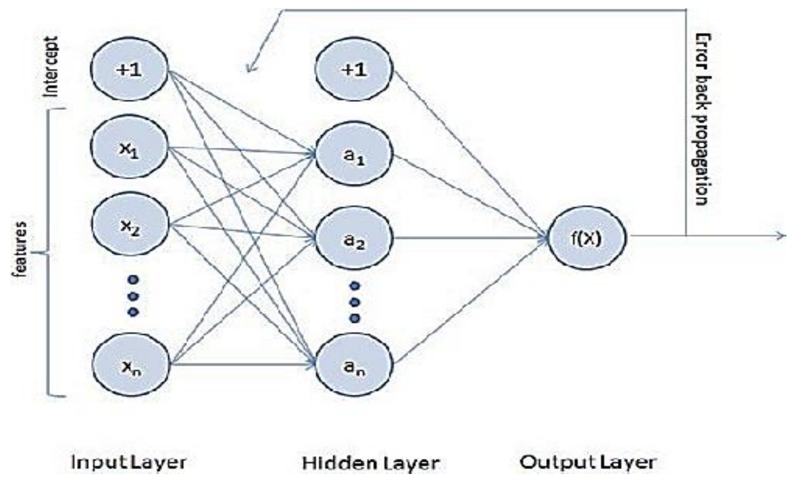

Fig 2.28. Multilayer perceptron representation with error backpropagation (Swamynathan, 2017).

2.9.3 Decision Tree

The decision tree is an algorithm based on the information theory concept developed by Shannon (1948). The entirety of the tree-based model is concerned with measuring the purity of information only. In machine learning, a statistical decision tree is used for modelling choices and outcomes based on some conditions. The Breiman *et al.* (1984) CART algorithm serves as the foundation for the Decision Tree Regressor. However, the decision trees now in use make use of a modified version of Quinlan's (1993) C4.5 algorithm.

A leaf node and an internal/decision node, which includes a root node, make up a decision tree. A root node is first initialized, after which it is divided into sub-trees. According to the splitting criteria, such as information gain, Gini impurity, and entropy for classification tasks, or Mean Squared Error (MSE), and Poisson for regression tasks, the optimal split is established. Based on the terminating requirements, the splits are categorized as either terminal/leaf nodes or decision/internal nodes. Each internal node is then processed independently till there are no internal nodes to separate, and this procedure continues.

Terminologies in Decision trees

1. Node splitting; means the data stored at a node is split based on some threshold condition. The threshold condition is determined by the quality of measured information with the help of the information measurement indexes such as Gini impurity, Mean squared error and Poisson.
2. Terminal/leaf node; there is no splitting beyond the terminal node. At this node, a decision is taken. The terminal node has the same function as the output layer in neural networks.

3. Pruning; is the act of reducing the depth of the decision tree by cutting off some nodes that do not meet the threshold condition. To reduce the complexity and avoid overfitting, pruning is applied.

Information theory metrics & equations

1. Gini impurity; Gini impurity is a mathematical measurement index whose concept is based on probability. It is a mathematical measurement that shows how pure the information in a dataset is. Concerning classification, G.I measure some mathematical information and based on that, we can deduce how pure a dataset is or the degree of class uniformity in the dataset.

   For a set of classes (C), for a given dataset (Q)

   $$G(\mathrm{Q}) = \sum_{c \epsilon C} P_c (1 - P_c) \quad (3.31)$$

   $$P_c = \frac{1}{N_{\mathrm{Q}}} \sum_{x \epsilon \mathrm{Q}} (y_{class=} c) \quad (3.32)$$

2. Entropy; entropy is a measure of disorderliness or randomness. In terms of impurity, entropy is used to increase purity by decreasing the randomness of impurity. Given by

   $$E(s) = -p_A . \log_2 P_A - p_B . \log_2 P_B \quad (3.33)$$

3. Information Gain; the concept of information gain is that it measures the reduction in uncertainty and it is a deciding factor for what particular node would be the root node. Information gain value increases as the uncertainty reduces. Information gain is defined in form of entropy and given by;

   $$I = E(Y) - E(Y/X) \quad (3.35)$$

   $E(Y)$ = Entropy of the full dataset

   $E(Y/X)$ = Entropy of the dataset based on some feature X

4. Mean Squared error; for regression problems, the CART algorithm uses the mean squared error to determine the prediction accuracy with respect to a feature as the root node. The mean squared error should be minimal at the terminal node.

   $$MSE = \frac{1}{n} \sum_{i=1}^{n} (Y_i - \widehat{Y}_i)^2 \quad (3.35)$$

The Scikit learn machine learning library included some other splitting criteria for regression tasks such as Friedman MSE, Absolute Error and Poisson.

The main goal of the decision tree or random forest in classification is to maximize information gain and minimize both Gini impurity and entropy. In regression, the goal is to minimize all the error metrics.

2.9.4 Random Forest

Breiman (2001a), who was motivated by the previous work of Amit and Geman (1997), developed the random forests algorithm. Random Forests were created as an alternative to boosting and are an extension of Breiman's bagging concept (Breiman, 2001b). The random forest is an extension of the decision tree model, researchers developed the random forest algorithm to improve the performance of the decision tree model. The shortcoming of the decision tree that led to the development of the random forest model was that the decision tree algorithm does not learn based on all of the features in a dataset and it is also prone to overfitting, but the random forest takes all of the features into consideration for learning and it is not sensitive to overfitting.

The random forest is an ensemble learner. Ensemble means the combination of multiple algorithms to be compounded as one. Concerning random forest, it would mean the combination of multiple decision trees built on different features selected at random. It is important to note that the same hyperparameters and principles that apply in the decision tree model also apply in the random forest model, but the improvement required that some new concept be introduced in the model.

The idea behind the random forest was to create multiple trees from randomly selected subsets of a dataset. By doing this, we explore and include the entire feature space and this results in an ensemble of various decision trees.

Main Concepts of Random Forest

1. Bootstrapping; suppose we have individual features x_1, x_2, x_3, x_4, x_5 belonging to a dataset C, the decision tree algorithm tries to select a single feature and with the help of the information measurement metrics, we can determine the root node and split based on just that single feature, but in Random Forest, all of the features are considered in building a tree. The bootstrapping concept simply means a random sampling with a replacement that is separate from the conventional stratified sampling. Bootstrapping helps to reduce the correlation and multi-collinearity in the generated trees since we require diverse configurations of decision trees. Random forest models with bootstrapping generalize in a better way since strong learners are generated.
2. Bagging; bagging involves two concepts, bootstrapping and aggregating. Results at the leaf node of every tree generated through bootstrapping are averaged, and then a single outcome is derived.
3. Other features such as N-estimators (Number of decision trees required to build a forest), max features (Number of features in a randomly selected subset of a dataset) and OOB-score (out-of-bag error) are also introduced in the random forest model.

In Fig. 2.9, a schematic representation is presented that outlines the sequential procedures involved in the application of the random forest algorithm to a dataset, with the primary objective of predicting a continuous variable. The algorithm involves constructing multiple decision trees, each using a randomly selected subset of input variables and observations, and then averaging the outputs to reduce the variance of the model. The model is then trained on a subset of the data, and the remaining data are used to evaluate the model's accuracy. This iterative process is repeated until a satisfactory level of prediction accuracy is achieved.

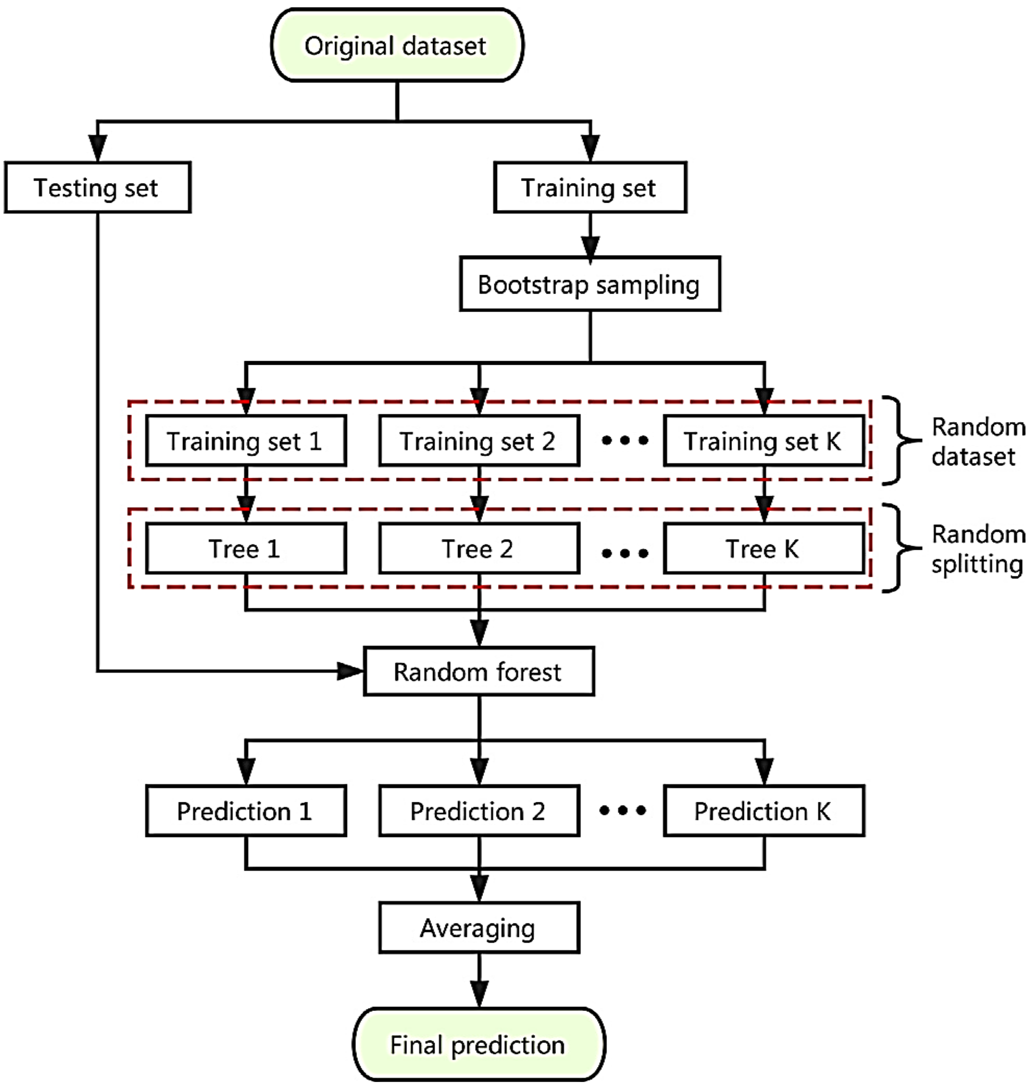

Fig 2.29. Schematic of random forest generation and prediction (Han *et al.*, 2019)

CHAPTER 3

RESEARCH METHODOLOGY

3.1 Data Collection & Analysis of Database

The ACI-DafStb shear database collected and compiled by Reineck *et al*. (2013) was utilized in this study to deterministically analyze the shear strength equations presented by the various national codes of design for structural concrete, Authorial models and machine learning-based models considered in this research. The shear database is characterized by shear strength resulting from experimental observation of simply supported reinforced concrete beams without stirrups. Geometric consideration of the beam specimen used in the experimental derivation of the shear strength values includes; Rectangular beams, T-section Flanged beams and I-section Flanged beams. To include data points that demonstrate only a practical parametric range of features in the dataset, some test results with an impracticable range of beam properties were filtered out. Hence, the test results did not have any form of bias.

Table 3.1 shows the criteria on which the collected shear test data was carefully filtered

Table 3.1 Criteria for excluding an experimental test in ACI-DafStb shear database

Beam Properties	**Criteria**
Compressive strength ($\boldsymbol{f_c}$)	< 10Mpa
Beam Width ($\boldsymbol{b_w}$)	<50mm
Shear Span – Effective Depth Ratio **(a/d)**	<2.4
Longitudinal Reinforcement percentage ($\boldsymbol{\rho l}$)	<0.139%
Effective Depth **(d)**	<57.2mm

The shear span to effective depth ratio (a/d) was not allowed to be less than 2.4 to avoid the effect of arch-action in the case of deep beams. Each beam specimen was characterized by the same mode of failure, diagonal tension shear failure. For longitudinal reinforcement, the selection process was automatically controlled by the ratio of allowable reinforcement ratio since shear failure cannot occur in over-reinforced concrete due to the premature crushing of concrete at the web region. A total of 224 data points were eliminated from the 1008 experimental shear test set. After the selection process was concluded, the database was finally built with 784 test results.

Table 3.2. Descriptive Statistics of Dataset

	$b_w(mm)$	a/d	$d(mm)$	$\rho l\%$	$f_{ck}(Mpa)$	$V(KN)$
Counts	784.00	784.0	784.00	784.0	784.00	784.00
Mean	218.54	3.50	345.50	2.2	35.32	98.10
Std, Dev	207.10	1.00	303.30	1.1	21.09	124.00
COV	0.95	0.29	0.88	0.5	0.60	1.26
Minimum	50.00	2.40	57.20	0.1	8.90	7.20
25%	150.00	2.90	204.60	1.2	22.23	41.22
50%	153.00	3.20	268.20	1.9	28.00	61.05
75%	203.00	4.00	336.00	2.7	39.42	106.15
Maximum	3005.00	8.10	3,000.0	6.6	135.00	1,308.40

Across all parameters, the dataset provided by Reineck *et al*. (2013) displays a high value of standard deviation which implies that the dataset has a wide scatter of parametric properties. Hence, the distribution of this dataset is suitable for the practical investigation of the shear models across a variety of parametric properties.

$$\sigma = \sqrt{\frac{\sum(x_i - \mu)^2}{N}}$$

σ = Dataset standard deviation

N = Size of the dataset

x_i = Singular data-point

μ = Mean of the dataset

From the table above, it can be seen that 588 test-data has effective beam depth (d) less than 336mm which is representative of the 75th percentile of the dataset, while 25% of the distribution has a percentage longitudinal ratio greater than 2.7%. The distribution of the shear span to effective depth ratio shows that the dataset is largely characterized by slender beams as 25% of the distribution has a slenderness ratio of less than 2.9 with a minimum value of 2.4.

3.2 Regression and correlation

Regression is a statistical method of determining the character and strength of the relationship between two numerical variables. Regression analysis can be easily carried out with a scattered plot. A scattered plot is a graph that shows the relationship between two quantitative variables either dependent and independent or non-dependent variables measured from a data population. The scattered plots below give a graphical representation of the relationship between the parameters that affect shear strength and the normalized experimental shear strength.

Normalization was done as a form of data pre-processing to scale down the existing range of data to a new range, thereby effectively managing the large variation in the dataset and bringing them closer. Fig. 3.1 shows the distribution of the experimental shear strength, and it can be seen that the data do not follow a perfect gaussian distribution, hence there is a need to scale the data before it can be used.

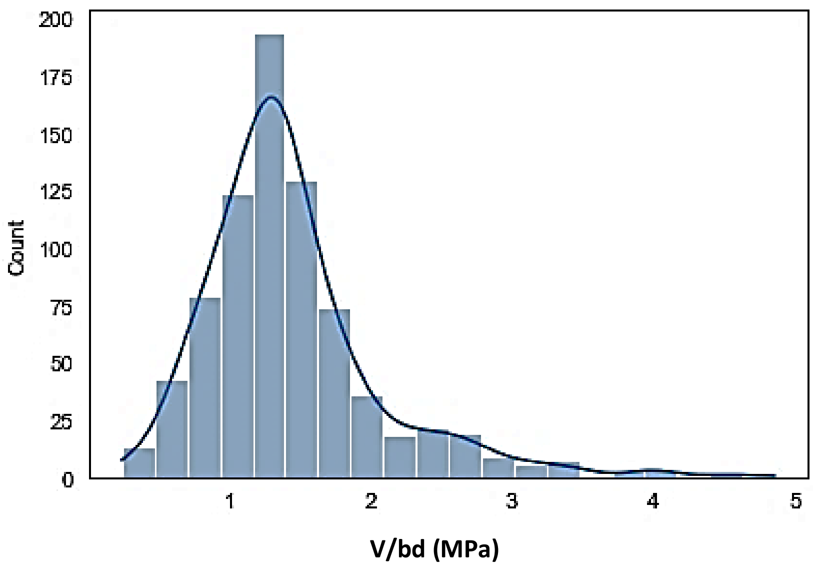

Fig 3.1 Distribution of normalized experimental shear strength (MPa)

Fig.3.2 infers that concrete strength mildly affects the shear strength. The gentle positive slope depicts that for every 20MPa increase in concrete compressive strength, there is a mild increase in the shear strength.

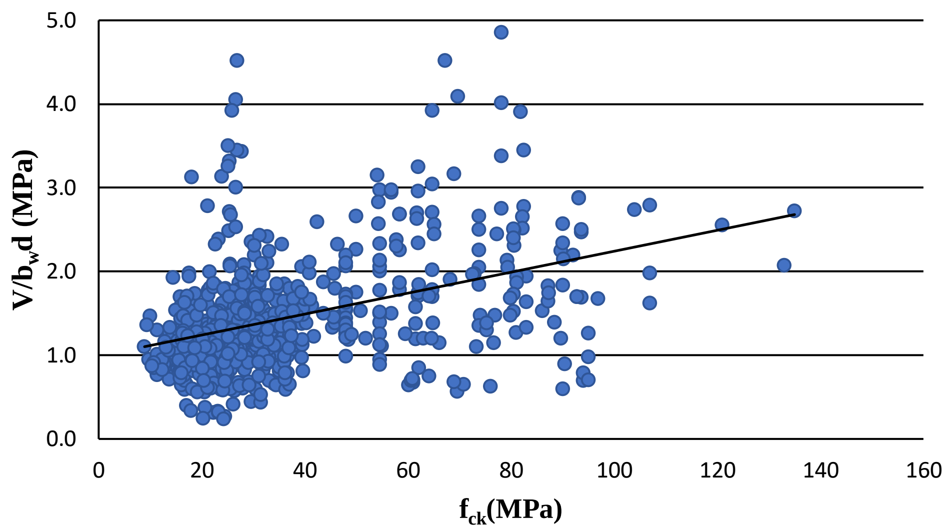

Fig 3.2 Scatter plot of normalized experimental shear strength against concrete strength MPa

In the compression chord capacity model developed by Cladera *et al.* (2016), the concrete strength was limited to 60MPa due to an observed large variability in the shear strength of members with high concrete compressive strength (Cladera *et al.*, 2019). Also from the plot, it was noticed that the shear strength is clustered when the concrete strength is within the range (8.90MPa- 40MPa), a large variability is noticed when concrete strength exceeds 60MPa.

The effective depth (d) plot against the normalized shear strength in Fig. 3.3 shows that the two parameters are inversely correlated. For every increase in the depth of beams provided in the database, there is a visible decrease in the experimental shear strength. The observable relationship between the aforementioned parameters in the database coincides with the experiment conducted by Slowick & Nowicki (2012), and the explanation of the size effect put forward by Collins & Kuchma (1999) and Reineck (1999).

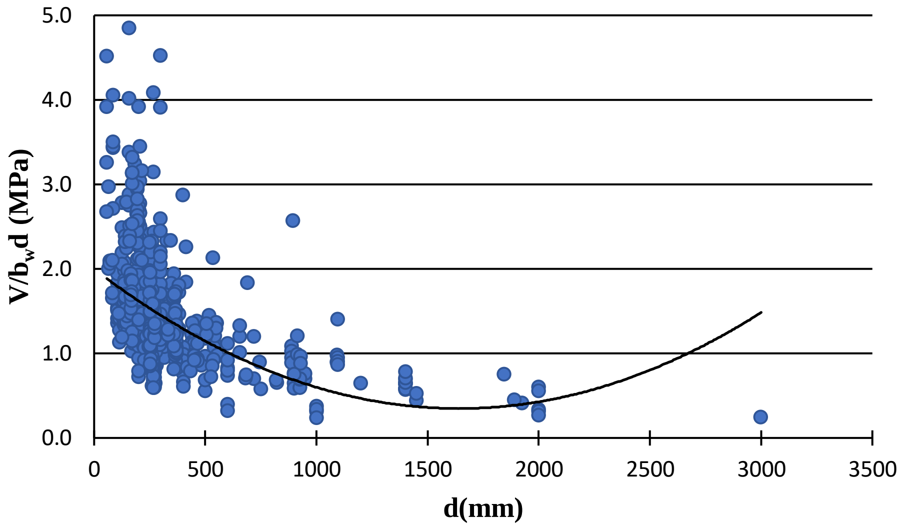

Fig 3.3 Scatter plot of normalized experimental shear strength against effective depth d

The scattered plot of the normalized experimental shear strength against the percentage of longitudinal reinforcement shows variability in the distribution of the experimental shear strength as the longitudinal reinforcement increases. From Fig. 3.4, it is seen that the response variable has a small scatter when the reinforcement ratio is between 0.139% - 2%, and a large variability is seen when the reinforcement ratio exceeds 2%. The EC2 adopts this practice in the modelling of empirical shear strength formula for beams without stirrups as they limit the percentage of longitudinal reinforcement ratio to 2%. Generally, the concrete strength increases as the reinforcement ratio increases, the 2% limitation may be as a form of control to avert web crushing due to over-reinforcing.

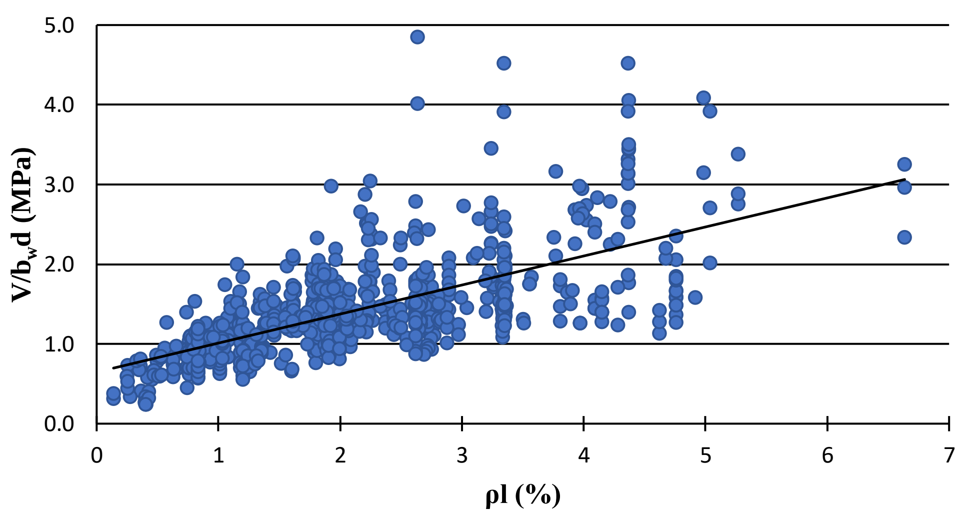

Fig 3.4 Scatter plot of normalized experimental shear strength against $\rho l(\%)$

Fig. 3.5 indicates there is an inverse relationship between the normalized experimental shear strength and the shear span-to-depth ratio. A decrease in the shear span to effective depth causes an increase in the shear strength. This indicates that a/d significantly affects shear strength. 5% of the experimental database is dominated by arch action, this is because their shear span – effective depth ratio is less than 2.5. Hence, for those 40 test points, an increased shear resistance can be seen from the plot below.

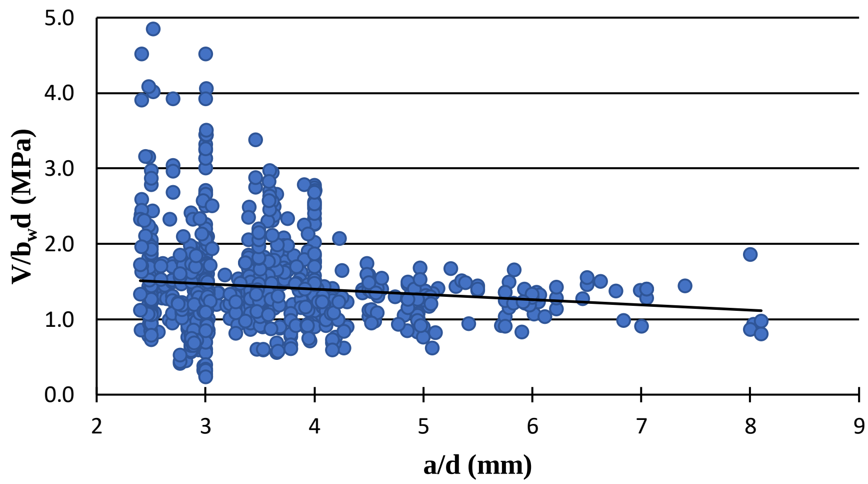

Fig 3.5 Scatter plot of normalized experimental shear strength against shear span/depth a/d

The plot below shows the relationship between the width of a beam and the normalized strength and a negative trend can be observed from the plot of both parameters.

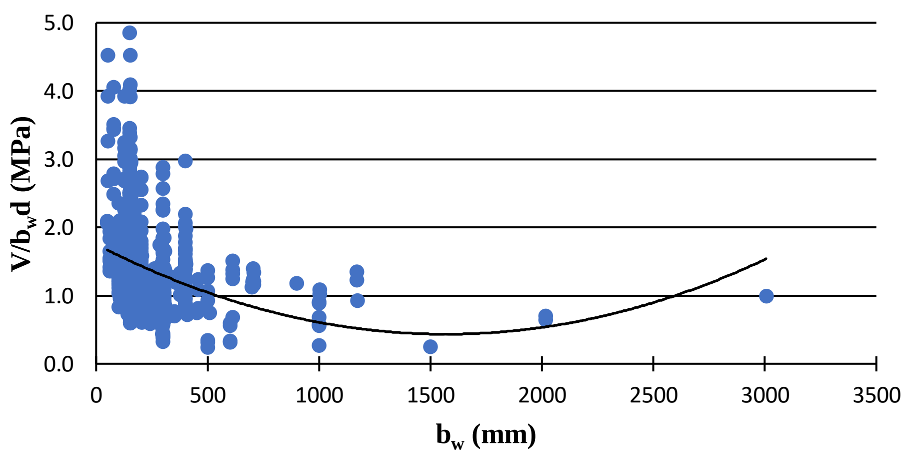

Fig 3.5 Scatter plot of normalized experimental shear strength against shear span/depth a/d

3.3 Coefficient of correlation

Correlation is a term used to explain the linear relationship that exists between two quantitative variables in terms of magnitude (strength) and direction. Correlation can be identified by carefully observing the slope of a scattered plot, a steep slope depicts a strong correlation with a high coefficient value, while a gentle slope indicates that there is no significant observable linear relationship between variables, hence a weak coefficient value. The value of the correlation coefficient can be deterministically measured with the correlation equation below;

$$r = \frac{1}{(n-1)s_x s_y}\sum(x_i - \mu_x)(y_i - \mu_y)$$

Where, n = Sample size

μ_x = Mean of variable X

μ_y = Mean of variable Y

s_x = Standard deviation of variable X

s_y = Standard deviation of variable Y

x_i = datapoint of variable X

y_i = datapoint of variable Y

The heatmap diagram in Fig. 3.6 displays and annotates the correlation between the factors that affect the shear strength of beams without transverse reinforcement. The heatmap is representative of the database provided by Reineck *et al*. (2013). From the diagram, it can be seen that the factors that affect shear strength are poorly correlated with each other. A typical example is the correlation between the effective depth of the beam and the concrete strength, which has a negative coefficient of correlation of less than 1% and no visible significant trend in the slope. Generally, the concrete compressive strength shows a poor correlation with other shear parameters. The inability to understand and establish a relationship between shear parameters as seen in the heatmap diagram is largely a contributing factor to the formulation of shear models and the variation in shear strength estimation.

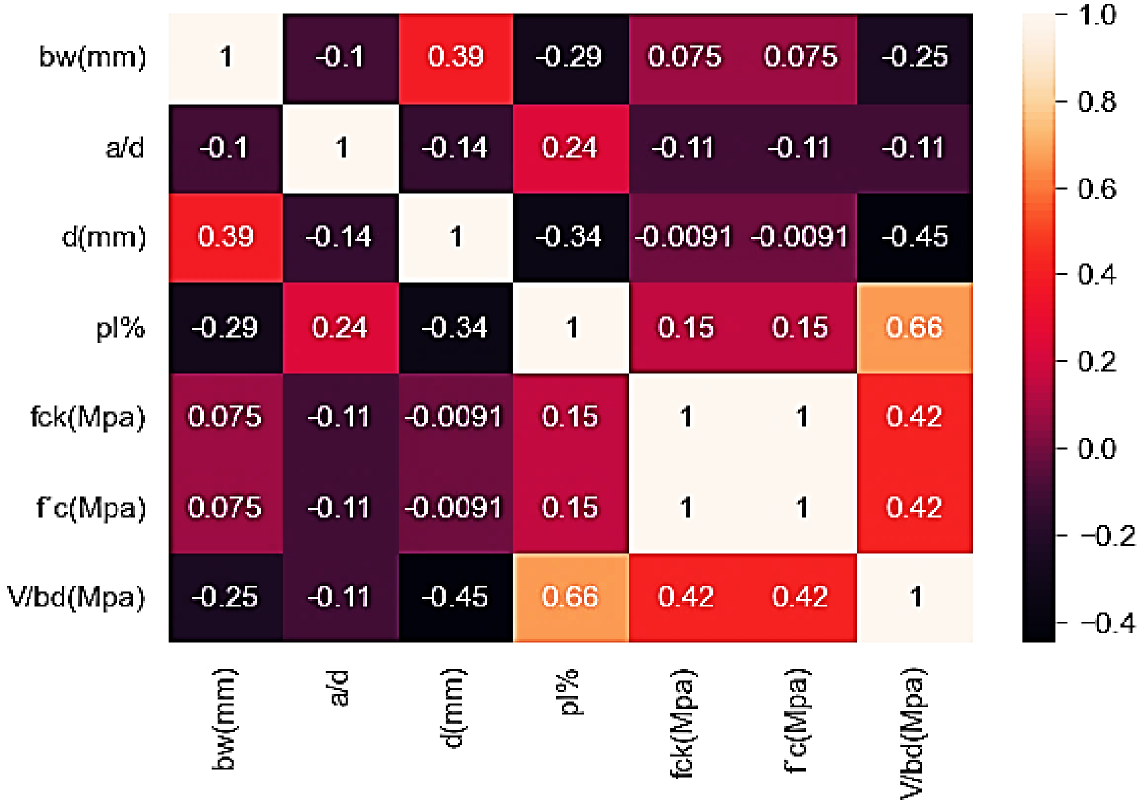

Fig 3.6 Heatmap showing poorly correlated shear parameters

Table 3.3 below shows how the shear parameters are correlated with the experimental shear strength in terms of strength and direction. The Table clearly shows that the shear strength of beams without shear reinforcement is mostly sensitive to the longitudinal reinforcement ratio, effective beam depth and the shear span- effective depth ratio. A positive 66% coefficient of correlation between the experimental shear strength and the longitudinal reinforcement ratio in the database indicates that for most of the test points, an increase in the longitudinal reinforcement leads to a corresponding increase in experimental shear strength. This trend can be classified as a fairly strong trend due to the correlation value.

From the literature, it has been established that as the depth of reinforced concrete beams increases, the shear strength decreases, this also holds for the dataset collected by Reineck *et al*. (2013). A negative 45% Coefficient of correlation between the experimental shear strength and the effective depth suggests that as the effective depth increases, the response of the experimental shear strength is such that it moderately decreases. The same can be said for the concrete compressive strength, but with a positive correlation. Information deduced from the database provided by Reineck *et al.* (2013) shows that the experimental shear strength is weakly correlated with the shear span-effective depth ratio (a/d) and the beam width. It should be noted that increasing the longitudinal percentage is not necessarily a good practice as some code of design limits its value to 3% to avoid premature web crushing.

Table 3.3. Correlation Of Shear Parameters with Shear Strength

Parameter	Coefficient of Correlation (%)	Direction
Shear span-depth ratio (a/d)	11	Negative
Effective depth (d)	45	Negative
Longitudinal reinforcement ratio ($\boldsymbol{\rho l}$%)	66	Positive
Compressive strength ($\boldsymbol{f_{ck}}$)	42	Positive
Beam width (b)	25	Negative

3.5 Deterministic analysis of shear resistance

A mean and design value deterministic analysis is a requisite for reliability investigation.

3.5.1 Mean value analysis

Mean value analysis provides us with the best estimate prediction of the shear strength from the models considered. All forms of bias are removed when conducting a mean value analysis thereby leaving us with a true prediction of shear from the models considered. To obtain mean value predictions, the characteristic values of concrete properties f_{ck}, f_c' are expressed at their mean value f_{cm} and partial factor of safety is taken as 1 or completely ignored.

EC2 and Fib Model Code 2010 suggest the relationship seen below for determining the mean value characteristic strength of concrete (f_{ck}).

$$f_{cm} = f_{ck} + 8MPa$$

f_{cm} = Mean value of concrete compressive strength (MPa)

f_{ck} = Characteristic cylinder strength of concrete compressive strength.

Some National codes of design such as ACI 318 and AS3600 do not include the characteristic value (f_{ck}) of concrete cylinder strength in their shear formulation, instead a special characteristic strength of concrete at 28 days (f_c') was used. To analytically relate the relationship between f_c' and f_{cm}, the database provided by Reineck *et al*. (2013) was thoroughly investigated and it was observed that the expression below holds in identifying the relationship between the two parameters.

$$f_c' = f_{ck} + 1.6MPa$$

From $f_{cm} = f_{ck} + 8MPa,$ it can be deduced that, $f_{ck} = f_{cm} - 8MPa$

By substituting f_{ck} into f_c' equation, we arrive at;

$$f_{cm} = f_c' + 6.4MPa$$

Special consideration was taken for the SANS 10100-1. (2000). The cube characteristic strength of concrete was used in the formulation of the shear model. Hence, a relationship between f_{cu} and f_{cm} has to be established. The strength and deformation characteristics for concrete in Table 3.4 given by EC2 show an analytical relation with values to derive concrete cylinder strength from concrete mean strength.

Table 3.4. Strength Classes for Concrete (MPa)

f_{ck}	**12**	**16**	**20**	**25**	**30**	**35**	**40**	**45**	**50**	**55**	**60**	**70**	**80**	**90**
f_{cu}	15	20	25	30	37	45	50	55	60	67	75	85	95	105
f_{cm}	20	24	28	33	38	43	48	53	58	63	68	78	88	98
f_{ctm}	1.6	1.9	2.2	2.6	2.9	3.2	3.5	3.8	4.1	4.2	4.4	4.6	4.8	5.0

For concrete class less than C50/60, the analytical expression for the mean concrete tensile strength is given as; $f_{ctm} = 0.30(f_{ck}^{2/3})$

For concrete class greater than C50/60, the analytical expression for the mean concrete tensile strength is given as;

$$f_{ctm} = 2.12(\ln(1 + (f_{cm}/10)).$$

The process for the mean value deterministic analysis of all code-based models and authorial models is illustrated in the figure below.

(Step1); Unbiased shear strength estimation for diagonal tension failure (V_u)

- *To determine the mean capacity of shear resistance for all models considered using the database that comprises experimental setup across all parametric ranges with failure due to diagonal tension failure.*

Input Parameters

1. Geometric properties and mean value of concrete properties (where applicable)

$f_{cm} = f_{ck} + 8Mpa,\ f_{cm} = f_c' + 6.4Mpa$

$f_{ctm} = 2.12(ln(1 + (f_{cm}/10)),\ f_{ctm} = 0.30(f_{ck}^{2/3})$

2 Equating partial factor of safety (γ_c) =1

Shear model evaluation

- *EC2 mean shear value prediction* ($\boldsymbol{V_{EC}}$) *– obtained using equation 2.3*
- *ACI 318-19* ($\boldsymbol{V_{ACI}}$)*- obtained using equation (C) in table 2.1*
- *AS 3600-2018* ($\boldsymbol{V_{AS}}$) *- obtained using equation 2.14*
- *SANS10100-1(2000)* ($\boldsymbol{V_{SANS}}$) *- obtained using equation 2.28*
- *MC 2010 (LOA II)* ($\boldsymbol{V_{MC-10(II)}}$) *- obtained using equation 2.31*
- *CCC Model* ($\boldsymbol{V_{CCC}}$) *- obtained using equation 2.55*
- *MASM* ($\boldsymbol{V_{MASM}}$)*- obtained using equation 2.43 – 2.45*
- *Modified SNiP code* ($\boldsymbol{V_{SNiP}}$) *- obtained using equation 2.70*
- *Ngoc Tran's Mechanical Model* ($\boldsymbol{V_{NLT}}$) *- obtained using equation 2.93*

(Step 2); Model Inference Comparison

- *Comparative analysis between the mean shear value of investigated models and experimental shear strength.*
- *Assessment of mean value predictions for specific test sections across a varied range of beam depth, concrete strength, shear span-effective depth ratio and longitudinal reinforcement.*

(Step 3); Contemplate the possible result

Visualize plots, discussions and observations.

Fig 3.7 Mean value deterministic analysis procedure

3.5.2 Design value analysis

For all shear models considered in this study, only the **EC2, SANS10100, MC10** and **CCC** express shear strength in both mean value and design value. When the shear strength is expressed in its design value, this means all form of design bias has been included in the shear model calculation thereby providing a more conservative estimation. It should be noted that the design value analysis does not give the true calibration of shear model performance.

Design values of material properties are derived deterministically by treating characteristic values of concrete as random variables and using them together with a partial factor of safety as input parameters.

$$f_{cd} = \frac{f_{ck}}{\gamma}, f_{\mathrm{ywd}} = \frac{f_{\mathrm{ywk}}}{\gamma}$$

The design value of any resistance model takes the format;

$$V_{Rd} = R\left[\frac{X_k}{\gamma_m}; a_d\right]$$

V_{Rd} represents the design resistance, X_k is the characteristic values of the material property, η conversion factor appropriates to the material property and a_d is the design geometric parameter.

Fundamental variables such as the geometries, steel percentage ratio and area of steel generally have their safety factored to be 1.0.

The procedure for the design value deterministic analysis of all code-based model and authorial model that uses design value is illustrated in the figure below.

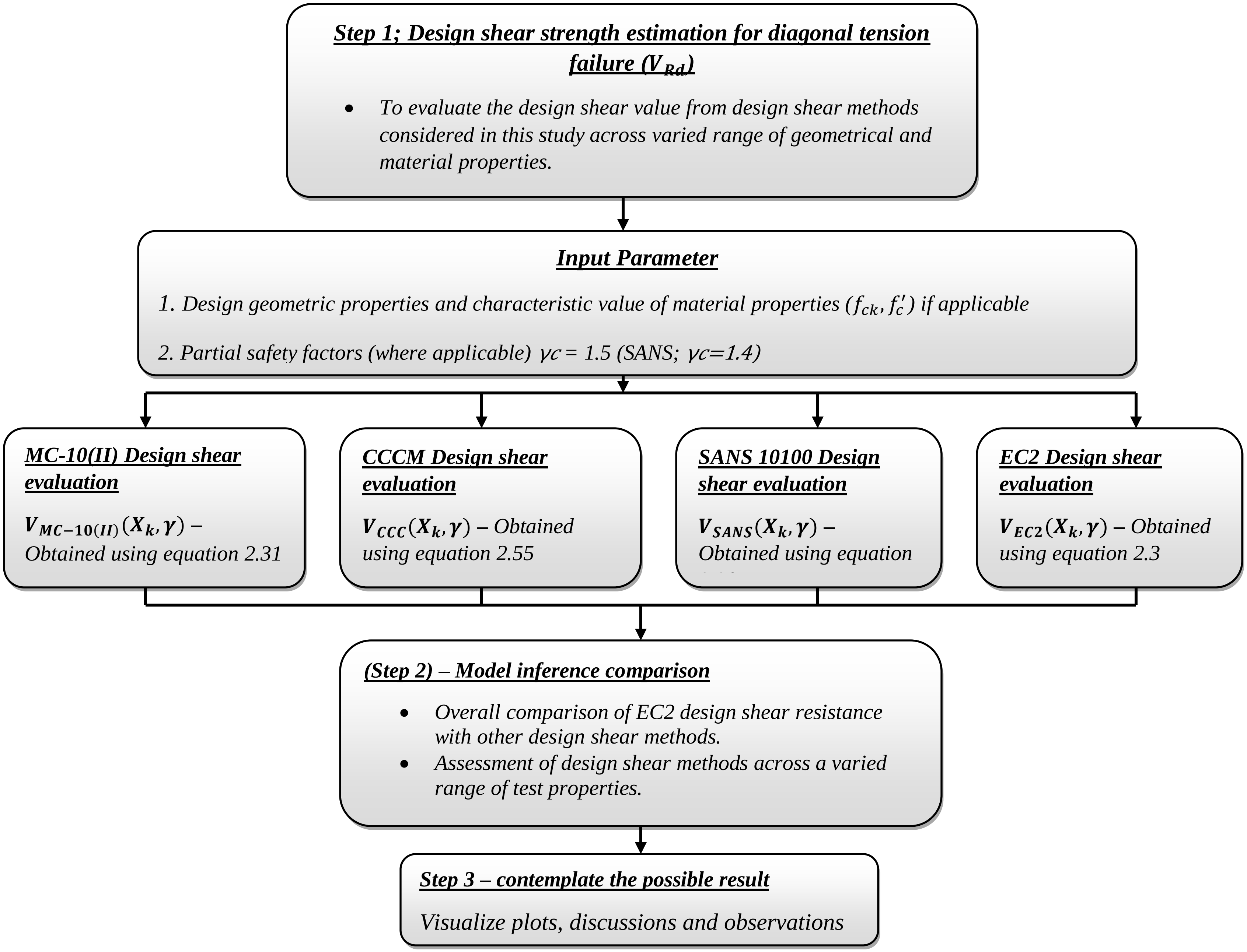

Fig 3.8 Design value deterministic analysis procedure

3.6 Machine learning model building and evaluation

In the study by Reinick et al. (2013), a total of 784 experimental setups were conducted. Of these, 588 experimental setups (75% of the total data) were randomly selected as the training data using a random state of 101 in the Scikit-learn framework. The selected training data was then used to train machine learning (ML) models across a 5-fold cross-validation with varying hyperparameters. The remaining 196 experimental setups (25% of the total data) were also randomly selected at a random state of 101 to serve as the testing data, which was then used to evaluate the predictive performance of the trained ML models.

Table 3.5. Descriptive statistics of the testing dataset for ML models

	$b_w(mm)$	a/d	$d(mm)$	$\rho l\%$	$f_{ck}(Mpa)$
Counts	196.00	196.0	196.00	196.0	196.00
Mean	222.57	3.49	343.55	2.2	33.81
Std, Dev	203.60	0.94	314.28	1.2	20.35
COV	0.92	0.27	0.92	0.55	0.60
Minimum	60.00	2.41	84.00	0.254	10.28
25%	150.00	2.90	191.30	1.3	22.15
50%	152.00	3.05	258.60	1.9	27.58
75%	283.00	4.00	355.60	2.82	36.58
Maximum	2016.00	8.10	2,000.0	5.27	106.9

Following the machine learning procedure, the obtained shear result has to be evaluated to determine the model which learned the relationship between variables in the dataset accurately and predicted the target value (shear resistance) with minimal error. The evaluation was based on statistical metrics namely the coefficient of determination (R^2), mean absolute error (MAE), root mean squared error (RMSE) and mean absolute percentage error (MAPE).

- Root mean squared error (RMSE)

  RMSE = $\sqrt{\frac{1}{n}\sum_{i=1}^{n}(y-x)^2}$

- Mean absolute percentage error (MAPE)

$$\text{MAPE} = \frac{100}{n}\sum_{i=1}^{n}\left|\frac{y-x}{y}\right|$$

- Coefficient of determination (R^2)

$$R^2 = \left[\frac{\sum_{i=1}^{n}(x-x')\,(y-y')}{\sqrt{\sum_{i=1}^{n}(x-x')^2\,(y-y'\sum_{i=1}^{n}(x-x')^2\,(y-y'))}}\right]^2$$

- Mean absolute error (MAE)

$$\text{MAE} = \frac{1}{n}\sum_{i=1}^{n}|y-x|$$

where n is the number of observations, y is the experimental shear strength, x is the predicted shear strength from machine learning models, y' and x' are the mean values of y and x.

The procedure adopted for building the machine learning algorithm and predicting shear strength is illustrated in Fig. 3.9.

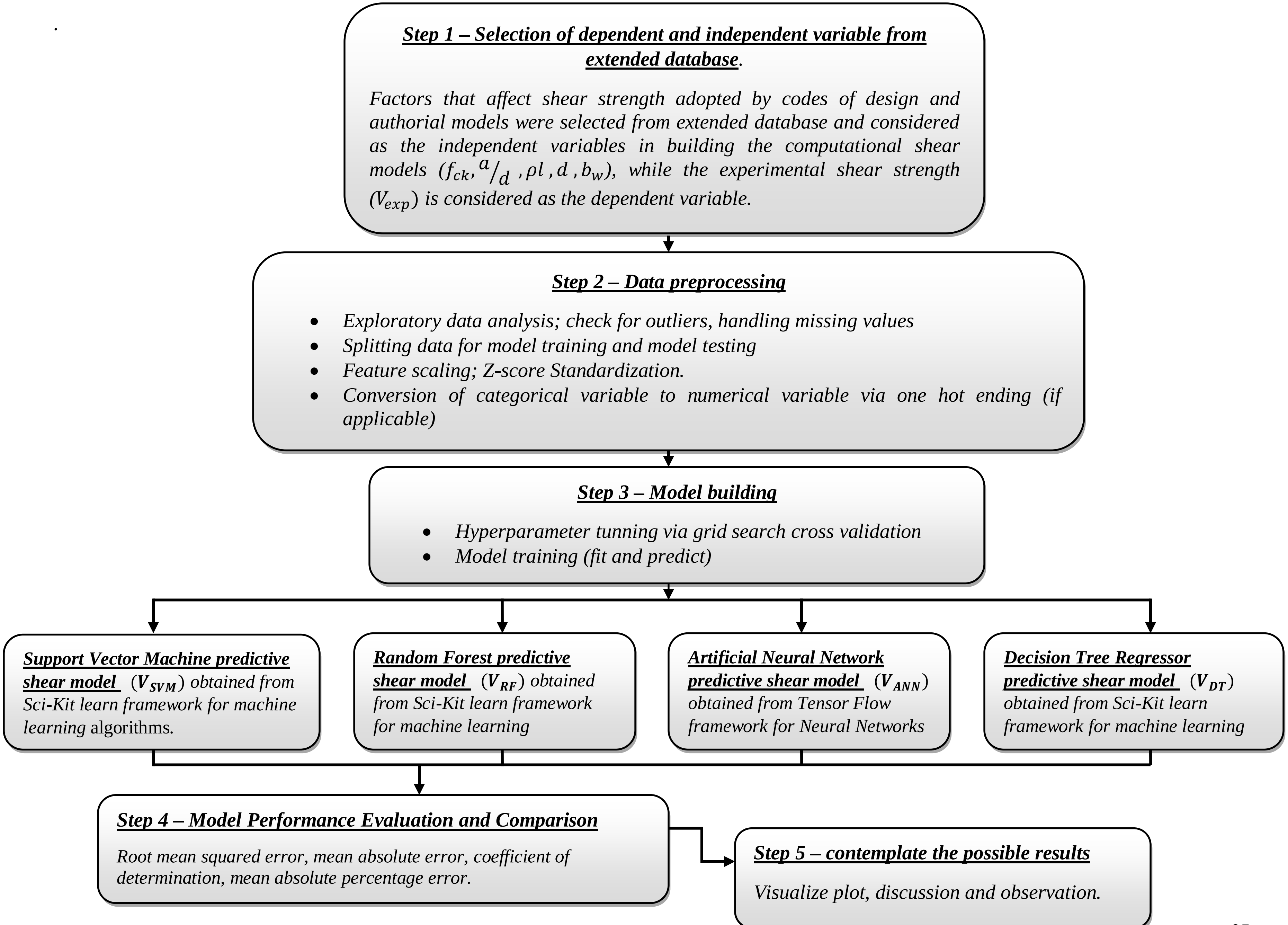

Fig 3.9 Procedure for developing machine learning models

3.7.0 Uncertainty modelling of Authorial, code-based and machine learning models

Model uncertainty is a measure that best describes the extent to which analytical and empirical models fail to express reality in its entirety. Statistical uncertainty modelling involves the derivation of model factors that gives a clearer understanding of the performance of the investigated models. The model factor is treated as a random variable which can be characterized by mean values, probability distribution functions and variances. The following criteria are considered for the performance evaluation of the model factor;

1. Model factor derivation and statistical analysis for considered models
2. Model factor sensitivity investigation with shear parameters
3. The suitable probability distribution function of model factor.

3.7.1 Model factor derivation

The model factor is calculated by comparing the experimental shear resistance observed from an individual test point to the respective shear strength derived from predictive shear models considered in this study. The vector properties (X) representative of the experimental shear strength is used as input parameters in the predictive models with further analysis resulting in a shear value. The methodology employed in determining the stochastic parameters of model uncertainty related to a single experimental observation, x , is adapted from the work of Holicky *et al*. (2013) as expressed below;

$$MF_x = \frac{V_{exp,x}}{V_{model,x}(X)}$$

MF_x = model factor related to a single experimental observation x

$V_{exp,x}$ = diagonal tension failure for individual experimental observation x

$V_{model,x}$ = mean shear resistance prediction obtained for the same experimental test point offered by the studied shear models.

X = vector of input variables including (beam depth (d), concrete strength (fcm), percentage longitudinal reinforcement (ρl), shear-span to depth ratio (a/d), width, (bw).

An MF value greater than 1 denotes conservatism and underestimation in the prediction of an investigated model while a value less than 1 denotes an overestimation and unconservative shear estimates.

3.7.1.1 Model factor based on EC2 ($\mathbf{V_{EC2}}$)

To determine the model uncertainty associated with the unbiased $EC2$ shear model for beams without stirrups characterized by diagonal tension failure, the expressions below are applied. The estimated model factor is represented as MF_{EC2}.

$$V_{EC2} = \left[0.18k(100\rho l f_{cm})^{1/3}\right]b_{\mathrm{w}}d \;\geq\; (0.035^{3/2} f_{cm}^{1/2})b_{\mathrm{w}}d = V_{min}$$

$$MF_{EC2,x} = \frac{V_{exp,x}}{V_{EC2,x}}$$

3.7.1.2 Model factor based on Fib Model Code 10 (II) ($\mathbf{V_{MC-10(II)}}$)

The unbiased Fib Model Code 10 (Level of approximation II) shear resistance model for beams without shear reinforcement is expressed as the equation below. The derived model factor is denoted as $MF_{MC-10(II)}$.

$$V_{MC-10(II)} = 0.9k_v\sqrt{f_{cm}}b_{\mathrm{w}}d$$

$$MF_{MC-10(II),x} = \frac{V_{exp,x}}{V_{MC-10(II),x}}$$

The parameter "k_v" has three separate expressions which distinguish the three levels of approximation and result in different outputs for the same beam properties. Here, the "k_v" adopted is that for the LoA II, as it modifies the MC-10 shear model to be specifically suited for beams without shear reinforcement.

3.7.1.3 Model factor based on ACI 318-19 ($\mathbf{V_{ACI}}$)

Only the concrete contribution from the nominal ACI 318-19 shear model is considered for the estimation of the shear resistance for beams without stirrups. The mean shear strength for the ACI shear model can be derived from the equation below.

$$V_{ACI} = \left[8\lambda_s\lambda(\rho)^{1/3}\sqrt{f_{cm}}\right]b_{\mathrm{w}}d$$

$$MF_{ACI,x} = \frac{V_{exp,x}}{V_{ACI,x}}$$

3.7.1.4 Model factor based on AS3600 – 2018 ($\mathbf{V_{AS}}$)

The unbiased predicted shear resistance V_{AS} is obtained based on the concrete contribution in the shear model provided by the Australian standard for concrete structures in 2018. The resistance model V_{AS} is expressed in the equation below. The derived model factor is denoted as MF_{AS}.

$$V_{AS} = k_v b_v d_v\sqrt{f_{cm}}$$

$$MF_{AS} = \frac{V_{exp,x}}{V_{AS}}$$

3.7.1.5 Model factor based on SANS-101000 ($\mathbf{V_{SANS}}$)

The South African standard for concrete design suggests an empirical derivation for estimating the shear strength contribution of concrete. The unbiased shear strength according to the *SANS10100* can be calculated by expressing the empirical model for shear at its mean values and without the inclusion of a safety factor as seen below.

$$V_{SANS} = 0.75(\frac{f_{cm}}{25})^{\frac{1}{3}}(\frac{100A_s}{b_{\mathrm{w}}d})^{\frac{1}{3}}(\frac{400}{d})^{\frac{1}{4}}$$

The derived model factor is denoted as MF_{SANS}

$$MF_{SANS} = \frac{V_{exp,x}}{V_{SANS}}$$

3.7.1.6 Model factor based on the compression chord capacity model ($\mathbf{V_{CCC}}$)

The compression chord capacity model is the only authorial model considered in this study that does readily express the shear strength in its mean value. The unbiased shear resistance prediction provided by the shear model by Cladera *et al*, (2016) can be calculated according to the expression below. The derived model factor is denoted as MF_{CCC}.

$$V_{CCC} = 0.3\zeta\frac{x}{d}f_{cm}^{2/3}b_{v,eff}d \;\; \nleq v_{cu,min} = 0.25(\zeta\frac{x}{d}+\frac{20}{d_0})f_{cm}^{2/3}b_{\mathrm{w}}d$$

$$MF_{CCC} = \frac{V_{exp,x}}{V_{CCC}}$$

3.7.1.7 Model factor based on the multi-action shear model ($\mathbf{V_{MASM}}$)

As the name implies, the multi-action shear model considers the shear resistance of a beam to be the summation of the shear contribution from the major shear transfer mechanism. This phenomenon is supported by assigning explicit expressions for each shear mechanism respectively. Only the contribution of the compression chord and the interface shear transfer is considered for beams without web reinforcement. The model expresses its parameters in their mean value without the inclusion of any form of bias. Hence, resulting in a true estimate of shear value. The derived model factor is denoted as MF_{MASM}.

$$V_{MASM} = \zeta\left[(0.88+)\frac{x}{d}+0.02\right]\frac{b_{v,eff}}{b}K_p + 167\frac{f_{ctm}}{E_{cm}}\frac{b_{\mathrm{w}}}{b}\left(1+\frac{2G_F E_{cm}}{f_{ctm}^2 d_0}\right)$$

$$MF_{MASM} = \frac{V_{exp,x}}{V_{MASM}}$$

3.7.1.8 Model factor based on the modified SNiP model (V_{SNiP})

Unbiased shear resistance prediction according to the modified SNiP model derived by Yerzhanov *et al*. (2019) can be estimated with the expression below with property values expressed in their mean values.

$$V_{SNiP} = 6\sqrt{\frac{1}{d} f_t b_w d}$$

$$MF_{SNiP} = \frac{V_{exp,x}}{V_{SNiP}}$$

3.7.1.9 Model factor based on the mechanical model by Ngoc Linh Tran (V_{NLT})

The best estimate for the shear strength by the mechanical model proposed by Tran (2020) can be derived through the expression below. The model factor is denoted as MF_{NLT}.

$$V_{NLT} = \frac{2}{3} f_{ct,ef} . bd \left[k_x + \frac{1.5G_F}{f_{ct,ef} \mathrm{w}_{cr}} (1 - k_x) \right]$$

$$MF_{NLT} = \frac{V_{exp,x}}{V_{NLT}}$$

3.7.2 Model factor based on machine learning models (V_{ML})

The dependent variable derived from each predictive supervised learning regression model considered in this study is compared to the respective shear strength from experimental observation to evaluate the model factor. The model factor would be evaluated with 25% of the database characterized by a randomized selection. The expression below follows

$$MF_{ML} = \frac{V_{exp,x}}{V_{ML}} = \left[MF_{ANN} = \frac{V_{exp,x}}{V_{ANN}};\ MF_{SVM} = \frac{V_{exp,x}}{V_{SVM}}; MF_{RF} = \frac{V_{exp,x}}{V_{RF}}; MF_{DT} = \frac{V_{exp,x}}{V_{DT}} \right]$$

MF_{ML} = Model factor based on machine learning predictive models

V_{ML}= prediction of shear strength as a dependent variable from machine learning models

MF_{ANN} = Model factor based on artificial neural network predictive model

V_{ANN}= prediction of shear strength based on artificial neural network algorithm.

MF_{SVM} = Model factor based on the architecture of support vector machine

V_{SVM}= prediction of shear strength based on support vector machine algorithm

MF_{RF} = Model factor of artificial intelligent models built on the random forest architecture

V_{RF}= prediction of shear strength as a dependent variable from random forest architecture.

MF_{DT} = Model factor based on the decision tree

V_{DT}= prediction of shear strength as a dependent variable from the decision tree model.

3.7.3 Statistical moment analysis of model factor

The model factor is regarded as a random variable with a distribution that may be statistically measured. Pearson coefficient of variation, mean, skewness and standard deviation are the pertinent statistical variables required for assessing the efficacy of a model factor.

A sample mean is a single value that best represents an entire group of scores (Neil, 2017). The sample mean is the commonly used measure of central tendency that most accurately reflects the population mean given by the expression below.

$$\mu = \frac{1}{n}\sum_{j=1}^{n} X_j \ ; \ \mu_{MF} = \frac{1}{n}\sum_{j=1}^{n} MF_j$$

When the mean of a model factor equals one over a range of deterministic analyses, this signifies that the model generalizes well over practical varied beam sections. A mean < 1 means the investigated model overestimates the shear resistance, conversely a mean > 1 means that the investigated model underestimates the shear resistance.

The standard deviation (σ) has been discussed earlier in section 3.1. Concerning the model factor, the standard deviation tells us how the model factors derived from individual test point distributed across a database scatters around the expected mean of 1. When the standard deviation is equal or close to zero, this implies that the majority of the model factor derived from a particular analytical model is clustered around the expected mean of 1. A high standard deviation signifies a poor model, uneven distribution of model factors and a high frequency of irregularity.

The degree to which the distribution of statistical data deviates from the normal distribution is shown by its skewness. Concerning the model factor, the frequency distribution has to be skewed towards a mean of 1.

$$\eta = \frac{\sum_{i=1}^{n}(x_i - \mu)^3}{[(n-1)*(n-1)*\sigma^3]}$$

The coefficient of variation (Ω) is commonly applied to measure variability in a dataset and this statistical measure must be restricted to the variables that are measured on scales with absolute zero (Marcin and Jan, 2013).

Here, $\Omega_{MF}(\%) = \frac{\sigma_{MF}}{\mu_{MF}} * 100$

3.7.4 Demerit point analysis

Collins (2001) used the demerit point analysis to assess the effectiveness of the examined shear resistance models in comparison to an experimental shear strength. It is important to keep in mind that demerit point analysis may only be used to evaluate design shear models, and not mean shear models when using it as a performance metric for shear models. The severity of each computed model factor is indicated by the associated demerit point. The sum of the percentages of the obtained model factors for each respective test point may be used to calculate the Total Demerit Point score, which represents how well the shear strength model performed overall. The Total Demerit Point's value affects the model's reliability.

Table 3.6 classification of the demerit points Collins (2001)

S/N	$V_{exp,x}/V_{(X_k,\gamma),x}$	Classification	Demerit Point
1	< 0.5	Highly hazardous	10
2	0.5 – 0.65	Dangerous	5
3	0.65 – 0.85	Marginal safety	2
4	0.85 – 1.30	Adequate safety	0
5	1.30 – 2.00	Conservative	1
6	> 2.0	Highly conservative	2

The compression chord capacity model and other shear methods from the South African Standard for concrete designs, Fib Model code 2010 and the Eurocode would be analyzed based on the demerit point analysis owing to their capability of expressing shear strength in its design value (inclusion of bias).

3.7.5 Sensitivity analysis

Sensitivity analysis investigates the effect of input parameters on an objective function with an end to determine the relative importance of each input parameter on the objective function (Baghi and Barros, 2017). According to Olalusi (2020), the observable sensitivity a model prediction portrays with respect to the model input parameters is a cause for concern in its reliability assessment provided there is no sufficient recalibration in the reliability analysis. For this research, the objective function would be the shear capacity of beams without shear reinforcement. Sensitivity analysis can be divided into 2 types; local sensitivity analysis and global sensitivity analysis.

In the global sensitivity analysis, the response function is evaluated by varying all the dependent parameters simultaneously, this in turn takes into account the influence of the interaction between parameters on the response function (Baghi and Barros, 2017). Hence, a global sensitivity analysis is carried out in this research. To determine the sensitivity of investigated shear models to basic input parameters, correlation and regression analysis as is carried out on the derived model factors.

Table 3.7. Pearson's correlation index (Franzblau, 1958).

Pearson Correlation Factor r	
0 - ± 0.2	Very weak or no correlation
0.2 - ± 0.4	Weak correlation
0.4 - ± 0.6	Moderate correlation
0.6 - ± 0.8	Strong correlation
0.8 - ± 1	Very strong correlation

3.7.6 Probabilistic modelling for model uncertainty

In structural reliability theory, a suitable characterization of the model uncertainty distribution function is paramount towards selecting a general probabilistic model. According to the JSCC (2001), the normal and lognormal distributions generally dominate the type of distributions used to describe actions, material properties and geometrical data. Hence, the lognormal distribution and the normal distribution would be considered possible distributions for the model factors.

3.7.6.1 Log-normal distribution

According to Modarres *et al*, (1999), the lognormal distribution is widely applied in reliability engineering and the model is appropriate for modelling failure processes resulting from the many small multiplicative errors. The mathematical expression of a log-normal probability distribution function is given below;

$$f(x) = \frac{1}{\sqrt{2\pi}\,\sigma x}\exp\left(-\frac{(\ln(x)-\mu)^2}{2\sigma^2}\right), x > 0$$

3.7.6.2 Normal distribution

The normal distribution is a basic statistical distribution. In a normal distribution, most of the values in the dataset are clustered in the middle of the range or around the mean while other data taper off symmetrically toward either extreme. The shape of a normal distribution takes on a bell curve, depicting that the data are evenly distributed. The probability density function of a normal distribution is given as;

$$f(x) = \frac{1}{\sqrt{2\pi}\,\sigma} e^{-\frac{1}{2}\left(\frac{x-\mu}{\sigma}\right)^2}$$

For a normal distribution, any value that lies beyond μ -3σ and μ +3σ is considered an outlier.

3.7.6.3 The goodness of fit test

To determine whether the model uncertainty distribution belongs to a proposed hypothesized theoretical distribution, a validity test has to be done. Hence, the goodness of fit test.

The goodness of fit test would be done using two measures;

1. The Chi-Squared test
2. Anderson darling goodness of fit test

Additionally, visualization plots which include probability plots and histogram plots with probability distribution function curves would be plotted and analyzed. Results from the goodness of fit test are corroborated with visualization plots to confirm the estimated probability distribution.

3.7.7 Reliability assessment and partial calibration approach

1. Preliminary reliability assessment using the FORM procedure to accentuate the safety performance regimes with respect to the parametric selection of test cases from the database. The procedure for the reliability assessment is seen in Fig 3.10.

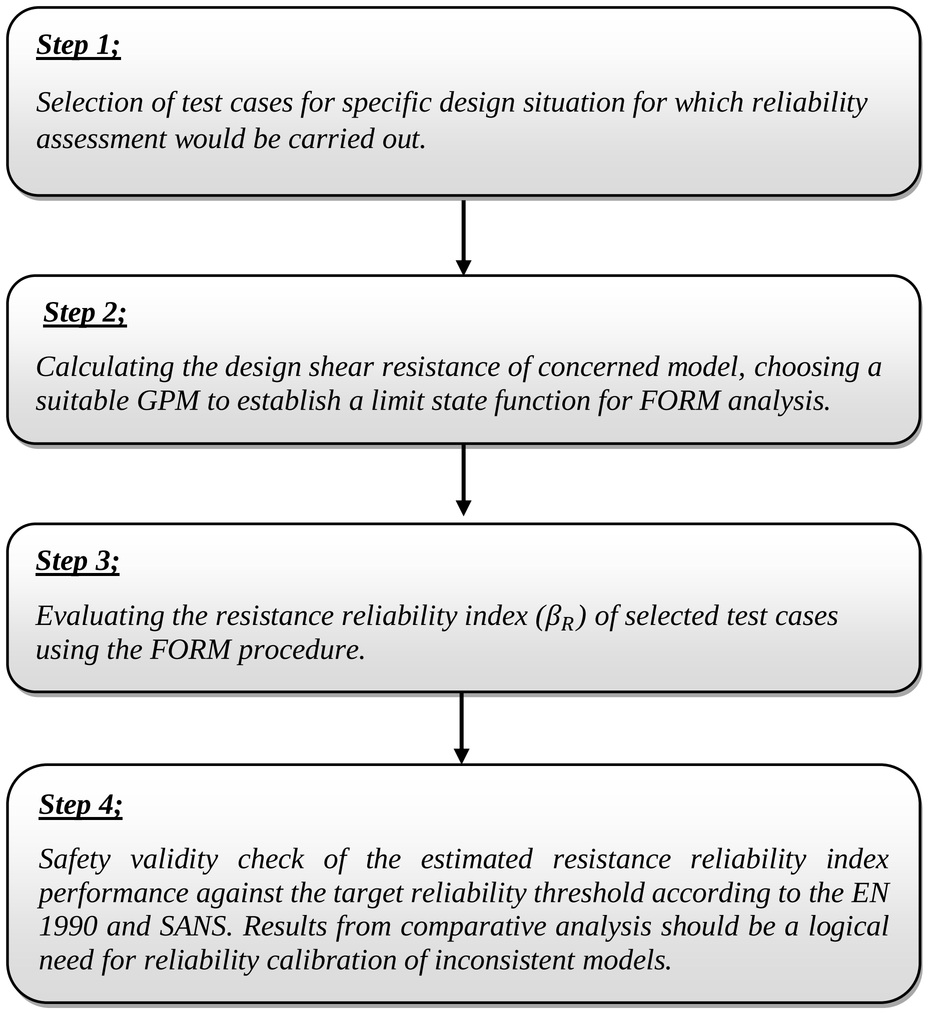

Fig. 3.10 Procedure for reliability investigation.

2. Derivation of preliminary model uncertainty partial factor for shear models using deterministic reliability calibration.

According to Mensah et al (2012), the most effective management of the reliability performance can be attained by deriving model uncertainty partial factors. Hence, the procedure for estimating the partial factors for model uncertainty is seen in Fig. 3.11.

Step 1; Identifying input parameter for partial factor of safety calibration for model uncertainty

- *Statistical moments of model factor necessary as input parameters in reliability investigation includes mean (μ_{MF}) and coefficient of variation (Ω_{MF}) derived from statistical analysis of model factor.*
- *Direction cosine (α_R) and target reliability (β)*

- *Determination of Direction cosine (α_R);α_R is taken as 0.8 if the COV of model uncertainty is higher than COV of geometrical and material properties i.e., model uncertainty dominates the model's safety performance, else, α_R is taken as 0.4×0.8 = 0.32.*
- *Target reliability (β) of level of reliability class 2 (RC2) structure according to the EN 1990 is adopted.*

Step 2; computation of model uncertainty partial factor (γ_{Rd}) *- derived input parameters are inserted into the equation;* $\gamma_{Rd} = 1/[\mu_{MF}.\exp(-\alpha_R.\beta.\Omega_{MF})]$

Step 3; Incorporating derived model uncertainty partial factor into resistance model design expression.

$$V'_{Rd} = V_{(X_k)}/(\gamma_M.\gamma_{Rd})$$

Step 4; anticipate the outcome

Observation, discussion and performance comparison

Fig. 3.11 Procedure for estimating the partial factor for model uncertainty according to EN 1990.

CHAPTER 4

RESULTS & DISCUSSION

4.1 Global comparison of shear mean value prediction to experimental shear strength

4.1.1 Global comparison using the perfect line analysis

The plot of the experimental shear strength ($\boldsymbol{V_{EXP}}$) against predicted shear strength ($\boldsymbol{V_{MODEL}}$) of 784 beams without shear reinforcement and parametric variations of test properties as compiled by Reinick *et al.* (2013) is presented in Fig. 4.0 and 4.1. Considering the perfect line of equality, the graphical visualizations in Fig. 4.0 show a trend comparison between the experimental shear strength observation and the best estimates of investigated models. The comparative study is achieved by examining the coefficient of determination (R^2), similarity and closeness between the trendline of predicted shear strength and the perfect line of equality.

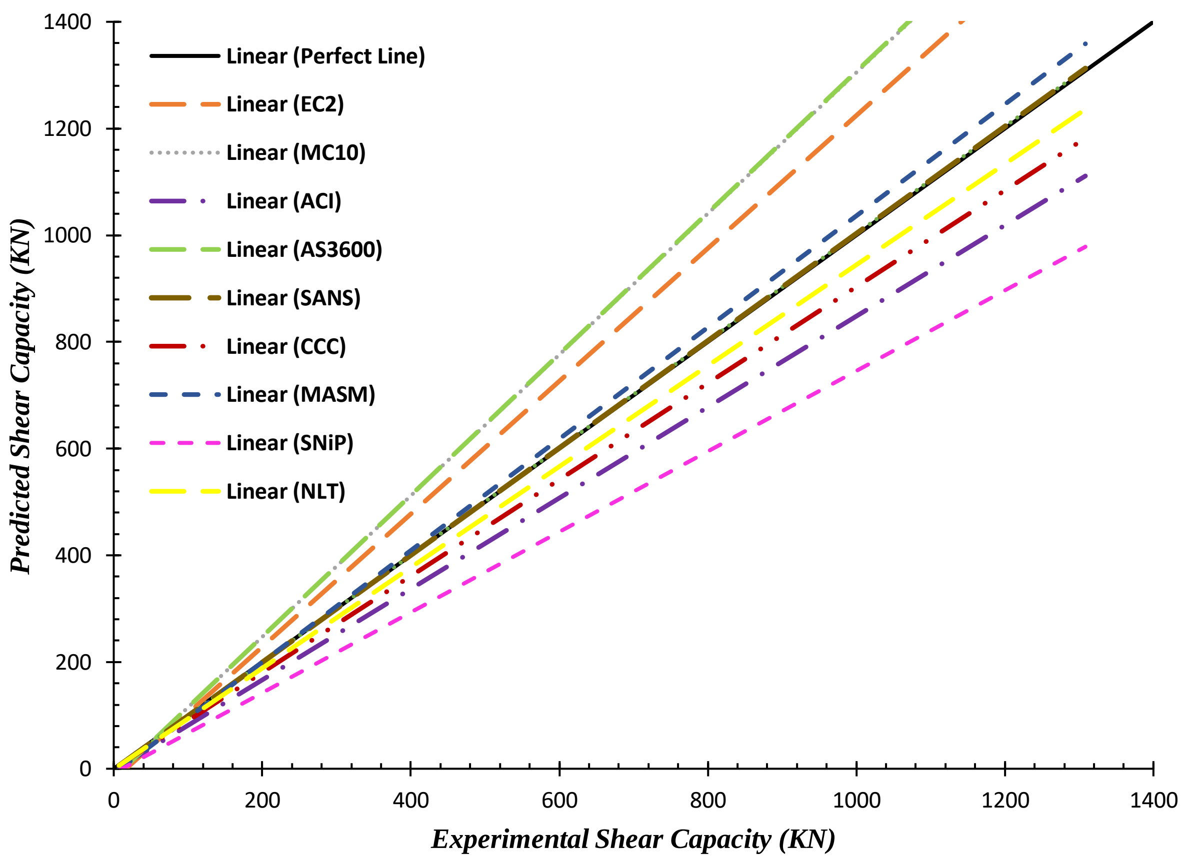

Fig. 4.0. Perfect line comparison plot of predicted shear value against experimental shear value.

4.1.1.1 Perfect line analysis

Fig.4.0 portrays the divergence of the trend line of the predicted shear strength with respect to the perfect line of equality where R^2 =1

.

1. The trendline of the predicted shear capacity V_{NLT}, V_{SANS}, V_{MASM} and V_{CCC} closely captures the perfect line of equality. The plot of the V_{MASM} in Fig.4.1e shows that the predicted values of V_{MASM} are more scattered compared to the V_{NLT}, V_{SANS} and V_{CCC} shear predictions, hence the choice of linear best fit of the V_{MASM} in Excel was based on few consistent predictions with experimental values. The closeness of the V_{MASM} trendline to the perfect line is negated based on its R^2 value = 0.8965 as compared to V_{NLT}, V_{SANS} & V_{CCC} which have R^2 values of 0.9375, 0.9151 and 0.9109 respectively.
2. The trendline of V_{EC}, V_{MC10}, V_{AS3600} & V_{SNiP} fails to capture the perfect line of equality. The plot of the V_{SNiP} in Fig.4.0 shows that the trendline diverges substantially below the line of equality with notable scatters around its trendline as seen in Fig.4.1g, this implies that the prediction of the modified Snip shear model performs poorly in comparison to the experimental value as it gives lower and overly conservative values of shear. Also, the R^2 value of V_{SNiP} = 0.8395 is indicative of its poor performance when compared to other shear models.
3. From fig.4.0, the trendline of V_{EC}, V_{MC10} & V_{AS3600} fails to reproduce the trendline of equality as it bears no comparison with the perfect line of equality. A deviation in trend above the perfect line of equality is observed while considering the plot of V_{EC}, V_{MC10} & V_{AS3600} as seen in fig.4.0 with much scatter around its trendline as seen in Figs.4.1a, 4.1f & 4.1c. Lower values of R^2 also indicate that the predictions of V_{EC} = 0.8956, V_{MC10} = 0.8849 & V_{AS3600} = 0.8849 are not as consistent with experimental values.
4. V_{ACI} shows similar predictions with experimental values at lower shear values, a deviation below the perfect line of equality is observed as the experimental shear value increases as seen in Fig. 4.0. The performance of the ACI shear model with respect to the experimental shear value at lower shear values is validated with an R^2 value of 0.929.

Generally, in descending order, the predictions that closely capture the perfect line of equality in terms of closeness of trend, a high value of R^2 and low scatter are V_{NLT}, V_{ACI}, V_{SANS} & $V_{CCC.}$

V$_{MODELS}$ against V$_{EXP}$

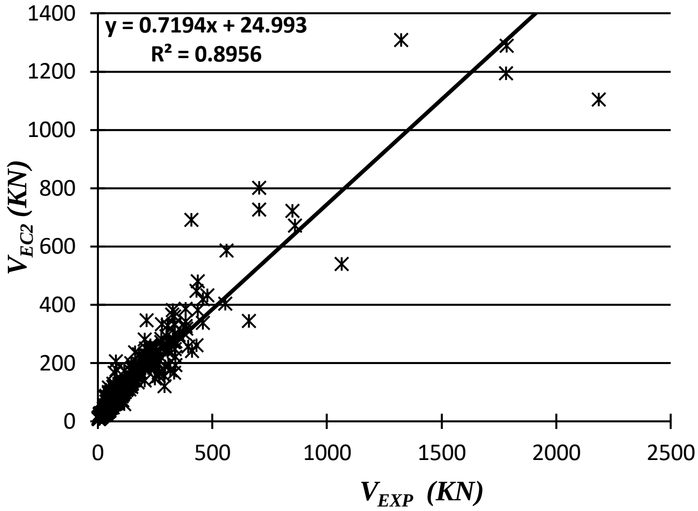

(a) ***V$_{EC}$***

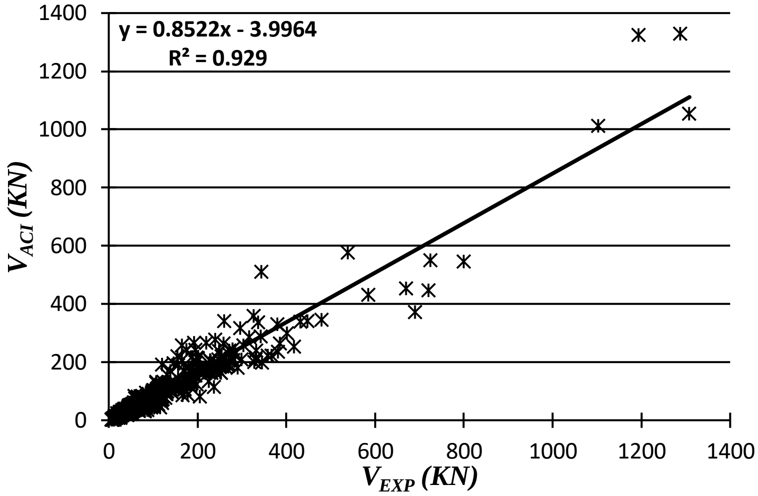

(b) ***V$_{ACI}$***

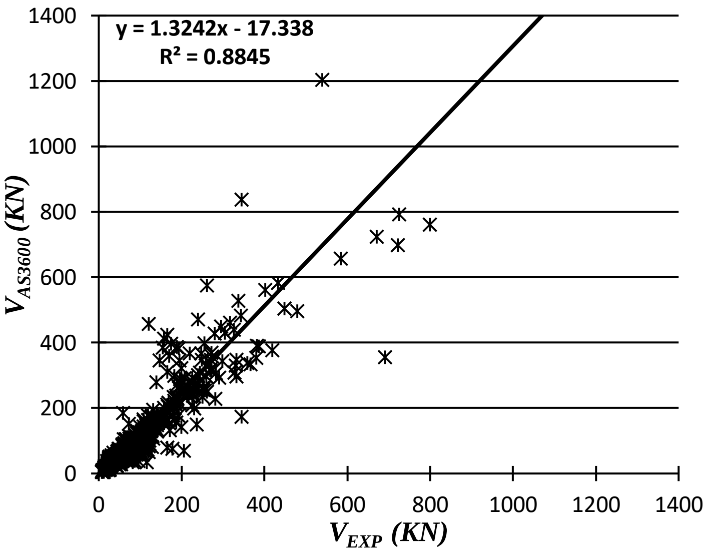

(c) ***V$_{AS3600}$***

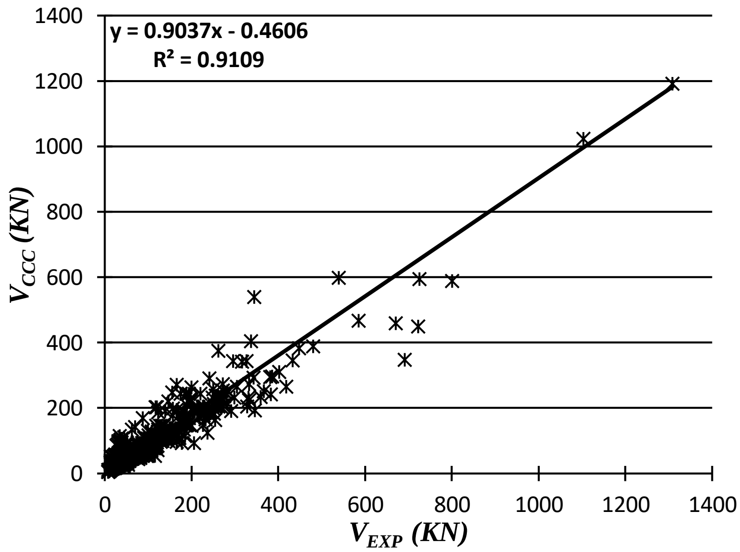

(d) ***V$_{CCC}$***

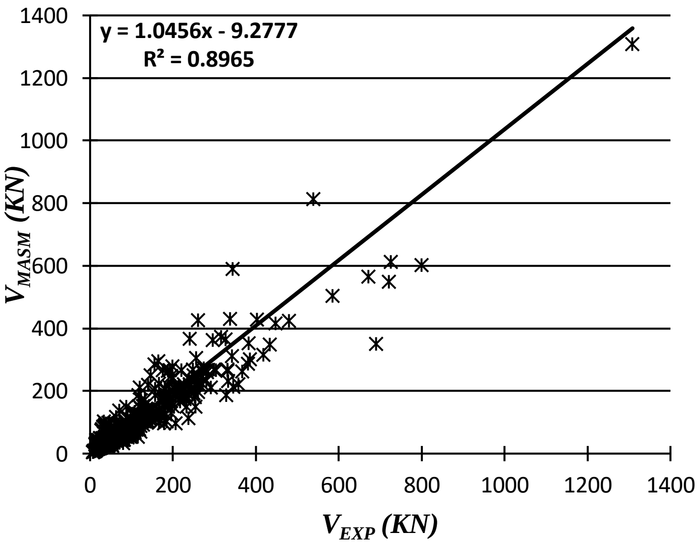

(e) ***V$_{MASM}$***

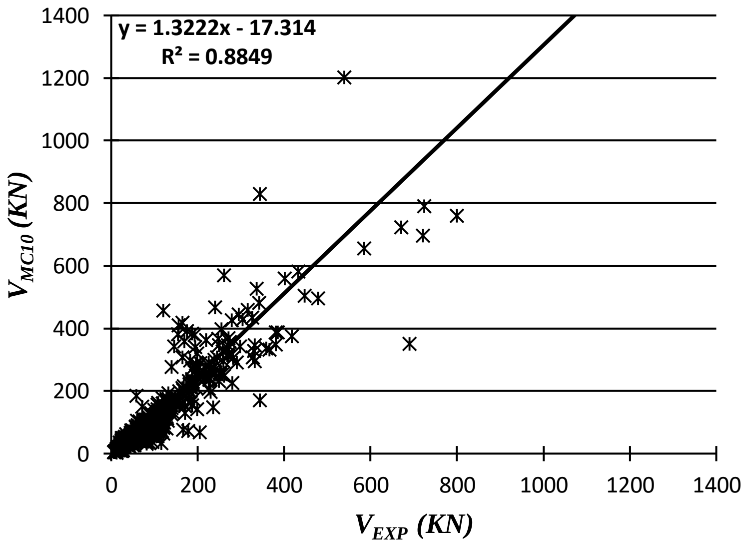

(f) ***V$_{MC1}$***

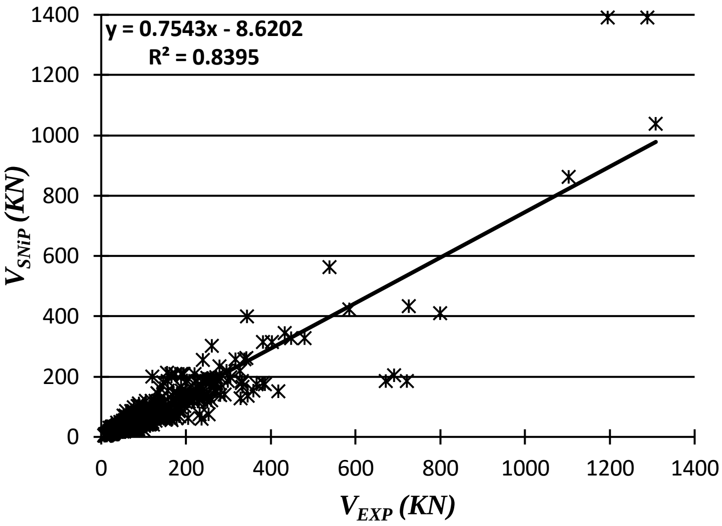

(g) V_{SNiP}

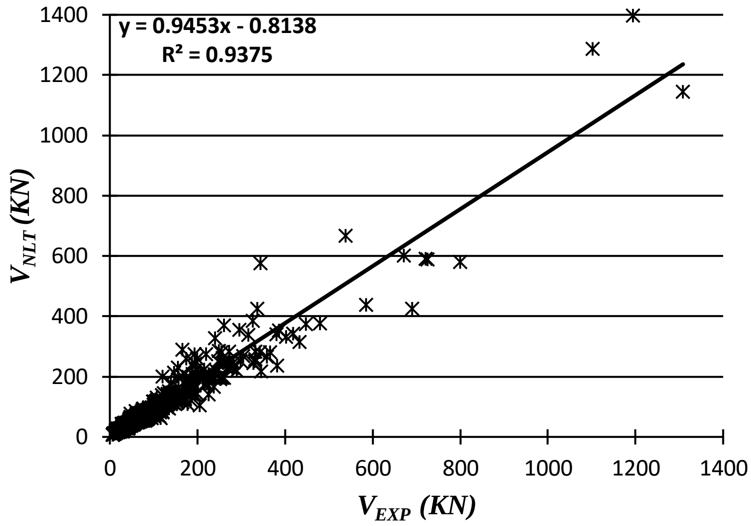

(h) V_{NLT}

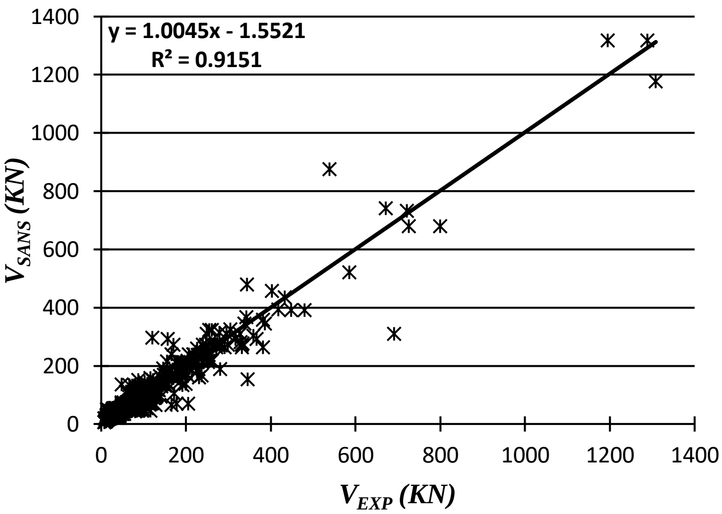

(i) V_{SANS}

Fig 4.1. Comparison of experimental shear strength (***V_{EXP}***) to predicted shear strength (***V_{MODEL}***) a) ***V_{EC2}***, b) ***V_{ACI}***, c) ***V_{AS3600}***, d) ***V_{CCC}***, e) ***V_{MASM}***, f) ***V_{MC10}***, g) ***V_{SNiP}***, h) ***V_{NLT}***, i) ***V_{SANS}***

4.1.1.2 Global comparison using the annotated heatmap

Fig.4.2 presents the heatmap of the unbiased shear values from investigated models and experimental shear values. The heatmap uses the Pearson correlation coefficient to determine the relationship between variables. The colour bar on the right side assigns a correlation intensity and annotation based on the extent to which shear values are correlated. The heatmap shows that V_{NLT} compares well with the experimental shear value with a correlation value of 0.97, while V_{SANS} and V_{ACI} rank second in this regard with a value of 0.96. The heatmap shows that of all the shear predictions, V_{SNiP} underperforms with a correlation value of 0.92. Second, to V_{SNiP} are the shear predictions of V_{MC10} and V_{AS3600} with a correlation value of 0.94. the shear Predictions from V_{CCC} and V_{MASM} give intermediate predictions with a correlation value of 0.95.

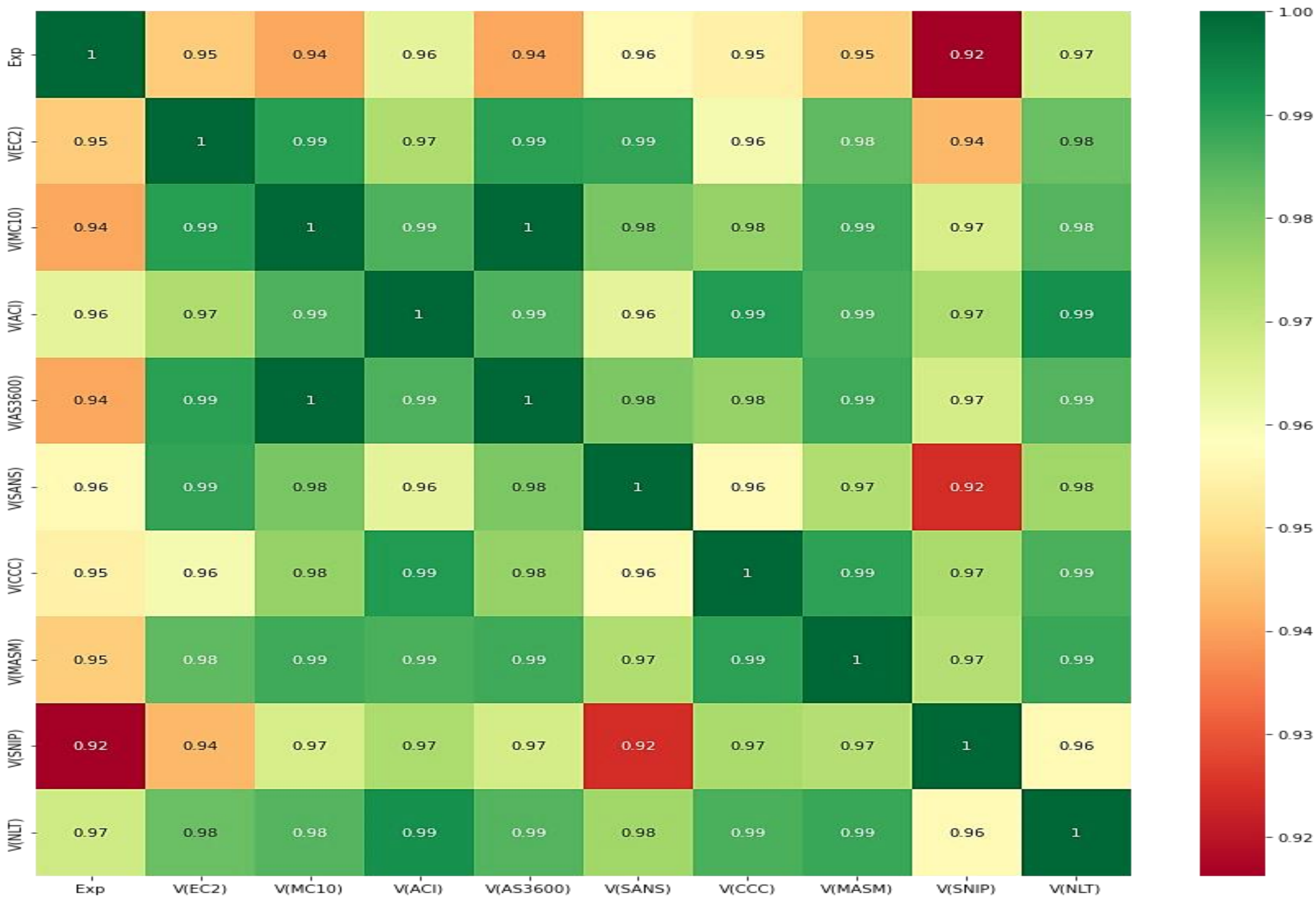

Fig.4.2 Heatmap with annotation showing the coefficient of correlation between experimental shear values and predicted shear values.

4.1.2. Global comparison of shear mean value prediction to experimental shear strength with respect to percentage longitudinal reinforcement

The plot of the normalized experimental shear strength $\left(\frac{V_{exp}}{b_{\mathrm{w}}d}\right)$ of reinforced concrete beams without shear reinforcement and parametric variations of test properties compiled by Reinick *et al.* (2014) against an incremental percentage of longitudinal reinforcement is presented in Fig. 4.3. The graphical visualization below gives a detailed comparison of the experimental observation of shear strength to the mean predicted shear value from investigated model's best estimates. The comparative study is achieved as shown in Fig. 4.3 by examining the similarity and closeness between the trendline of normalized experimental shear strength and the trendlines of normalized mean shear value according to (1) EN 1992-1-1 $\left(\frac{V_{EC2}(X_m)}{b_{\mathrm{w}}d}\right)$, (2) Fib Model Code 10 $\left(\frac{V_{MC-10(II)}(X_m)}{b_{\mathrm{w}}d}\right)$, (3) ACI 318-19 $\left(\frac{V_{ACI}(X_m)}{b_{\mathrm{w}}d}\right)$, (4) AS 3600-18 $\left(\frac{V_{AS}(X_m)}{b_{\mathrm{w}}d}\right)$, (5) SANS10100 $\left(\frac{V_{SANS}(X_m)}{b_{\mathrm{w}}d}\right)$, (6)CCCM $\left(\frac{V_{CCC}(X_m)}{b_{\mathrm{w}}d}\right)$, (7) MASM $\left(\frac{V_{MASM}(X_m)}{b_{\mathrm{w}}d}\right)$, (8) Modified Snip $\left(\frac{V_{SNiP}(X_m)}{b_{\mathrm{w}}d}\right)$, (9) Mechanical Model $\left(\frac{V_{NLT}(X_m)}{b_{\mathrm{w}}d}\right)$. Given that the data being analyzed (shear parameters) has a nonlinear relationship, a poly fit was employed in Fig. 4.3–4.5 rather than a linear fit. A poly fit provides for a more flexible fit to the data as it can capture more complex nonlinear relationships between the variables than a linear fit.

The following remarks were established from Figs. 4.3 and 4.4

1. An increasing trend of normalized experimental observations as the percentage longitudinal reinforcement increases ($pl\%$) was observed.
2. The trendline of V_{NLT} perfectly captures the trendline of the experimental shear strength with respect to its behaviour across the range of longitudinal reinforcement ratio. The trendline of V_{SANS} bears the closest comparison with V_{NLT} but a slight deviation above the experimental trendline is seen as the ratio of longitudinal reinforcement increases beyond 3% providing slightly higher shear capacity predictions.
3. Across the range of longitudinal reinforcement ratio, V_{SNiP} provides overly conservative shear predictions with very low shear values as the longitudinal reinforcement ratio increases. The trendline of the V_{ACI} ranks second to the V_{SNIP} as it also fails to capture the experimental shear trend by providing conservative shear predictions across the range of longitudinal reinforcement ratios considered.
4. V_{CCC} and V_{MASM} bear comparison with the experimental shear values between 0% – 4% of longitudinal reinforcement ratio with slightly lower shear values, higher shear prediction is

observed as the reinforcement ratio increases beyond 4% for the range of longitudinal reinforcement ratio considered.

5. The trend of V_{MC10} and V_{AS3600} is similar to the experimental shear trend only at 0-3% range of reinforcement ratio with slightly higher values of shear at 0 -2% of longitudinal reinforcement ratio. At $pl\%$ > 3%, V_{MC10} and V_{AS3600} provide consistent unconservative shear predictions for the parametric range considered.
6. The trend of the V_{EC2} shows a different behaviour from every other predictive model in its response to increasing longitudinal reinforcement ratio. The following observations were deduced from the V_{EC2} plot;
    - At 0 – 2% longitudinal reinforcement ratio, the trendline of V_{EC2} bears close comparison with the experimental shear trendline with a correlation value of up to 98% providing almost the same shear predictions as the experimental shear values.
    - At $pl\%$ >2, the trendline of the V_{EC2} starts to deviate below the experimental shear strength line i.e., V_{EC2} starts to provide conservative shear predictions when $pl\%$ > 2 with marginal increment until $pl\%$ = 3.
    - when pl% is between 3 – 4%, the EC2 shear model shows no observable trend in its prediction of shear capacity.
    - At a higher longitudinal reinforcement ratio > 4%, a marginally continued decrease in the shear prediction is observed up until the failure point. While for the same parametric range, the experimental shear strength gives a continued increased prediction.
    - At extreme values of longitudinal reinforcement ratio, the V_{EC2} tends to be more conservative than the V_{SNiP} in its shear prediction.
    - At $pl\%$ > 4, the V_{EC2} tends to be more conservative than V_{ACI} with a significant difference in prediction at extreme values of longitudinal reinforcement ratio for the range considered.

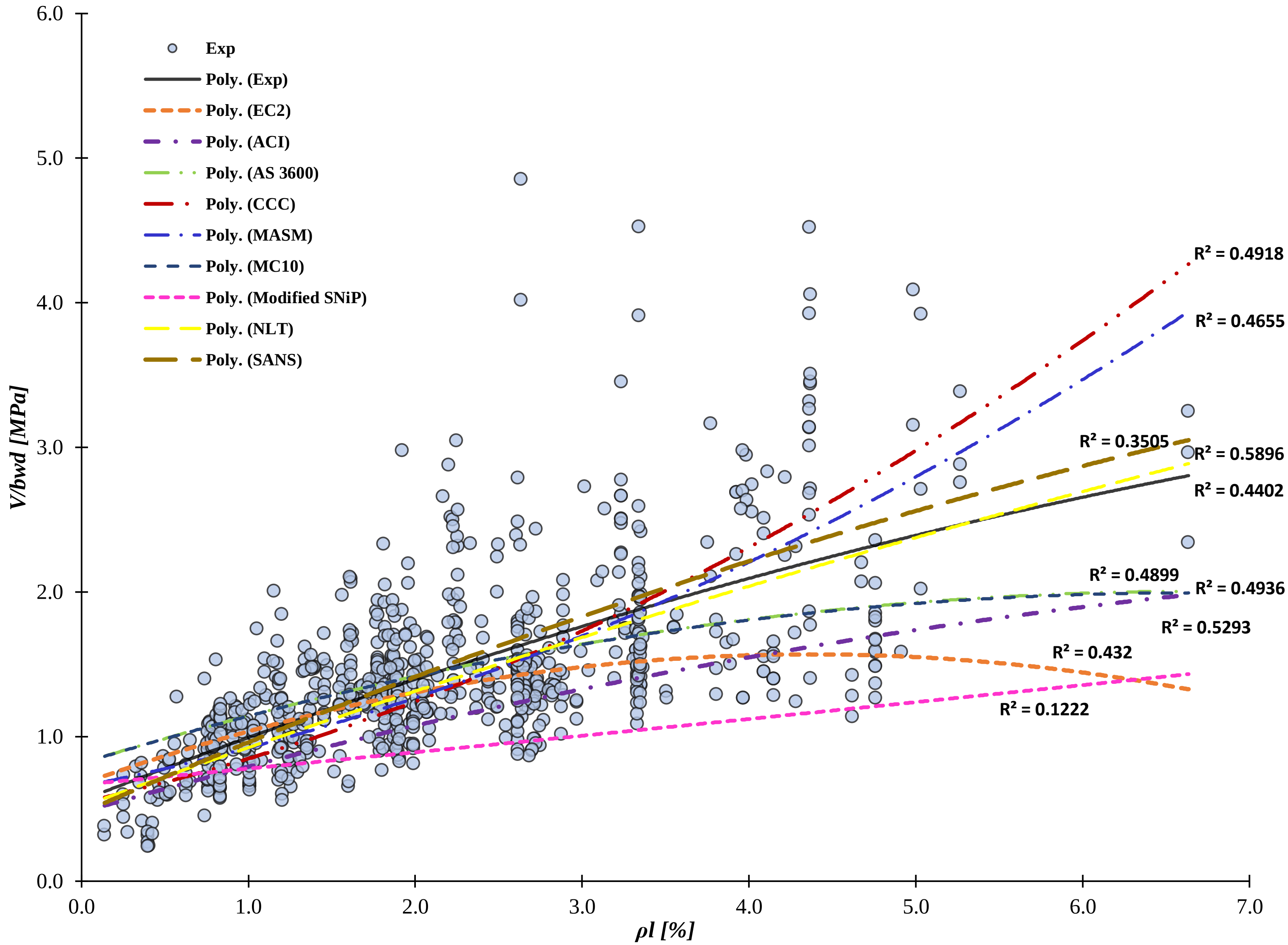

Fig.4.3 Comparison of normalized mean shear capacity to experimental observation with respect to ρl

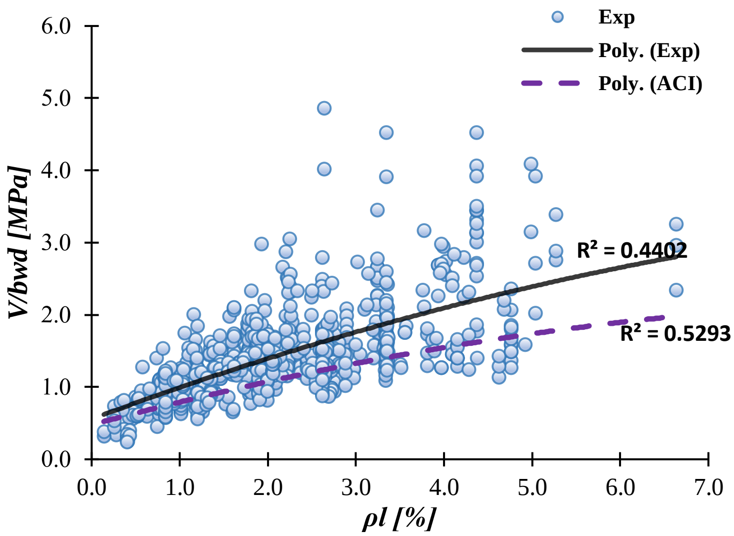
Exp
Poly. (Exp)
Poly. (ACI)
R² = 0.4402
R² = 0.5293
V/bwd [MPa]
ρl [%]

(a)

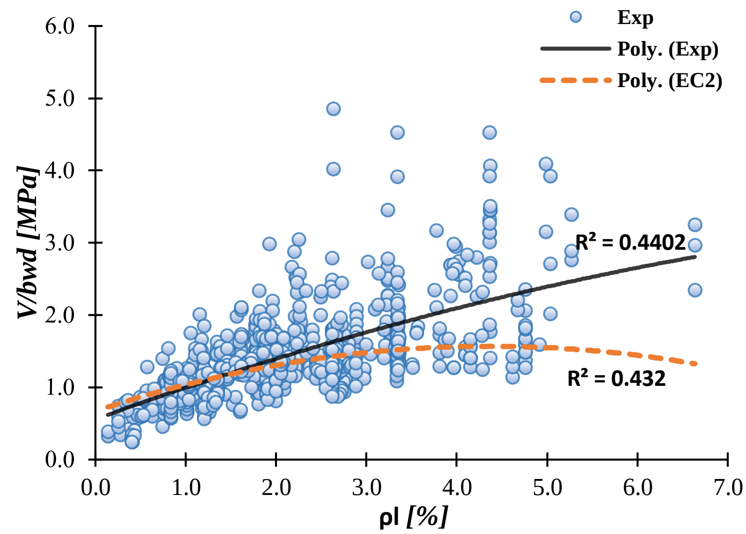
Exp
Poly. (Exp)
Poly. (EC2)
R² = 0.4402
R² = 0.432
V/bwd [MPa]
ρl [%]

(b)

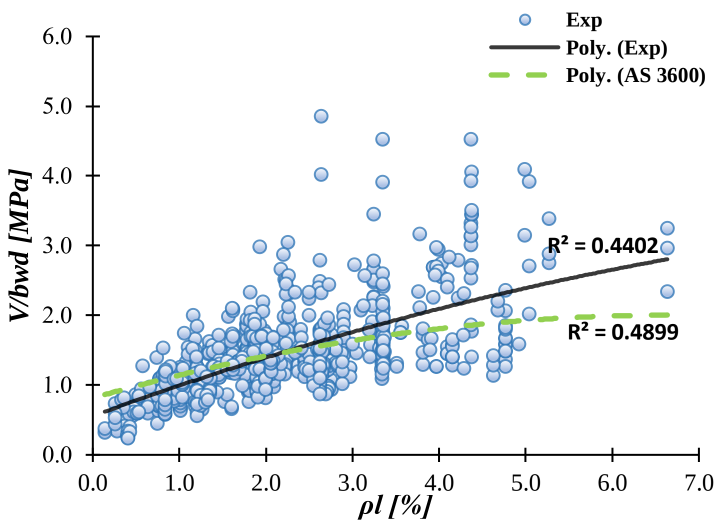
Exp
Poly. (Exp)
Poly. (AS 3600)
R² = 0.4402
R² = 0.4899
V/bwd [MPa]
ρl [%]

(c)

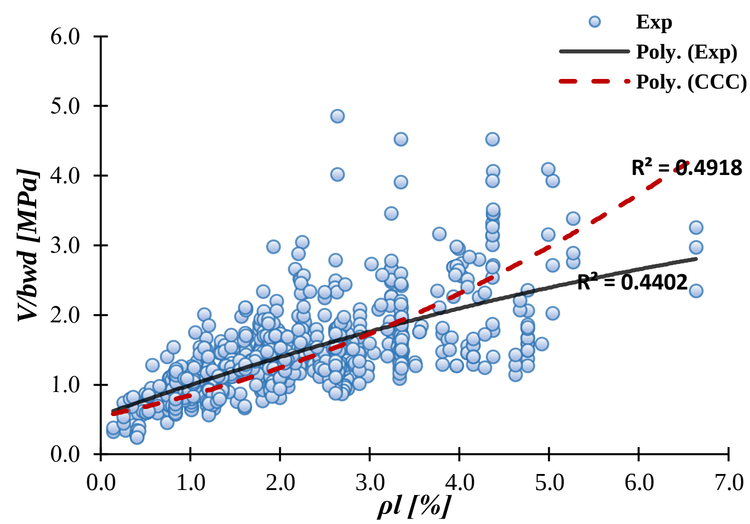
Exp
Poly. (Exp)
Poly. (CCC)
R² = 0.4918
R² = 0.4402
V/bwd [MPa]
ρl [%]

(d)

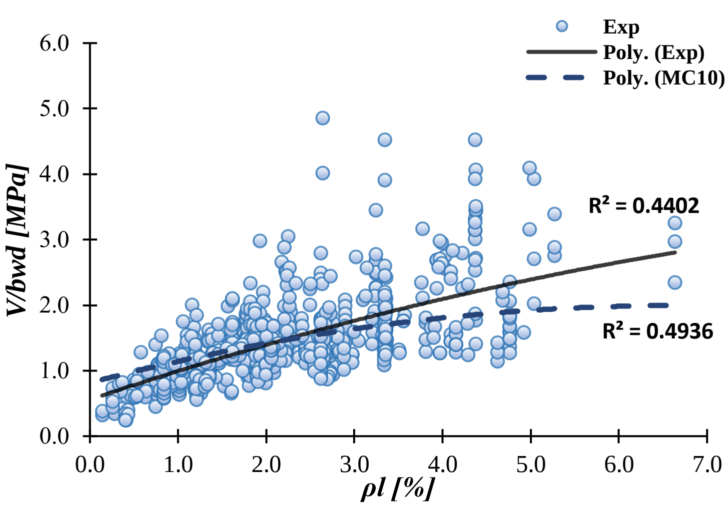
Exp
Poly. (Exp)
Poly. (MC10)
R² = 0.4402
R² = 0.4936
V/bwd [MPa]
ρl [%]

. (e)

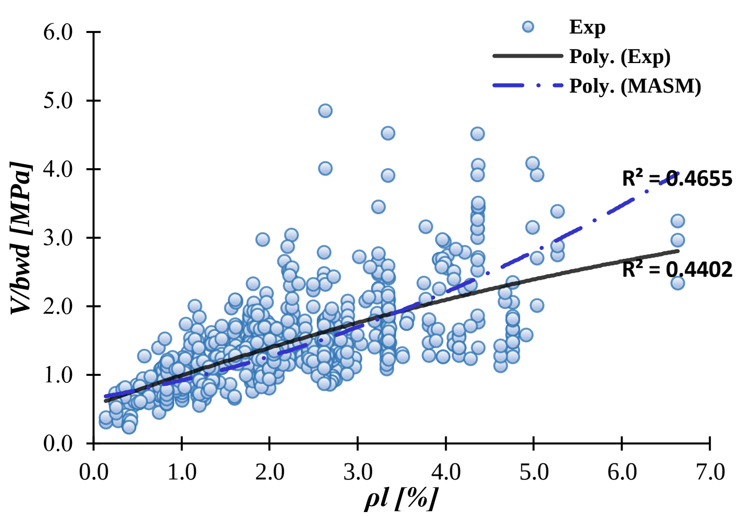
Exp
Poly. (Exp)
Poly. (MASM)
R² = 0.4655
R² = 0.4402
V/bwd [MPa]
ρl [%]

(f)

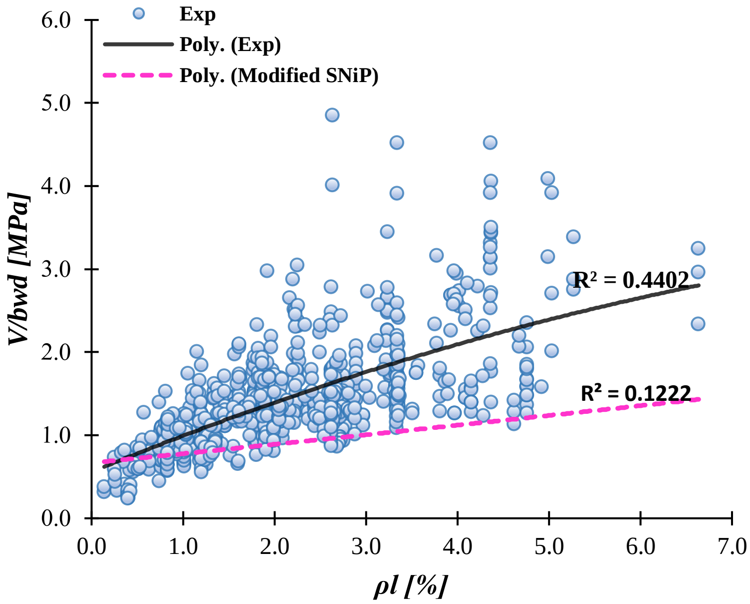

(g)

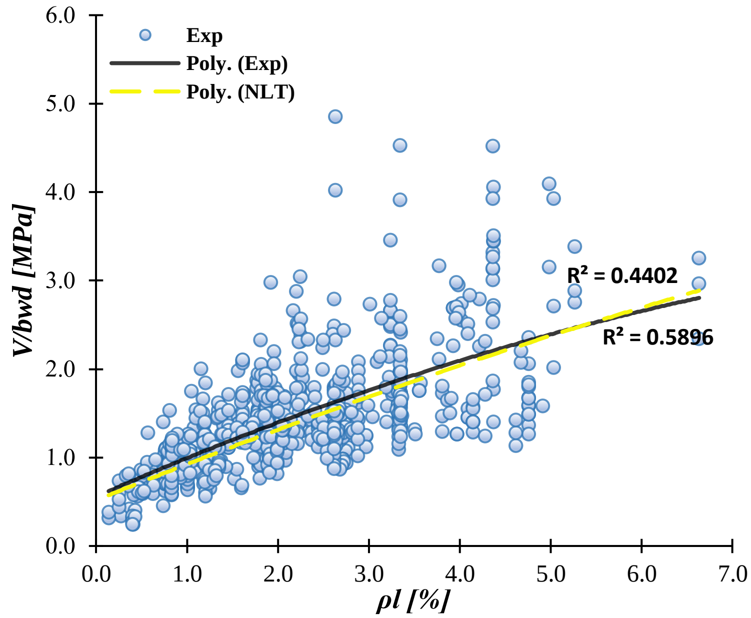

(h)

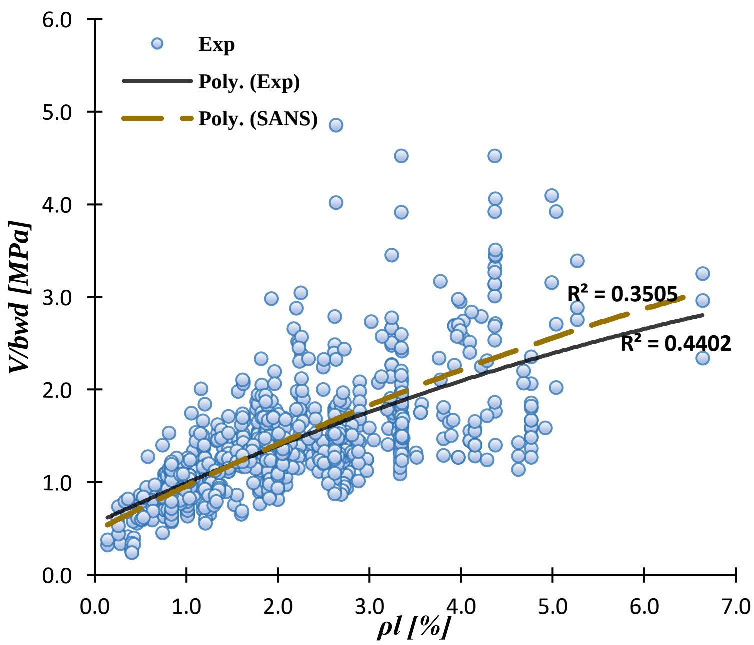

(i)

Fig 4.4. Comparison of normalized experimental shear strength $\left(\frac{V_{exp}}{b_w d}\right)$ to normalized predicted shear strength a) V_{EC2}, b) V_{ACI}, c) V_{AS3600}, d) V_{CCC}, e) V_{MASM}, f) V_{MC10}, g) V_{SNiP}, h) V_{NLT}, i) V_{SANS}

4.1.3. Global comparison of shear mean value prediction to experimental shear strength with respect to percentage longitudinal reinforcement

The following observations were drawn from Fig. 4.5

1. The trendline of V_{NLT} perfectly captures the experimental shear trend for the range of concrete strength considered. V_{EC2} provides a closer comparison to the accurate predictions of V_{NLT} with a marginal rate of increase in shear capacity as the concrete strength increases.
2. The trend of V_{MC10}, V_{AS3600}, V_{CCC} & V_{MASM} compares well with the experimental shear trendline providing an approximate prediction when the concrete strength is < 80MPa. V_{MC10}, V_{AS3600}, V_{CCC} & V_{MASM} starts to give conservative predictions with a continual decrease in shear predictions as the concrete strength increases beyond 80MPa for the parametric range considered.
3. V_{SANS} did not succeed in capturing the trend of experimental shear strength as no significant trend is recognized for the plot of V_{SANS} against f_{cu}(Mpa). The behaviour of the predicted shear value from the SANS shear model for beams without stirrups is majorly caused by the limit placed on the allowable concrete strength ($f_{cu} \leq$ 40MPa).
4. V_{SNIP} fails to capture the trendline of the experimental shear strength by providing overly conservative shear predictions as the concrete strength increases. V_{ACI} also fails to capture the experimental shear strength trend, but with predicted values less conservative than the V_{SNIP}.
5. Aside from the V_{NLT} and V_{EC2}, every other considered shear model fails to completely or approximately capture the trend of experimental shear strength for the considered range of concrete strength.
6. At extreme values of concrete strength, shear failure tends to occur as shear predictions of V_{MC10}, V_{AS3600}, V_{CCC}, V_{MASM} & V_{SNiP} continually decrease towards zero upon incremental concrete strength.

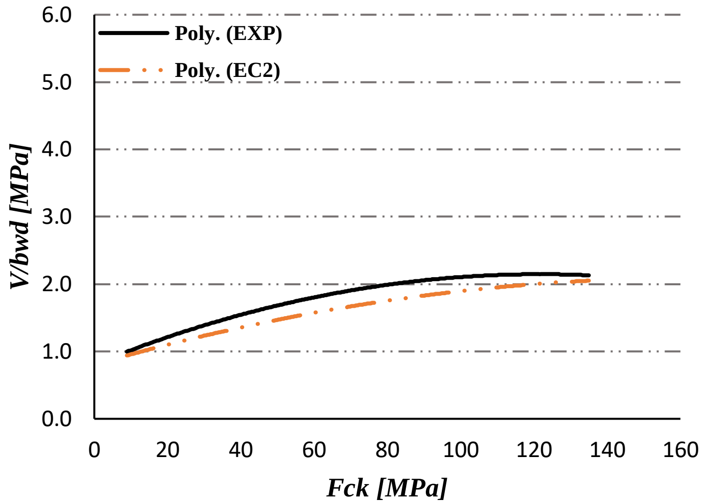

(a) V_{EC2}

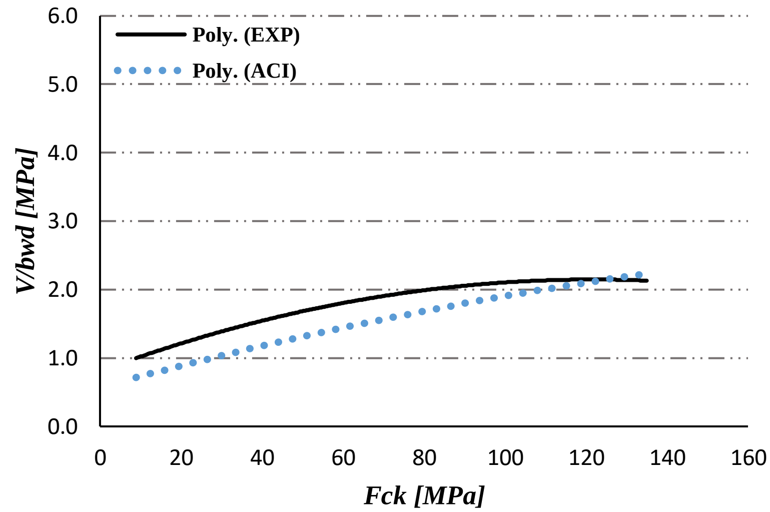

(b) V_{ACI}

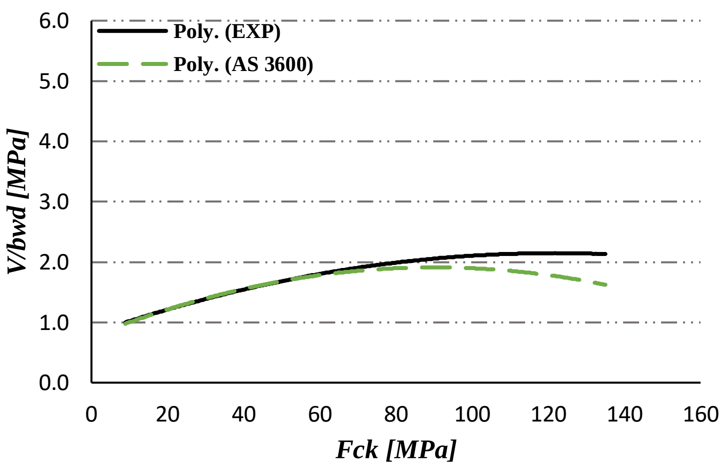

(c) V_{AS3600}

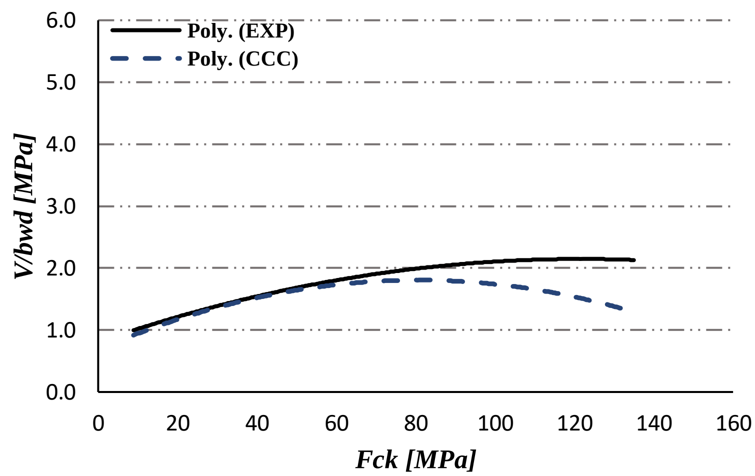

(d) V_{CCC}

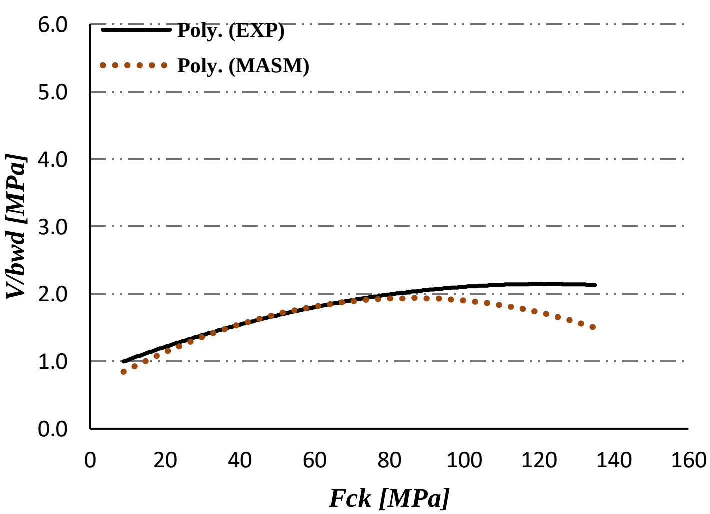

(e) V_{MASM}

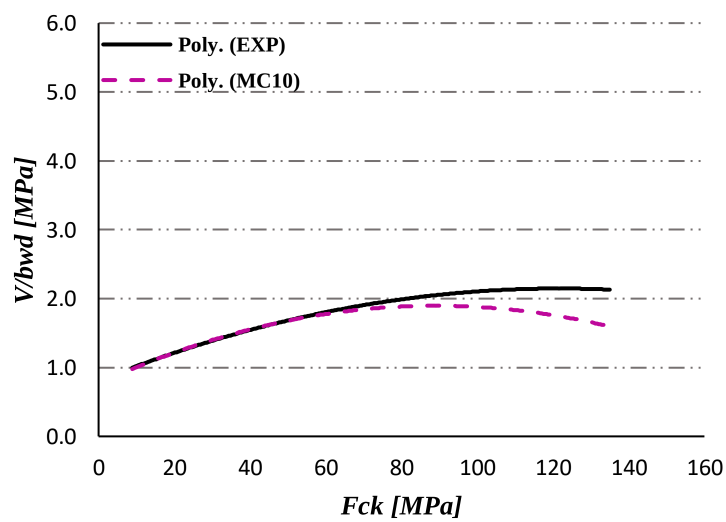

(f) V_{MC10}

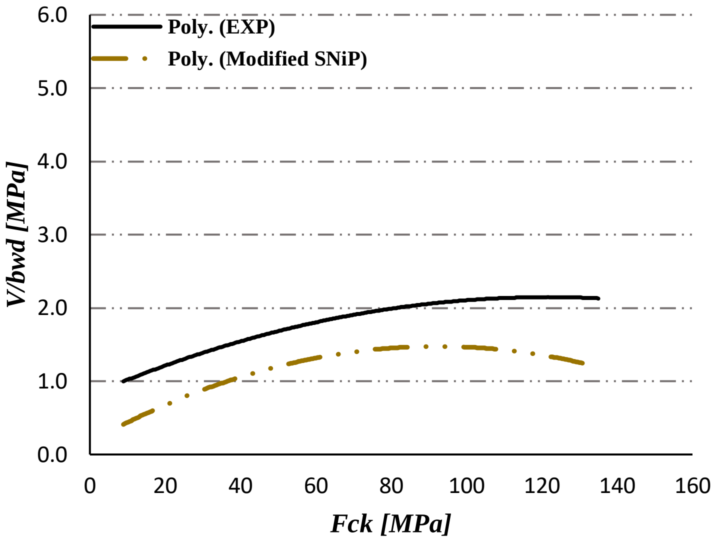

(g) ***V_{SNiP}***

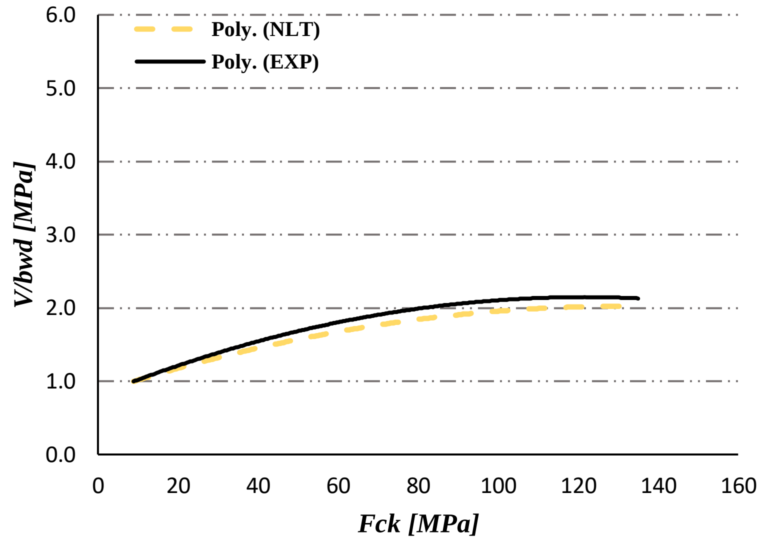

(h) ***V_{NLT}***

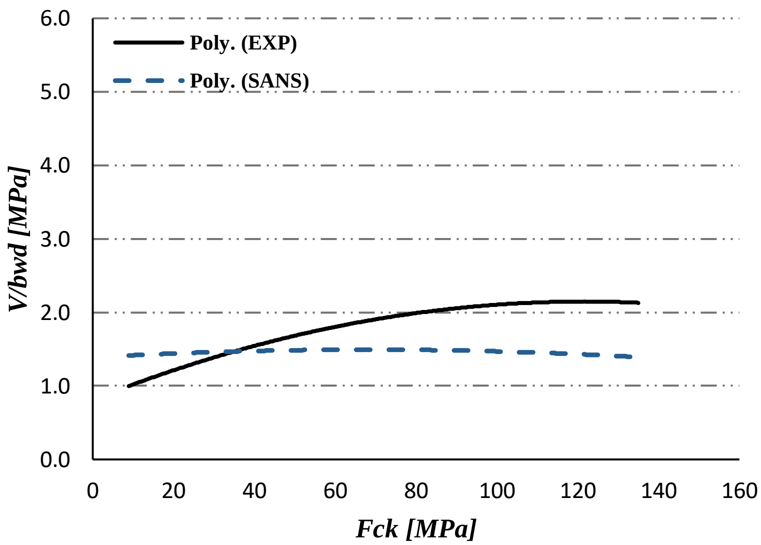

(i) ***V_{SANS}***

Fig 4.5. Comparison of normalized experimental shear strength $\left(\frac{V_{exp}}{b_w d}\right)$ to normalized predicted shear strength with respect to concrete strength. A) $\boldsymbol{V_{EC2}}$, b) $\boldsymbol{V_{ACI}}$, c) $\boldsymbol{V_{AS3600}}$, d) $\boldsymbol{V_{CCC}}$, e) $\boldsymbol{V_{MASM}}$, f) $\boldsymbol{V_{MC10}}$, g) $\boldsymbol{V_{SNiP}}$, h) $\boldsymbol{V_{NLT}}$, i) $\boldsymbol{V_{SANS}}$

4.2 Comparison of experimental shear strength to the EC2 and other shear design value

Estimates from design approaches (design value predictions) presented in section (3.5.2) are compared to experimental shear observations. Trends of normalized design values $(\frac{V_{Rd(X_{k},\gamma)}}{b_w d})$ which includes $\left(\frac{V_{EC2}(X_{k},\gamma)}{b_w d}\right)$, $\left(\frac{V_{MC-10(II)}(X_{k},\gamma)}{b_w d}\right)$, $\left(\frac{V_{SANS}(X_{k},\gamma)}{b_w d}\right)$ and $\left(\frac{V_{CCC}(X_{k},\gamma)}{b_w d}\right)$ are plotted against the experimental observations. Design shear values from $EC2, MC-10(II), SANS-101000\ and\ CCCM$ are derived from the same beam geometrical properties, concrete strength and longitudinal reinforcement ratio that corresponds with experimental observations. Shear models from ACI 318-19, AS 3600-18, MASM, Modified Snip and the mechanical model by Tran (2020) are not considered in this section because they only provide best-estimate predictions. In design value analysis, the range of values is widened due to the use of conservative estimates of shear obtained from the analysis. Therefore, a logarithmic scale is employed to fit the design value data, as it is a useful tool for analyzing data that covers a wide range of values. Additionally, logarithmic scales help reduce the impact of outliers in nonlinear data.

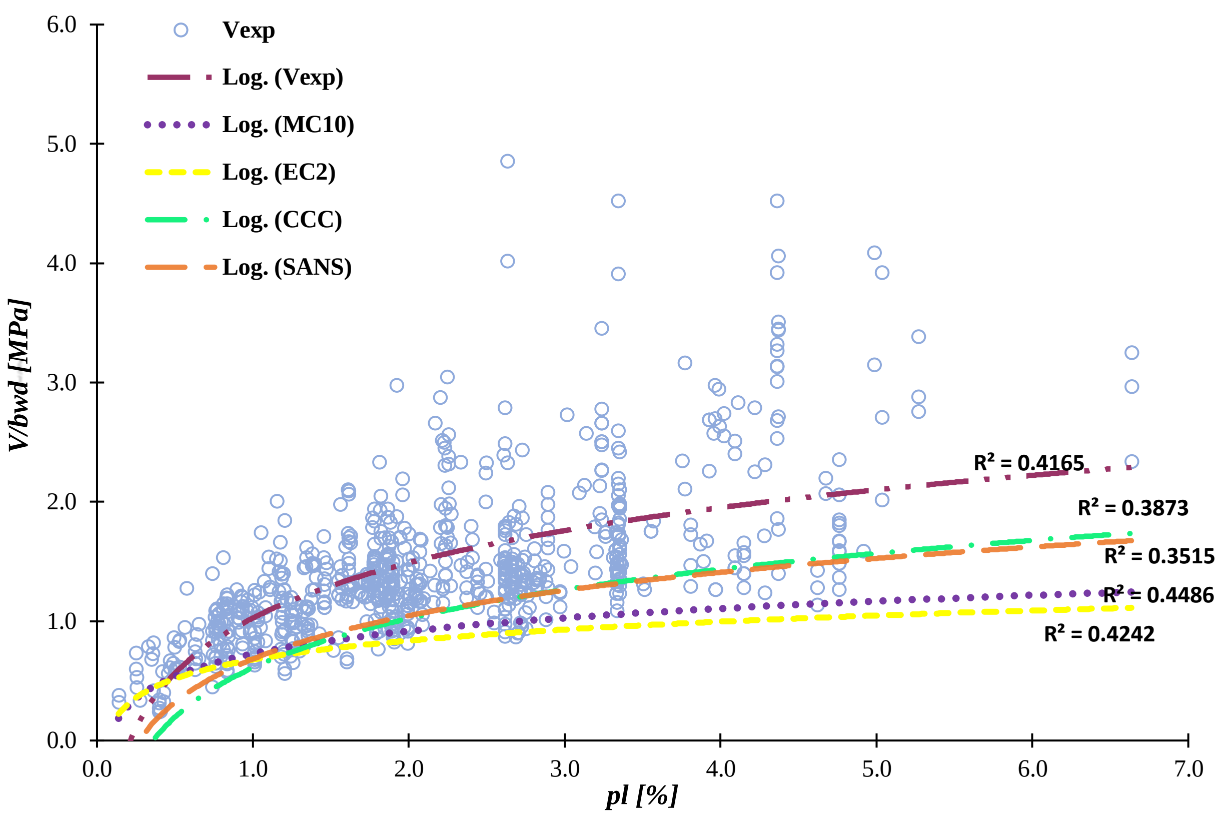

Fig.4.6 Comparison of normalized design shear capacity to experimental observation with respect to ρl (%)

The following observations were deduced from Fig.4.6 above

1. All considered design approaches provide conservative shear predictions with varying extents of conservatism.
2. At a longitudinal reinforcement ratio > 2%, V_{CCC} and V_{SANS} provide lesser conservative estimates of shear capacity compared to the V_{EC2} and V_{MC10} for the parametric range.
3. When contrasted with other shear design procedures, the EC2 design capacity provides the most conservative trend line.
4. Of the various design techniques taken into account in this study, at high levels of reinforcing bars percentage, the CCC design approach's trend line is the least conservative.

4.3 Statistical analysis of model factor observations

This section analyses the derived model factor for the investigated shear models by considering the statistical moments, distribution of model factors, identification of outliers, sensitivity analysis and appropriate probability distribution function.

4.3.1 Statistical moment

Table 4.1 Statistics of the model factors across the whole dataset

	MF_{EC2}	MF_{MC10}	MF_{ACI}	MF_{AS3600}	MF_{CCC}	MF_{MASM}	MF_{SNiP}	MF_{NLT}	MF_{SANS}
Counts	784	784	784	784	784	784	784	784	784
Mean	1.10	1.0	1.31	1.0	1.14	1.11	1.65	1.02	1.05
Std	0.30	0.34	0.31	0.34	0.28	0.28	0.52	0.16	0.28
COV (%)	27	34	24	34	25	25	32	16	27
Skewness	2.33	2.52	1.70	2.50	0.041	0.007	1.19	0.51	1.53
Min	0.41	0.26	0.63	0.26	0.28	0.31	0.60	0.57	0.28
Max	3.18	3.43	3.26	3.41	2.23	2.28	4.15	1.98	2.95
25%	0.93	0.82	1.12	0.82	1.02	0.98	1.32	0.94	0.87
50%	1.04	0.92	1.27	0.92	1.16	1.13	1.57	1.06	0.99
75%	1.18	1.09	1.44	1.09	1.28	1.25	1.88	1.17	1.12
Max/Min	7.76	13.19	5.17	13.12	8.00	7.35	7.00	3.47	10.54
Kurtosis	9.13	10.35	5.72	10.28	1.99	1.63	2.54	1.27	6.96

From Table 4.1, the investigation shows that MF_{NLT} has the smallest bias of 1.02 and a very low dispersion around the mean. The marginal scatter around the mean value is traceable to its standard deviation value (σ_{MF}) of 0.16, that is, the derived model uncertainty for each of the 784 tests is much closer to the distribution mean value showing consistency in its prediction. A coefficient of variation Ω_{MF} = 16% suggests that the model factor distribution for V_{NLT} has a low variability but is slightly higher than the recommended measure of variation for model uncertainty as stated by JCSS (2009) by 6%. These findings confirm that shear predictions of the mechanical model by Ngoc Linh Tran compare well with experimental shear values as it does not overpredict or underpredict shear values.

Both MF_{CCC} and MF_{MASM} have similar COV values of about 25%. As both shear models were derived by the same authors applying the same shear mechanism philosophy, this was anticipated. Though, it should be noted that the CCC shear model is a simplification of MASM with the major assumption that the uncracked compression chord is the main resisting or predominant transfer action in the considered failure state, hence eliminating other shear transfer mechanisms. This simplification resulted in the CCC model giving a more conservative shear prediction with just a 3% margin as compared to the MASM model, though in both cases, the models tend to underestimate the shear predictions by 14% ($\mu_{MF(CCC)}$=1.14) and 11% ($\mu_{MF(MASM)}$=1.11). Moreover, their COV values are higher than the threshold of 10% for model uncertainty in structural reliability models as recommended by JCSS (2001) and Holicky et al (2009). This is indicative of the random nature of shear mechanisms and the generally known arduousness in modelling their behaviour.

From Table 4.1, MF_{MC10} and MF_{AS3600} has the same mean (μ_{MF} = 1.0), the same standard deviation ($\sigma_{MF} = 0.34$) & the same coefficient of variation (34%), although there are differences in other statistical parameters as seen in Table 4.2. A mean of 1.0 indicates that shear models from (MC10 & AS3600) have no form of bias in shear resistance prediction, but the standard deviation = 0.34 suggests that the distribution of MF_{MC10} and MF_{AS3600} has a large scatter around the respective mean value. Also, a COV% value of 34% denotes that there is a low consistency in the shear prediction as there is a large variation between the mean value and predicted values. Hence, the standard deviation (σ_{MF}) and the Coefficient of variation (Ω_{MF}) negates the accuracy in the prediction of V_{MC10} & V_{AS3600}. The similarity in the statistical moments of both models is because the Fib Model Code adopted the term "k_v" from the Australian shear provision for beams without stirrups and incorporated into their level II approximation shear model which is only for beams without shear reinforcements as utilized in this research. Hence, a similar performance is expected.

The unbiased shear resistance function V_{EC2} persistently underpredicts shear capacity by offering estimations 10% more conservative than actual shear values, as evidenced by the result that MF_{EC2} has a mean value of 1.10. Irregularity in predictions for shear model uncertainty is indicated by the scatter of

0.30, which suggests a significant dispersion of MF_{EC2} around the mean. A variability index of 27% also indicates this.

Quantification of the model uncertainty associated with ACI showed that MF_{ACI} underestimates the shear resistance. A mean of (μ_{MF} = 1.31) suggests that the ACI shear model gives estimates that are 31% more conservative as compared to experimental shear values. The standard deviation and coefficient of variation also suggest a large scatter around the mean and inconsistency in shear prediction with values of 0.31 & 24%.

The investigation also shows that MF_{SANS} has a small bias of 1.05 but a high dispersion around the mean. The large scatter around the mean value can be ascribed to its standard deviation value (σ_{MF}) of 0.28, that is, the distribution of MF_{SANS} is such that they are far below or above the mean value.

Statistical moments of MF_{SniP} seem to be the least favourable among all the investigated shear models. V_{SniP} shear strength predictions showed a poor correlation to the experimental results with its model factors (MF_{SniP}) having a mean value of μ_{MF} = 1.65 and standard deviation σ_{MF}= 0.56.

The statistical moments show that the SniP shear model is overly conservative as it provides very low shear resistance estimates. A high deviation value indicates that the distribution is highly scattered around its mean. The measure of variation in MF_{SniP} also questions the integrity of this model in its consistency in shear capacity prediction (Ω_{MF} = 32%).

Table 4.2 Statistics of mean value model factors for flanged beams

	MF_{EC2}	MF_{MC10}	MF_{ACI}	MF_{AS3600}	MF_{CCC}	MF_{MASM}	MF_{SNiP}	MF_{NLT}	MF_{SANS}
Counts	64	64	64	64	64	64	64	64	64
Mean	1.45	1.28	1.56	1.28	0.57	0.64	1.96	1.00	0.71
Std	0.57	0.61	0.58	0.61	0.26	0.30	0.69	0.20	0.33
COV (%)	39	48	37	48	46	47	35	20	46
Skewness	1.34	1.36	1.16	1.36	1.11	1.15	1.30	0.42	1.17
Min	0.88	0.66	0.92	0.66	0.28	0.31	1.16	0.64	0.28
Max	3.18	3.18	3.26	3.18	1.22	1.42	4.15	1.47	1.60
25%	1.04	0.88	1.17	0.88	0.41	0.44	1.48	0.85	0.49
50%	1.17	1.02	1.33	1.02	0.48	0.53	1.64	0.98	0.58
75%	1.67	1.48	1.76	1.48	0.72	0.77	2.36	1.11	0.95
Max/Min	3.61	4.82	3.54	4.82	4.36	4.58	3.58	2.30	5.71
Kurtosis	0.68	0.78	0.31	0.78	0.02	0.07	1.19	0.40	0.33

Information from Table 4.2 shows that EC2, MC10, ACI, AS3600 and Modified SNiP shear resistance models for beams without shear reinforcement underestimate the shear resistance for flanged beams. The test was conducted on 64 flanged beam specimens with varied material properties.

It was found that V_{SNIP}, V_{ACI} and V_{EC2} are extremely conservative when predicting the shear capacity of a reinforced concrete flanged beam without shear reinforcement with a mean value of model factor (μ_{MF}) = 1.96, 1.56 and 1.45. A corresponding high deviation from their respective mean value and large variation in prediction was also discovered. Shear predictions from V_{MC10} and V_{AS3600} tend to be less conservative as compared to V_{SNIP}, V_{ACI} and $V_{EC2.}$ The mean of the model factors was found to be 1.28, denoting a 28% conservatism. It was also found that MF_{MC10} and MF_{AS3600} are widely scattered around their mean value (σ_{MF} = 0.61) with a large extent of variation (Ω_{MF} = 48%).

$MF_{CCC,}$ MF_{MASM} & MF_{SANS} were found to have a mean of (μ_{MF}) = 0.57, 0.64 &0.71. this implies that these models generally overpredict the shear capacity for flanged beams without shear reinforcement. A high COV and high scatter were also identified. See Table4.2.

Statistical moments of MF_{NLT} for flanged beams seem to be consistent with that of the full database. A 2% drop in the mean value and a 25% increase in the measure of variability were recorded, this brings the statistical properties to (μ_{MF} = 1, $\Omega_{MF} = 20\%$).

Table 4.3 Statistics of mean value model factors for rectangular beams

	MF_{EC2}	MF_{MC10}	MF_{ACI}	MF_{AS360}	MF_{CCC}	MF_{MASM}	MF_{SNiP}	MF_{NLT}	MF_{SANS}
Counts	720	720	720	720	720	720	720	720	720
Mean	1.07	0.98	1.29	0.98	1.19	1.15	1.62	1.05	1.07
Std	0.25	0.30	0.26	0.29	0.22	0.24	0.50	0.17	0.27
COV (%)	23	31	20	30	18	21	31	17	26
Skewness	1.53	2.33	0.96	2.30	0.77	0.79	1.04	0.56	2.48
Min	0.41	0.26	0.63	0.26	0.60	0.54	0.60	0.57	0.28
Max	2.65	3.43	2.63	3.41	2.23	2.28	3.97	1.98	2.95
25%	0.92	0.81	1.12	0.81	1.05	1.02	1.31	0.95	0.90
50%	1.03	0.92	1.27	0.92	1.18	1.15	1.55	1.07	1.00
75%	1.16	1.08	1.42	1.08	1.30	1.26	1.85	1.17	1.13
Max/Min	6.46	13.19	4.17	13.12	3.72	4.22	6.62	3.47	10.54
Kurtosis	5.55	11.96	2.40	11.75	2.45	2.33	2.12	1.52	12.09

From Table 4.3, MF_{MC10} and MF_{AS3600} both has a mean (μ_{MF}) = 0.98 (close to 1 as seen in table 4.1). This is indicative of a slight overprediction of the V_{MFC10} and V_{AS3600} by 2%. A large scatter around the mean shows how uncertain the predictions of these models can be.

MF_{SniP} has a mean value of 1.62 and a standard deviation of 0.50. predictions from the SNiP shear models continue to give overly conservative values across all databases (full database, flanged sections and rectangular sections). A high bias as seen in the case of MF_{SniP} suggests that V_{SniP} has a very poor performance in estimating shear capacity compared to other shear models. Its high coefficient of variation and the standard deviation is also indicative of its uncertainty measure in predicting shear resistance.

The mean (μ_{MF}) of MF_{NLT} increased by 3% as compared with the full database mean value. A mean value of 1.05 is just 5% conservative. Predictions from the V_{NLT} model are also characterized by a low scatter of model factors around the mean value and low variability in the model factors distribution. The statistical moments of MF_{NLT} indicate that the mechanical model best predicts the shear capacity and represents reality (experimental observations of shear) well as it is characterized by a low bias, low scatter and low variation in the distribution of model factor.

Table 4.4 Statistical design value model factors for the whole database

	$\boldsymbol{MF_{EC2}}$	$\boldsymbol{MF_{MC10}}$	$\boldsymbol{MF_{CCC}}$	$\boldsymbol{MF_{SANS}}$
Counts	784	784	784	784
Mean	1.72	1.60	1.63	1.48
Std	0.48	0.54	0.42	0.33
COV (%)	28	34	26	22
Skewness	2.34	2.38	-0.26	0.55
Min	0.65	0.43	0.41	0.45
Max	4.99	5.15	3.18	3.47
25%	1.46	1.31	1.42	1.32
50%	1.63	1.49	1.65	1.48
75%	1.86	1.75	1.86	1.65
Max/Min	7.68	11.98	7.76	7.71
Kurtosis	9.14	9.43	1.28	3.19

From table 4.4, it can be seen that all shear expression for the considered design resistance models generally underpredicts the shear strength. This is due to the inclusion of safety factors and the use of characteristic values of material properties rather than mean values.

Of all considered models, the statistics of MF_{EC2} shows that its degree of conservatism exceeds every other model with a mean value μ_{MF} = 1.72. The standard deviation σ_{MF} = 0.48 is also worthy of attention as it signifies a large scatter around the mean of 1.72. Lastly, the uncertainty associated with shear predictions following the V_{EC2} is validated by a high measure of variation Ω_{MF} = 0.28.

Though 48% conservative, the statistics of MF_{SANS} seems to be more favourable among the considered shear methods. The mean value of model factor realizations associated with the V_{SANS} the shear method was seen to be the smallest of the derived μ_{MF}. In terms of model factor distribution, MF_{SANS} realization seems to be more clustered around the mean as compared to the realizations from the alternative shear methods and also less uncertain as seen in table 4.4 owning to a value of σ_{MF} = 0.33 and Ω_{MF} = 0.22 which is the smallest across the database.

The uncertainty surrounding the shear prediction following the V_{MC10} is significant as it has the highest scatter around the mean, σ_{MF} = 0.54, which signifies inconsistency in shear prediction. Despite having a mean value of 1.60, implying a conservatism less than MF_{EC2} and MF_{CCC}, the large scatter and notable coefficient of variation Ω_{MF} = 0.34 suggest an uncertainty concern.

4.3.2 Histogram of model factors

The histogram reveals the following characteristics, which may not be explicitly visible initially:

- An indication of the skewness or symmetricity of the model factor distribution.
- How spread out the observed MF realization are
- The extent to which the observed data is scattered about the measure of central tendency
- Modality of MF realizations.
- Erroneous data that does not belong with other data of interest (outliers)
- Point of increasing conservative bias.

After a close examination of the histogram's plots (representing nine datasets of model factor observations), the following observations were made from Fig.4.7.

- Near the mean MF, most of the data points are consolidated.
- Excluding MF_{CCC} & MF_{MASM}, the majority of the observations are not symmetric about the peak frequency, suggesting that the sampling distribution is not normal for certain points. As skewness is often associated with a log-normal distribution, this suggests that a low-reliability prediction of shear strength is expected as a consequence of the distribution of the model factor realization.
- The histogram's spans show how much variance there is.

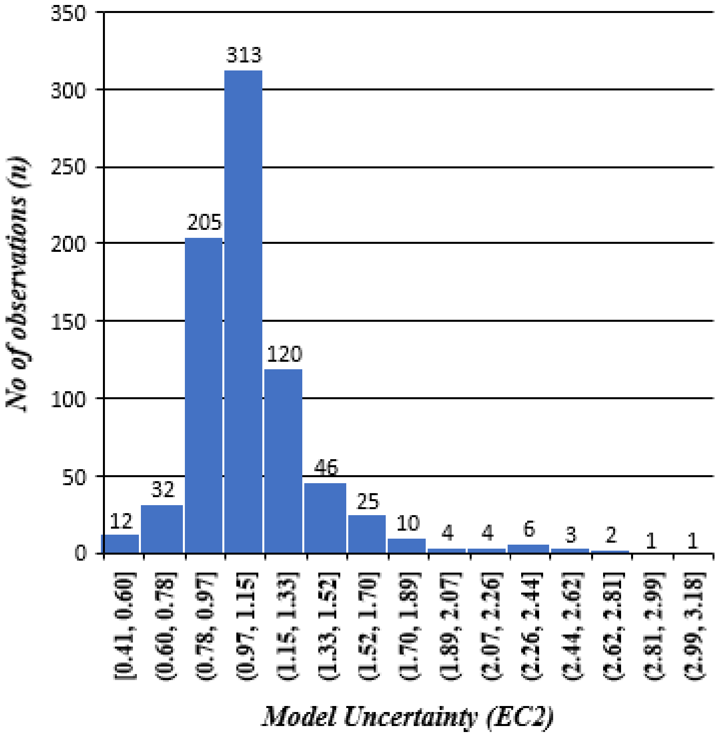

(a) MF_{EC2}

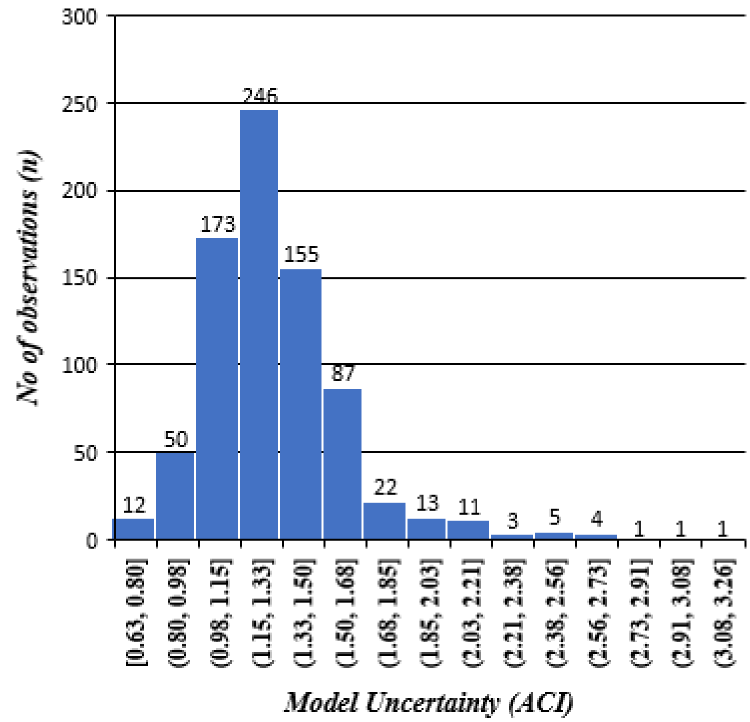

(b) MF_{ACI}

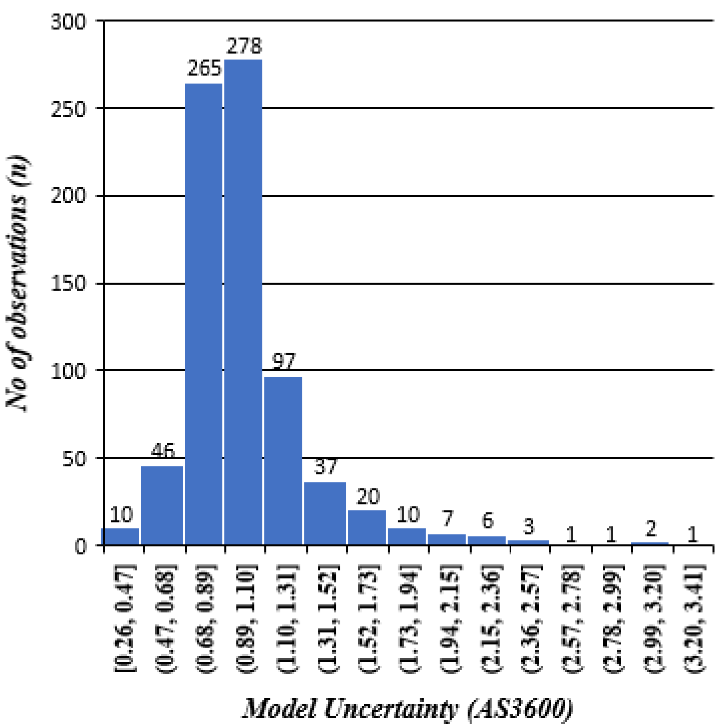

(c) MF_{AS3600}

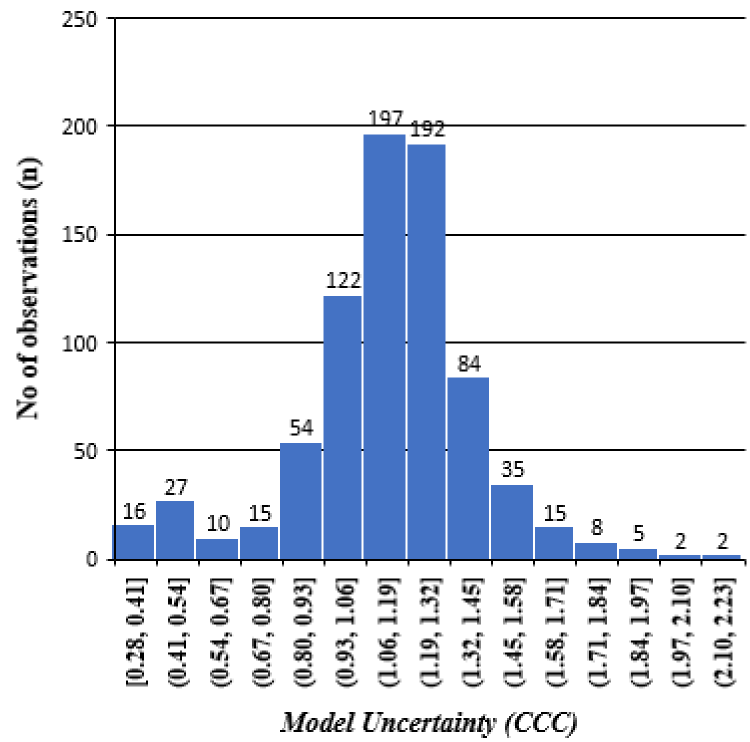

(d) MF_{CCC}

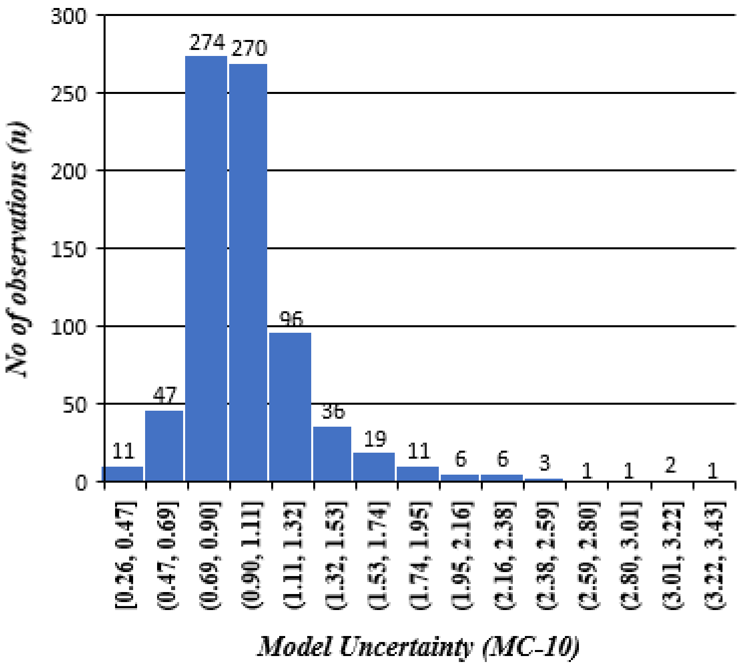

(e) MF_{MC-10}

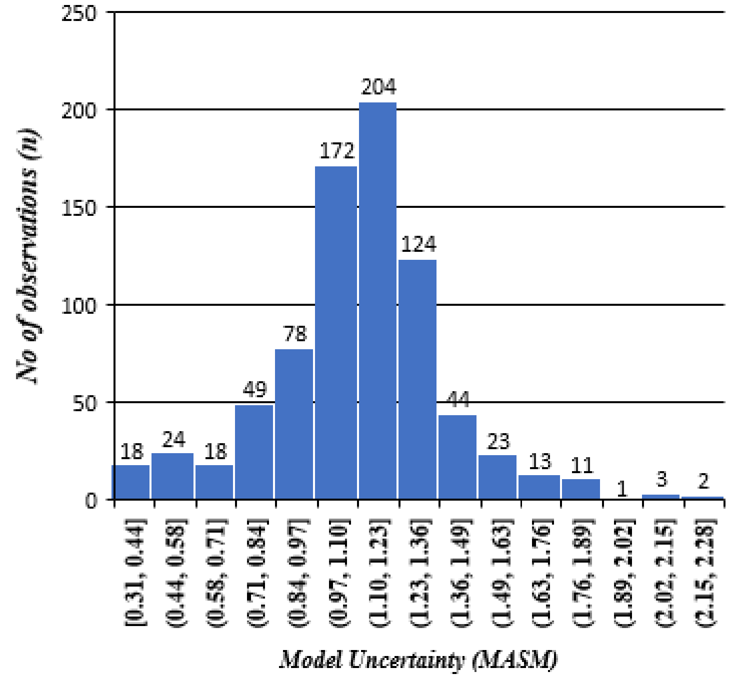

(f) MF_{MASM}

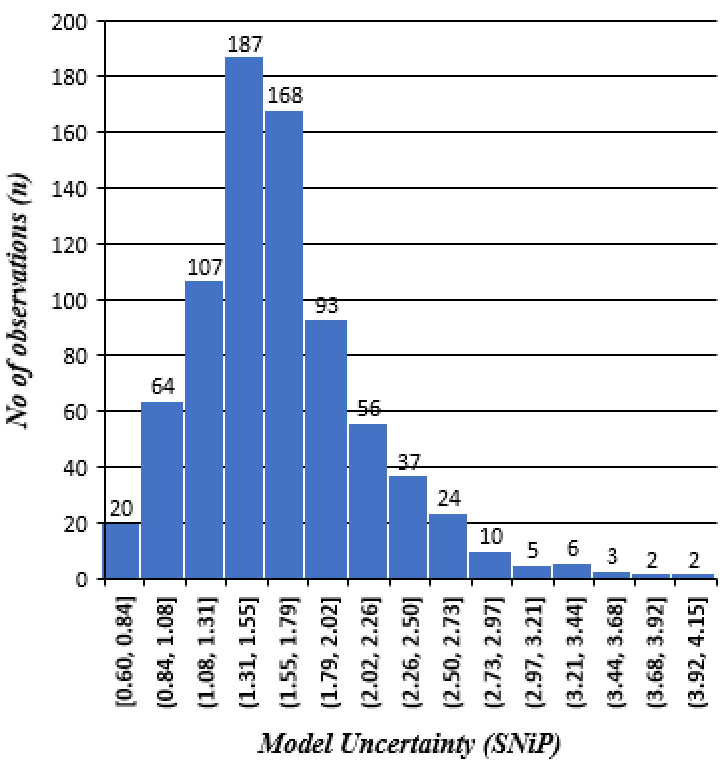

(g) MF_{SNiP}

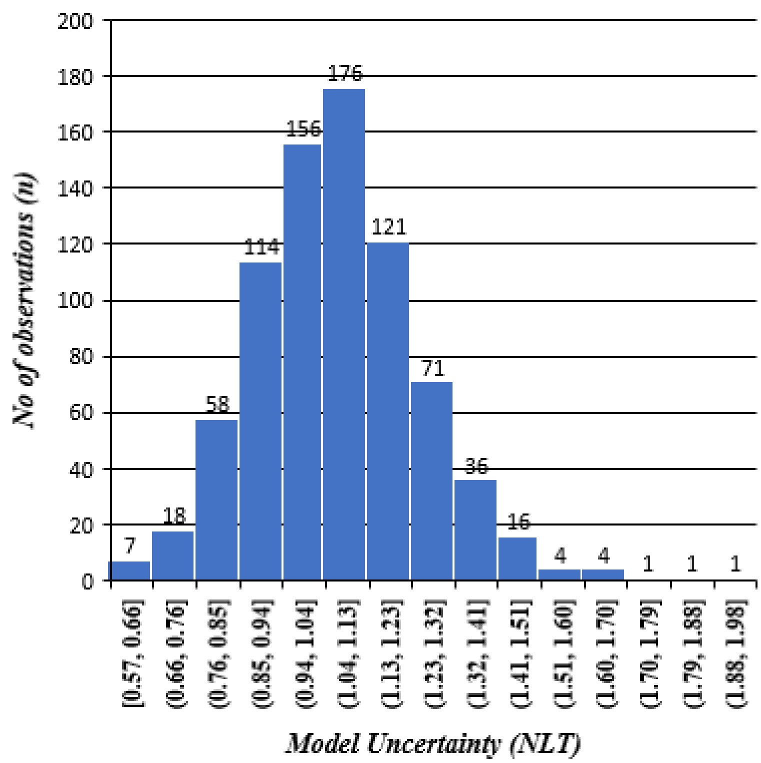

(h) MF_{NLT}

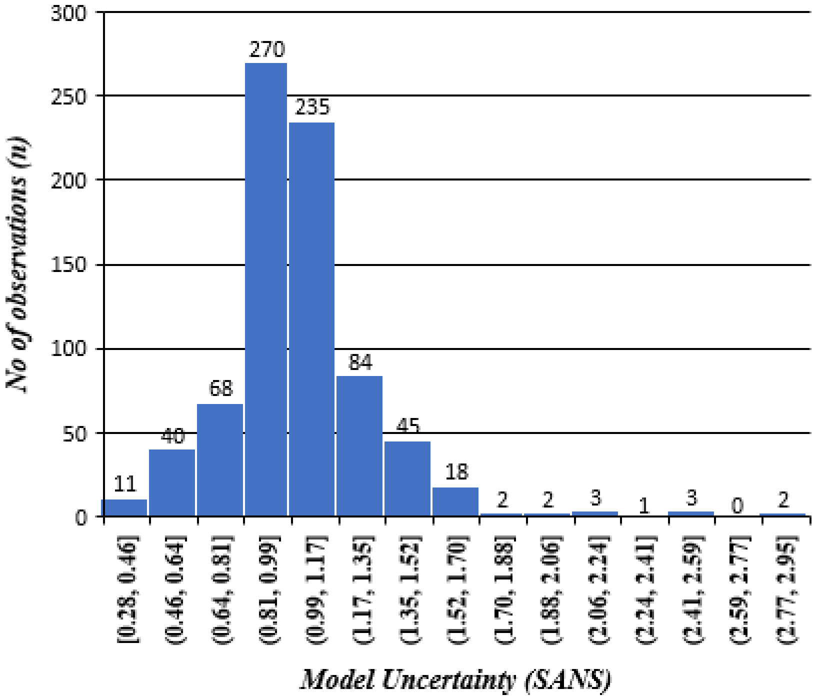

$(\boldsymbol{i})$ $\boldsymbol{MF_{SANS}}$

Fig. 4.7 Histograms of the model factors

4.3.3 Identification of outliers

Outliers also reveal the extent of variation and abnormality in a distribution. Fig 4.8 presents the boxplot, a statistical tool, that shows the summary of the distribution of MF realizations in terms of the minimum, maximum, 25th percentile, median or 50th percentile, 75th percentile and the outliers present in a data distribution.

From Fig 4.8, the plot shows that MF_{NLT} has the least outliers in comparison to other model factor realizations. For all 784 data points, only 6 points were considered outliers with 5 points positioned above $\mu + 3\sigma$ and just one point below $\mu - 3\sigma$. 0.77% of MF_{NLT} is considered an outlier which is quite insignificant. Hence, the unsubstantial quantity of outliers discovered infers there is no form of variation or an inconsequential variability in MF_{NLT}.

From Fig 4.8, the plot shows that MF_{CCC}, MF_{MASM}, MF_{SANS}, MF_{ACI}, MF_{SNiP} has more outliers in comparison to the MF_{NLT} realization with some outliers ranging between 1.5% - 2% of the entire data points. This signifies an increased variability in model factors distribution as compared to MF_{NLT}.

From Fig 4.8, the plot infers MF_{AS3600}, MF_{MC10}, MF_{EC2} has the most extent of variability as more numbers of outliers were found in comparison to the MF realizations of other shear models with some outliers ranging between 2.5% - 3% of the entire data points.

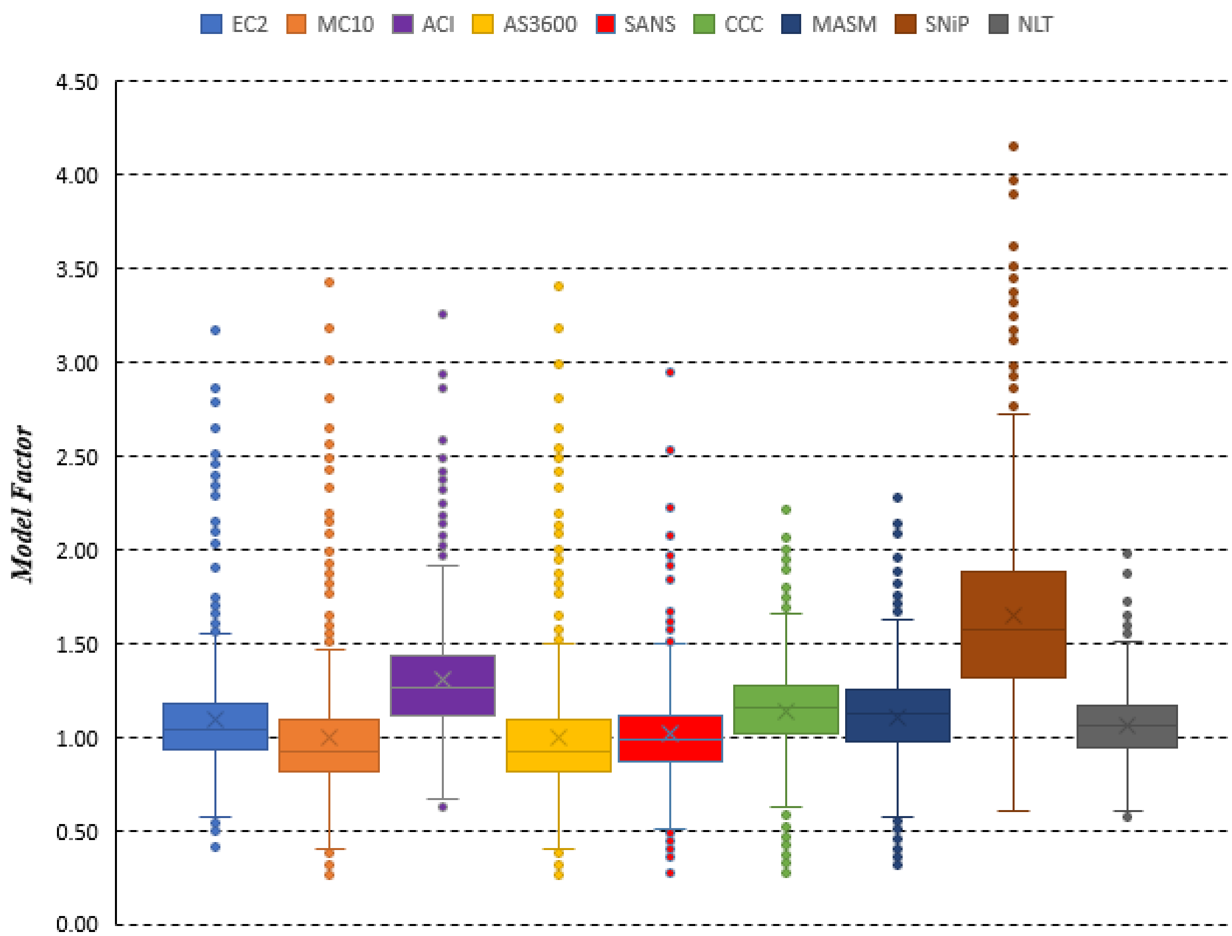

Fig 4.8 Box-plot of the model factors

4.3.4 Sensitivity analysis of model factors

In this section, separate parametric scatter plots for MF_{EC2}, MF_{ACI}, MF_{AS3600}, MF_{CCC}, $MF_{MC10-II}$, MF_{MASM}, MF_{SNiP}, MF_{NLT} and MF_{SANS} against the major influencing shear strength parameters are presented in Figs. 4.9 – 4.17. The lines that better describe the trend of different MF realizations with shear parameters are shown on the plots. Corresponding trend equations and coefficient of determination (R^2) values are also indicated to give a robust examination. A stronger coefficient of determination R^2 signifies a strong trend between model factor realization and shear parameters which is exactly what to look out for. Lesser values of R^2 Pose no threat as there is no cause for concern. A significant trend implies a strong R^2 value which also implies an inadequate consideration of the shear parameter in shear model formulation.

Table 4.5 Pearson correlation coefficient between model factors and shear parameters

	Pearson Correlation coefficient r				
	$\boldsymbol{b_w(mm)}$	$\boldsymbol{a/d}$	$\boldsymbol{d(mm)}$	$\boldsymbol{\rho l}(\%)$	$\boldsymbol{f_{ck}[MPa]}$
$\boldsymbol{MF_{EC2}}$	-0.22	-0.22	-0.34	0.5	0.018
$\boldsymbol{MF_{ACI}}$	-0.13	-0.33	-0.12	0.12	-0.25
$\boldsymbol{MF_{MC\text{-}10}}$	-0.18	-0.28	-0.26	0.35	0.068
$\boldsymbol{MF_{AS3600}}$	-0.18	-0.28	-0.26	0.35	0.061
$\boldsymbol{MF_{CCC}}$	0.039	-0.24	0.14	-0.22	-0.13
$\boldsymbol{MF_{MASM}}$	-0.032	-0.17	0.033	-0.061	-0.21
$\boldsymbol{MF_{SNiP}}$	-0.13	-0.12	0.077	0.42	-0.32
$\boldsymbol{MF_{NLT}}$	0.086	0.083	0.12	-0.18	-0.0038
$\boldsymbol{MF_{SANS}}$	0.027	-0.40	-0.018	0.075	0.48

4.3.5 Sensitivity analysis discussion of model factors

4.3.5.1 $\mathbf{MF_{EC2}}$ trend analysis

Correlation with d

From Fig. 4.9(a), MF_{EC2} shows a weak negative trend with the beam effective depth (d) with a Pearson correlation coefficient of -0.34 as seen in Table 4.4. The plot shows that the mean shear function of EC2 provides conservative estimates of shear capacity at d < 500mm. a decreasing conservative bias for the range of beam depth considered is seen as beam depth increases beyond 500mm. V_{EC2} generally overpredicts the shear capacity of beams (d > 500mm) without stirrups. Variation in the performance of V_{EC2} across the range of depth is due to the improper calibration of this concrete term.

Correlation with b_w, a/d & f_{ck}

MF_{EC2} displays a weak negative trend with a/d and bw with a correlation value of -0.22 according to the Pearson correlation matrix as seen in Table 4.4. shear predictions of the EC2 shear model tend to become unconservative as the beam width and shear span – effective depth ratio increases beyond 500mm and 5 respectively. While the concrete strength (f_{ck}), no significant trend is identified for the relationship with MF_{EC2} as a correlation value of 0.018 was recorded. This is indicative of the meticulousness in calibrating the concrete strength term during the formulation of EC2 shear model expression.

Correlation with pl

Figure 4.9 e displays a suggestive trend between MF_{EC2} and pl, with a positive correlation value of 0.50. as seen in Table 4.6. The graph demonstrates that as pl increases, V_{EC2} dramatically underestimates capacity at high pl ratios. Marginally unconservative estimates of V_{EC2} is achieved at a minimal amount of longitudinal reinforcement ratio (pl < 2 %). The conservatism of the EC2 shear model at low pl ($pl <$ 2%) is caused by the limitation placed on the allowable percentage of longitudinal reinforcement. This suggests that pl is $V_{EC2's}$ most important parameter.

4.3.5.2 MF_{ACI} trend analysis

Correlation with b_w, d & pl

The plot of MF_{ACI} shows an insignificant trend with b_w, d & pl with a correlation coefficient of –0.13, -0.12 & 0.12 respectively. The absence of any observable trend suggests that these shear parameters were perfectly calibrated in the ACI shear provision for beams without stirrups. Moreover, it is worth mentioning that V_{ACI} consistently underestimates the shear capacity across the range of considered parameters with a very weak trend observation which is quite negligible. The introduction of a properly calibrated size effect modification term (λ_s) in the ACI 318-19 shear provision is the reason the model factor is insensitive to beam depth (d) as compared to the shear provision in ACI 318 -14.

Correlation with a/d & f_{ck}

MF_{ACI} displays a fairly significant negative correlation with a/d & f_{ck} with a weaker correlation seen in the plot of MF_{ACI} against a/d. A decreasing conservative bias is observed for the plot of MF_{ACI} against a/d with a correlation value of -0.33. The sensitivity of MF_{ACI} to the a/d ratio is a result of its neglection in the ACI shear provision. Similarly, a weak negative correlation is seen between MF_{ACI} and f_{ck}. A decreasing conservative bias is seen as the concrete strength increases (fig 4.10e) with a correlation value of -0.25.

4.3.5.3 $\mathbf{MF_{AS3600}}$ & $\mathbf{MF_{MC10}}$ trend analysis

The model factor distribution of V_{AS3600} and V_{MC10} displays the same correlation coefficient and response to increasing shear parameters.

Correlation with $\mathrm{b_w}$& $\mathrm{f_{ck}}$

From Figures 4.11, 4.13 and Table 4.4, the trends in MF_{AS3600} & MF_{MC10} with the concrete strength (fck) and the beam width (b_w) shows no significant correlation. Both model factors have a correlation coefficient of -0.18 with the beam width, while a value of 0.061 and 0.068 was seen as the correlation coefficient of MF_{AS3600} & MF_{MC10} against f_{ck}.

Correlation with $\mathrm{a/d, d}$ & pl

MF_{AS3600} & MF_{MC10} displays a fairly significant negative trend with $\mathrm{a/d}, d$ & pl with a correlation coefficient of -0.28, -0.26 and -0.35 respectively. From Figures 4.11c & 4.13c, it can be observed that the model factors were initially unconservative at ρl<2% and started to become conservative at ρl > 2%. In like manner, V_{AS3600} & V_{MC10} begins to overestimate the shear capacity at d > 500mm and a/d >3.

4.3.5.4 $\mathbf{MF_{CCC}}$ trend analysis

MF_{CCC} only showed weak correlations with $\mathrm{a/d}$ (-0.24) & pl (-0.22), while a very weak or nonexistent relationship was seen as indicated by the Pearson correlation matrix in the plot of MF_{CCC} against b_w, d & f_{ck} with correlation coefficient values of 0.039, 0.14 and -0.13 respectively.

A decreasing conservative bias is seen as the shear span to effective depth ratio and longitudinal reinforcement ratio increase. At ρl < 4 – 4.5%, the model factor distribution is characterized by conservative estimates. While at ρl > 4 – 4.5%, MF_{CCC} becomes less conservative in cases when there are fewer data points.

4.3.5.5 $\mathbf{MF_{MASM}}$ trend analysis

Correlation with $\mathrm{d, bw, pl, a/d, f_{ck}}$

MF_{MASM} realizations only displayed a weak relationship with the concrete strength f_{ck} owing to a correlation coefficient of -0.21. a minimal decrease in conservative bias is seen as the concrete strength increases with MF_{MASM} being unconservative at f_{ck}> 80Mpa.

MF_{MASM} showed no observable trend with other parameters influencing shear capacity. Insignificant correlation coefficient values as seen in table 3.8 were assigned to these parameters ($d = 0.033,\ bw, = -0.032,\ pl = -0.061, a/d = -0.17$).

4.3.5.6 MF_{SNiP} trend analysis

Correlation with $\mathrm{d, bw, a/d}$

Fig 4.15 (a), (b) and (d) showed that MF_{SNiP} did not display any major trend with the effective depth d, beam width bw and the shear span to effective depth ratio a/d with insignificant correlation coefficient values of 0.077, -0.13 and -0.12 respectively as seen in table 3.8. The insensitivity of the MF_{SNiP} to the effective depth was not unexpected as the term (d) was adequately recalibrated with the same extended database of 784 beams without shear reinforcement compiled by Reinick et al (2014).

Correlation with $\mathrm{pl}, \mathrm{f_{ck}}$

The plot of MF_{SNiP} displayed a significant positive trend (r = 0.42) with the longitudinal reinforcement ratio and a negative trend (r = -0.32) with the concrete strength. In Fig 4.15 c, an increasing conservative bias is seen as the longitudinal reinforcement ratio increases with a majority (More than 85%) of the data point being conservative, this implies that the SNiP method does not adequately account for the longitudinal reinforcement ratio in shear resistance. Fig 4.15e suggests a decreasing trend between MF_{SNiP} and increasing concrete strength f_{ck} with a correlation coefficient of -0.32.

4.3.5.7 MF_{NLT} trend analysis

$Correlation$ with $d, b\mathrm{w}, pl, a/d\ , f_{ck}$

The plots of MF_{NLT} against all the shear parameters showed no trend that is worthy of attention as no serious relationship can be identified between MF_{NLT} realizations and the considered influencing shear factors. From table 4.4, the correlation coefficients were found to be negligible.

$(b\mathrm{w} = 0.086, \mathrm{d} = 0.12, pl = -0.18\ , \frac{a}{d} = 0.083, f_{ck} = -0.0038)$.

4.3.5.8 MF_{SANS} trend analysis

MF_{SANS} displayed no form of interrelationship with the beam width, effective depth and longitudinal reinforcement ratio with an inconsequential correlation coefficient of 0.027, -0.018 and 0.075 respectively. MF_{SANS} shows a strong trend with a/d $(r = -0.40)$ & f_{ck} $(r = 0.48)$, an increasing conservative bias is seen in the plot of MF_{SANS} against incremental values of f_{ck}. At f_{ck} < 40Mpa, a greater part of the MF_{SANS} realizations tend to be unconservative. This does not hold as the concrete strength crosses beyond 40Mpa, because the majority of the data point becomes conservative as seen in fig 4.17c. similarly, in the plot of MF_{SANS} realization against the shear span – effective depth ratio, a decreasing conservative bias is observed as a majority of datapoint starts to provide unconservative estimates at a/d > 4. The sensitivity of MF_{SANS} to the concrete strength is due to the limitation placed on the permissible concrete strength $(f_{ck} \leq 40MPa)$, while inadequate calibration or neglection of the

"a/d" term in the SANS10100 shear provision may be the cause of MF_{SANS}'s sensitivity to the shear span to effective depth ratio.

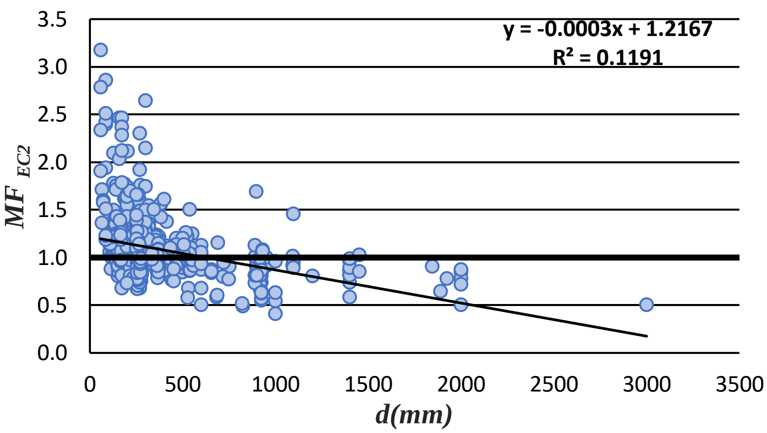

(i) $\boldsymbol{MF_{EC2}\ versus\ d}(\boldsymbol{mm})$

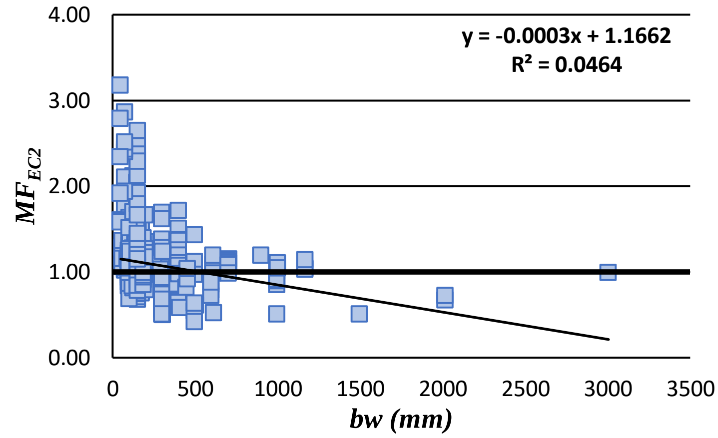

(ii) $\boldsymbol{MF_{EC2}\ versus\ b_w}(\boldsymbol{mm})$

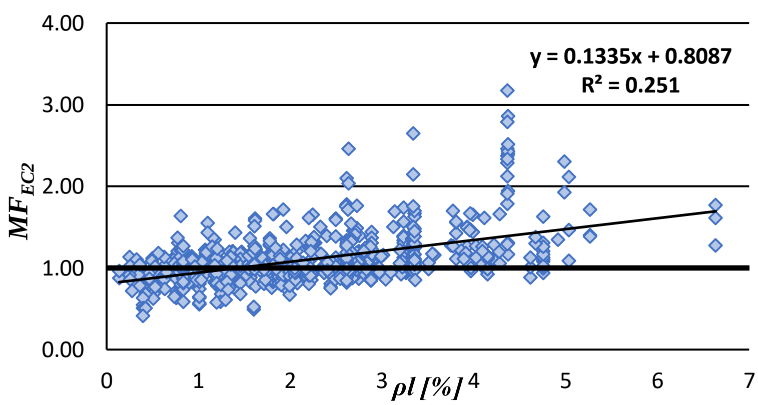

(iii) $\boldsymbol{MF_{EC2}\ versus\ \rho l}(\%)$

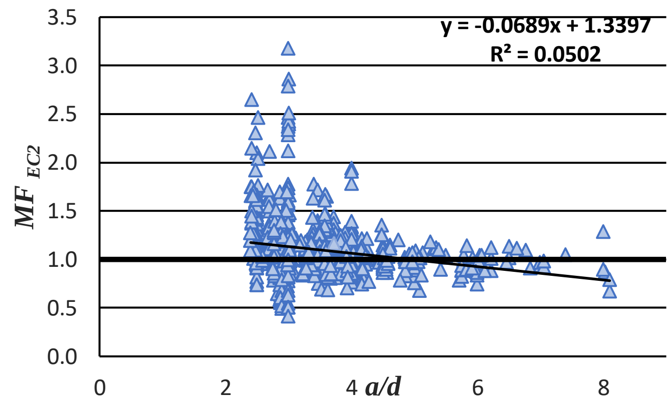

(iv) $\boldsymbol{MF_{EC2}\ versus\ a/d}$

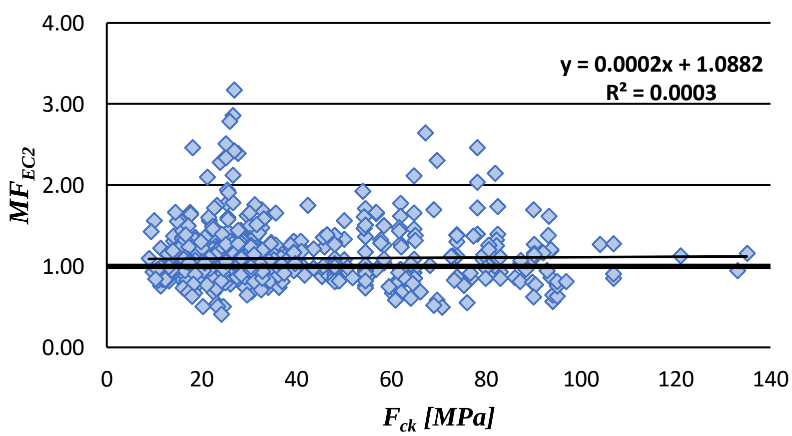

$(\boldsymbol{V})\ \boldsymbol{MF_{EC2}\ versus\ f_{ck}}(\boldsymbol{MPa})$

Fig 4.9. Sensitivity plot of $\boldsymbol{MF_{EC2}}$ against (i) d (ii) bw (iii) ρl (iv) a/d (v) fck

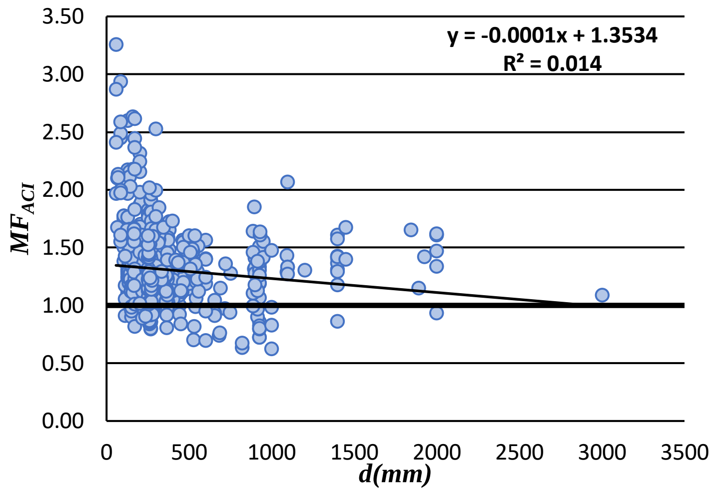

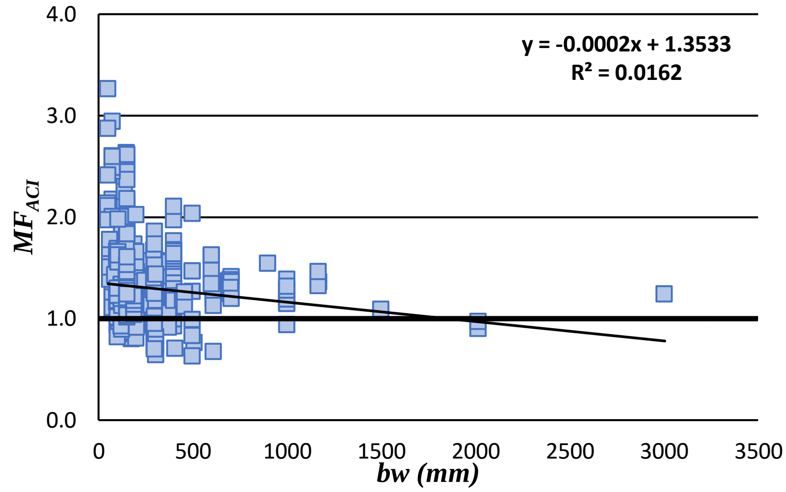

(i) MF_{ACI} *versus* $d(mm)$

(ii) MF_{ACI} *versus* $b_w(mm)$

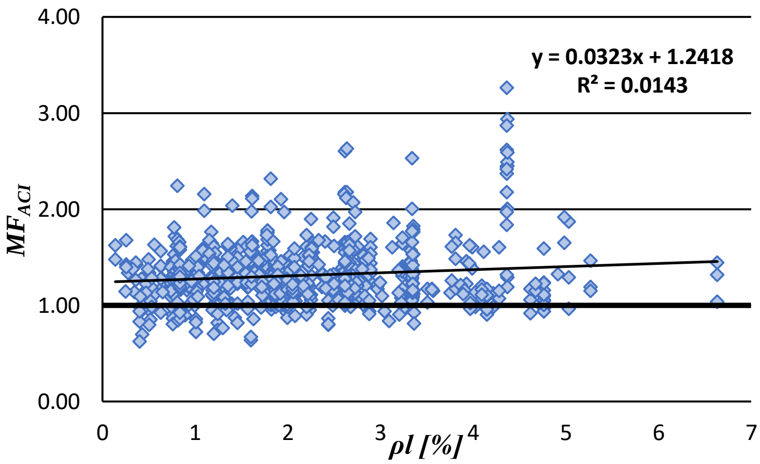

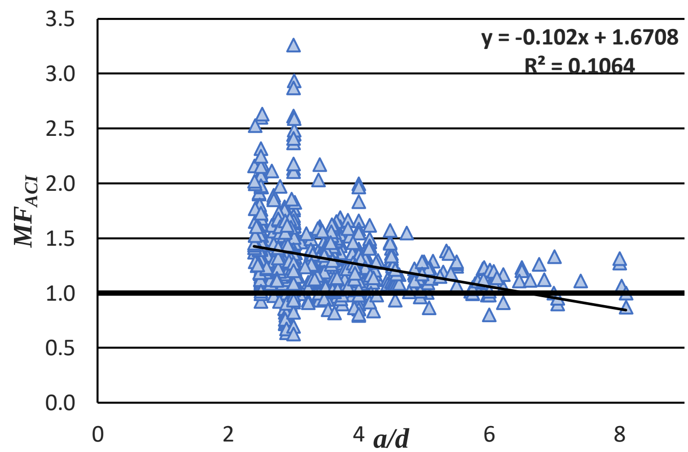

(iii) MF_{ACI} *versus* $\rho l(\%)$

(iv) MF_{ACI} *versus* a/d

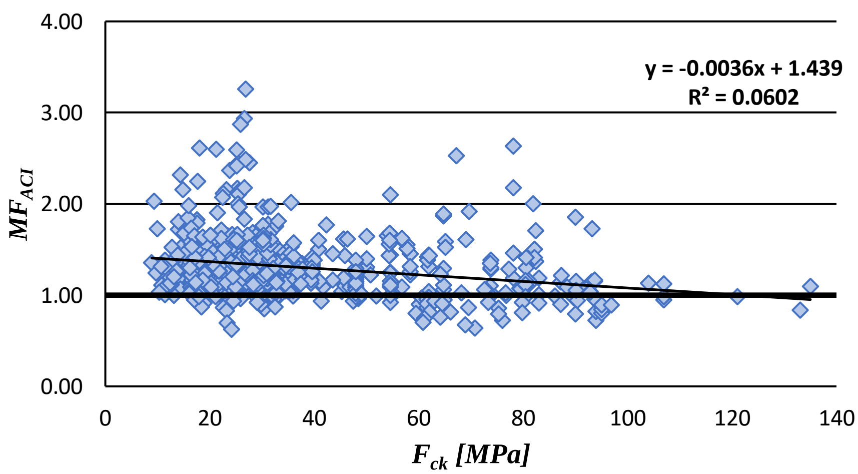

(v) MF_{ACI} *versus* f_{ck} (MPa)

Fig. 4.10. Sensitivity plot of MF_{ACI} against (i) d (ii) bw (iii) ρl (iv) a/d (v) fck

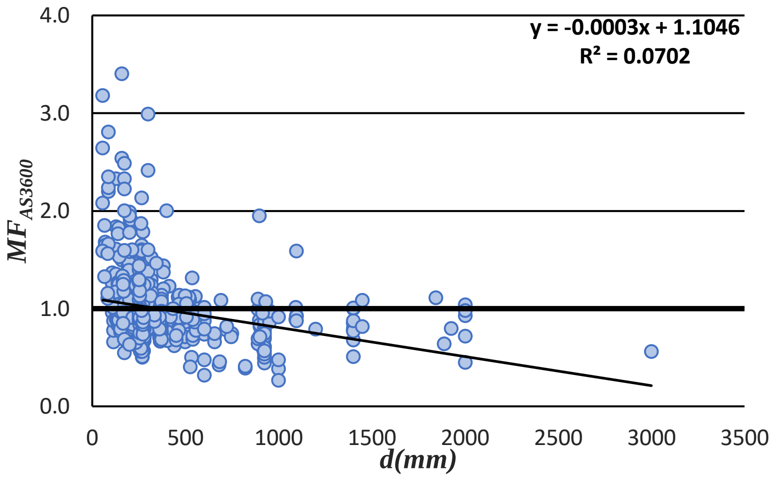

(i) $\boldsymbol{MF_{AS3600}\ versus\ d(mm)}$

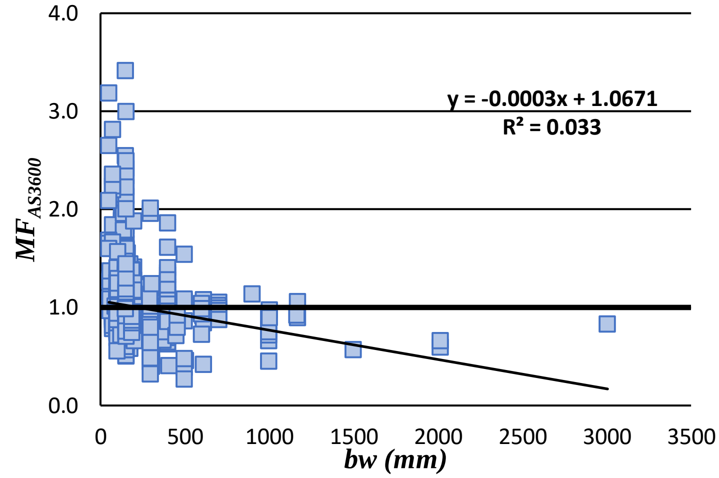

(ii) $\boldsymbol{MF_{AS3600}\ versus\ b_{\mathrm{w}}(mm)}$

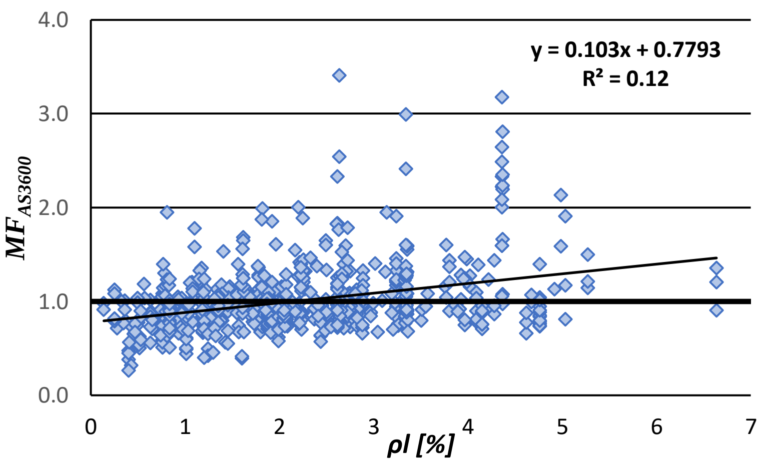

(iii) $\boldsymbol{MF_{AS3600}\ versus\ \rho l}(\%)$

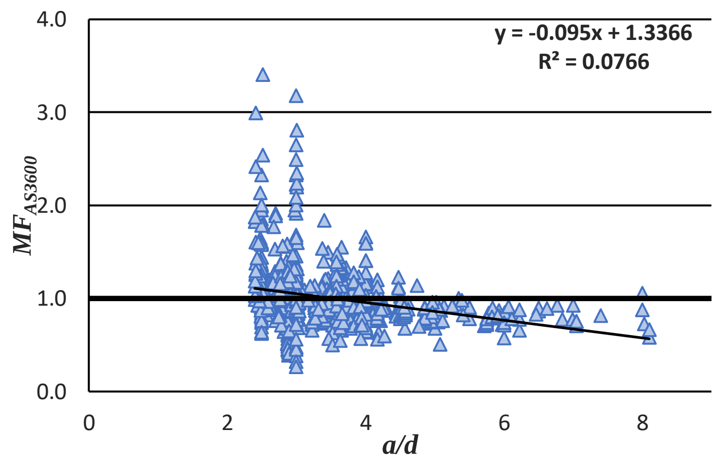

(iv) $\boldsymbol{MF_{AS3600}\ versus\ a/d}$

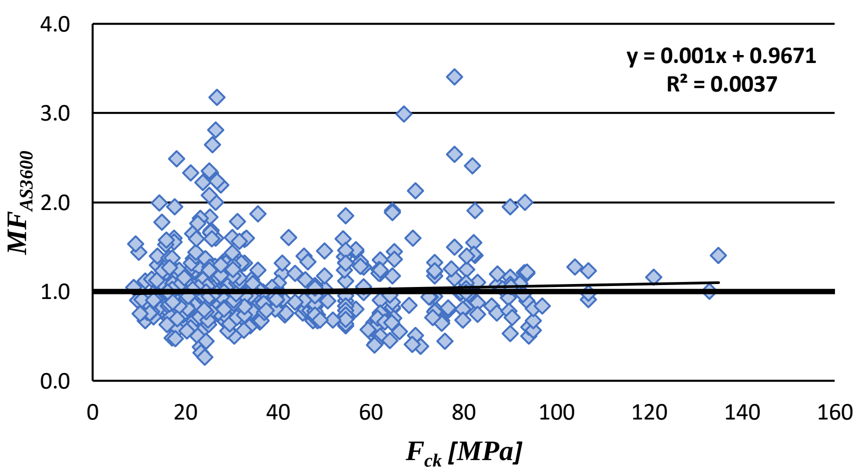

(v) $\boldsymbol{MF_{AS3600}\ versus\ f_{ck}(MPa)}$

Fig. 4.11. Sensitivity plot of $\boldsymbol{MF_{AS3600}}$ against (i) d (ii) bw (iii) ρl (iv) a/d (v) fck

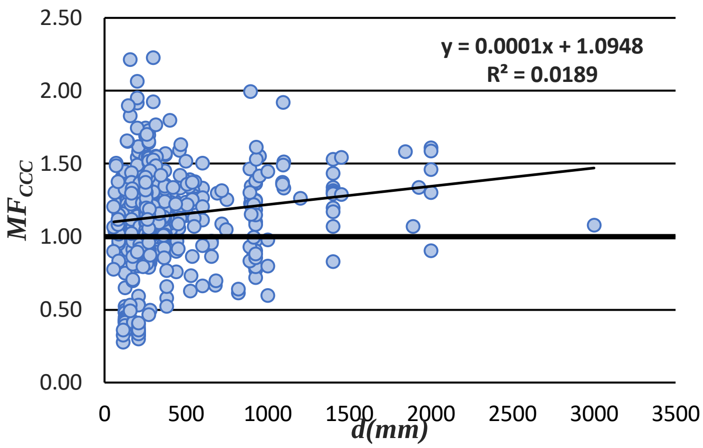

(i) MF_{CCC} *versus* $d(mm)$

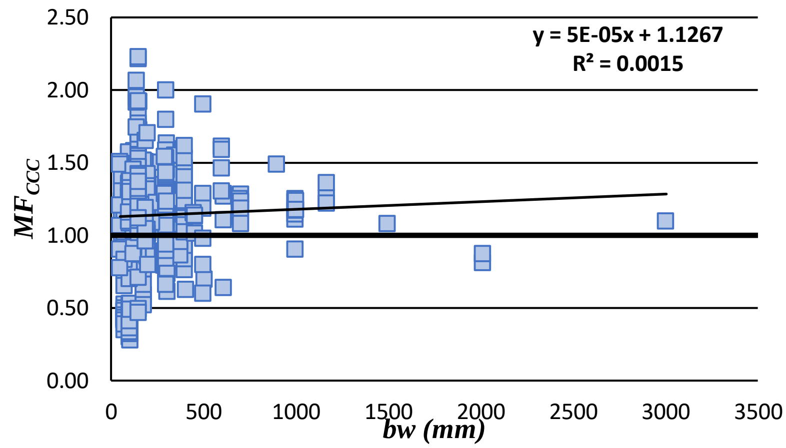

(ii) MF_{CCC} *versus* $b_w(mm)$

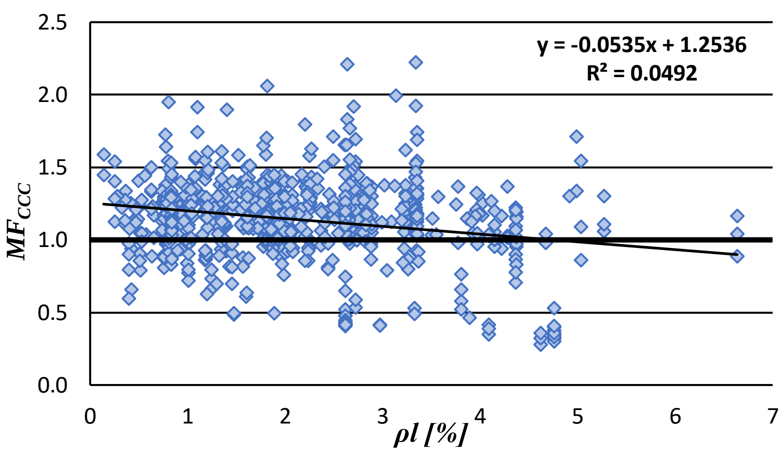

(iii) MF_{CCC} *versus* $\rho l(\%)$

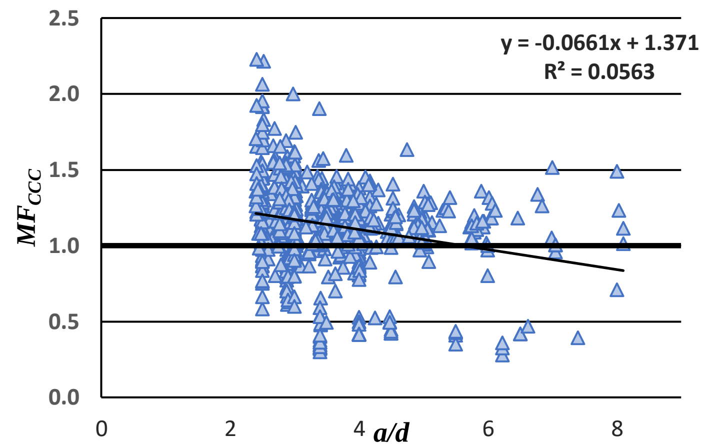

(iv) MF_{CCC} *versus* a/d

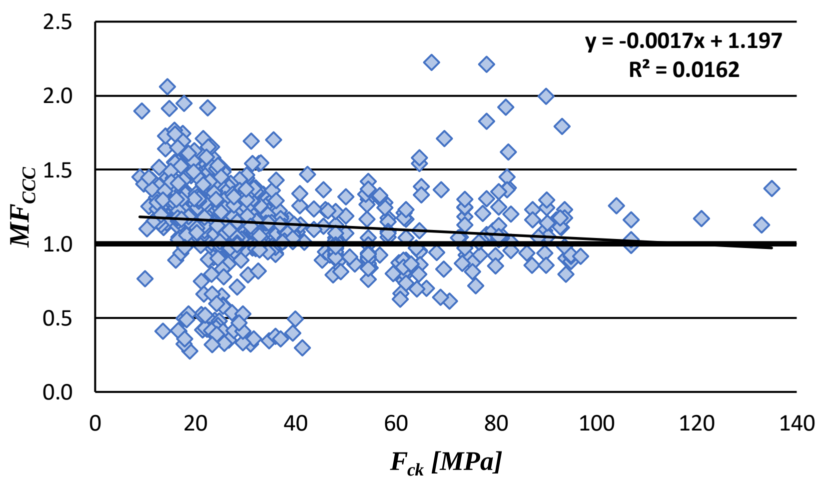

(v) MF_{CCC} *versus* $f_{ck}(MPa)$

Fig. 4.12. Sensitivity plot of MF_{CCC} against (i) d (ii) bw (iii) ρl (iv) a/d (v) fck

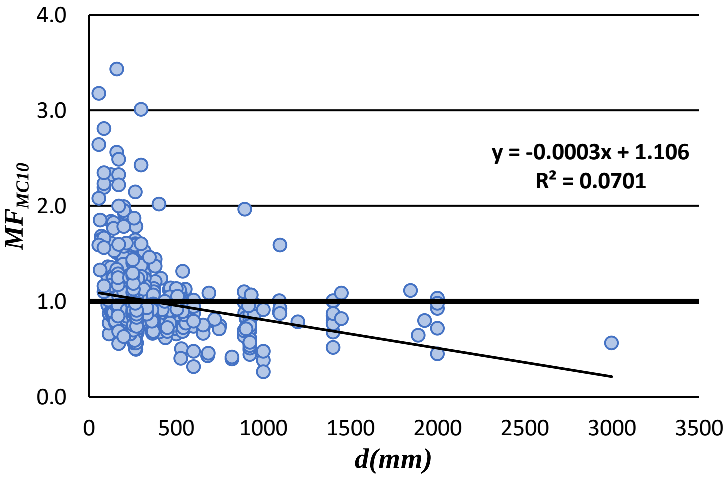

(i) MF_{MC10} $versus$ $d(mm)$

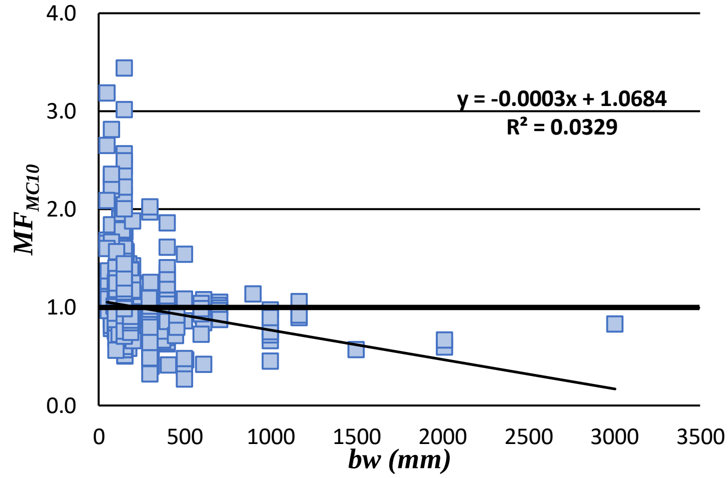

(ii) MF_{MC10} $versus$ $b_w(mm)$

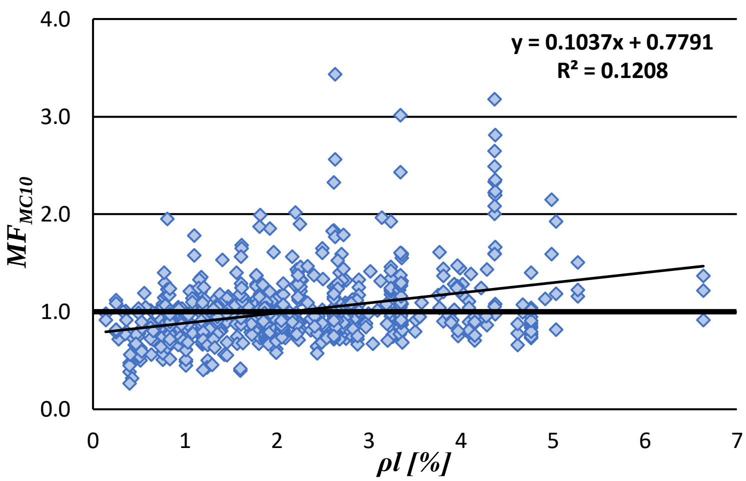

(iii) MF_{MC10} $versus$ $\rho l(\%)$

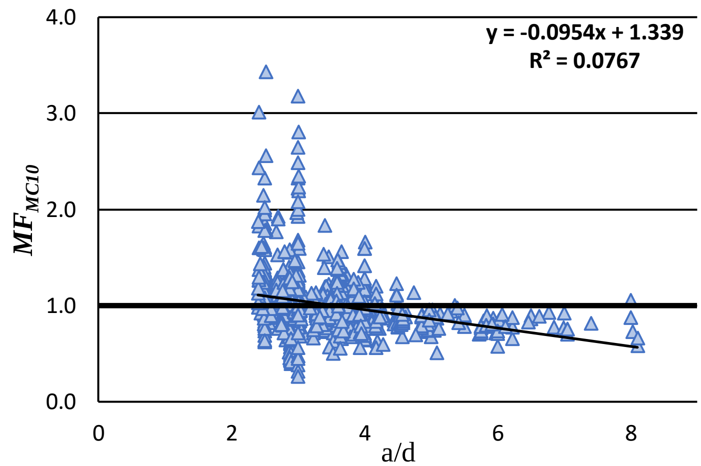

(iv) MF_{MC10} $versus$ a/d

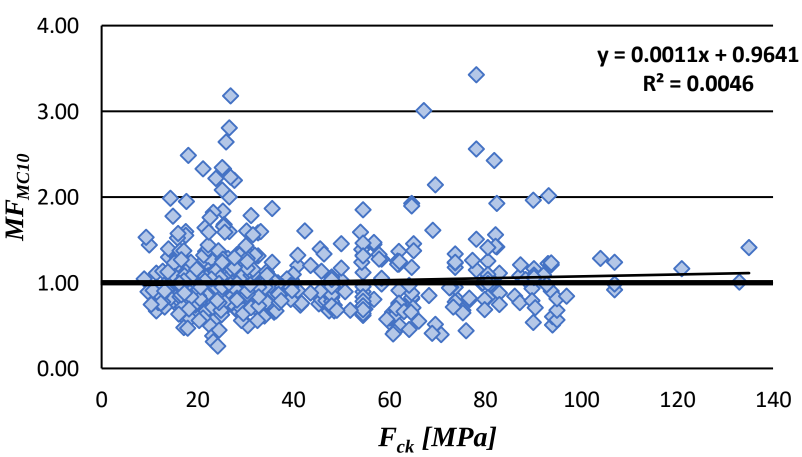

(v) MF_{MC10} $versus$ $f_{ck}(MPa)$

Fig. 4.13. Sensitivity plot of MF_{MC10} against (i) d (ii) bw (iii) ρl (iv) a/d (v) fck

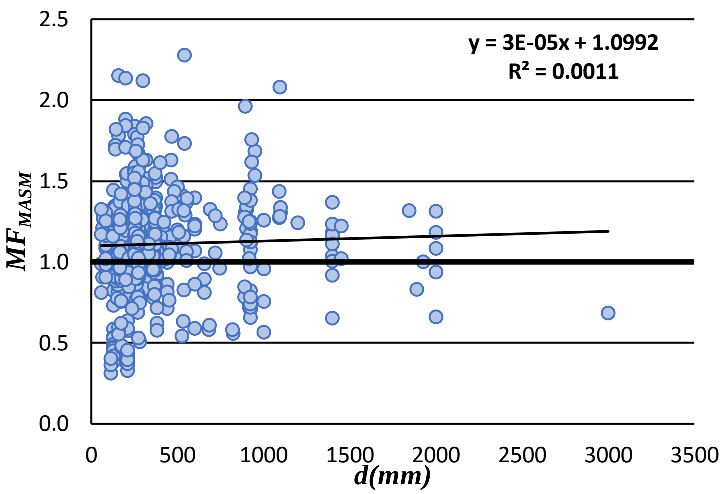

(i) MF_{MASM} $versus$ $d(mm)$

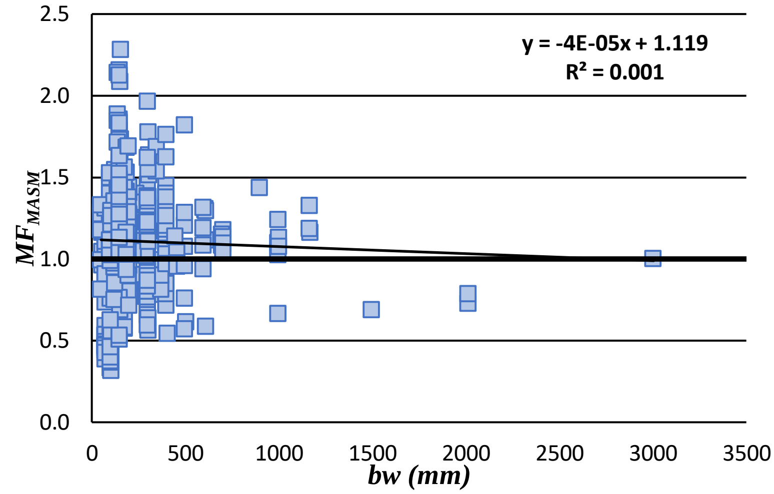

(ii) MF_{MASM} $versus$ $b_w(mm)$

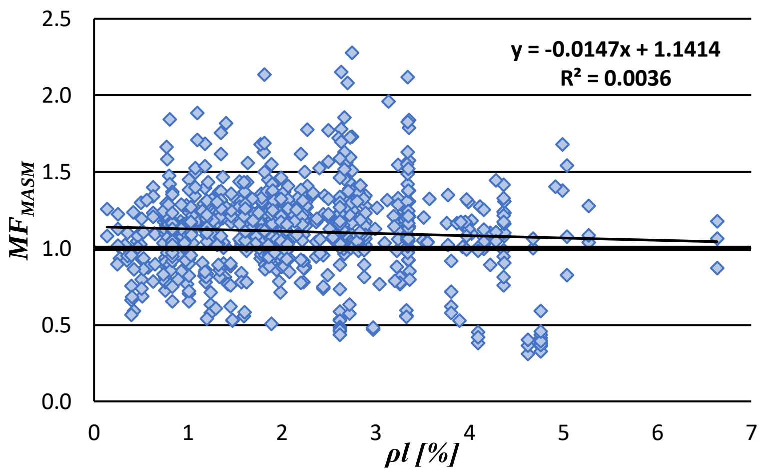

(iii) MF_{MASM} $versus$ $\rho l(\%)$

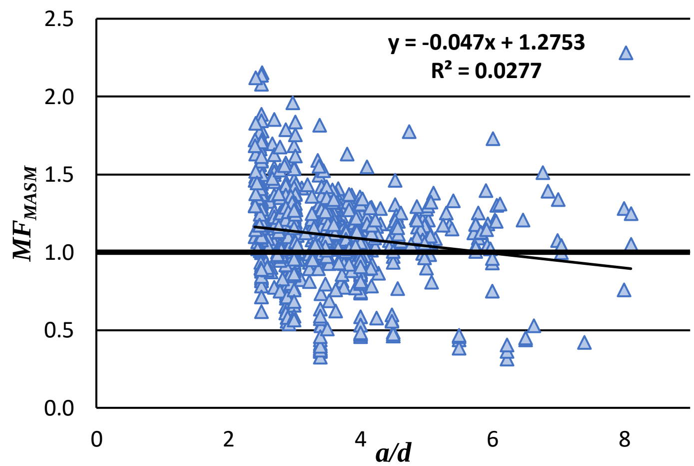

(iv) MF_{MASM} $versus$ a/d

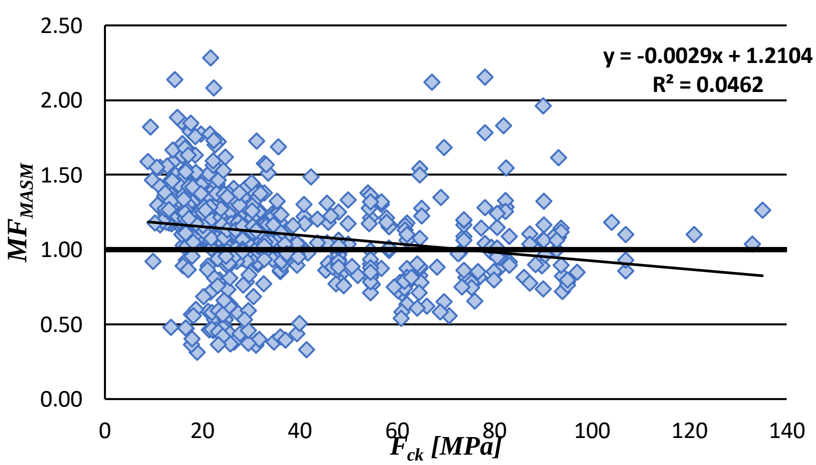

(v) MF_{MASM} $versus$ $f_{ck}(MPa)$

Fig. 4.14. Sensitivity plot of MF_{MASM} against (i) d (ii) bw (iii) ρl (iv) a/d (v) fck

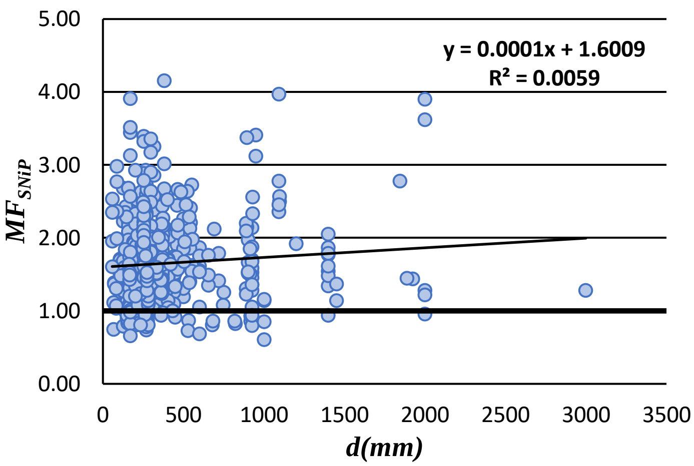

(i) MF_{SNiP} *versus* $d(mm)$

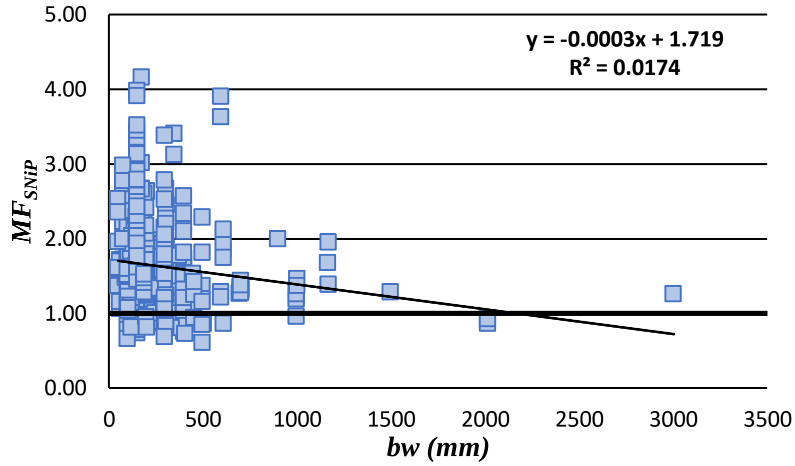

(ii) MF_{SNiP} *versus* $b_{\mathrm{w}}(mm)$

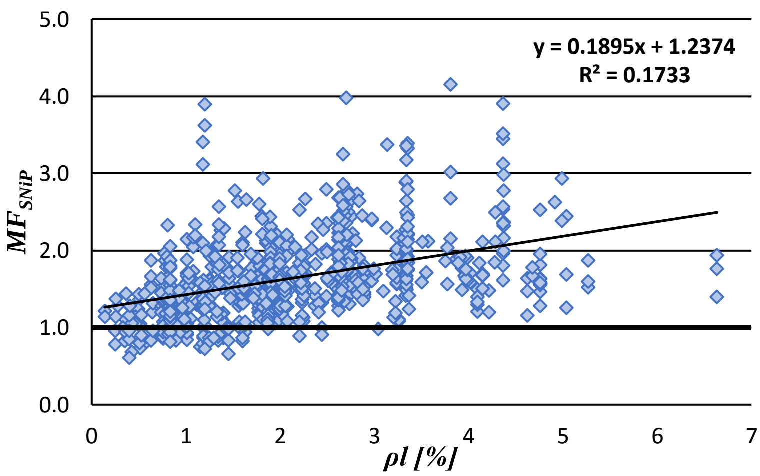

(iii) MF_{SNiP} *versus* $\rho l(\%)$

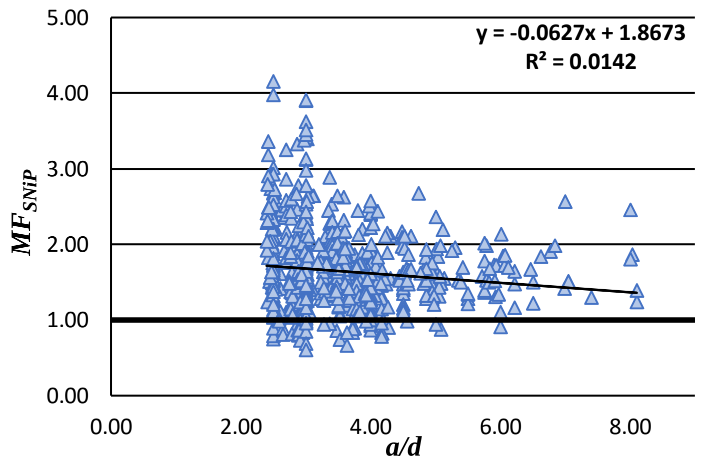

(iv) MF_{SNiP} *versus* a/d

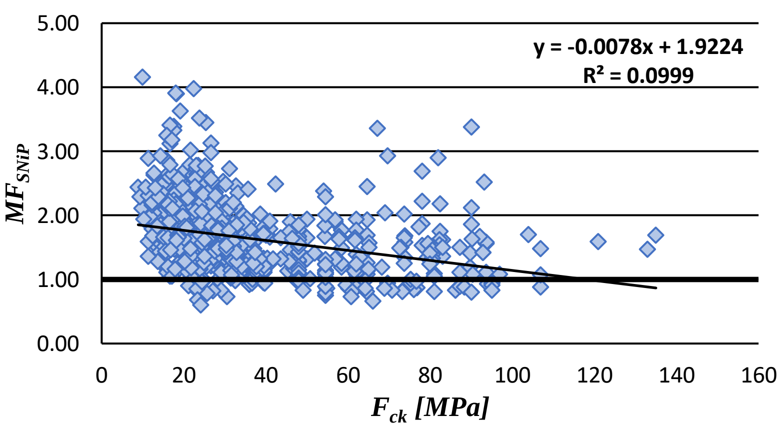

(v) MF_{SNiP} *versus* $f_{ck}(MPa)$

Fig. 4.15. Sensitivity plot of $\boldsymbol{MF_{SNiP}}$ against (i) d (ii) bw (iii) ρl (iv) a/d (v) fck

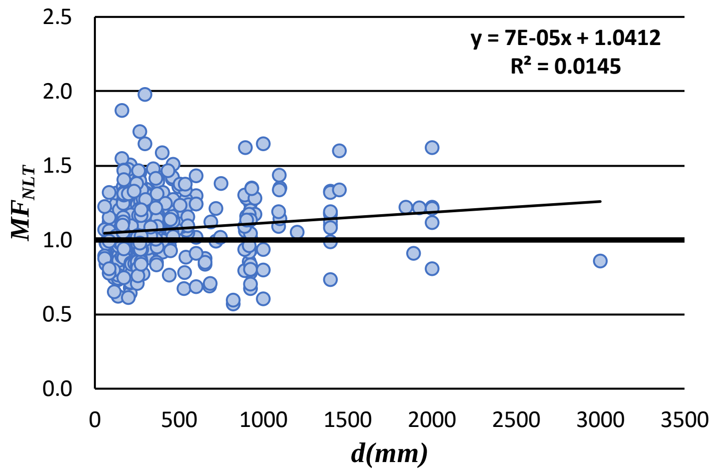

(i) MF_{NLT} $versus$ $d(mm)$

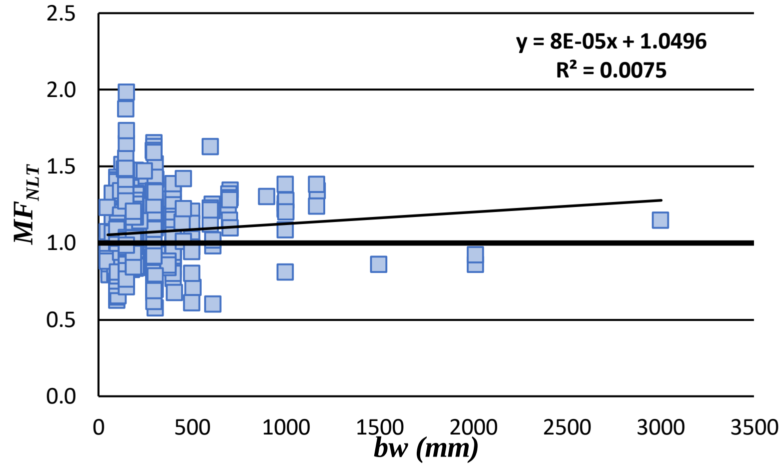

(ii) MF_{NLT} $versus$ $b_w(mm)$

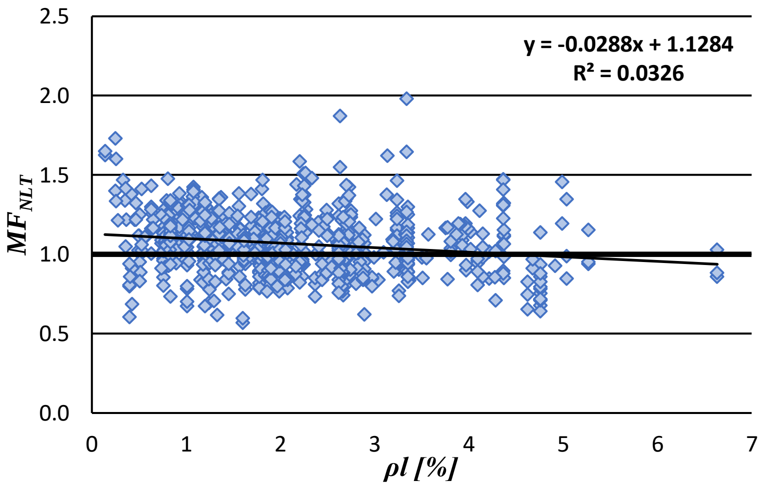

(iii) MF_{NLT} $versus$ $\rho l(\%)$

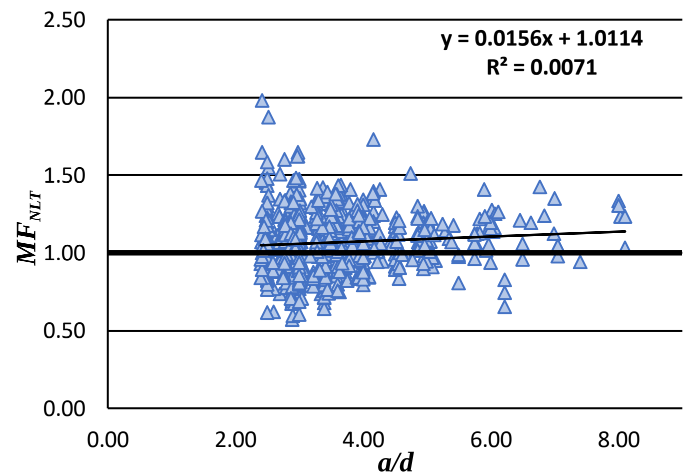

(iv) MF_{NLT} $versus$ a/d

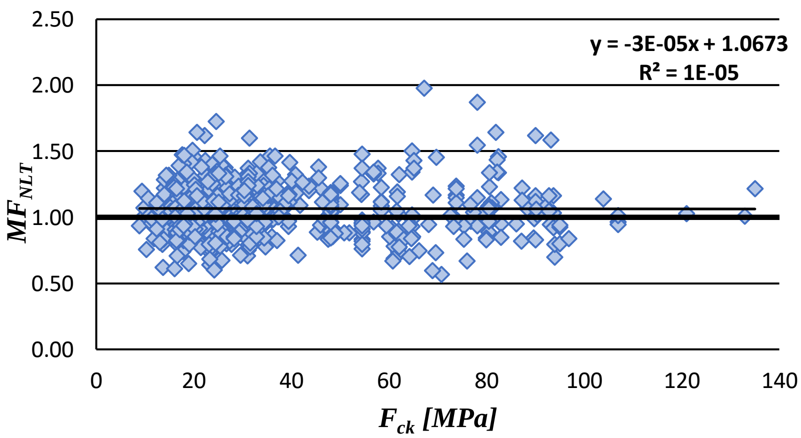

(v) MF_{NLT} $versus$ $f_{ck}(MPa)$

Fig. 4.16. Sensitivity plot of MF_{NLT} against (i) d (ii) bw (iii) ρl (iv) a/d (v) fck

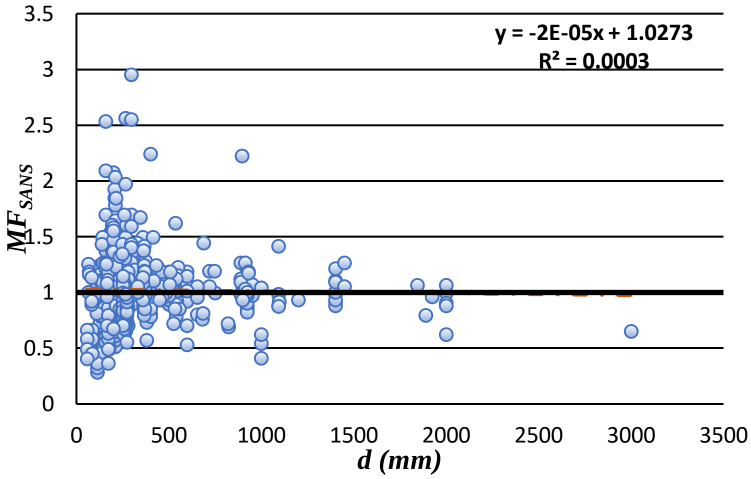

(i) MF_{SANS} $versus$ $d(mm)$

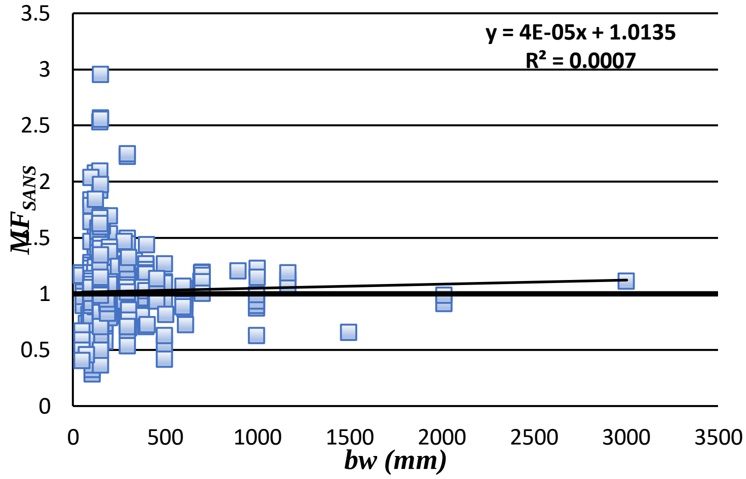

(ii) MF_{SANS} $versus$ $b_w(mm)$

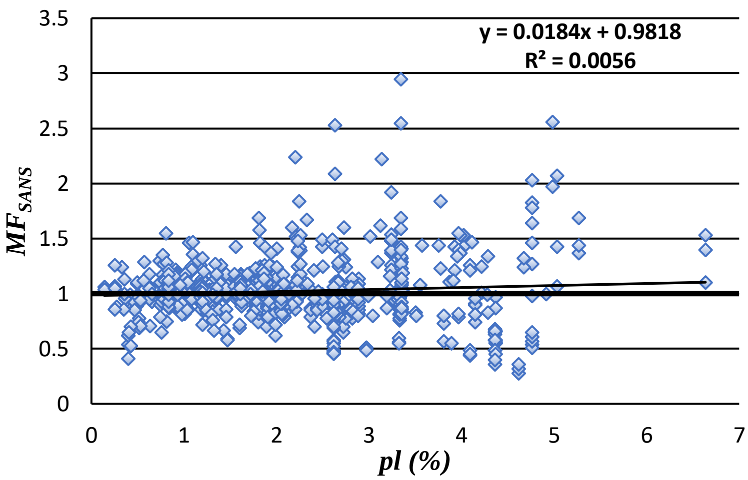

(iii) MF_{SANS} $versus$ $\rho l(\%)$

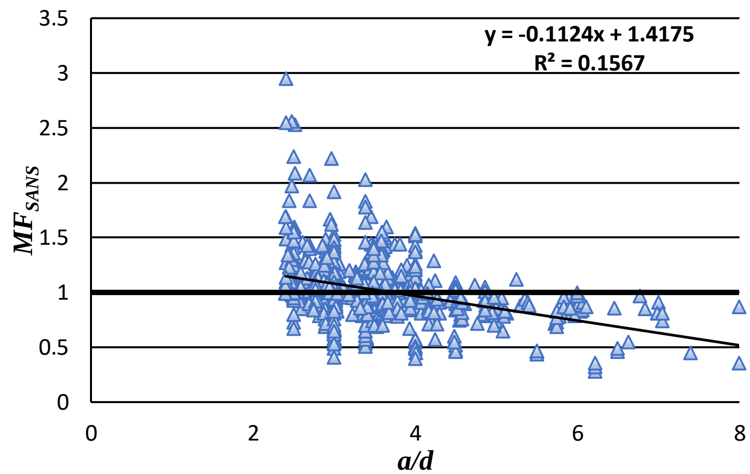

(iv) MF_{SANS} $versus$ a/d

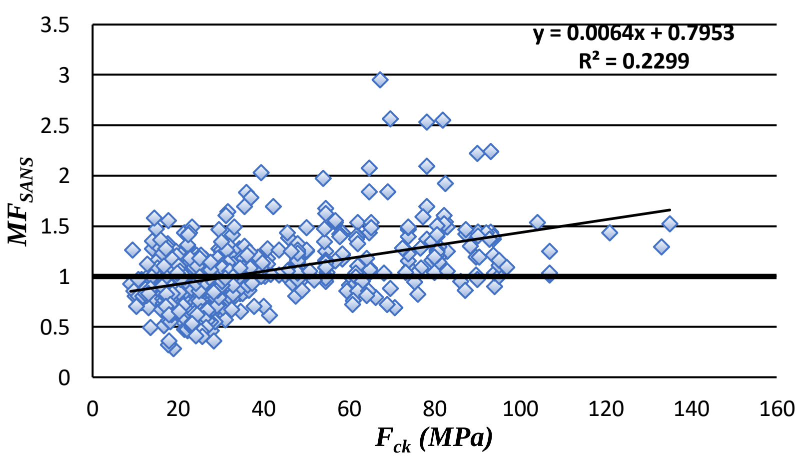

(v) MF_{SANS} $versus$ $f_{ck}(MPa)$

Fig. 4.17 Sensitivity plot of MF_{SANS} against (i) d (ii) bw (iii) ρl (iv) a/d (v) fck

4.3.6 Choice of probabilistic model

The distribution fitter application in the MATLAB R2021 suite was used to fit the model factor distribution derived from the considered shear model with respective plots as shown in Fig. 4.18. This was done to identify the distribution function for each model as is required for classifying the quality of reliability estimates (Mcleod, 2019). A non-parametric analysis that corroborates the findings from the plots was also done. Lastly, parametric statistical measures such as the Pearson coefficient of skewness and kurtosis value as seen in Table 4.1 was used to conclude the distribution of model factor realizations.

The model factor realization tends to be highly negatively or positively skewed if the following condition is satisfied; -1 ≤ η_{MF} ≥1. While a distribution is said to be fairly or moderately skewed if -0.5 ≤ η_{MF} ≥0.5. In both cases, each scenario depicts abnormality in the normal distribution but normality in the log-normal distribution. It's worth knowing that the closer the coefficient of skewness is to zero, the more normal the data is, as a perfectly normal distribution is said to have a skewness coefficient of zero.

Plots from the distribution fitter (fig 4.18) show that the model factor realizations MF_{CCC} and MF_{MASM} are normally distributed as the log-normal distribution curve failed to capture the data points (Fig. 4.18 h & i). Also, the formation of a bell curve that perfectly fits the distribution as is typical of a normal distribution (Fig. 4.18) was seen to outperform the curve of the Log-Normal and Weibull distribution indicating that the underlying distribution is normal. The skewness coefficient of MF_{CCC} and MF_{MASM} which has a value of 0.041 and 0.007 respectively suggests that the distribution is not skewed in any way as both values are very close to zero. Lastly, to authenticate the findings, the Anderson darling and chi-square goodness of fit test gave a P value of 5.67 which is considerably greater than the 5% significant value (0.05). Hence, the non-parametric test confirmed that the null hypothesis that the underlying distribution is normal was accepted.

Having established the distribution of MF_{CCC} and MF_{MASM} it is only logical to expect optimal reliability in shear resistance prediction, since a 2- parameter lognormal distribution results in a lower prediction of reliability as compared to the normal distribution, but the variability ($\Omega_{MF} = 25\% > 10\%$) makes the reliability uncertain.

Results from the non-parametric test conducted for MF_{NLT} revealed that the null hypothesis that the underlying distribution is normal was barely rejected with a significance P-value of 0.055 which is negligibly higher than 0.05. A Pearson coefficient of skewness of 0.52 suggests that the distribution is mildly skewed, while the plots (fig 4.18 o & p) show that the Log-Normal distribution curve was slightly more favourable than the Normal and Weibull distribution curve in fitting MF_{NLT}. This investigation shows that MF_{NLT} has a very low degree of abnormality and the distribution is almost normal. Hence, it is safe to expect a reliable prediction and a moderate assessment of reliability not necessarily conservative.

Probability distribution assessment shows that the other model factor realizations MF_{EC2}, MF_{AS3600}, $MF_{MC10,}$ $MF_{ACI,}$ MF_{SNiP} and MF_{SANS} are largely characterized by lower prediction of shear reliability as every attempt to determine the underlying distribution showed favouritism for the Log-Normal distribution. Firstly, a positive skewness was identified in the histogram of each respective plot. Secondly, the tail end extending to the right side indicated that the extent of variation is out of bounds for a gaussian distribution. Thirdly, the significance P-value for the Anderson darling and chi-square goodness of fit test was significantly lower than 0.05 signifying that the null hypothesis was rejected. Another indication is the Pearson coefficient of skewness which was considerably higher than 1.

In conclusion, investigation shows that MF_{NLT} is the most suitable choice of probabilistic model as it provides a more consistent and moderate reliability prediction as compared to other models.

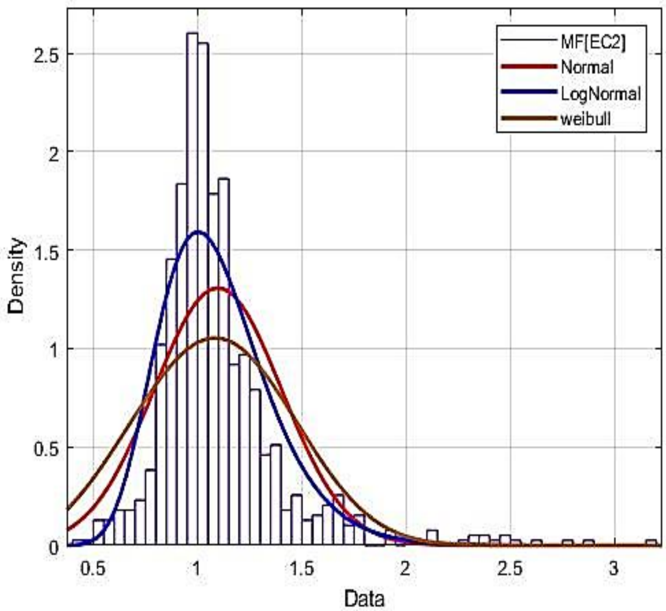

(a) Probability distribution function of MF_{EC2}

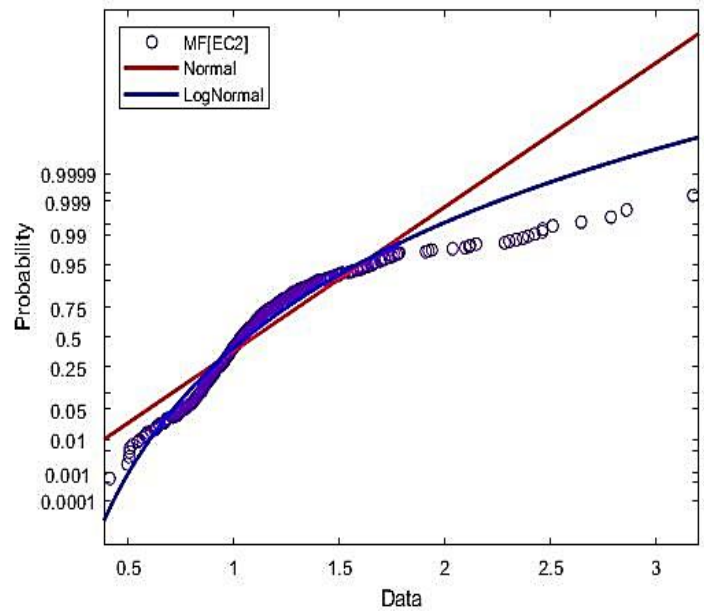

(b) Probability plot of MF_{EC2}

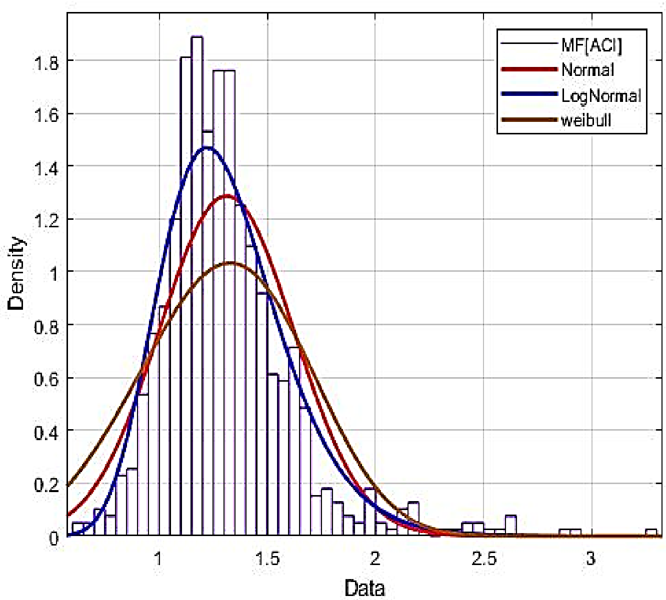

(c) Probability distribution function of MF_{ACI}

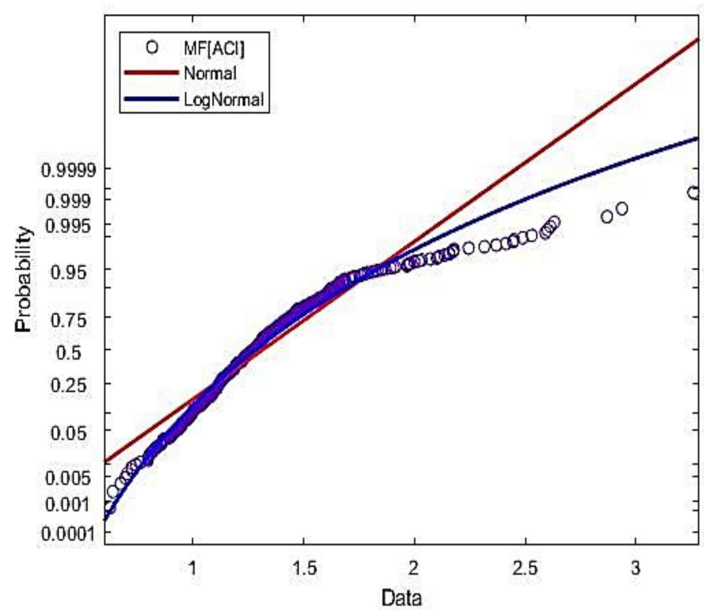

(d) Probability plot of MF_{ACI}

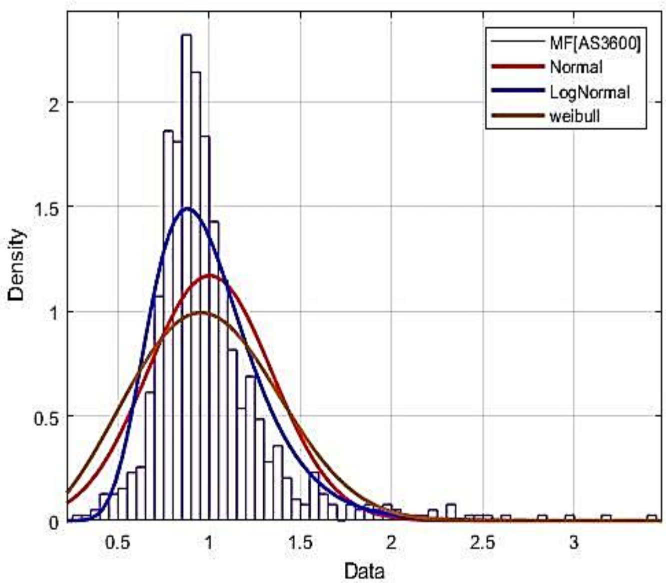

(e) Probability distribution function of MF_{AS3600}

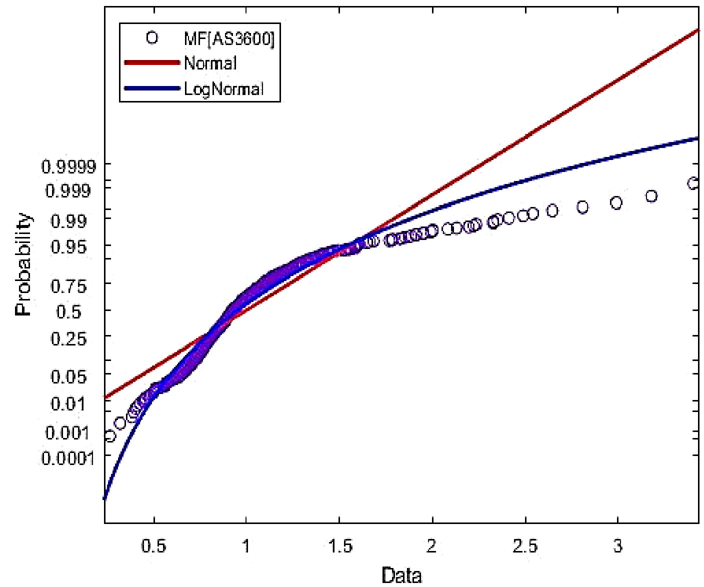

(f) Probability plot of MF_{AS3600}

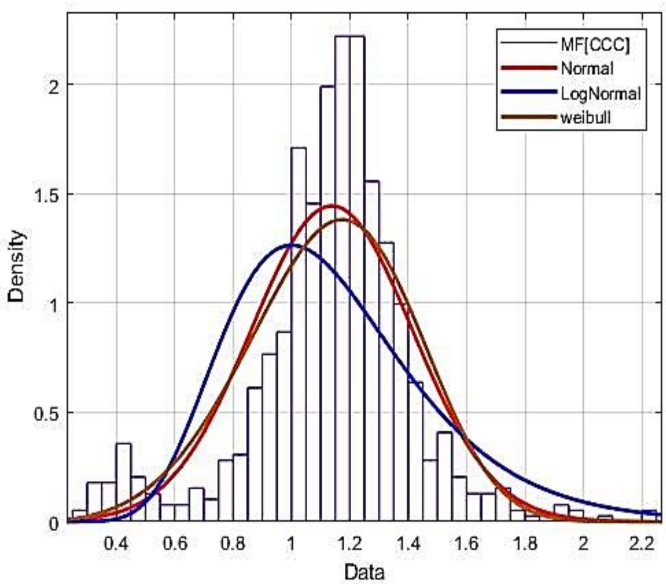

(g) Probability distribution function of MF_{CCC}

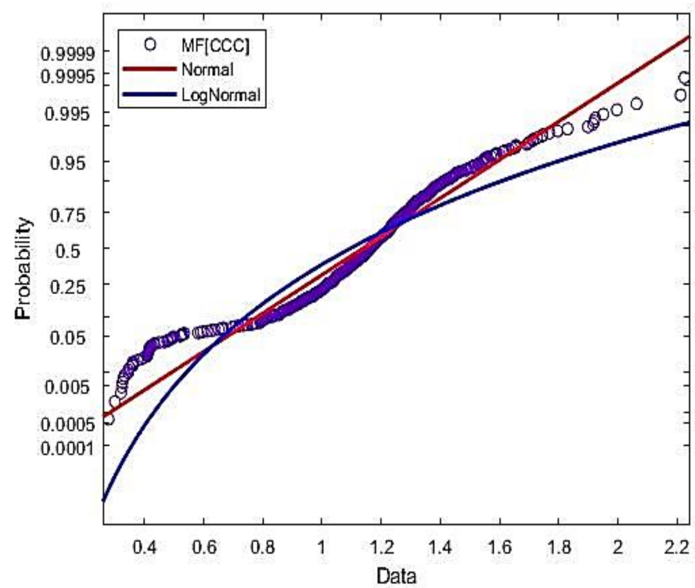

(h) Probability plot of MF_{CCC}

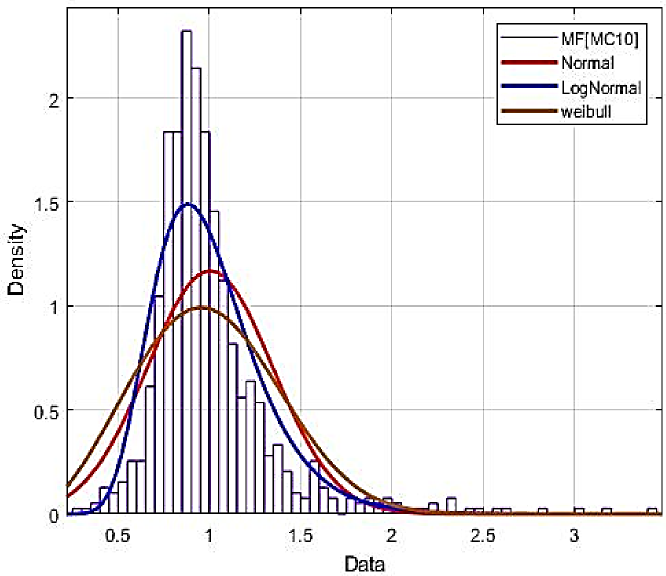

(i) Probability distribution function of MF_{MC10}

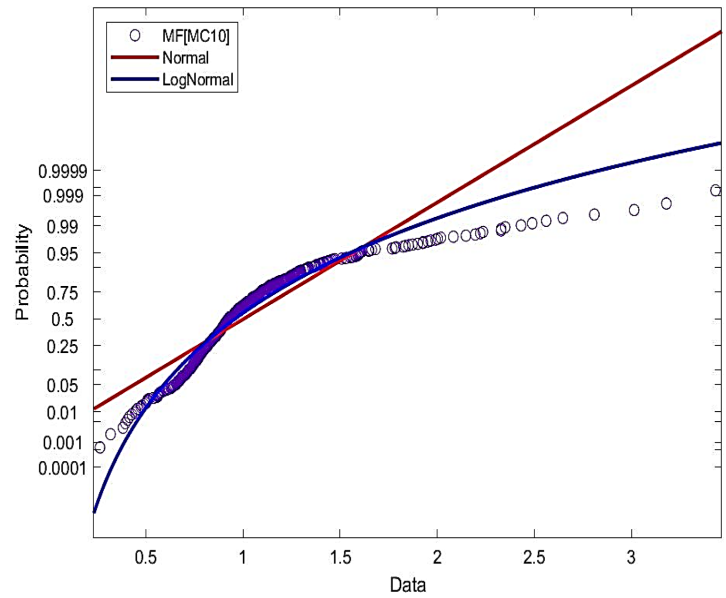

(j) Probability plot of MF_{MC10}

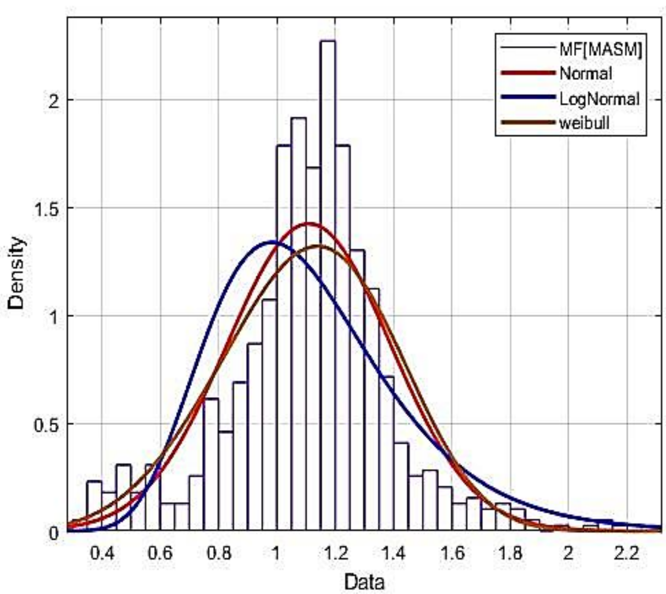

(k) Probability distribution function of MF_{MASM}

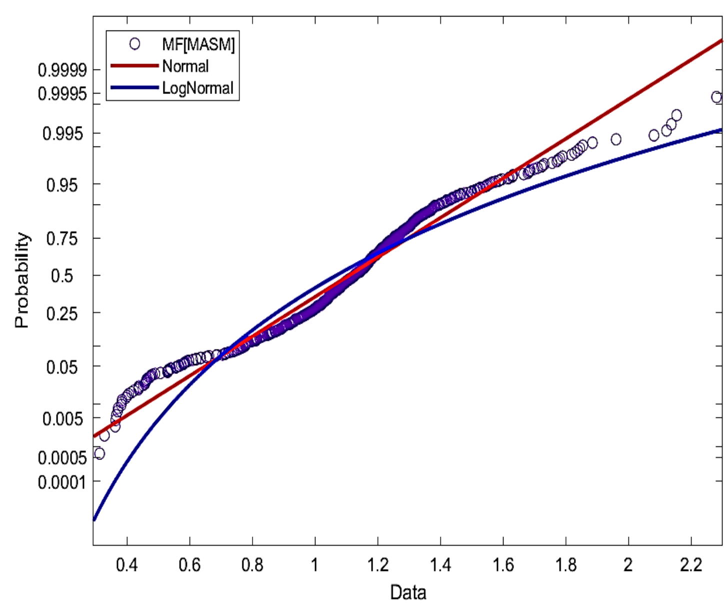

(l) Probability plot of MF_{MASM}

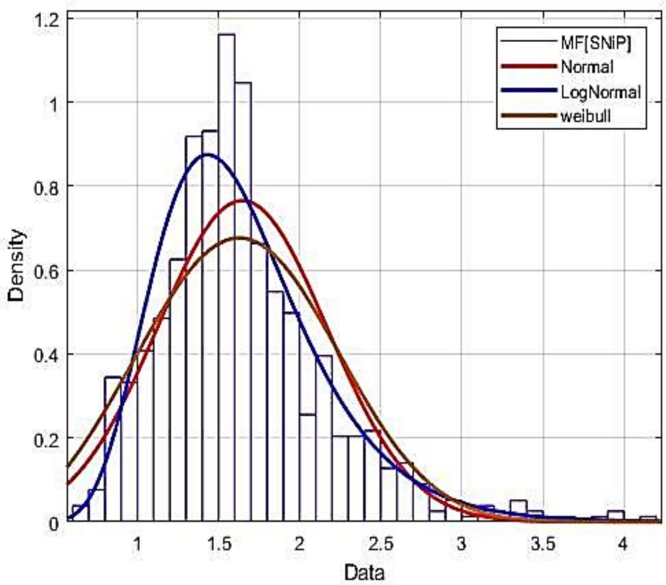

(m) Probability distribution function of MF_{SNiP}

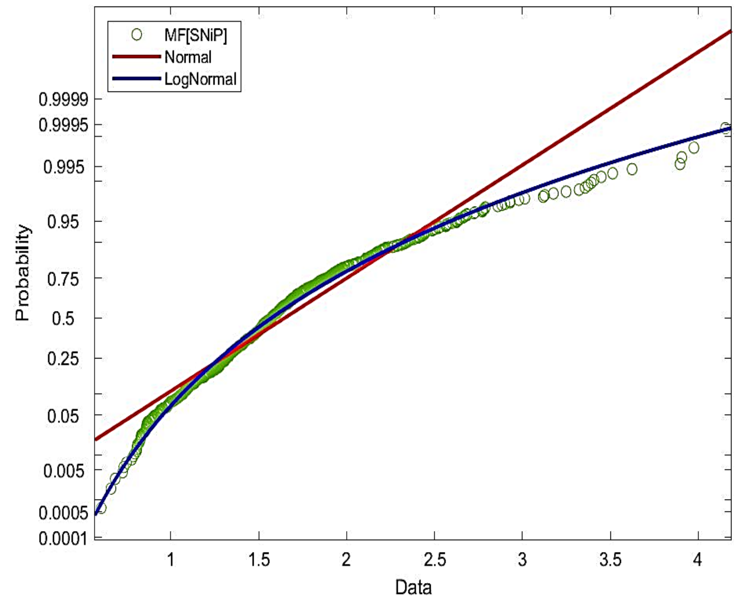

(n) Probability plot of MF_{SNiP}

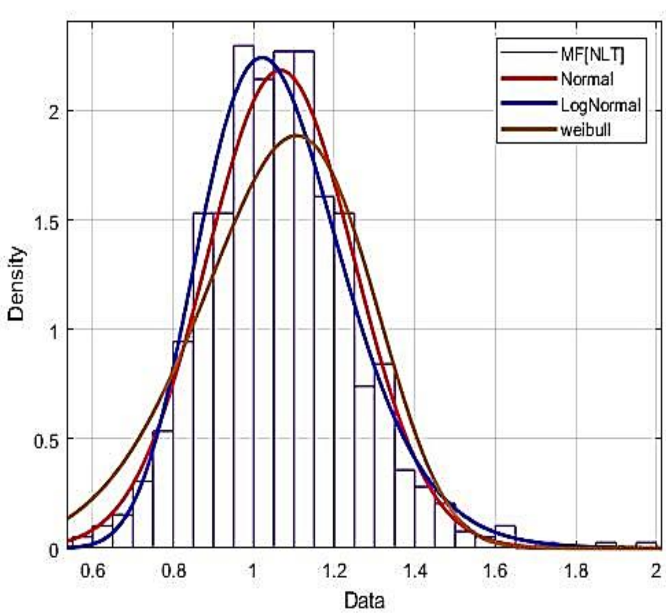

(o) Probability distribution function of MF_{NLT}

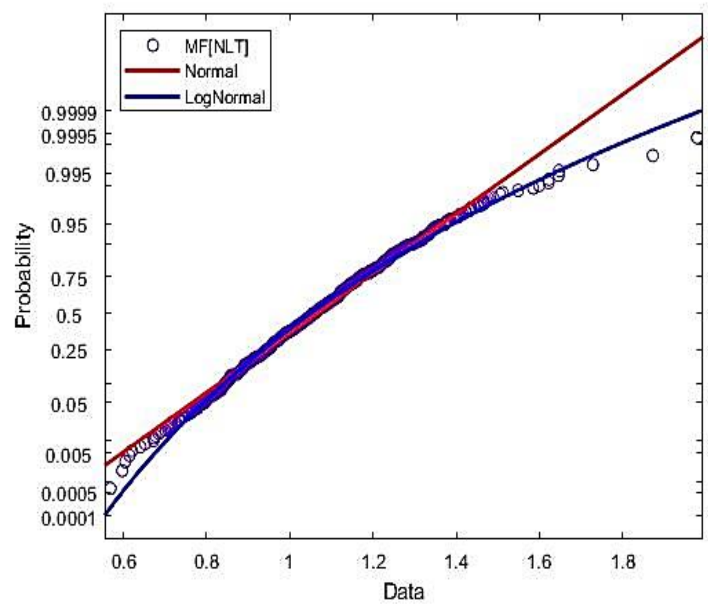

(p) Probability plot of MF_{NLT}

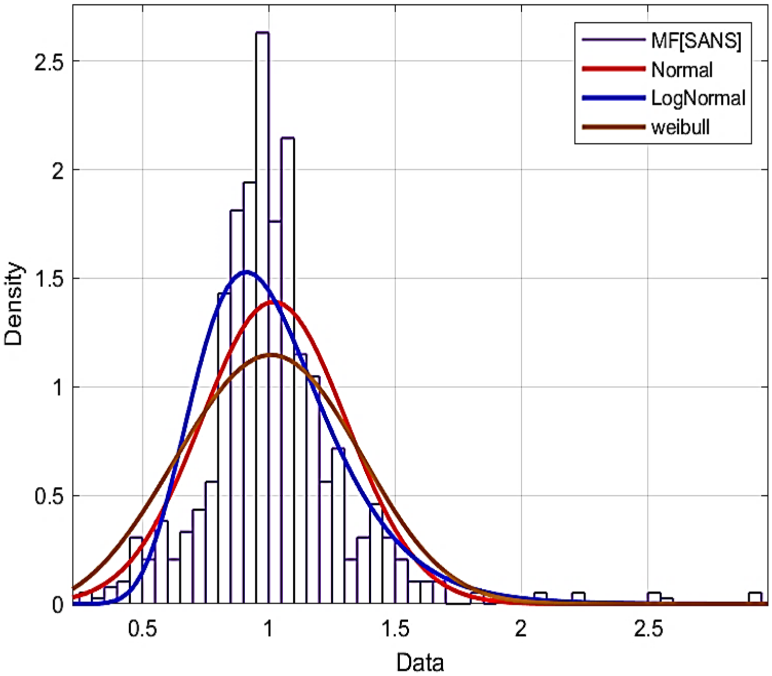

(q) Probability distribution function of MF_{SANS}

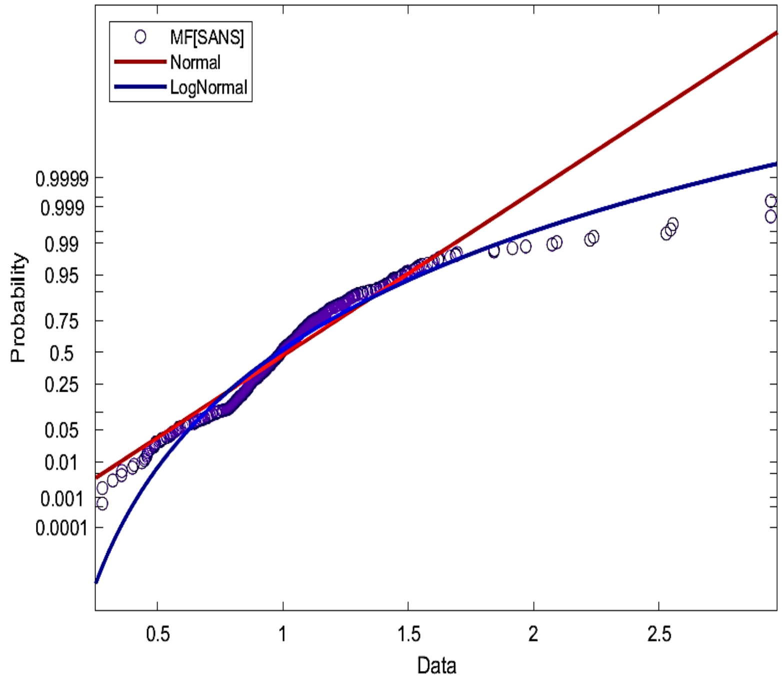

(r) Probability plot of MF_{SANS}

Fig 4.18 Model uncertainty probability fitting & distribution plots for conventional shear models.

4.3.7 Demerit point analysis for design shear value

The shear strength method's total performance is represented by the TDP (Total Demerit Point) score. The shear technique is more accurate in predicting the shear strength of reinforced concrete beams when TDP is less. The analysis system is used to assess how well the researched shear models perform in foretelling the shear strength of experimental beams from the database. In Table 3.5, the DP score for each categorization has been summarized. Table 4.6 presents the determined TDP score for the shear models, which is seen in Figure 4.19. As mentioned earlier in section 3.7.4, the demerit point analysis only applies to shear methods that can be expressed in terms of their respective design values such as those considered in this section.

Table 4.6 Total demerit point Analysis

Range	Classification	DP	MF_{EC2} (%)	MF_{MC10} (%)	MF_{CCC} (%)	MF_{SANS} (%)
<0.5	Extremely dangerous	10	0	0	0	0
0.5 – 0.65	Dangerous	5	0	1	3	1
0.65 – 0.85	Low safety	2	1	2	2	3
0.85 – 1.30	Appropriate safety	0	9	21	11	20
1.30 – 2.00	Conservative	1	74	62	69	71

> 2.0	Extremely Conservative	2	16	14	14	5
Total demerit point (TDP)			**108**	**99**	**116**	**92**

The following were deduced from the table above

- Based on the investigation, SANS had the lowest score with a TDP of 92, hence it has a better performance than the other 3 shear models. V_{MC10} is the closest to V_{SANS} out of all the models investigated with a TDP score of 99.
- The TDP scores for the V_{EC2} and V_{CCC} models are 108 and 116, respectively.
- The EC2 shear model and the CCC shear model were the poorest of the examined processes. The EC2 shear techniques received a high TDP because they provided the majority of overly conservative predictions.

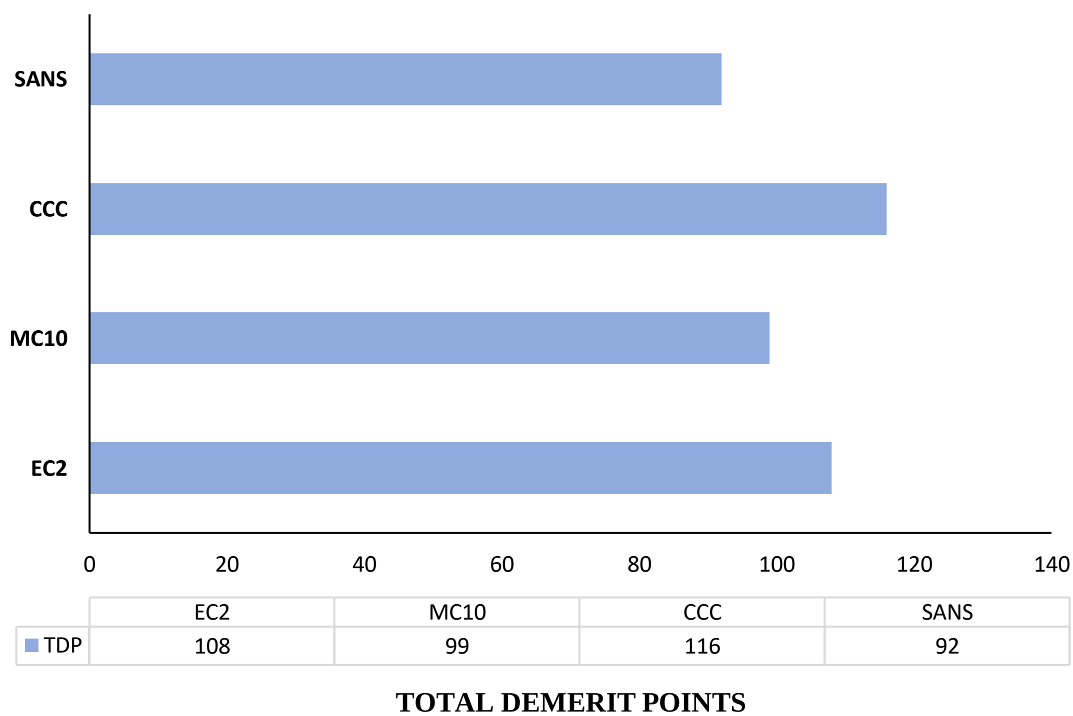

Fig 4.19. Bar Plot of Demerit Point Analysis

4.4 Comparison of experimental shear strength to machine learning shear predictions (Subset of Database)

4.4.1 comparison of predictions from machine learning models to experimental shear strength

Fig 4.19 and 4.20 presents the plot of experimental shear strength (V_{EXP}) against predicted shear capacity from machine learning models (V_{ML}) using 196 testing set of beams (rectangular and flanged) without shear reinforcement and parametric variations of properties randomly selected from the database compiled by Reinick *et al.* (2013). Considering the perfect line of equality, the graphical visualizations below show a trend comparison between the experimental shear strength observation and the outputs from the considered machine learning algorithms. The comparative study is achieved by examining the coefficient of determination (R^2), the scatter of predicted data points, and the similarity and closeness between the trendline of A.I based models and the perfect line of equality.

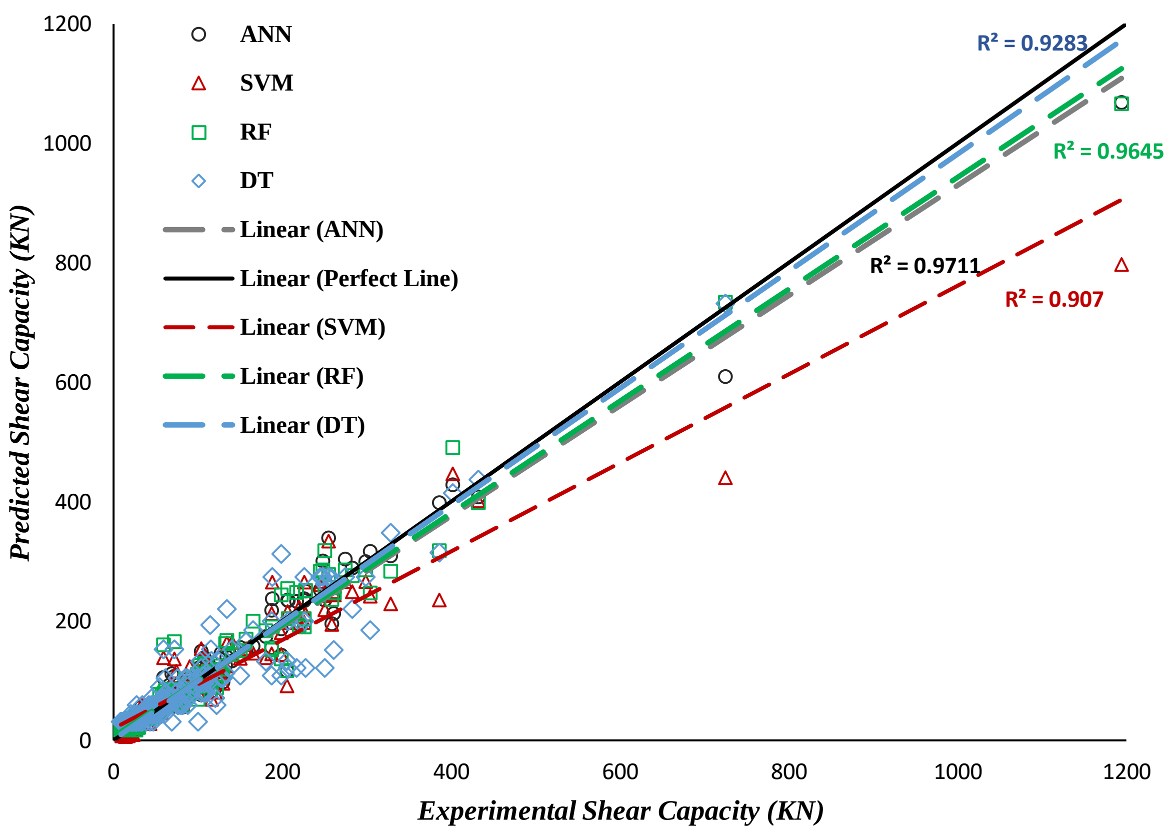

Fig 4.20. Perfect line comparison plot of machine learning shear capacity prediction against experimental shear value.

The following observations were established from the close examination of Fig. 4.19 & 4.20

- The trendline of shear prediction from the support vector machine model failed to accurately capture the perfect line as it significantly deviates below the perfect line of equality as the experimental shear strength increases. This implies that predictions from the support vector machine model have an increasing conservative bias as the experimental shear strength increases. Lower predictions of shear values may be due to the choice of hyperparameters selected by the grid search cross–validation function from the sci-kit learn model selection tool. Also, from Fig 4.20, it can be seen that the scatter of the datapoint around the trendline seems to be much as compared to the plots of other A.I based models, implying that the predictions are not as consistent. Predictions from the SVM also displayed the lowest value of $R^2 = 0.907$.
- The trendline of shear predictions from the decision tree algorithm displays a perfect comparison with the perfect line of equality. But a close examination reveals the shortcoming in the predictions of V_{DT} thereby negating the visual accuracy. Firstly, because it appeared to follow the V_{SVM}'s trend, a significant scatter of data points around the trendline was observed. Secondly, a coefficient of determination (R^2) value of 0.9283 finally suggests that the predictions from the decision tree don't come close in comparison to the perfect line of equality as compared to predictions from V_{ANN} & V_{RF}.
- V_{ANN} & V_{RF} provides a similar estimation of shear capacity. Howbeit, predictions from the Artificial Neural Network seem slightly more accurate than the Random Forest shear predictions. Plots from Fig.4.19 shows that the trendline of V_{ANN} & V_{RF} bears close comparison with the perfect line of equality with fewer scattered points observed around V_{ANN}'s trend. V_{RF} provides a better estimate of shear strength in terms of closeness of trendline to the line of equality, parametric coefficient of determination (R^2) = 0.9645 and less scatter of datapoint as compared to V_{SVM} and V_{DT}.
- The highest value of $R^2 = 0.9711$, lowest observed scatter around the trendline and close capturing of the perfect line of equity infer V_{ANN} is most favourable in shear capacity prediction as compared to other A.I based shear models.

v_{ML} against v_{exp}

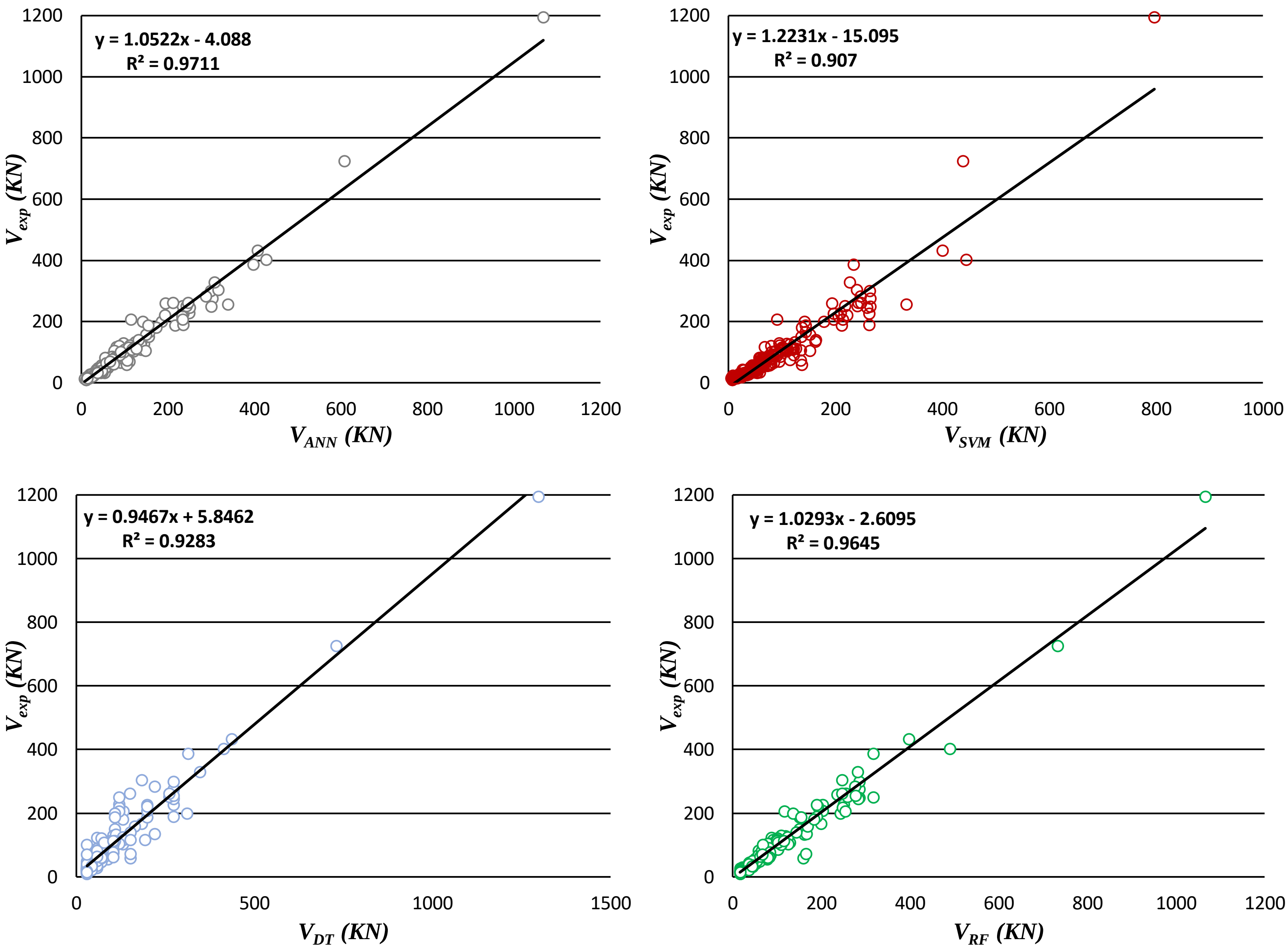

Fig 4.21. Comparison of experimental shear strength (***V_{EXP}***) to machine learning predicted shear strength (***V_{ML}***)

a) ***V_{ANN}***, b) ***V_{SVM}***, c) ***V_{DT}***, d) ***V_{RF}***

4.4.2 Comparison using the annotated heatmap

Fig.4.21 presents the heatmap of the A.I based shear predictions for machine learning models and experimental shear values. The heatmap uses the Pearson correlation coefficient to determine the relationship between variables. The colour bar at the right side indicates the intensity of correlation and assigns a coefficient based on the extent to which shear values are related. The heatmap shows that V_{ANN} compares well with the experimental shear value with a correlation value of 0.99, while V_{RF} comes second to V_{ANN} with a correlation value of 0.98. The heatmap shows that of all the machine learning shear predictions, V_{SVM} seems to be the least favourable with a correlation value of 0.95. Second to V_{SVM} is the shear prediction of V_{DT} with a correlation value of 0.96.

It is worth mentioning that the shear predictions from the Random Forest supervised learning model have a very close similarity with the prediction from the Deep Neural Network model with a correlation coefficient of 0.98.

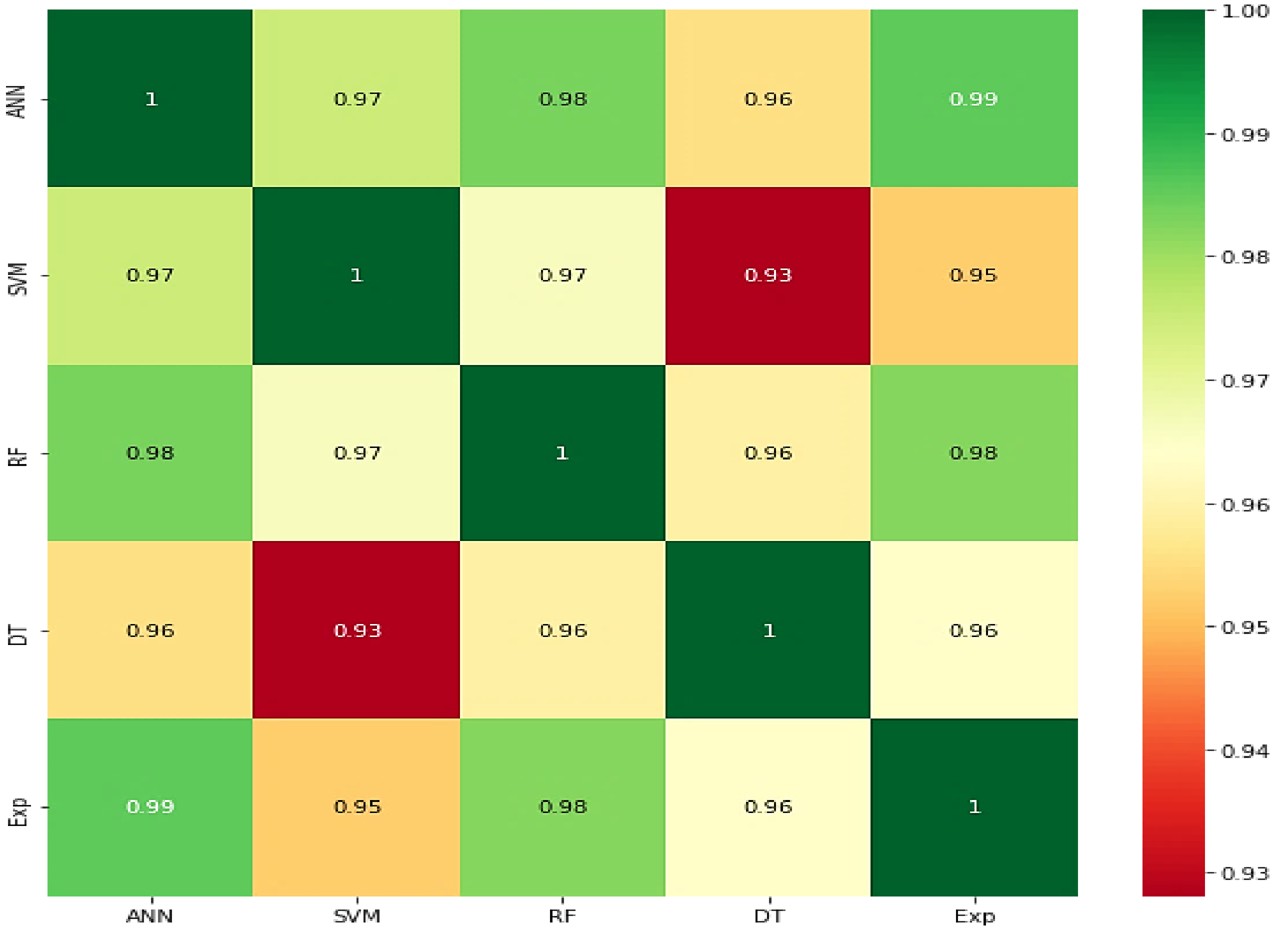

fig.4.22 Heatmap with annotation showing the coefficient of correlation between experimental shear values and predicted shear values from machine learning models.

4.4.3. Comparison of machine learning prediction to experimental shear strength with respect to percentage longitudinal reinforcement

A subset of the database provided by Reinick et al (2014) consisting of 196 beams randomly selected as test data following the machine learning sequence is compared with the experimental shear strength. The predictions from the machine learning algorithm are normalized to converge as (1) $\left(\frac{V_{ANN}}{b_w d}\right)$, (2) $\left(\frac{V_{RF}}{b_w d}\right)$, (3) $\left(\frac{V_{DT}}{b_w d}\right)$, (4) $\left(\frac{V_{SVM}}{b_w d}\right)$. Trendlines of normalized machine learning shear predictions are compared to experimental observations $\left(V_{exp}\right)$.

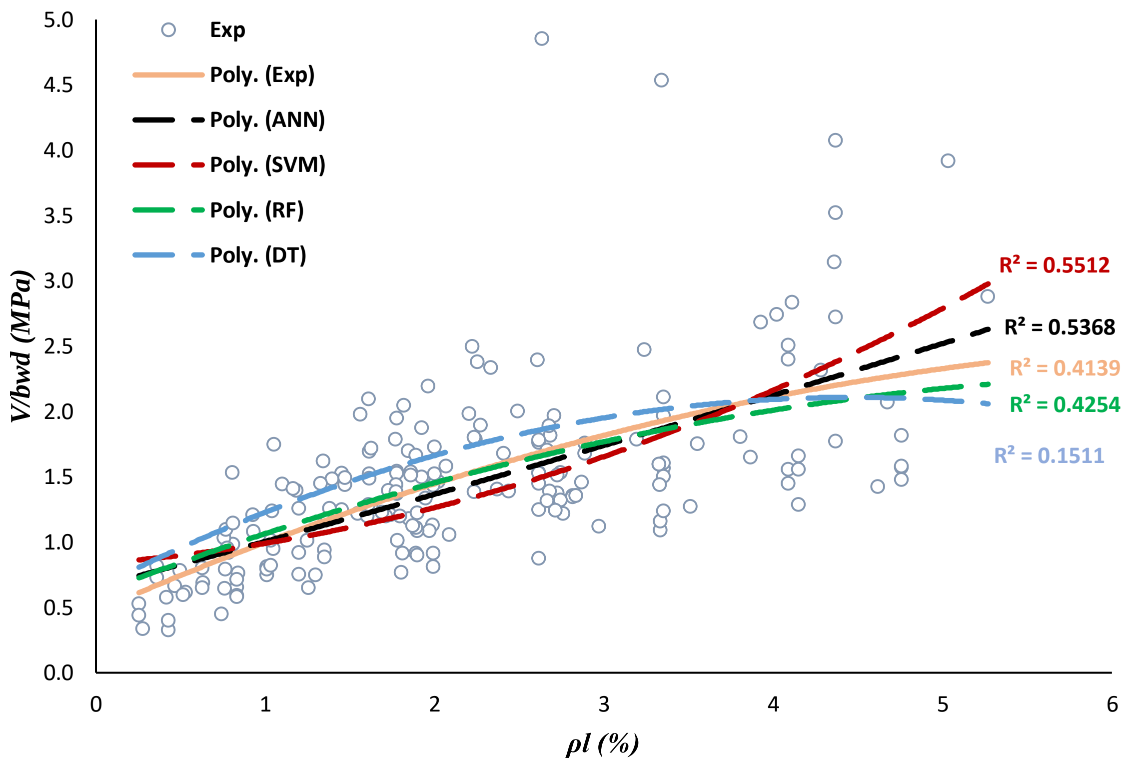

Fig 4.23. Comparison of normalized A.I based shear predictions to experimental observation with respect to pl%

From Fig 4.23, the following were observed

- The trendline of the normalized shear prediction from the decision tree M.L model failed to capture the experimental trendline as it initially appears to be above the experimental trendline implying that for each experimental shear prediction at ρl < 4%, V_{DT} provides unconservative shear estimates. The trendline of V_{DT} deviates below the experimental trendline as the longitudinal reinforcement ratio increases beyond 4%. This insinuates V_{DT} tends to provide conservative shear predictions at ρl > 4%.

- Initially, V_{SVM} provides unconservative estimates of shear capacity as the trendline starts above the experimental trendline at ρl < 1%. An increase in the longitudinal reinforcement ratio ρl > 1% causes the shear prediction from the support vector model to become fairly conservative up until when ρl > 4% and overestimation once again dominates the shear prediction of V_{SVM}.
- Fig 4.23 shows that the trendline of normalized V_{ANN} captures the experimental trendline perfectly well with a slight deviation above the experimental trend at ρl > 4%. This denotes that at a higher longitudinal reinforcement ratio, V_{ANN} provides a marginally unconservative shear estimate.
- The trends of V_{RF} bear the closest comparison to the trend of $V_{ANN,}$ this means the shear predictions from the Random Forest supervised learning model also compare well with the experimental shear strength but slightly underestimate the shear capacity.

4.4.3.1 Error trend observation

Fig 4.24 shows that the errors associated with V_{ANN} &V_{SVM} displayed an insignificant trend with the parametric range of longitudinal reinforcement, contrarily V_{DT} &V_{RF} showed a positive trend to increasing longitudinal reinforcement ratio suggesting that prediction error increases as ρl increases. Also, at ρl < 4% V_{DT} is characterized by unconservative shear predictions as a negative error indicates a higher shear prediction value and a positive error indicates a conservative shear prediction. The sensitivity of V_{RF} prediction to ρl is quite inconsequential.

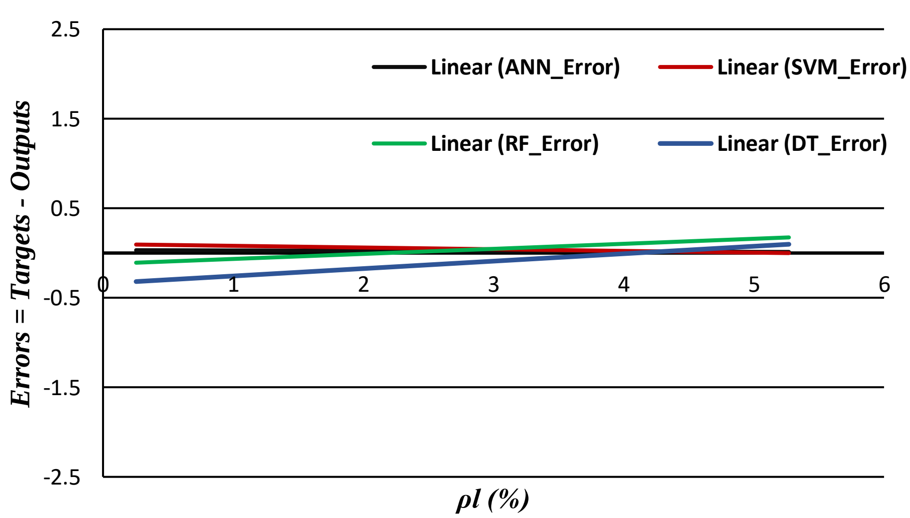

Fig 4.24 Plots of normalized error against ρl

4.5 Statistical analysis of machine learning model factor observations

This section adopts descriptive statistics to analyze the derived model factor distribution for the machine learning models by considering the statistical moments, histogram of model factors, identification of outliers with a box plot, sensitivity analysis and appropriate probability distribution plots.

Table 4.7 Statistical parameters of model factors from A.I based shear models.

	MF_{ANN}	MF_{SVM}	MF_{RF}	MF_{DT}
Counts	196	196	196	196
Mean	1.00	1.07	1.00	1.04
Std	0.18	0.32	0.19	0.38
COV%	18%	30%	19%	37%
Skewness	0.60	1.99	0.20	1.78
Max	1.79	2.58	1.77	3.32
75%	1.11	1.16	1.10	1.12
50%	1.00	1.02	1.00	0.95
25%	0.90	090	0.88	0.77
Min	0.56	0.42	0.37	0.29
Max/Min	3.20	6.14	4.78	11.45
Kurtosis	1.64	6.12	1.62	7.32

From Table 4.7, MF_{ANN} and MF_{RF} both have a mean of 1, this indicates that there is no form of bias in the shear prediction from these A.I-based models. Moreover, the measure of dispersion which is close to zero suggests that the realizations of both MF_{ANN} and MF_{RF} are minimally scattered around the mean with MF_{ANN} having a standard deviation value of 0.18 while σ_{MF} for MF_{RF} = 0.19. The coefficient of variation also infers a nominal variability in the realizations of both MF_{ANN} and MF_{RF} with values of $\Omega_{MF(ANN)}$= 18%, $\Omega_{MF(RF)}$= 19%. The low degree of variability in the model factor realizations buttresses the certainty in the shear predictions of V_{ANN} and V_{RF}, though the COV% is slightly higher than the 10% recommended value given by JCSS (2001).

MF_{SVM} has a mean value of 1.07 which is indicative of a small bias and 7% conservatism while MF_{DT} is just 4% conservative with a mean value of 1.04. Although the small bias indicates that the shear models built on the architecture of support vector machine and decision trees are somewhat accurate in shear prediction, the wide dispersion of the realized model factors around the mean brings to light the uncertainty in the performance of DT and SVM models in shear prediction with $\sigma_{MF(SVM)}$=0.32,

$\sigma_{MF(DT)}$= 0.38. Also, the coefficient of variation as seen in table 4.5 suggests a significant degree of variation in their model factor realization considerably greater than the recommended extent of variation for shear models by the JCSS (2001).

4.5.1 Histogram of model factor realizations for A.I based shear models.

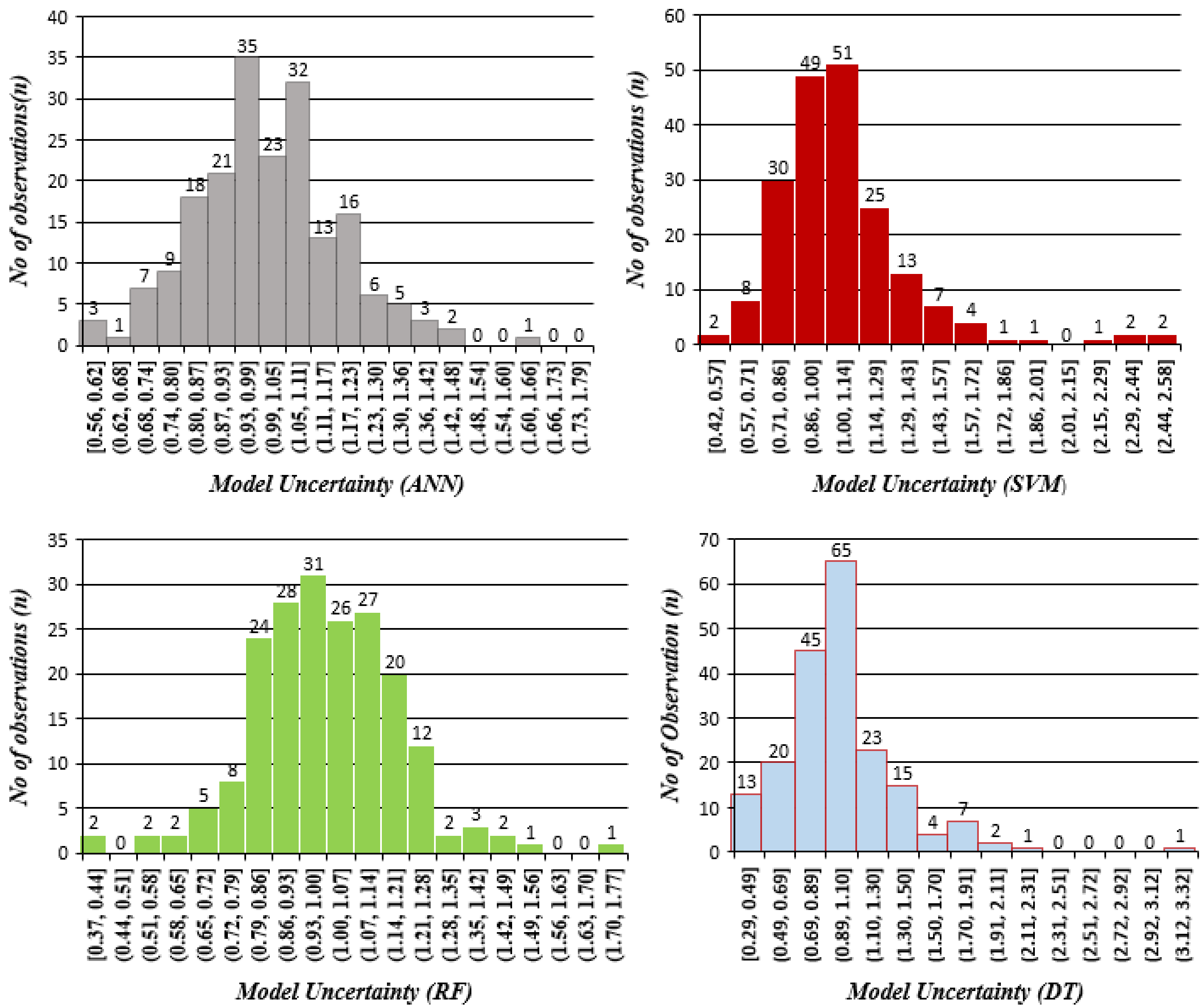

Fig 4.25 Histogram of machine learning model factors

4.5.2 Histogram of the prediction error of A.I based shear models

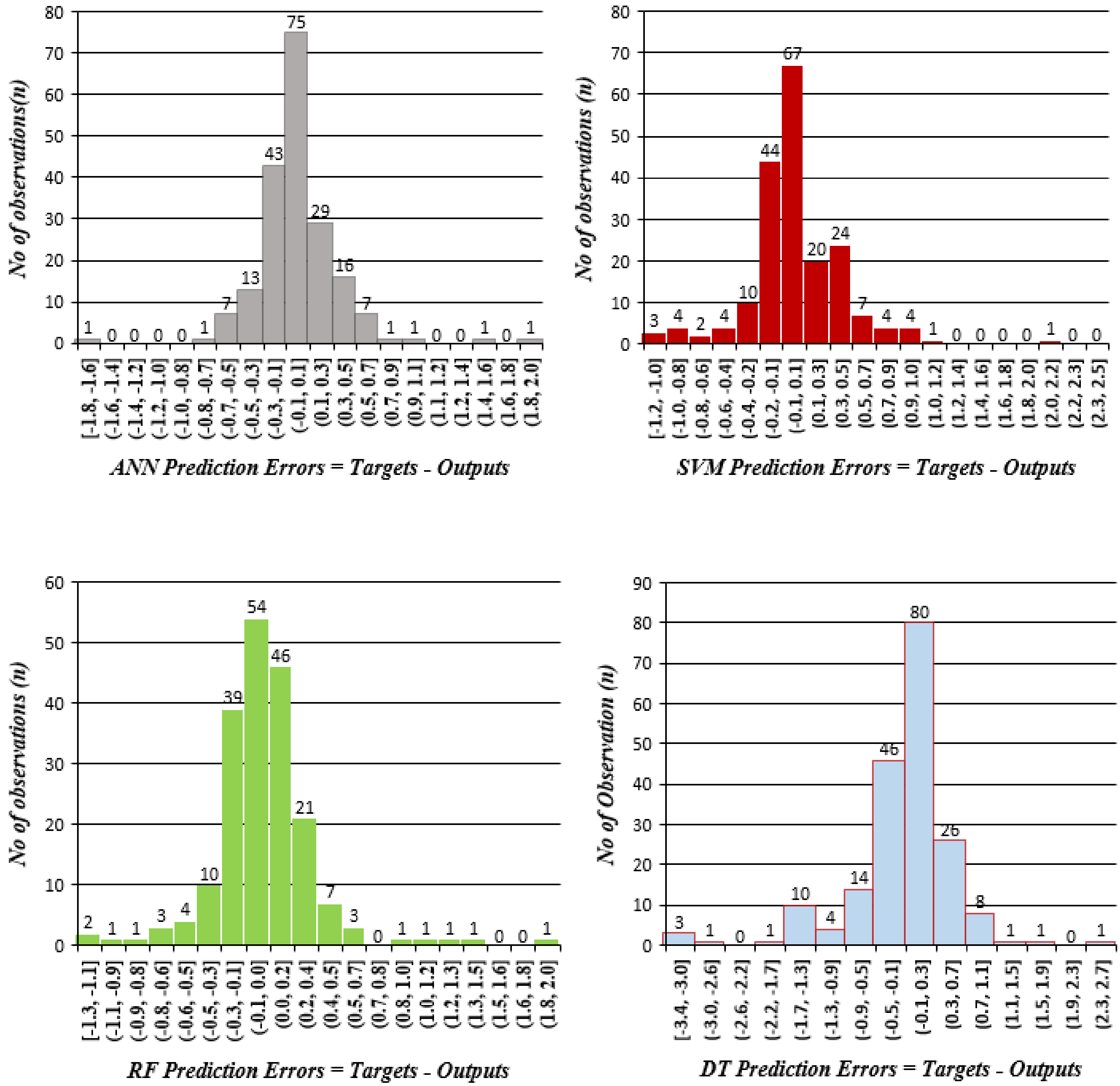

Fig 4.26 Error plot of machine learning model predictions

4.5.3 Identification of outliers

Realizations from Fig. 4.27 are as follows;

- With consideration to all 196 data points randomly selected for the A.I based shear prediction, only 4 points were regarded as outliers in the ANN shear model factor realization. From the MF_{ANN} realizations, only one point lies below $\mu - 3\sigma$ and three points above $\mu + 3\sigma$. The compactness of the model factor distribution MF_{ANN} suggests that at extreme values of MF, MF_{ANN} does not excessively overestimate or underestimate shear capacity.
- The box plot of MF_{RF} looks similar to that of MF_{ANN} but with 2 more outliers laying outside $\mu - 3\sigma$, making it 6 identified outliers, 3 above the maximum and 3 below the minimum.
- The boxplot of MF_{DT} shows that the majority of the data points below the 75th percentile are unconservative as the 75th percentile of the model factor distribution is slightly higher than 1. All of the outliers in MF_{DT} lie above the maximum.
- MF_{SVM} has 8 outliers in its distribution as seen in fig 4.26 which is 4% of the entire dataset. As a result, some variability is seen in the distribution of MF_{SVM}.

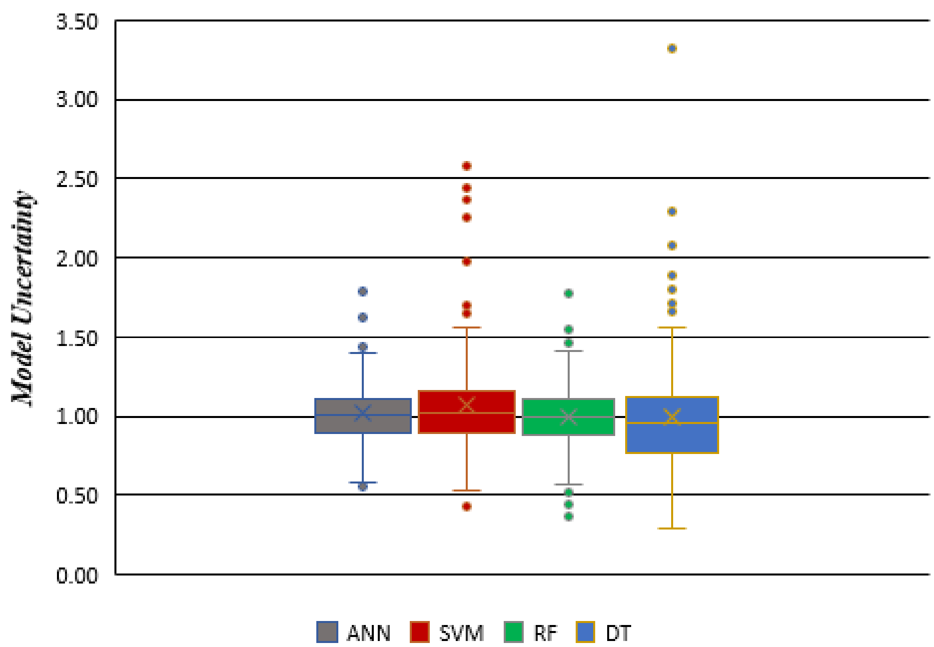

Fig 4.27 Box plots of A.I based model factors

4.5.4 Trend analysis of model factors derived from machine learning models

Scatter plots for MF_{ANN}, MF_{SVM}, MF_{RF} and MF_{DT} against the main parameters that affect shear strength are presented in Figs 4.28 – 4.31. The sensitivity of model factors to shear parameters is investigated by closely examining the plots in Figs 4.28 – 4.31 for trends and corroborating the findings with information deduced from Table 4.8. The lines that give the best description of the observed trend are shown on the plots. Corresponding trend equations and coefficient of determination (R^2) values are also included in the plot to support the examination.

Table 4.8. Pearson correlation matrix of machine learning model factors to shear parameters

	Pearson Correlation coefficient r				
	$b_w(mm)$	a/d	$d(mm)$	$\rho l(\%)$	$f_{ck}[MPa]$
MF_{ANN}	0.023	-0.18	-0.14	0.036	0.24
MF_{SVM}	0.018	-0.071	-0.11	0.0033	-0.021
MF_{RF}	0.025	-0.29	0.0012	0.2	0.21
MF_{DT}	0.2	-0.18	0.052	0.27	0.25

4.5.4.1 MF_{ANN} trend analysis

Close examination of Fig. 4.28 revealed that MF_{ANN} only showed a weak positive correlation with the concrete strength with a correlation coefficient r = 0.24. The weak positive correlation is indicative of a marginal increasing conservative bias as the concrete strength increase. The plot also revealed that MF_{ANN} showed no significant trend with the remaining shear strength parameters.

4.5.4.2 MF_{SVM} trend analysis

The assessment of Fig. 4.29 showed that MF_{SVM} has no form of correlation with all of the factors affecting shear strength. This was validated by an insignificant correlation coefficient as seen in table 4.6.

4.5.4.3 MF_{RF} trend analysis

From fig 4.30, MF_{RF} displayed a weak sensitivity to the shear span – effective depth ratio (a/d), longitudinal reinforcement ratio (ρl) and concrete strength with a coefficient correlation of -0.29, 0.2 and 0.21 respectively. While no trend was seen for the beam width (b_w) and depth (d).

4.5.4.4 MF_{DT} trend analysis

The parametric coefficient analysis in Table 4.8 shows that MF_{DT} realizations have a weak correlation with the beam width, longitudinal reinforcement ratio and concrete strength with designated coefficients of 0.2, 0.27 and 0.25. While an insignificant trend was observed for the relationship between MF_{DT} and the shear span – effective depth ratio and the effective depth as well.

Though the Pearson correlation coefficient suggests a weak positive relationship between MF_{DT} and the beam width, but a close examination of Fig. 4.31(b) shows that the fairly steep slope of the trendline suggests a fairly significant relationship between the two variables.

Generally, all machine learning models displayed a very poor sensitivity to the shear parameters as compared to how conventional shear models respond to shear parameters.

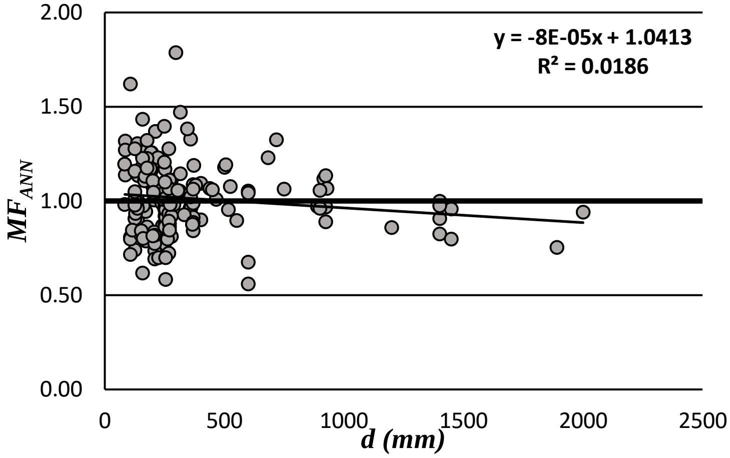

(i) $MF_{ANN}\ versus\ d(mm)$

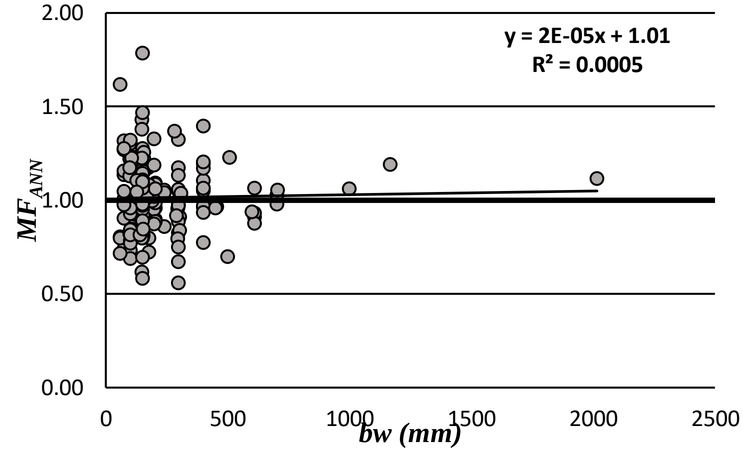

(ii) $MF_{ANN}\ versus\ b_{\mathrm{w}}(mm)$

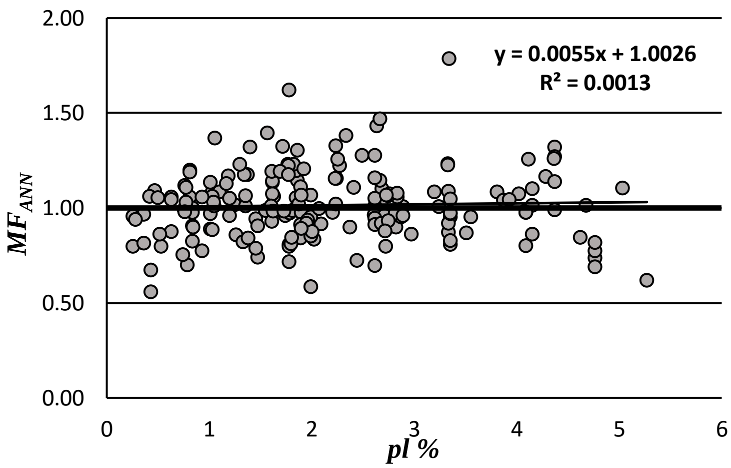

(iii) $MF_{ANN}\ versus\ \rho l$

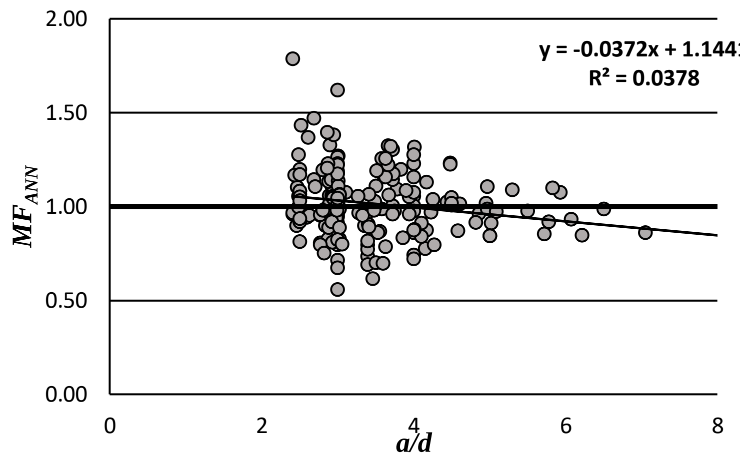

(iv) $MF_{ANN}\ versus\ a/d$

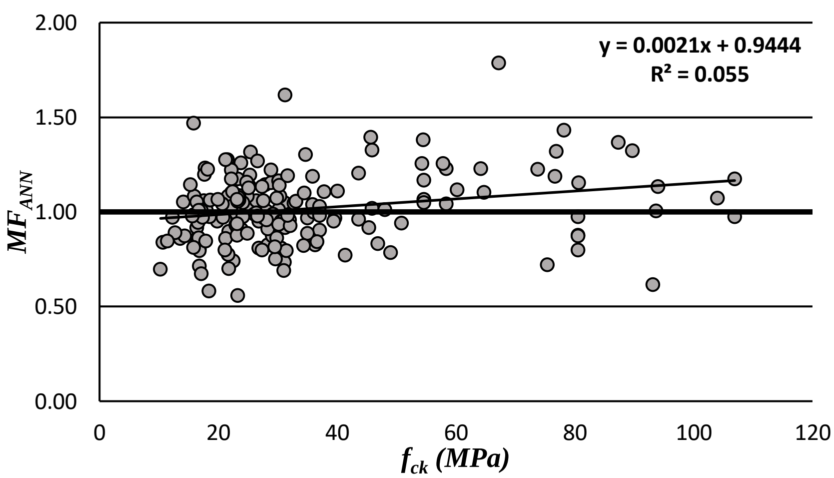

(v) $MF_{ANN}\ versus\ f_{ck}$

Figure 4.28. Sensitivity plot of $\boldsymbol{MF_{ANN}}$ against (i) d (ii) bw (iii) ρl (iv) a/d (v) fck

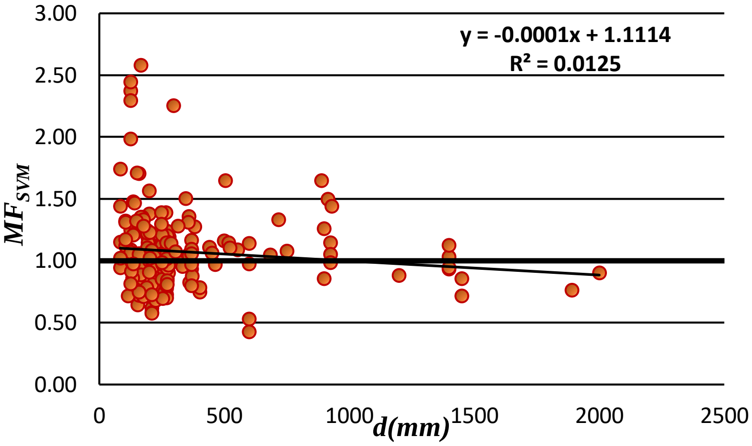

(i) $\boldsymbol{MF_{SVM}\ versus\ d(mm)}$

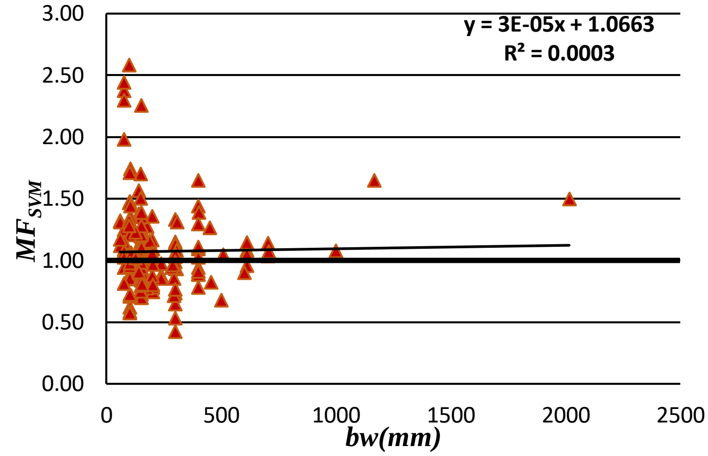

(ii) $\boldsymbol{MF_{SVM}\ versus\ b_{w}(mm)}$

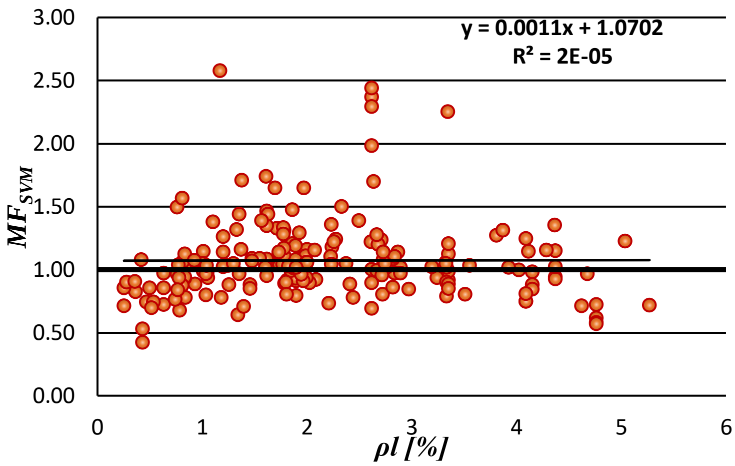

(iii) $\boldsymbol{MF_{SVM}\ versus\ \rho l}$

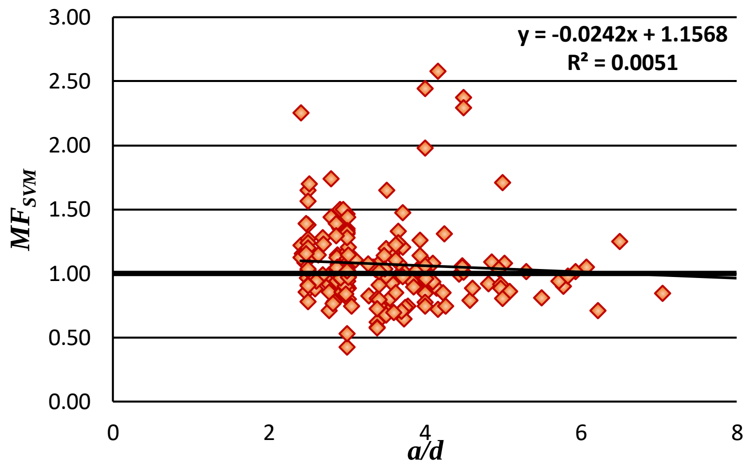

(iv) $\boldsymbol{MF_{SVM}\ versus\ a/d}$

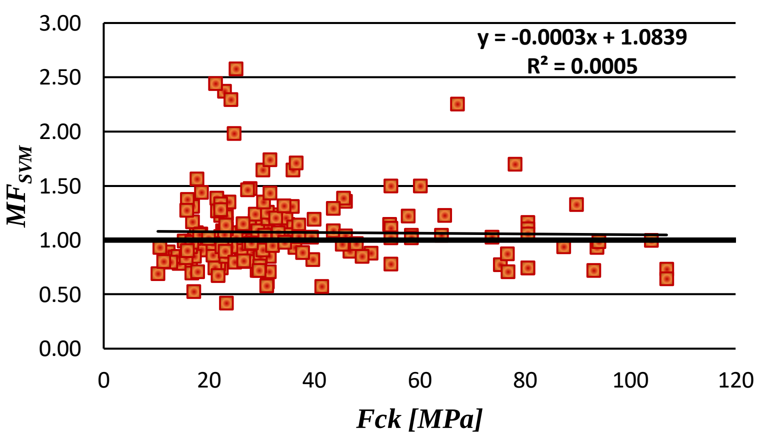

(v) $\boldsymbol{MF_{SVM}\ versus\ f_{ck}}$

Figure 4.29. Sensitivity plot of $\boldsymbol{MF_{SVM}}$ against (i) d (ii) bw (iii) ρl (iv) a/d (v) fck

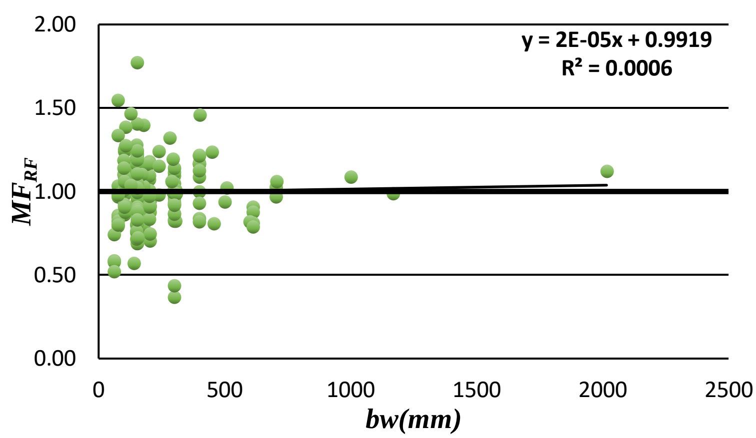

(i) MF_{RF} *versus* $d(mm)$

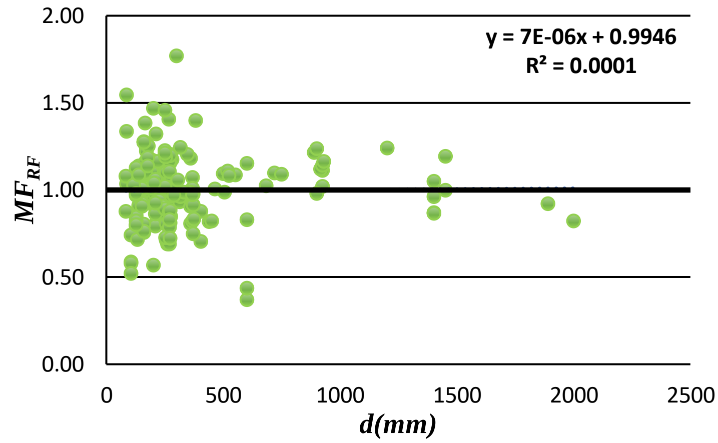

(ii) MF_{RF} *versus* $b_{\text{w}}(mm)$

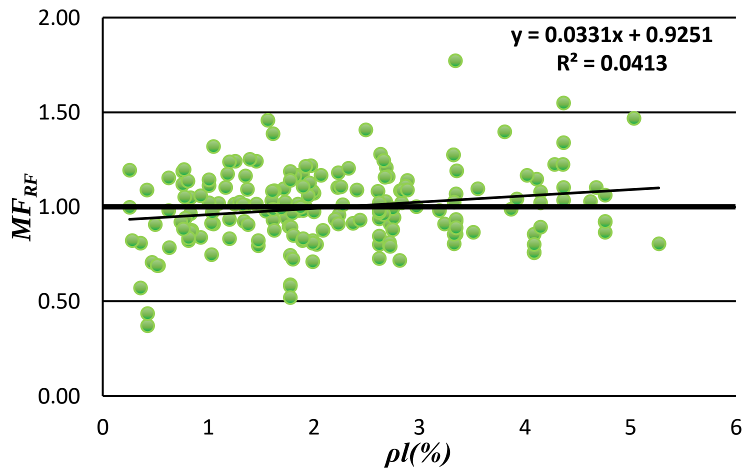

(iii) MF_{RF} *versus* ρl

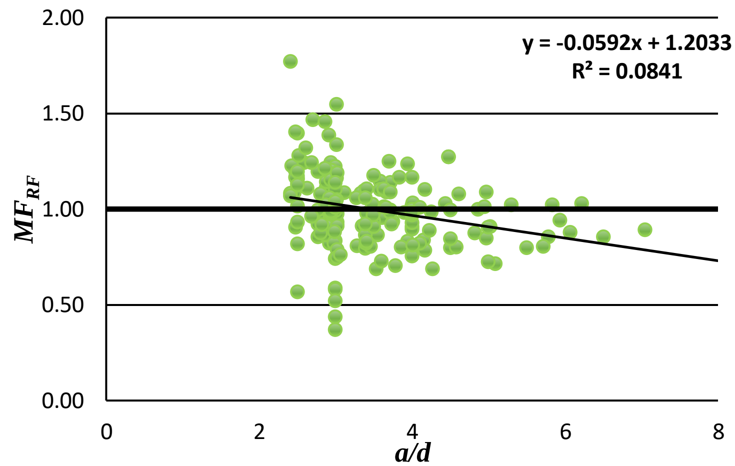

(iv) MF_{RF} *versus* a/d

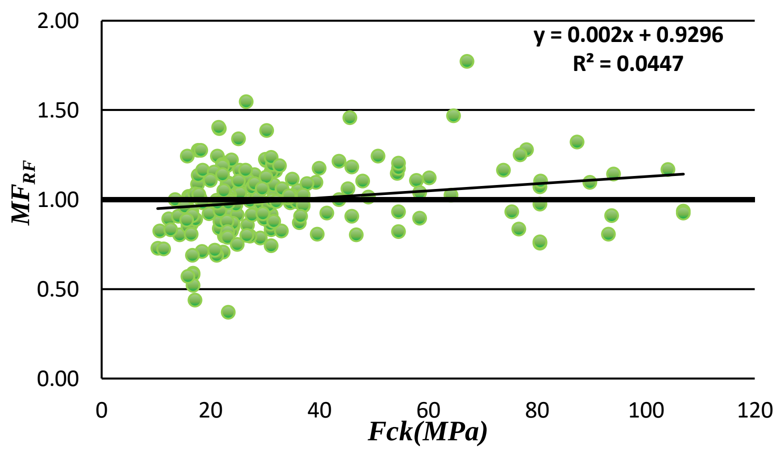

(v) MF_{RF} *versus* f_{ck}

Figure 4.30. Sensitivity plot of MF_{RF} against (i) d (ii) bw (iii) ρl (iv) a/d (v) fck

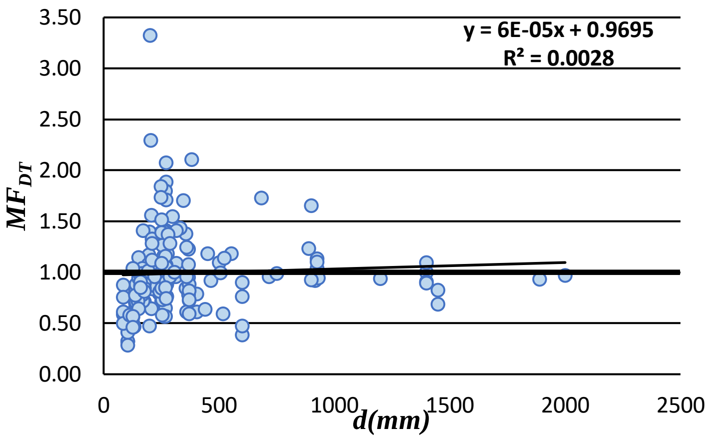

(i) MF_{DT} versus $d(mm)$

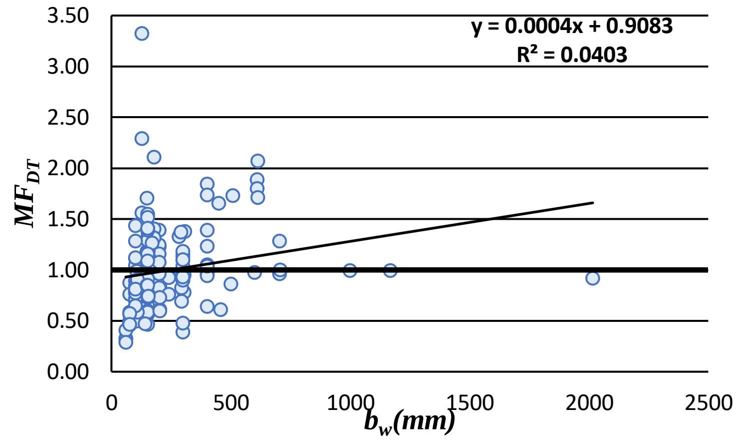

(ii) MF_{DT} versus $b_{\mathrm{w}}(mm)$

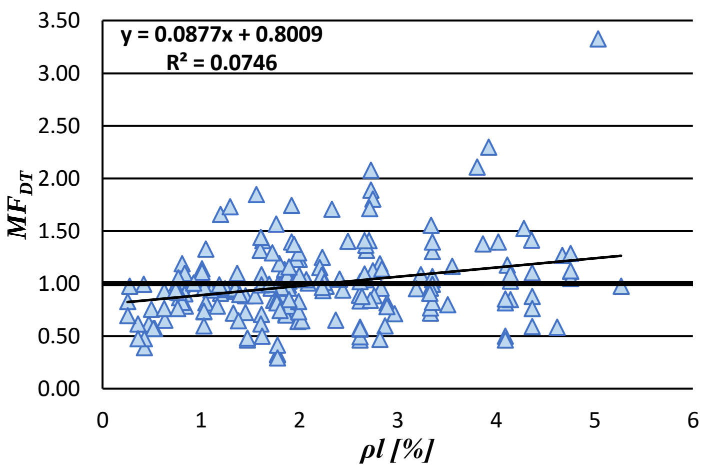

(iii) MF_{DT} versus ρl

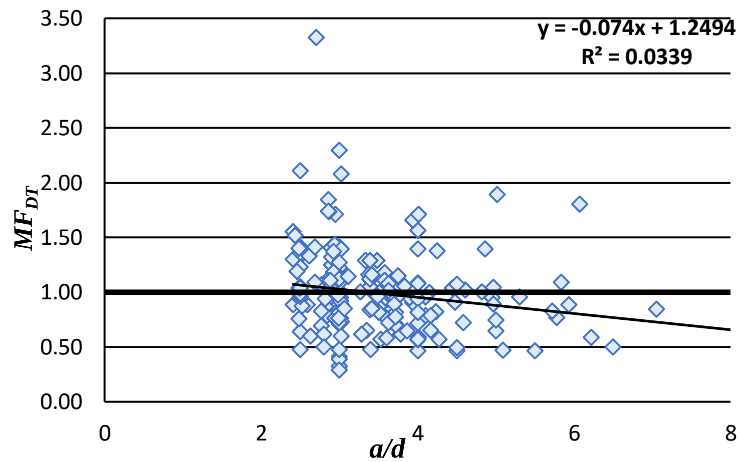

(iv) MF_{DT} versus a/d

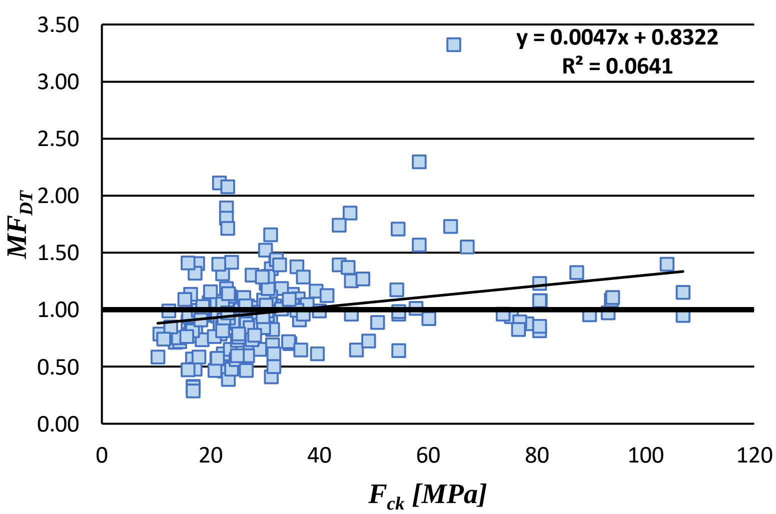

(v) MF_{DT} versus f_{ck}

Figure 4.31. Sensitivity plot of MF_{DT} against (i) d (ii) bw (iii) ρl (iv) a/d (v) fck

4.5.5 Probability distribution function of realized A.I based the model factor

The null hypothesis for the choice of the probability distribution function in MF_{DT} & MF_{SVM} was rejected as the non-parametric analysis gave a significance P-value considerably lower than 0.05, which indicates that the underlying distribution is a Log-Normal distribution. The corresponding Pearson coefficient of skewness (1.78 & 1.99) which is greater than 1 shows that the realizations of MF_{DT} & MF_{SVM} are highly positively skewed. This also indicates that MF_{DT} & MF_{SVM} is not normally distributed. Another clue to defining the distribution is the careful observation of plots in fig 4.28 (c, d, g, h) which shows that the Log-Normal curve fits both distributions

Both of the non-parametric tests (Anderson Darling & Chi-Square) conducted for MF_{ANN} almost did not reject the null hypothesis that the underlying distribution is normal as the significance P-value of 0.06 and 0.072 was higher than the recommended P-value of 0.05 with just a minimal margin. A Pearson skewness coefficient of 0.60 suggests that the distribution is fairly skewed, while the plots (fig 4.28 a & b) show that the Log-Normal distribution curve was slightly a better fit than the Normal distribution. This investigation shows that MF_{ANN} has a minimal degree of abnormality and the distribution is almost normal. Hence, it is safe to expect a reliable prediction and a moderate assessment of reliability not necessarily conservative.

The goodness of fit test for MF_{RF} shows that the null hypothesis was not rejected. Failure to reject the hypothesis was due to the P-value from the non-parametric analysis which was found to be 0.041 and 0.033, implying that the underlying distribution is normal. The Pearson skewness coefficient = 0.2 also corroborated the findings from the non-parametric analysis due to its closeness to zero. In addition, fig 4.28 (a & b) supported the findings showing that the distribution curve has no excessive tail extension as it is for a normal distribution and the log-normal distribution curve tends to be a better fit than the normal distribution curve.

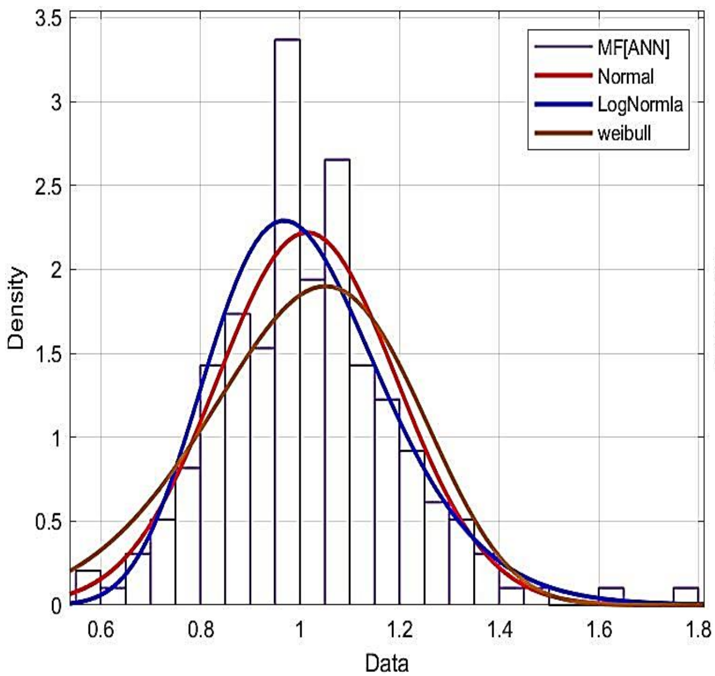

(a) Probability Distribution Function of MF_{ANN}

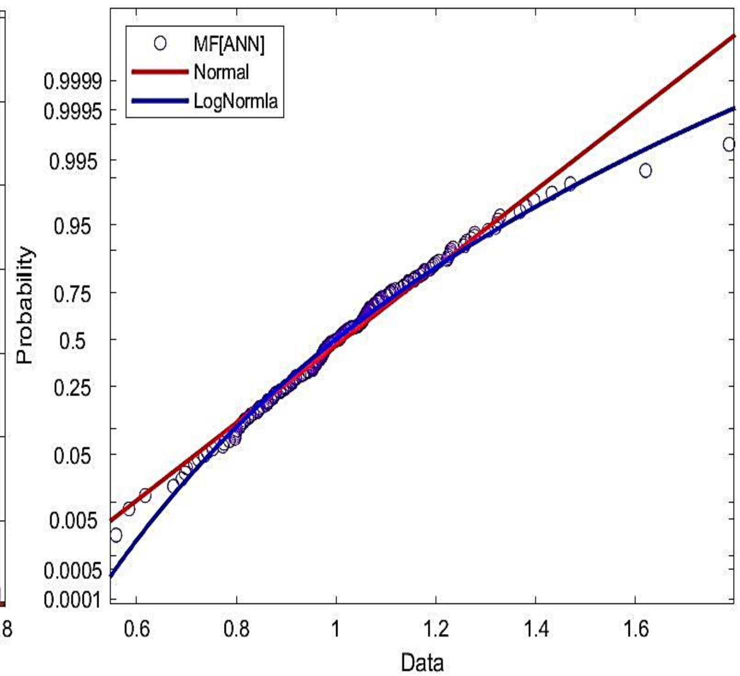

(b) Probability Plot of MF_{ANN}

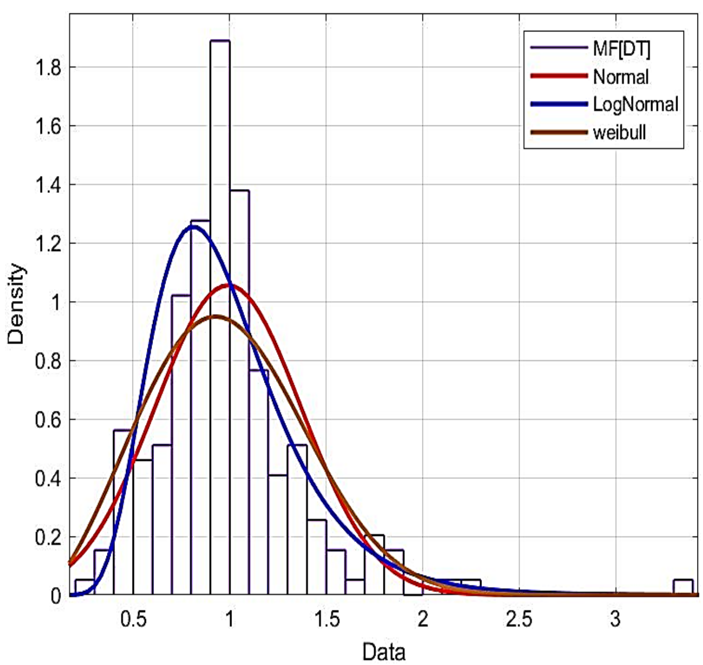

(c) Probability Distribution Function of MF_{DT}

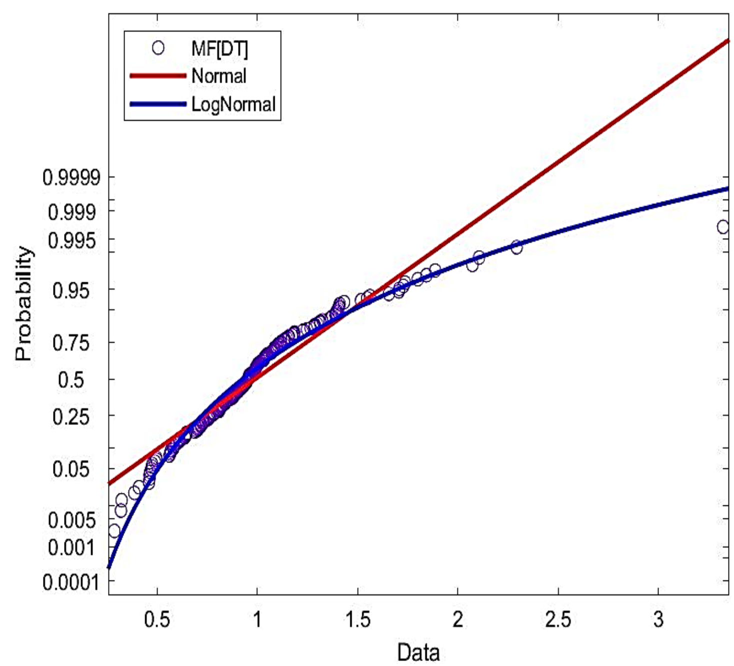

(d) Probability Plot of MF_{DT}

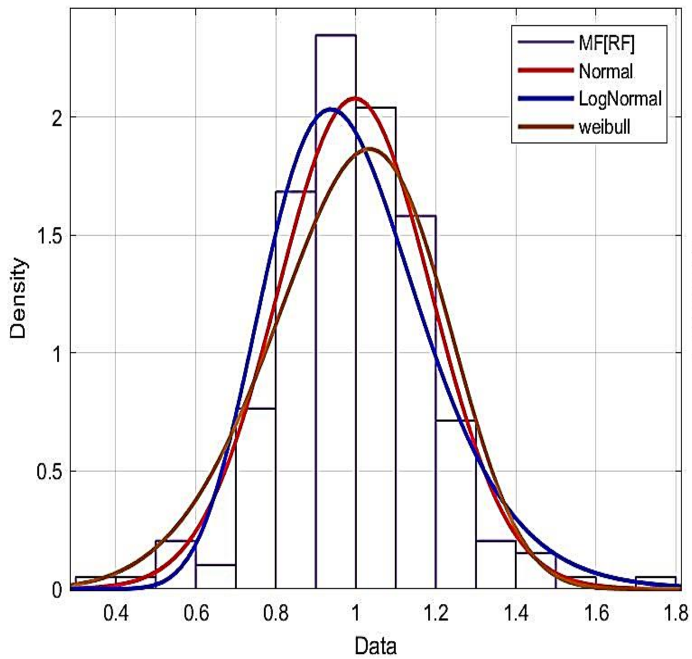

(e) Probability Distribution Function of MF_{RF}

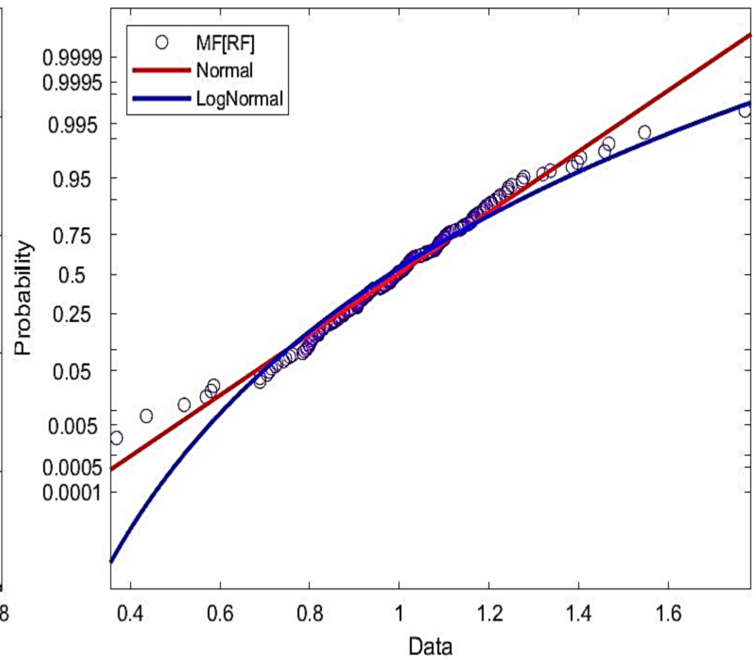

(f) Probability Plot of MF_{RF}

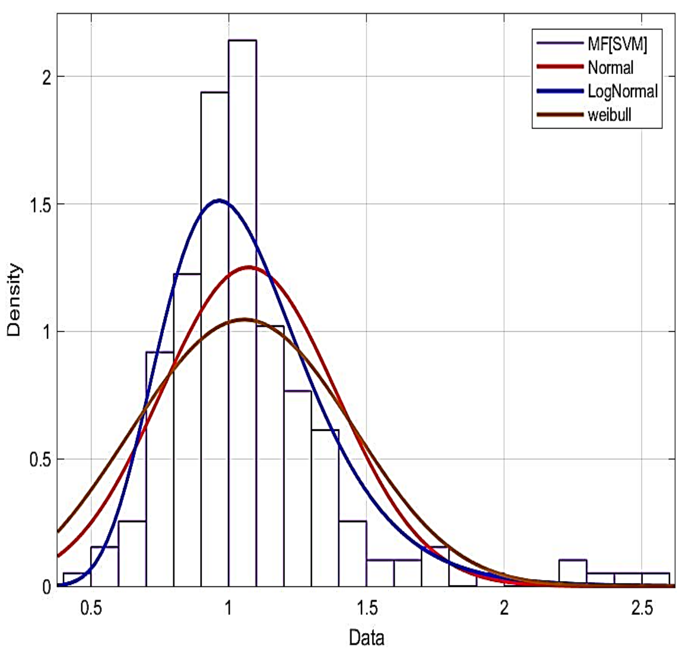

(g) Probability Distribution Function of MF_{SVM}

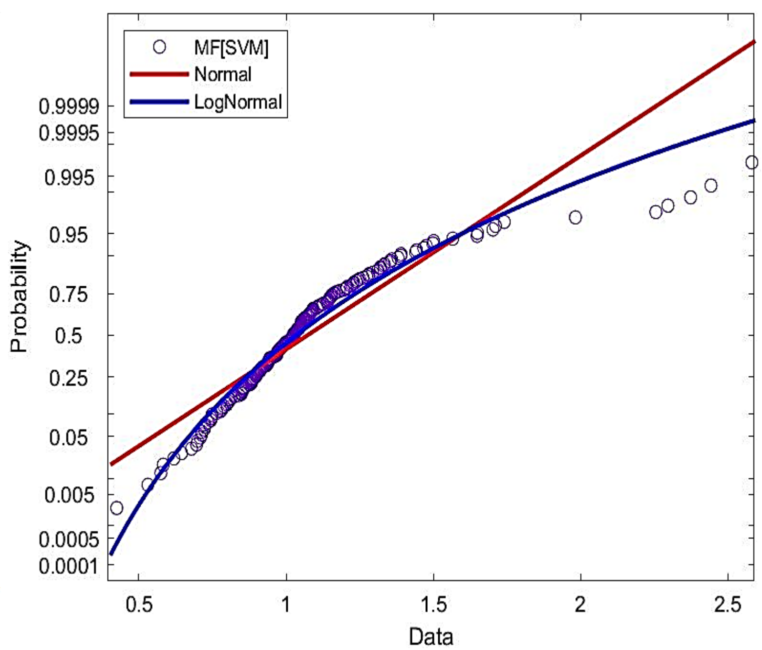

(h) Probability Plot of MF_{SVM}

Fig 4.31 Model uncertainty probability fitting & distribution plots for conventional shear models.

4.5.6 Performance evaluation of ML shear results

A comparison of the ANN, SVM, RF and DT shear model in terms of MAE, MAPE, RMSE and R^2 values is presented in Table 4.9 and plotted in Fig 4.32.

Table 4.9. Evaluation score for machine learning shear prediction

Evaluation Metrics	ANN	SVM	RF	DT
Mean Absolute Error (MAE)	12.00	18.00	13.29	20.50
Mean Absolute Percentage Error (MAPE)	0.14	0.22	0.15	0.26
Root Mean Squared Error (RMSE)	21.47	42.95	23.10	33.15
Coefficient of Determination (R^2)	0.97	0.91	0.96	0.93

Table 4.9. above, the following were established

- Data from Table 4.9 showed that the ANN shear prediction model's performance assessment metrics were better than those of the alternative machine learning models taken into consideration in this study. According to the values of MAE = 12, MAPE =0.14, and RMSE = 21.47, the ANN model comes near to accurately predicting the real shear resistance over the range of parameters taken into consideration with a coefficient of determination R^2 = 0.97.
- The evaluation metrics of the RF model prediction are the closest to ANN’s prediction with just a minimal performance margin.
- The DT shear model's performance data appear to be superior to the SVM shear model. When compared to the SVM shear model, the DT shear model performed better on the most crucial evaluation criteria, RMSE and R^2.

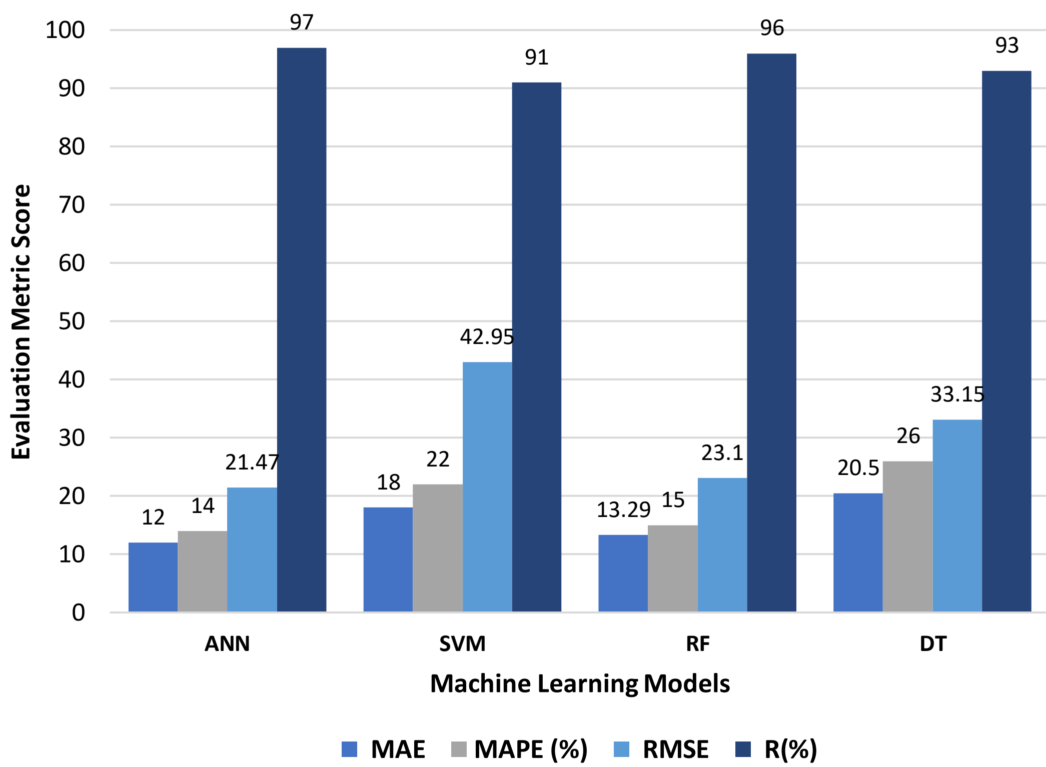

Fig 4.32 Bar chart displaying the metrics score of ML models shear result.

4.5.7 Optimal hyperparameter of ML models selected via cross-validation.

The grid-search cross-validation in the model–selection sub-library of the sci-kit learn ML library package was used to perform a 5 – fold cross-validation with a specified parameter grid that contains the most important combination of hyperparameters required for an optimal model tunning. After the hyperparameter tunning, the grid search CV selected the best parameters upon which the architecture of the ML models was built. See table 4.10 below.

Table 4.10. Optimal hyperparameters of models

Model	**Hyperparameter Grid**	**Optimal Hyperparameters**
SVM	C: 0.001, 0.01, 0.1, 0.5, 1, 2	2
	Kernel: Linear, Rbf, Poly, Sigmoid	Linear
	Scale: Auto, Gamma	Gamma
	Degree: 2, 3	2
	Epsilon: 0, 0.01, 0.1, 0.5, 1, 2	0.5

RF	N estimators: 64, 80 Criterion: squared error, absolute error, Poisson Max depth: 40, 50,37,35 Min samples split: 3, 5, 2 Min impurity decrease: 0.00001, 0.005, 0.000008 Min samples leaf: 1,2 Max features: auto, sqrt, log2 Max leaf nodes: 30,40,45,50 Bootstrap: True, False Random state: 101, 73, 80	64 squared error 37 2 0.000008 1 Auto 45 True 73
DT	Criterion: squared error, absolute error, Poisson, Friedman MSE Splitter: Best, Random. Max depth: 40, 50,60,70,80,90,100 Min samples split: 3, 5, 10,20, 25 Min impurity decrease: 0.00001, 0.005, 0.000008 Min samples leaf: 1,2,3,4,5 Max features: auto, sqrt, log2 Max leaf nodes: 3, 5, 10, 15, 30, 40	Squared error Random 40 3 0.000008 1 Auto 40
ANN	Number of hidden layers Learning rate The activation function in both layers Optimizer Loss function Mini-batch size Epochs	2 0.01 ReLU Adam Optimizer MSE 16 500

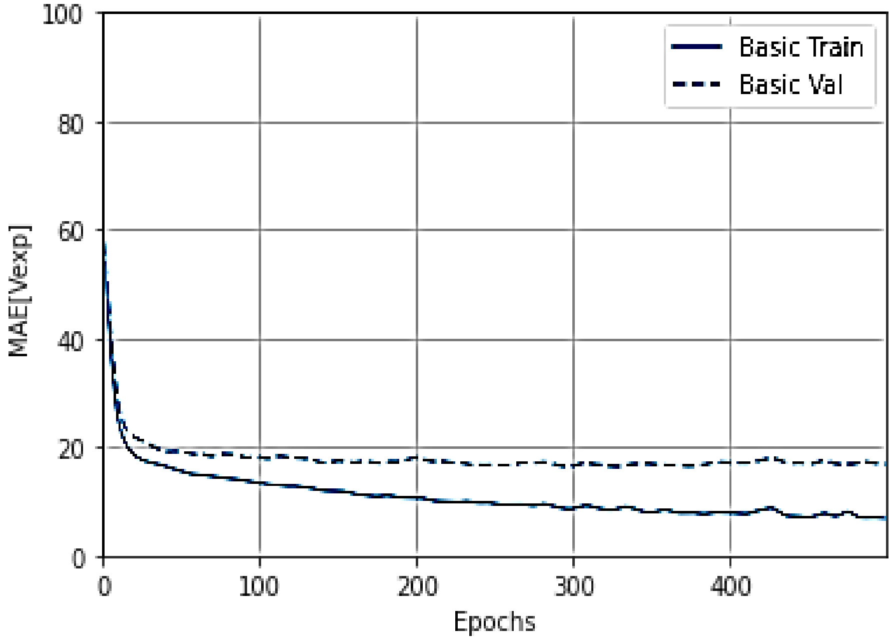

Fig 4.32 performance of ANN with respect to MAE.

CHAPTER 5

MODEL UNCERTAINTY PARTIAL FACTOR RELIABILITY CALIBRATION; A SIMPLIFIED RELIABILITY ANALYSIS

5.1 Overview

According to Taerwe (1993), it is imperative to calibrate uncertainties in models if the measure of dispersion has a coefficient greater than 0.2. This was corroborated by the argument made by Sykora et al. (2012) saying that for safe models with a coefficient of variation less than 0.2, it is unnecessary to require an additional calibration of modelling uncertainty.

Direction cosines yielded during prior reliability assessment of shear methods has revealed that the safety performance of models is largely influenced by model factor. Hence, Mensah et al (2013) agreed that the most effective management of reliable performance for any resistance method is to provide a specially calibrated partial factor for model uncertainties that will account for the uncertainty associated with shear methods.

The partial factor for model uncertainty γ_{Rd} for any shear method can easily be derived according to the procedures established in EN 1990 as seen below.

$$\gamma_{Rd} = 1/[\mu_{MF}.\exp(-\alpha_R.\beta.\Omega_{MF})]$$

Here,

μ_{MF} and Ω_{MF} = statistical moments of model factor realizations in terms of mean value and coefficient of variation respectively.

α_R = FORM Sensitivity Factor (Direction Cosine)

β = Target Reliability Index

According to EN 1990, the derived model uncertainty partial factor can be incorporated into the design shear methods to mitigate the effect of identified uncertainties in shear reliability predictions. See equation below

$$V'_{Rd} = V_{(X_k)}/(\gamma_M.\gamma_{Rd})$$

$V_{(X_k)}$ = Shear resistance due to characteristic properties of input parameters

γ_M = Partial resistance factor to account for material and geometric uncertainties, which can also be set as the partial safety factor of concrete (γ_c=1.5) as a safe assumption should a proper probabilistic calibration of γ_M be neglected.

V'_{Rd} = Calibrated design resistance

All of the expressions above only apply to design shear methods. The works of Konig et al (1985), Taerwe (1993) and Sykora et al (2012) have shown how the mean shear methods can be calibrated to correctly include the effect of the partial safety factor of model uncertainty.

5.1.1 FORM sensitivity factor

The model uncertainty partial factor is significantly affected by the choice of the FORM sensitivity factor which overall influences the degree of calibration of design shear expressions since the model uncertainty partial factor is a function of the FORM sensitivity factor.

The table below describes the criterion for selecting a sensitivity factor.

Table 5.1. Selection of FORM sensitivity factor

	Criterion [Dominancy of Model Uncertainty]	$\boldsymbol{\alpha_R}$
1	If COV% of model uncertainties > COV% of the geometrical and material properties, model uncertainty is dominant.	0.8
2	If COV% of model uncertainties < COV% of the geometrical and material properties, model uncertainty is non-dominant.	0.4 * 0.8 = 0.32

5.1.2 Selection of target reliability Index β

According to Sykora and Holicky (2012), a more practical assessment of the actual performance of existing structures can be arrived at by employing probabilistic methods to describe uncertainties of basic variables as a probabilistic model would. Hence, Specifying the target reliability index is a requisite for the probabilistic assessment of existing structures.

The target reliability values as specified in (EN 1990, 2002) relate the reliability class to a respective consequence of failure. Additionally, the indexes were fundamentally intended for new structures. (EN 1990, 2002) recommends the target reliability index for two reference periods (1 and 50 years). The target reliability index values for each reliability class correspond approximately to the same reliability level. For instance, the reliability index β for an RC2 structure = 3.8, meaning this index can only be used if probabilistic models of basic variables are related to the reference period of 50 years.

Table 5.2 presents the recommended target reliability according to EN 1990.

Table 5.2 Target Reliability index for different reference periods according to (EN 1990, 2002)

	EN 1990 target values for reliability index			
Reliability class	Failure consequence	Reliability Index (1-year reference period)	Reliability Index (50-year reference period)	Examples
RC1	Low for loss of human life, and economic, social or environmental small or negligible	4.2	3.3	Agricultural buildings
RC2	Medium for loss of human life, economic, social or environmental considerable	4.7	3.8	Residences, offices
RC3	High for loss of human life, or economic, social or environmental very great	5.2	4.3	Bridges, public buildings.

5.2 Model uncertainty partial factor related to EC2 shear resistance model for beams without stirrups using deterministic reliability verification

The partial factor can be used to account for the uncertainty associated with the EC2 shear design methods. Since the underlying distribution for MF_{EC2} has been identified as a log-normal distribution, the approach earlier stated can be applied for a deterministic reliability verification. It is mandatory to identify the distribution of MF_{EC2} since a lower prediction of reliability is associated with a lognormal distribution, hence the need for model uncertainty partial factor of safety calibration.

$$\gamma_{Rd} = 1/[\mu_{MF}.\exp(-\alpha_R.\beta.\Omega_{MF})]$$

Input parameters

β = 3.8

α_R = 0.32 (since model uncertainty is non-dominant) (Olalusi and Spyridis, 2020)

μ_{MF} = 1.10, Ω_{MF} = 27% = 0.27

$\gamma_{Rd} = 1/[1.10 * \exp(-0.32 * 3.8 * 0.27)]$

γ_{Rd} = 1.26

Table 5.3 Variation of EC2 model uncertainty partial factor $\boldsymbol{\gamma_{Rd}}$ with target reliability index $\boldsymbol{\beta}$

Target reliability index ($\boldsymbol{\beta}$)	3	3.2	3.4	3.6	3.8	4	4.2	4.4
Model Uncertainty factor ($\boldsymbol{\gamma_{Rd}}$)	1.18	1.20	1.22	1.24	1.26	1.29	1.31	1.33

Fig 5.1 Variation of derived EC2 partial factor $\boldsymbol{\gamma_{Rd}}$ with β for = 0.4x0.8 = 0.32.

5.3 Model Uncertainty Partial Factor related to SANS shear resistance model for beams without stirrups using deterministic reliability verification

Input parameters

β = 3.8

α_R = 0.32 (since model uncertainty is non-dominant) (Olalusi and Spyridis, 2020)

μ_{MF} = 1.05, Ω_{MF} = 27% = 0.27

$\gamma_{Rd} = 1/[1.05 * \exp(-0.32 * 3.8 * 0.27)]$

γ_{Rd} = 1.32

Table 5.4 Variation of SANS model uncertainty partial factor $\boldsymbol{\gamma_{Rd}}$ with target reliability index $\boldsymbol{\beta}$

Target reliability index ($\boldsymbol{\beta}$)	3	3.2	3.4	3.6	3.8	4	4.2	4.4
Model Uncertainty factor ($\boldsymbol{\gamma_{Rd}}$)	1.24	1.26	1.28	1.30	1.32	1.35	1.37	1.39

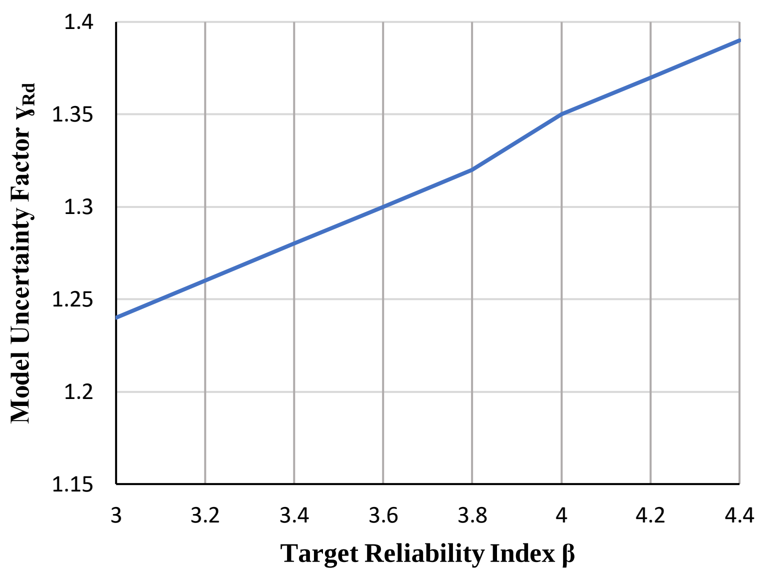

Fig 5.2 Variation of derived SANS partial factor $\boldsymbol{\gamma_{Rd}}$ with β for = 0.4x0.8 = 0.32.

Although, the analysis done in this study showed that all of the shear models taken into consideration, with the exception of Tran (2020)'s model, had a COV>0.2, indicating that model uncertainty calibration is required for all of these models. The EC2 and SANS shear models were the only ones to which the calibration processes were used. The justification for this is provided in the next paragraphs.

As of September 2021, the EC2 has been adopted by all European Union member states and by some other countries outside of the EU, such as Norway, Switzerland, and Turkey. Therefore, at least 31 countries have adopted the EC2 as their standard for the design of concrete structures. The EC2 shear model was chosen for calibration over other shear models because it applies to a larger variety of nations. Further studies to calibrate shear models not taken into account in this section are advised by this research.

As the study was conducted in South Africa, the decision to include the SANS shear model in this part is primarily based on how the research can influence and contribute to the South African design standard.

CHAPTER 6

CONCLUSION AND RECOMMENDATION

6.1 Overview

The inability of investigated shear models to adequately replicate trends as seen in experimental observations indicates significant underlying uncertainties inherent in the shear strength models for beams without shear reinforcement. The identified uncertainties may be a result of model oversimplification or the neglection of important shear parameters leading to an overestimation or underestimation of shear strength and an inconsistent prediction across the parametric range. The shear reliability prediction of an investigated model is based on its insensitivity to the considered range of shear parameters, marginal or no form of bias in the mean value of model factors realization, minimal coefficient of variation, a low scatter of model factor realizations around the mean and also the ratio of maximum model factor to the minimum (MF_{max}/MF_{min}) should be minimal. Additionally, the choice of probability distribution function affects the reliability predictions of investigated shear models and it is a good indication of the performance of a model.

Further investigations revealed that there was no clause from national codes or authorial publications that the investigated models have been calibrated to account for deliberately structured trends associated with increasing shear strength parameters. Uncertainties discovered after a thorough assessment of the considered models gave rise to safety and economic concerns as would be discussed in the following sections. The performance of a shear model mustn't result in over-conservatism or significant unconservative estimates, as overly conservative estimation leads to an uneconomic performance of shear models while significant unconservative prediction raises concerns for the safety performance of shear models.

6.2 Accomplishments of research objectives

To assess and quantify the uncertainties in shear models which includes shear expressions from code-based models (such as EN 2003, ACI 318, AS 3600, *Fib* Model Code 2010 and SANS10100), authorial models (such as CCC, MASM, NLT and the modified SNiP shear model) and machine learning based shear models (ANN, SVM, RF and DT) to arrive at a probabilistic model which would be recommended for future reliability analysis, the following objectives were actualized.

1. A robust understanding of the mechanism of shear failure and contributing shear transfer actions in reinforced concrete beams with and without shear reinforcement with proper consideration of

the influence of shear parameters on the response of beams without stirrups to shear as outlined in section

2. An in-depth knowledge of the underlying principles or phenomenon employed in the formulation of the considered shear capacity models together with the included limitations is a form of bias.
3. Mathematical intuition behind the development of supervised machine learning models and deep neural networks with implementation in python (An object-oriented programming language) and the use of python library packages such as Pandas, NumPy, Sci-Py, machine learning library (Sci-Kit learn) and Neural Network library packages such as TensorFlow and Keras API.
4. Proper application of structural reliability assessment methods which includes concepts such as deterministic assessments, probabilities and statistics.
5. In Chapter 4, model factors of the investigated 9 shear techniques were measured and statistically analyzed. The obtained model factors were parametrically related to significant shear design parameters for observable trends and were found to be sensitive to some shear parameters, though the mechanical models seemed to be less sensitive to the shear parameters. Correlation and regression analysis revealed negligible, mild and significant sensitivity of model factors to important parameters that influence shear strength. The model factor statistics derived were used as an indicator of the uncertainty in the reliability prediction of shear models. After the reliability investigation, a partial factor that would account for model uncertainties in shear models was derived for the EC2 and SANS shear models alongside the justification in the latter part of section 5.3.
6. Finally, a general probabilistic model that is suitable for a futuristic full reliability assessment of shear models without shear reinforcement was identified for both non-AI-based models and A.I based models and would be recommended in the subsequent section.

6.3 Limitation of research

The database provided by Reinick et al (2013) which was utilized in this research comprises extreme values of shear parameters which would normally be identified as outliers following a Z-score or box-plot identification of outliers. If these data points were considered outliers, this would defeat the aim of shear reliability investigation across a wide parametric range. Additionally, limiting the range of data would be an indirect inclusion of bias. Hence, proper data standardization was done instead of removing those points that were identified as outliers.

In addition, removing those data points would reduce the available data for training and evaluating the machine learning models resulting in a poorly generalized model.

6.4 Assessment of model uncertainty for shear reliability

The statistical analysis's conclusion is as follows:

- The model factor MF_{EC2} following the V_{EC2} shear method has a mean value of 1.10 and a standard deviation of 0.30, confirming that the unbiased shear resistance function of EC2 generally underpredicts shear capacity. Hence the EC2 unbiased shear resistance is said to have an uneconomic performance. The scatter around the mean = 0.30 and the variability in shear prediction = 27% revealed the degree of uncertainty of the V_{EC2} shear method.
- The parametric assessment revealed that MF_{EC2} is significantly sensitive to the effective depth and amount of longitudinal tensile reinforcement with a correlation coefficient of -0.34 and 0.50 respectively. This signifies that EC2 does not adequately account for the longitudinal reinforcement ratio and the size effect. At a high amount of longitudinal shear reinforcement EC2 shear method for beams without stirrups exhibits an uneconomical performance as it overly underpredicts shear capacity at high values of ρl. safety concern arises as the effective depth increases beyond 500mm indicating that at $d > 500$mm, reliable safe predictions following the V_{EC2} shear approach is uncertain.
- Sensitivity of V_{EC2} to the beam width and shear-span-to-depth ratio also suggest an inadequate calibration of these shear parameters.
- MF_{ACI} has a mean value of μ_{MF} = 1.31 and a standard deviation of σMF = 0.31 implying that shear predictions associated with the ACI shear methods are generally characterized by a significant degree of over-conservatism (underprediction). V_{ACI} was seen to have a significant negative correlation with the shear-span to effective depth ratio a/d and a milder sensitivity to the concrete strength. This implies that it is unsafe to apply the ACI shear approach to very slender beams without stirrups. Generally, the sensitivity to shear parameters poses a question of adequate calibration of the size effect in the ACI shear method.
- Close examination of the shear approach presented by the fib model code level II approximation and the Australian concrete design standard revealed a systematic negative trend with $\mathrm{a/d}, d$ & pl with a correlation coefficient of -0.28, -0.26 and -0.35 respectively. Both shear models displayed unsafe performances at ρl < 2% and are seen to be uneconomical at a high amount of longitudinal reinforcement. In like manner, shear predictions following the V_{AS3600} & V_{MC10} shear methods tend to be unsafe for use at d > 500mm and a/d >3. These identified trends are symbolic of the inadequate consideration of the respective shear parameters in model formulation.
- Safety concerns associated with the performance of the mechanical compression chord capacity model (CCC) at a high slenderness ratio (very slender beams) and high amount of longitudinal

reinforcement are not so alarming, this is because there is a paucity of overly unconservative estimates at an extreme parametric range of $\mathrm{a/d}$ & pl. Though conservative, the statistics of the model factor realization of V_{CCC} is somewhat satisfactory with a mean value of 1.14, a standard deviation of 0.28 and a coefficient of variation of 0.25.

- The model factor MF_{MASM} associated with the V_{MASM} shear method has a mean value of 1.11 and a standard deviation of 0.28, affirming that the mean shear function MASM generally underpredicts shear capacity. No alarming safety or economic concern was associated with this model as the investigation failed to identify any deliberately structured bias.
- Investigation showed that the performance of the Modified SNiP shear method raises alarming economical concerns. Decreasing conservative bias still kept a majority of the model factors significantly above a value of 1. This over-conservatism is a result of the neglect of important shear parameters as the Modified SNiP shear method comprises only very basic shear parameters. Significant sensitivity to pl is indicative of the neglection of this term, while sensitivity to concrete compressive strength is a result of incomplete information when deciding to substitute compressive strength for tensile strength following the assumption that "In shear model formulation, cognizance should be given to the concrete tensile strength rather than concrete compressive strength".

  Generally, the modified SNiP shear approach greatly underpredicts shear capacity with a mean value of 1.65, a standard deviation of 0.52 and a variation coefficient of 0.31.
- Uncertainty assessment revealed that the unbiased shear provision for RC beams without stirrups in the South African standard for concrete design was not adequately calibrated for concrete strength and shear-span to effective depth ratio. The assessment showed that applying the SANS shear method at a high shear span to an effective depth ratio (very slender beams) is an unsafe practice as all of the predictions at this high slenderness ratio provided increasing unconservative estimates, hence exaggerating shear capacity. This systematic trend calls for a deliberate effort to account for the slenderness ratio. Shear predictions at concrete strength > 40MPa follow an increasing conservative bias (uneconomic performance).
- Of all the shear models considered in this study, code-based models (such as EN 2003, ACI 318, AS 3600, *Fib* Model Code 2010 and SANS10100), authorial models (such as CCC, MASM, NLT and the modified SNiP shear model) and machine learning based shear models (ANN, SVM, RF and DT), V_{NLT} is the best predictor of shear capacity. All indicators employed in the reliability assessment showed V_{NLT} to be the most suitable candidate that gives predictions synonymous with experimental shear observations. MF_{NLT} was the most favourable candidate in terms of statistical moments with a mean of 1.02, a standard deviation of 0.16 and a coefficient of

variation of 16%. The degree of scatter around the mean value is significantly small compared to other investigated shear models as seen in table 4.1. The marginal measure of dispersion indicates there is no form or negligible degree of uncertainty associated with the V_{NLT} . The insensitivity of the V_{NLT} shear model to main shear parameters is indicative of its consistency and reliability in prediction across considered parametric range.

- Investigations from the machine learning shear predictions showed all A.I based shear methods to be a good predictor of shear capacity in terms of the mean value, dispersion of data points, the presence of outliers and sensitivity to shear parameters. The highest bias seen in the machine learning shear result was in the case of MF_{SVM} which was just 7% conservative, this is relatively small compared to the conservatism seen in MF_{ACI} = 31% conservative, MF_{CCC} = 14% conservative, MF_{SNiP} = 65% conservative. Though the only shortcoming of MF_{SVM} and MF_{DT} was their descriptive statistics that showed the variability of MF_{SVM} and MF_{DT} to be relatively large with a variation coefficient of 0.30 and 0.37 respectively. The degree of dispersion calls for certainty concerns in reliable shear predictions. Unlike MF_{SVM} and MF_{DT}, shear predictions from MF_{ANN} and MF_{RF} proved to be more reliable as they both had a lower variation index of 0.18 and 0.19 respectively with a mean of 1.00. Both MF_{ANN} and MF_{RF} are undisputedly reliable in shear prediction, but MF_{ANN} is the better predictor due to its less sensitivity to shear parameters.

In conclusion, a good predictive shear resistance model is one with a mean close to 1 (low bias), low standard deviation (minimal dispersion), low variability index (consistency in shear prediction) and a weak sensitivity to parameters influencing shear capacity (adequate consideration of shear parameters). Furthermore, such a model can be adopted as a probabilistic model in future reliability assessments of alternative shear design methods. Out of all the shear models considered in this study, the shear method based on structural mechanics proposed by Ngoc Linh Tran (V_{NLT}) meets the requirements for a good model as stated above and is considered the best predictor of shear capacity. While considering soft computation, V_{ANN} and V_{RF} meets the demand for a suitable model and can also be adopted as a probabilistic model for reliability analysis.

6.5 Recommendations

6.5.1 Main recommendations from the dissertation

1. To account for the uncertainty associated with the EC2 and SANS10100 shear methods, a model uncertainty partial factor ($\boldsymbol{\gamma_{Rd(EC2)}}$= 1.26 & $\boldsymbol{\gamma_{Rd(SANS)}}$ = 1.32) for the target reliability level of reliability class 2 (RC2) recommended for residential buildings and offices for a reference period of 50yrs according to EN 1990 is recommended.

2. The mechanical model by Ngoc Linh Tran is suggested as a probabilistic model for future reliability assessments of alternative shear techniques since the investigation showed it to be the best predictor of shear strength as it properly reflects shear failure and has the lowest uncertainty level in its model factor statistics.
3. Generally, mechanical model based on the theory of structural mechanics, fracture mechanics and crack theory should be assessed for reliable shear predictions and adopted by National codes in place of the conventional empirical models which has a lot of assumptions and neglection of important shear parameters resulting in uncertainties.
4. The investigation conducted in this study showed that the EC2 shear method overpredicts shear at larger beam depths, leading to unsafe designs. Hence, for safe design practices, it is recommended that the present state of the EC2 shear method should not be used in estimating the shear capacity of beams depth > 500mm until the size effect concern has been addressed following an adequate calibration.

6.5.2 Recommendations for future research

1. The mechanical model proposed by Tran (2020) should be used as a general probabilistic model for the full reliability assessment of any alternative shear design provision for beams without shear reinforcement.
2. The underestimation of shear capacity following the ACI shear methods for beams without shear reinforcement calls for a proper reliability calibration.
3. The procedures highlighted in the work of Konig *et al.* (1985), Taerwe (1993) and Sykora *et al*. (2012) should be adopted to correctly include the effect of the partial safety factor of model uncertainty for the Modified SNiP shear method.

LIST OF REFERENCES

ACI-ASCE Committee 426 (1973). The shear strength of reinforced concrete members. *ACI Structural Journal, Proc*.,70:1091–187.

Aldakheel, F., Satari, R., & Wriggers, P. (2021). Feed-Forward Neural Networks for Failure Mechanics Problems. (C. M. A., Ed.) *Applied Sciences*. DOI: https://doi.org/10.3390/app11146483

Amani, J., & Moeini, R. (2012). Prediction of shear strength of reinforced concrete beams using adaptive neuro-fuzzy inference system and artificial neural network. *Scientia Iranica*, No.19(2), 242–248.

Amit, Y. and Geman, D. (1997). Shape quantization and recognition with randomized trees. *Neural Computation*, Vol 9(7), Pp. 1545-1588.

Angelakos, D., Bentz, E. and Collins, M. (2001). Effect of Concrete Strength and Minimum Stirrups on Shear Strength of Large Members. *ACI Structural Journal*, vol. 98, no. 3, pp. 290-300

AS 3600-2018 (2018) Concrete Structures. Sydney: Standards Australia Limited.

Autrup, F., Jorgensen, H.B. and Hoang, L.C (2021). *Conference paper: Experimental investigation of dowel action in RC beams without shear reinforcement.*

Baghi, H. and Barros, J. (2018) Design-oriented approach to predict the shear strength of reinforced concrete beams. *Fib international federation of structural concrete*, Vol. 19, pp. 98 – 115.

Bazant, Z. and Sun, H. (1987). Size effect in diagonal shear failure: influence of aggregate size and stirrups. *ACI Material Journal*, vol. 84, no. 4, pp. 259–71.

Bentz, EC., Vecchio, FJ. and Collins, MP. (2006). Simplified modified compression field theory for calculating the shear strength of reinforced concrete elements. *ACI Structural Journal*, Vol. 103, No. 4, pp. 614–624.

Borishansky, M. S. (1961). Shear strength of reinforced concrete elements (UDC 624.075.3: 624.012 45) (pp. 85–95). Amsterdam: *International Council for Building Research, Studies and Documentation - CIB.*

Breiman, L., Friedman, J., Olshen, R.A and Stone, C.J. (1984) Classification and Regression Trees. First Edition ISBN 9780412048418. Belmont, CA: Wadsworth International Group.

Breiman, L. (2001) Bagging Predictors. *Machine Learning*, Vol 45 (1) pp. 5–32.

Breiman, L. (2001). Bagging Predictors. *Machine Learning*, Vol 24 (2), Pp. 123–140.

Campana, S., Fernandez Ruiz, M., Anastasi, A and Muttoni, A. (2013). Analysis of shear transfer actions on one-way RC members based on measured cracking pattern and failure kinematics. *Magazine of Concrete Research*, Vol. 56, no.6, pp. 386–404.

CEN European Committee for Standardization. Eurocode 2. Design of concrete structures – general rules and rules for buildings. EN 1992-1-1, Brussels, Belgium; 2004. p. 225.

Chou, J.S., Tsai, C.F., Pham, A.D and Lu, Y.H. (2014). Machine learning in concrete strength simulation: multi-nation data analytics. *Construction and Building Materials* 73 (2014) 771–780.

Chowdury, S. and Loo, YC. (2018). The New Australian Concrete Structures Standard AS 3600:2018 – Aspects of its Complexity and Effectiveness. *Athens Journal of Technology and Engineering*, Vol.6, No.3, pp. 163-178.

Cladera, A. and Marı, A. (2004). Shear design procedure for reinforced normal and high-strength concrete beams using artificial neural networks. Part II: Beams with stirrups. *Engineering Structures*, vol. 26, No. 7, pp. 927–936.

Cladera, A., Mari, A., Ribas, C., Bairan, J. (2015). Mechanical-based shear model for assessment of reinforced and/or prestressed concrete beams. SMAR 2015 – *Third conference on smart monitoring assessment and rehabilitation of civil structures*.

Cladera, A., Mari, A., Ribas, C., Oller, E., Bairan, J.M., Duarte, N. and Menduina, R. (2019). A simplified model for the shear strength in RC and PC beams, and for punching shear in slabs, with or without shear reinforcement, including steel, FRP and SMA. SMAR 2019 – *Fifth conference on smart monitoring assessment and rehabilitation of civil structures*.

Collins, M. and Kuchma, D. (1999). How safe are our large, lightly reinforced concrete beams, slabs and footings? *ACI Structural Journal*, vol. 96, no.4, pp. 482-490.

Collins, M. (2001). Evaluation of shear design procedures for concrete structures. A Report prepared for the CSA technical committee on reinforced concrete design.

Collins, M.P., Bentz, E.C., Quach, P. T., Fisher, A.W. and Proestos, G.T. (2015). Predicting the shear strength of concrete structures. *The New Zealand concrete industry conference 2015.*

CSA Committee A23.3. (2004). Design of concrete structures (pp. 214). Mississauga: Canadian Standards Association.

Deng, L., Chu, H., Shi, P., Wang, W. and Kong, X. (2020). Region-based CNN method with deformable modules for visually classifying concrete cracks. *Applied Sciences*, Vol.10(7):2528. https://doi.org/10.3390/app10072528.

EN 1990 (2002). Eurocode – Basis of structural design. European Standard, European Committee for Standardization, Brussels.

Engen, A.B, Hendriks, M.A.N., Kohler, J., Overli, J.A and Aldstedt, E. (2016). A Quantification of the Modelling Uncertainty of Non-linear Finite Element Analyses of Large Concrete Structures.

Fenwick RC, Paulay T. Mechanisms of shear resistance of concrete beams. (1968) *Journal of Structural Division (ASCE)*, Vol. 94, No.10, pp. 2325–2350.

Fernandez Ruiz, M., Muttoni, A. and Sagaseta, J. (2015). Shear strength of concrete members without transverse reinforcement: A mechanical approach to consistently account for the size and strain effects. *Engineering Structures*, vol. 99, pp. 360 – 372. DOI: http://dx.doi.org/10.1016/j.engstruct.2015.05.007

Fédération Internationale du Béton (fib) (2010). Shear and punching shear in RC and FRC elements, fib Bulletin, vol 57.

Fédération Internationalé du Béton (fib) (2013). Fib Model Code for Concrete Structures 2010.

Filatov, V. B. (2017). Strength calculation of inclined sections of reinforced concrete elements under transverse bending. *Materials Science and Engineering*, IOP Conference Series, 262(012160).

Frosch, R. and Wolf, T. (2003). Simplified Shear Design of Prestressed Concrete Members. *Joint Transportation Research Program*, Pp.192 – 203.

Franzblau, A. N. (1958). A primer of statistics for non-statisticians.

Gino, D., Bertagnoli, G., La Mazza, D., & Mancini, G. (2017). A quantification of model uncertainties in NLFEA of RC shear walls subjected to repeated loading. *Ingegneria Sismica*, *34*(3), 79-92.

Han, Q., Gui, C., Xu, J and Lacidogna, G. (2019). A generalized method to predict the compressive strength of high-performance concrete by improved random forest algorithm. *Construction and building materials* 226 (2019) 734 – 742.

Haykin, S. (2009). Neural networks and learning machines. Third edition 2009 ISBN-13: 978-0-13-147139-9.

Hillerborg A. (1983) Analysis of a single crack. In: Wittmann FH, editor. *Fracture mechanics of concrete.* Amsterdam, Netherlands: Elsevier; pp. 223–249.

Holicky, M. (2009). Reliability analysis for structural design. First edition 2009 ISBN: 978-1-920338-11-4.

Holický, M., Retief, J.V. and Wium, J.A. (2010). Partial factors for selected reinforced concrete members: Background to a revision of SANS 10100-1. *SAICE Journal*, 52 (1), 36-44.

Holický, M., Retief, J. and Sýkora, M. (2015). Assessment of model uncertainties for structural resistance. *Probabilistic Engineering Mechanics*. DOI: http://dx.doi.org/10.1016/j.probengmech.2015.09.008

Hordijk DA. (1992). Tensile and tensile fatigue behaviour of concrete, experiments, modelling and analyses. *Heron Journal*, Vol. 37, No.1, pp. 3–79.

Huber, U.A. (2005). Reliability of Reinforced Concrete Shear Resistance. MSc dissertation, Dept. of Civil Eng., Univ. of Stellenbosch, Stellenbosch, South Africa.

Hunegnaw, C.B. and Aure, T.W. (2021). Effect of orientation of stirrups in combination with shear span to depth ratio on the shear capacity of RC beams. *Journal Heliyon*, Vol.7. e08193. DOI: https://doi.org/10.1016/j.heliyon.2021.e08193

Muller, A.C and Guido, S. (2016). Introduction to machine learning with python; a guide for a data scientist. First edition.

ISO, S. (2015). 2394. General Principles on Reliability for Structures. Zurich: ISO.

Japan Society of Civil Engineers (JSCE). (1986). Specification for design and construction of concrete structures: Design. Tokyo: SP1

Jayasinge, T., Gunawardena, T. and Mendis, P. (2022). Assessment of shear strength of reinforced concrete beams without shear reinforcement: A comparative study between codes of practice and artificial neural network. *Case studies in construction materials*. Vol. 16. 01102. DOI: https://doi.org/10.1016/j.cscm.2022.e01102

JCSS. JCSS Probabilistic Model Code. (2001). Joint Committee on Structural Safety, Zurich. ISBN 978-3-909386-79-6

JCSS probabilistic model code (2006), Zurich.

Jelic´, I., Pavlovic´, MN. and Kotsovos, MD. (1999). A study of dowel action in reinforced concrete beams. *Magazine of Concrete Research*, Vol. 51, No.2, pp 131–141.

Jung, S and Kim, K. (2008). Knowledge-based prediction of shear strength of concrete beams without shear reinforcement. *Journal of engineering structures*, Vol. 30, pp. 1515 – 1525. DOI: https://doi.org/10.1016/j.engstruct.2007.10.008

Kani G.N.J. (1967). How safe are our large reinforced concrete beams? *ACI Journal*, Vol. 64, No.12, pp. 128 – 141.

Kim, J.K. and Park, Y.D. (1996). Prediction of Shear Strength of Reinforced Concrete Beams without Web Reinforcement. *ACI Materials Journal*, Vol. 93, No. 3, pp. 213-222.

Krefeld W, Thurston CW. (1966) Contribution of longitudinal steel to the shear resistance of reinforced concrete beams. *ACI Journal*, Vol.63, No.3, pp. 325–344.

Kuchma, D., Kim, K., Kim, S., Sun, S., Akamat, A. and Hawkins, N. (2004). Simplified Shear Design of Structural Concrete Members. *Concrete Bridge Conference*.

Kukreja, H., Bharath, N., Siddesh, C.S and Kuldeep, S. (2016). An introduction to the artificial neural network. *International Journal of Advance Research and Innovative Ideas in Education*. Vol.1, No.5, Pp. 27 – 30.

Lee, D.H., Han, S.J., & Kim, K.S. (2017). Simplification and verification of dual potential capacity model for reinforced concrete beams subjected to shear. *Structural Concrete*, Vol.18, No.2, pp. 278–291.

Lukas, K. and Vladimir, C. (2016). Model Uncertainties of FEM Nonlinear Analyses of Concrete Structures. *Solid State Phenomena* Vol. 249, pp 197-202.

Marí, A., Bairán, J., Cladera, A., Ollera, E. and Ribas, C. (2015). Shear-flexural strength mechanical model for the design and assessment of reinforced concrete beams. *Structure and Infrastructure Engineering*: Maintenance, Management, Life-Cycle Design and Performance, DOI: http://dx.doi.org/10.1080/15732479.2014.964735

Mari, A., Barian, J.M., Cladera, A. and Oller, E. (2015). Shear design and assessment of reinforced and prestressed concrete beams based on a mechanical model. *Journal of structural engineering*, 04016064-17. DOI: https://doi.org/10.1061/(ASCE)ST.1943-541X.0001539

Mcloed, C.H., Viljoen, C.B and Retief, J.V. (2016). Quantification of model uncertainty of EN1992 crack width prediction model. University of KwaZulu-Natal, Durban, South Africa.

McCulloch, W.S., and Pitts, W. (1943). A logical calculus of the ideas immanent in nervous activity. *Bulletin of Mathematical Biophysics*. Vol. 5, Pp. 115–133.

Mcloed, C.H., Viljoen, C.B and Retief, J.V. (2017). Conference paper; Determining model uncertainty associated with concrete crack models for members in tension. University of KwaZulu-Natal, Durban, South Africa.

Mcleod, C.H., (2019) Model Uncertainty in the Prediction of Crack Widths in Reinforced Concrete Structures and Reliability Implications. PhD dissertation, Department of civil engineering, Stellenbosch University, South Africa.

Mensah, K.K. (2015). Reliability Assessment of Structural Concrete with Special Reference to Stirrup Design. PhD dissertation, Dept. of Civil Eng., Univ. of Stellenbosch, Stellenbosch, South Africa.

Mensah, K. K., Retief, J. V. and Barnardo-Viljoen, C. (2013). Eurocode 2's Variable Strut Inclination Method for shear, its modelling uncertainty and reliability calibration. *In Proceedings of fib Symposium on Engineering a Concrete Future: Technology Modeling & Construction.*

Michelucci, U. (2018). Applied deep learning: A case-based approach to understanding deep neural networks. ISBN-13 (pbk): 978-1-4842-3789-2. https://doi.org/10.1007/978-1-4842-3790-8

Modarres, M., Kaminsky, M and Krivtsov, V. (1999). Reliability engineering and Risk analysis: A practical guide.

Mosley, B., Bungey, J. and Hulse, R. (2007). Reinforced Concrete Design to Eurocode 2 (6th edition.). Palgrave Macmillan, New York, USA.

Muttoni, A., & Fernández Ruiz, M. (2008). Shear strength of members without transverse reinforcement as a function of critical shear crack width. *ACI Structural Journal*, 105(2), 163–172.

Nadolski, V., and Sykora, M. (2014). Uncertainty In Resistance Models for Steel Members. Transactions of the VŠB – Technical University of Ostrava No.2, 2014, Vol.14, Civil Engineering Series paper 28.

Nakamura, T., Iwamoto, T., Fu, L., Yamamoto, Y., Miura, T. and Gedik, Y.H. (2018). Shear Resistance Mechanism Evaluation of RC Beams Based on Arch and Beam Actions. *Journal of Advanced Concrete Technology*, Vol. 16, pp. 563-576.

National Standard of the People's Republic of China. (2010). Code for design of concrete structures (GB 50010-2010). Beijing: Ministry of Housing and Urban-Rural Development of the People's Republic of China.

Nawy, E. G. (2009). Prestressed Concrete (5th ed.). Upper Saddle River, NJ: Prentice Hall.

Neil, J.S. (2017). Statistics for people who (think they) hate statistics. 6th Edition. The University of Kansas.

Olalusi, O.B. (2018). Reliability Assessment of Shear Design Provisions for Reinforced Concrete Beams with Stirrups. PhD Dissertation, Department of Civil Engineering, University of Stellenbosch, South Africa.

Olalusi, O.B and Spyridis, P. (2020). Machine learning-based models for the concrete breakout capacity prediction of single anchors in shear. *Advances in engineering software*, Vol.147 102832. DOI: https://doi.org/10.1016/j.advengsoft.2020.102832

Olalusi, O.B, and Spyridis, P. (2020). Probabilistic Studies on the Shear Strength of Slender Steel Fiber Reinforced Concrete Structures. *Journal of applied sciences*, No.10;6955. DOI: https://doi.org/10.3390/app10196955

Olalusi, O.B and Viljoen, C. (2017). Towards Effective General Probabilistic Representation for Shear Resistance: *12th International Conference on Structural Safety and Reliability (ICOSSAR). TU Wien Vienna, Austria.*

Olalusi, O.B, and Viljoen, C. (2019). Assessment of simplified and advanced models for shear resistance prediction of stirrup-reinforced concrete beams. *Engineering structures*, Vol. 189, Pp. 96 – 109.

Olalusi, O.B and Awoyera, P.O. (2021). Shear capacity prediction of slender reinforced concrete structures with steel fibres using machine learning. *Engineering structures* 227 (2021) 111470.

Parsi, S. S., Mertz, G., & Whittaker, A. S. (2022). Evaluation of design equations for out-of-plane shear strength of deep concrete sections in nuclear power plant buildings. *Nuclear Engineering and Design*, *386*, 111545.

Quinlan, R. (1993) C4.5: Programs for Machine Learning. Morgan Kaufmann Publishers, San Mateo.

Riberio, A.B., Calixto, J.M.F and Diniz, S.M.C. (2016). Assessment of epistemic uncertainties in the shear strength of slender reinforced concrete beams. *Engineering Structures*, Vol.116, pp. 140–147.

Reineck, K. (1991). The ultimate shear force of structural concrete members without transverse reinforcement is derived from a mechanical model (SP-885). *Structural Journal*, vol. 88, no. 5, pp.592 - 602.

Reineck, K.-H., Bentz, E. C., Fitik, B., Kuchma, D. A., & Bayrak, O. (2013). ACI-DAfStb database of shear tests on slender reinforced concrete beams without stirrups. *ACI Structural Journal*, Vol. 110, No.5, pp. 867–875.

Retief, J.V. (2007) Personal communication.

Subramanian, N. (2016). Design of reinforced concrete structures.

SANS 10100-1. (2000). The structural use of concrete – Part 1: Design. South African Bureau of Standards, Pretoria.

Sayyad, Atteshamuddin, S., Subhash, V., Patankar. (2013). Effect of stirrup orientation on the flexural response of RC deep beams. *American Journal of Civil Engineering and Architecture*, Vol.1, No.5, pp. 107–111. Available online at. http://pubs.sciepub.com/ajcea/1/5/4.

Shannon, C. E. (1948). A mathematical theory of communication. *Bell Systems Technical Journal*, Vol. 27, pp. 379–423 and pp. 623–656.

Sherwood E.G, Bentz E. and Collins M. (2008). Effect of Aggregate Size on Beam-Shear Strength of Thick Slabs, *ACI Structural Journal*, Vol. 104, No. 2, pp. 180-190.

Sherwood, E.G., Evan, C.B. and Michael, P.C. (2008). Where is shear reinforcement required? Review of research results and design procedures. *ACI Structural Journal*. Vol. 104, pp.590–600.

Shetty, M.S. (2005) Concrete Technology: Theory and Practice. S. Chand & Company, Ram.

Sigrist, V., Bentz, E., Fernández Ruiz, M., Foster, S. and Muttoni, A. (2013). Background to the *fib* Model Code 2010 shear provisions – part I: beams and slabs. *Structural Concrete*, Vol.14, no. 3, pp. 195 – 203.

Skansi, S. (2018). Introduction to Deep Learning. Zagreb, Zagreb, Croatia: Springer International Publishing AG, Retrieved August 25, 2021, from https://doi.org/10.1007/978-3-319-73004-2.

Slowik, M. (2012). Experimental study of shear failure mechanism in concrete beams. *Proceedings of the International Symposium* “Brittle Matrix Composites”, Vol. 10. Pp 345 – 354.

Slowik, M. (2014). Shear failure mechanism in concrete beams. *Procedia material science*, Vol. 3, No.3, pp. 1977 – 1982.

Slowik, M. (2018). The analysis of failure in concrete and reinforced concrete beams with different reinforcement ratios. *Archive of the applied mechanic journal*. DOI: https://doi.org/10.1007/s00419-018-1476-5

Słowik, M. and Nowicki, T. (2012). The analysis of diagonal crack propagation in concrete beams. *Computational Materials Science*, vol. 52, no. 1, pp. 261-267.

Smola, A.J. and Scholkopf, B. (2003). A tutorial on support vector regression.

Sneed, L.H. and Ramirez, J. (2010). Influence of effective depth on the shear strength of concrete beams – An experimental study. *ACI structural journal*, Vol.107, No.5, pp 554- 562.

SNIP 2.03.01-84. (2012). Concrete and reinforced concrete structures (pp.162). Moscow: Ministry of Regional Development of the Russian Federation.

Song, J., Kang, W., Kim, K. and Jung, S. (2010) Probabilistic shear strength models for reinforced concrete beams without shear reinforcement. *Structural engineering and mechanics journal*, Vol. 34, No. 1, pp 15- 38.

Swamynathan, M. (2017). Mastering Machine Learning with Python in Six Steps. ISBN-13 (pbk): 978-1-4842-2865-4, DOI 10.1007/978-1-4842-2866-1. Bangalore, Karnataka, India.

Sykora, M., Krejsa, J and Holicky, M. (2004). Model uncertainty for shear resistance of reinforced concrete beams with shear reinforcement according to EN 1992-1-1. *Civil engineering series*, Vol.13, No.2, Paper.48.

Sykora, M., Cervenka, V and Holicky, M. (2012). Assessment Of Model Uncertainties in The Analysis of Reinforced Concrete Structures. 18th international conference, *Engineering mechanics*. Paper 200, pp. 1263 – 1272.

Sykora, M., Holicky, M., Prieto, M and Tanner, P. (2014) Uncertainties in resistance models for sound and corrosion-damaged RC structures according to EN 1992-1-1. *Journal of materials and structures*. DOI 10.1617/s11527-014-0409-1

Sykora, M., Krejsa, J., Mlcoch, J., Prieto, M and Tanner, P. (2017). A technical paper: Uncertainty in shear resistance models of reinforced concrete beams according to fib MC2010, fib. *International Federation for Structural Concrete (2018)*, Pp 1 – 12.

Taerwe, L. (1993). Towards a consistent treatment of model uncertainties in reliability formats for concrete structures, *CEB Bulletin d'Information 'Safety and Performance Concepts'. Lausanne: CEB.*

Tao Zhang, Phillip Visintin & Deric J. Oehlers (2016): Shear strength of RC beams without web reinforcement, *Australian Journal of Structural Engineering*, DOI: https://doi.org/10.1080/13287982.2015.1122502

Taylor, R. and Brewer, R.S. (1963). The effect of the type of aggregate on the diagonal cracking of reinforced concrete beams. *Magazine of Concrete Research*. Vol. 115, No. 44, pp. 87–92.

The fib (International Federation for Structural Concrete). (2015). The fib in Russia: New standards. Structural Concrete, 16(1), 149–150.

Tran N.L., (2020). A mechanical model for the shear capacity of slender reinforced concrete members without shear reinforcement. *Engineering Structures*, Vol. 219. DOI: https://doi.org/10.1016/j.engstruct.2020.110803

Tran, N.L. and Graubner, C.A. (2018). Uncertainties of concrete parameters in the shear capacity calculation of RC members without shear reinforcement. *BETON-UND STAHLBETONBAU International Probabilistic Workshop 2018. Technische Universität Darmstadt Institut für Massivbau*.

Vapnik, V. and Lerner, A. (1963). Pattern recognition using the generalized portrait method. Automation and Remote Control, 24: 774–780.

Vapnik, V. and Chervonenkis, A. (1964). A note on one class of perceptron. Automation and Remote Control, 25.

Vecchio, FJ. And Collins, MP. (1986). The modified compression-field theory for reinforced concrete elements subjected to shear. *ACI Structural Journal*, Vol. 83, No. 2, pp. 219–231.

Vegera, P., Khmil, R. and Blikharskyy, Z. (2016). The shear strength of reinforced concrete beams without shear reinforcement. *Journal of civil engineering*, environment and architecture. Vol. 32. Pp. 447 – 457. DOI: https://doi.org/10.7862/rb.2015.209

Wakjira, T.G., Ibrahim, M., Ebead, U. and Alam, M.S. (2022). Explainable machine learning model and reliability analysis for flexural capacity prediction of RC beams strengthened in flexure with FRCM. *Engineering Structures* 255 (2022) 113903. https://doi.org/10.1016/j.engstruct.2022.113903

Yang, Y (2014). Shear Behavior of Reinforced Concrete Members without Shear Reinforcement: A New Look at an Old Problem. Doctoral Thesis, Dept. of Civil Eng., Delft University of technology.

Yerzhanov, M., Ju, H., Zhang, D., Moon, S.W., Kim, J. & Lee, D. (2019). The shear strength model of reinforced concrete beams without stirrup is used in the CIS countries. *Journal of Structural Integrity and Maintenance*. Vol4, no.1, pp.15-25, DOI: https://doi.org/10.1080/24705314.2019.1565056

Zararis, P. (2003). Shear Strength and Minimum Shear Reinforcement of Reinforced Concrete Slender Beams, *ACI Structural Journal*, Vol. 100, No. 2, pp. 203–215.